

# How upward seepage of alkaline groundwater sustains plant species diversity of mesotrophic meadows

GIJSBERT CIRKEL





**How upward seepage of alkaline groundwater  
sustains plant species diversity of mesotrophic  
meadows**

Dirk Gijsbert Cirkel

## **Thesis Committee**

### **Promotors**

Prof. Dr S.E.A.T.M. van der Zee  
Personal Chair Ecohydrology  
Wageningen University

Prof. Dr J.P.M. Witte  
Extraordinary Professor at the Systems Ecology Group  
VU University Amsterdam

### **Other members:**

Prof. Dr M.F.P. Bierkens, Utrecht University  
Prof. Dr W. de Vries, Wageningen University  
Prof. Dr R. van Diggelen, Antwerpen University (Belgium)  
Dr A.J.P. Smolders, Research Center B-WARE, Nijmegen

This research was conducted under the auspices of the Graduate School SENSE

# How upward seepage of alkaline groundwater sustains plant species diversity of mesotrophic meadows

Dirk Gijsbert Cirkel

## **Thesis**

submitted in fulfilment of the requirements for the degree of doctor  
at Wageningen University

by the authority of the Rector Magnificus

Prof. Dr M.J. Kropff,

in the presence of the

Thesis Committee appointed by the Academic Board

to be defended in public

on Friday 16 May 2014

at 11 a.m. in the Aula

How upward seepage of alkaline groundwater sustains plant species diversity of mesotrophic meadows

171 pages

Cirkel, D.G.

PhD thesis, Wageningen University, Wageningen, NL (2014)

With references, with summaries in English and Dutch

ISBN 978-90-6173-912-4

**Abstract**

**&**

**Nederlandse samenvatting**

## Abstract

Wet mesotrophic meadows depending on upward seepage of fresh alkaline groundwater, regarded as the Dutch crown jewels of biodiversity, have declined dramatically in both surface area and botanical quality over the last century. Nowadays, these low productive meadows are only found in protected nature reserves, usually small ones, isolated in an intensively used agricultural landscape. The high biodiversity is explained by the supply of unpolluted, base rich groundwater, which ensures a relatively high and stable groundwater level and leads, in combination with a limited amount of infiltrating precipitation water, to small scale water quality gradients in the soil. These gradients range from base rich, mesotrophic with a circumneutral pH to base poor oligotrophic and more acid conditions in the root environment of the plants. As a result, plant species with different environmental preferences can grow next to and interwoven with each other. Deep intensive drainage in the agricultural areas surrounding the reserves resulted in reduced seepage intensities, and increased influence of infiltrated precipitation water in the soil. As a result, the buffering capacity of many Dutch fen meadow soils decreased and small scale hydrochemical gradients disappeared, resulting in a loss of biodiversity. To restore seepage dependent meadow ecosystems to their full floristic glory, water management measures should aim at restoring seepage intensities and high groundwater levels, whilst at the same time preserving small scale abiotic gradients. This requires delicate measures, which are only feasible with enough knowledge about the hydrological and biogeochemical processes driving the small scale abiotic gradients. So far however, knowledge was insufficient to take such measures effectively.

A usually unknown factor is the quantity of the upward flowing groundwater. Since in situ measuring of upward groundwater fluxes is virtually impossible; one has to derive these fluxes by calibrating hydrological models on measurable quantities such as groundwater and surface water levels. However, seepage data derived in such a way can be subject to profound uncertainty and inaccuracy. This thesis presents a method to estimate seepage intensities from data provided by piezometers and water level gauges and provides insight in the maximum level of accuracy and the minimum level of uncertainty associated with seepage intensity estimates. In most cases, upward flowing groundwater does not reach the root zone but is diverted to ditches, or, in nature areas to gullies and streams. On top of this flow system a lens shaped pocket of infiltrated precipitation water develops. The interface between this so called precipitation lens and underlying groundwater oscillates due to weather variability. As a result, mixing of the two water types occurs, potentially limiting solute loss out of the soil profile. Modelling this mixing behaviour is typically very computationally demanding. In this thesis the dispersive and chromatographic mixing behaviour was explored theoretically, which resulted in insights in how to incorporate mixing behaviour in less computationally demanding approaches.

Based on field measurements and (conceptual) modelling exercises, this thesis shows that shallow flow patterns of seepage and infiltrating precipitation water are strongly dependent on complex interactions between topography and local (ephemeral) drainage systems. The infiltration and exfiltration fluxes of groundwater and precipitation water appeared to directly influence the dynamics of chemical transport in the precipitation lens, in the deeper groundwater, and particularly in the transition zone between the two. The resulting small scaled water quality gradients were reflected in the strong spatiotemporal variation of soil-pH. Furthermore, this thesis shows that this strong spatiotemporal variation can seriously bias empirical relations between abiotic site factors such as soil acidity and vegetation response. In many ecological studies abiotic conditions are determined by taking a single soil sample from the root zone, or bulking several root zone samples per plot. In this way, important information on small scale spatial variation of abiotic conditions is either not taken into account, or lost due to the bulking of samples. These results emphasize the need for systematic sampling and quantification of within plot variation of abiotic conditions in space and time. Moreover, a good interpretation of the processes determining the abiotic conditions of a site (e.g. the sulphate cycling presented in chapter 4) is only possible by combining spatial and temporal biogeochemical and hydrological data.

This thesis provides integrating insights into the hydrological and biogeochemical relationships between upward seeping groundwater, infiltrating precipitation water and vegetation patterns. These insights contribute to sound management of seepage dependent meadows and to a better understanding of the eco-hydrological effects of changes in water management, changes in climatic conditions and contamination of inflowing groundwater.

Keywords: Upward seepage, Fen meadows, Parameter estimation, Precipitation lens, Solute transport, Oscillating concentration fronts, Dispersive and chromatographic mixing, Sulphate reduction, Internal eutrophication, Pyrite oxidation, Soil pH, Heterogeneity; Rhizosphere processes, Microtopography, Surface runoff

## Nederlandse samenvatting

Door kwelwater gevoede natte hooilanden, zoals blauwgraslanden, worden wel beschouwd als de Nederlandse kroonjuwelen van biodiversiteit. Ze zijn de afgelopen eeuw sterk achteruitgegaan, zowel in oppervlakte als in botanische kwaliteit. Tegenwoordig vindt men deze laagproductieve hooilanden alleen nog in beschermde natuurgebieden. Het gaat hierbij om veelal kleine reservaten, die geïsoleerd liggen in een intensief gebruikt agrarisch landschap. De hoge biodiversiteit van de hooilanden wordt verklaard door de toestroming van schoon en baserijk grondwater. Dit resulteert in relatief hoge en stabiele grondwaterstanden en, gecombineerd met een beperkte hoeveelheid infiltrerend regenwater, in kleinschalige waterkwaliteitsgradiënten in de bodem. Daardoor ontstaat er op zeer korte afstand (orde grootte: enkele decimeters) een variatie in het wortelmilieu van de planten die uiteenloopt van baserijke, mesotrofe en pH-neutrale omstandigheden tot basenarme, oligotrofe en zuurdere omstandigheden. Als gevolg hiervan kunnen vele plantensoorten die verschillen in hun milieuvorkeuren vlak naast elkaar voorkomen.

De bijna overal in Nederland uitgevoerde intensieve drainage van agrarische gebieden en toegenomen grondwateronttrekking heeft geresulteerd in een verminderde kwelintensiteit, en toenemende invloed van infiltrerend regenwater in de bodem van kwelafhankelijke reservaten. Als gevolg hiervan is de buffercapaciteit van veel bodems in natuurgebieden gedaald en zijn kleinschalige hydrochemische gradiënten verdwenen zodat de biodiversiteit is afgenomen. Om de volledige botanische glorie van kwelafhankelijke ecosystemen te herstellen, dienen waterbeheersmaatregelen zich te richten op het herstellen van kwelintensiteiten en hoge grondwaterstanden, in nauwe samenhang met het herstel van kleinschalige abiotische gradiënten. Dit vereist op maat gesneden maatregelen, die alleen haalbaar zijn met voldoende kennis over de voor de kleinschalige abiotische gradiënten sturende hydrologische en biogeochemische processen. Vooral nog is echter de kennis nog vaak onvoldoende om dergelijke maatregelen effectief uit te kunnen voeren.

Een veelal onbekende factor is de lokale hoeveelheid omhoog stromende grondwater. Aangezien in-situ meten van opwaartse grondwaterstroming vrijwel onmogelijk is, is men aangewezen op het afleiden van deze fluxen uit de kalibratie van hydrologische modellen aan meetbare grootheden, zoals grond- en oppervlaktewaterstanden. De op deze wijze afgeleide kwelfluxen zijn echter onderworpen aan significante onzekerheden en onnauwkeurigheden. Dit proefschrift presenteert een methode voor het schatten van kwelintensiteiten op basis van gemeten grond- en oppervlaktewaterstanden. De methode geeft inzicht in de maximaal haalbare nauwkeurigheid en de minimale onzekerheid die verbonden zijn aan de inschatting van de kwelintensiteit.

In veel gevallen zal het omhoog stromende grondwater niet de wortelzone bereiken, maar worden omgeleid naar sloten en greppels, of, in meer natuurlijke gebieden naar geultjes en beken. Bovenop dit stromingssysteem vormt zich een lensvormige hoeveelheid geïnfiltrerd regenwater. De grens tussen deze zogenaamde neerslaglens en het

onderliggende kwelwater oscilleert door variaties in het weer. De hierdoor optredende menging van beide typen water voorkomt in potentie uitloging van stoffen uit het bodemprofiel. Het modelleren van dit menggedrag vergt zeer veel rekenkracht. In dit proefschrift is het dispersieve en chromatografische menggedrag daarom theoretisch onderzocht. Deze analyse resulteerde in inzicht in minder rekenkracht vereisende benaderingen voor het simuleren van het menggedrag.

Op basis van veldmetingen en (conceptuele) modellen laat dit proefschrift zien dat ondiepe stromingspatronen van kwel en infiltrerend neerslagwater sterk afhankelijk zijn van complexe interacties tussen topografie en lokale (kortstondige) afvoersystemen. Deze stromingspatronen bleken op hun beurt van invloed te zijn op het chemische transport in de neerslagens, het diepere grondwater, en in het bijzonder in de overgangszone tussen deze twee. De resulterende kleinschalige kwaliteitsgradiënten kwamen tot uiting in de sterke spatiotemporele variatie van de bodem-pH. Bovendien laat dit proefschrift zien dat deze variatie sterk vertekenend kan werken op empirische relaties tussen abiotische standplaatsfactoren, zoals de zuurgraad, en de vegetatierespons. In ecologische studies worden abiotische kenmerken veelal bepaald door het nemen van een enkel grondmonster uit de wortelzone, of het mengen van meerdere wortelzonemonsters per plot. De zo belangrijke informatie over kleinschalige ruimtelijke variatie aan abiotische omstandigheden wordt hierdoor respectievelijk genegeerd of weggepoetst. Het is daarom nodig dat bodemonsters voortaan systematisch worden genomen en dat de variatie in abiotische omstandigheden in ruimte en tijd binnen vegetatieplots wordt gekwantificeerd. Bovendien is een goede interpretatie van de processen die de lokale standplaatscondities aansturen (bijvoorbeeld de sulfaatcyclus gepresenteerd in hoofdstuk 4) alleen dan mogelijk, wanneer voldoende ruimtelijke en temporele biogeochemische en hydrologische gegevens worden verzameld.

Dit proefschrift verschaft een integraal inzicht in de hydrologische en biogeochemische relaties tussen kwelwater, infiltrerend neerslagwater en vegetatiepatronen. Dat inzicht is van belang voor het beheer van kwelafhankelijk graslanden, bijvoorbeeld doordat het kan bijdragen aan een juiste beoordeling van de ecohydrologische gevolgen van ingrepen in de waterhuishouding, van klimaatverandering en van de instroming van vervuild grondwater.

...



# CONTENTS

	Abstract & Nederlandse samenvatting	v
<b>Chapter 1</b>	Introduction	1
<b>Chapter 2</b>	Estimating seepage intensities from groundwater level time series by inverse modelling; a sensitivity analysis on wet meadow scenarios	13
<b>Chapter 3</b>	Mixing behaviour at oscillating fronts	37
<b>Chapter 4</b>	Sulphate reduction and calcite precipitation in relation to internal eutrophication of groundwater fed alkaline fens	65
<b>Chapter 5</b>	The influence of spatiotemporal variability and adaptations to hypoxia on empirical relationships between soil acidity and vegetation	95
<b>Chapter 6</b>	Microtopography as a driving mechanism for ecohydrological processes in shallow groundwater systems	117
<b>Chapter 7</b>	Synthesis and outlook	139
	Bibliography	147
	Dankwoord	165
	List of publications	168
	Curriculum Vitae	170



CHAPTER

**1**

| **Introduction**

## Dutch crown jewels of biodiversity

This thesis focusses on the hydrological and chemical functioning of wet mesotrophic meadows that depend on upward seepage of fresh alkaline groundwater (hereafter: wet mesotrophic meadows). These ecosystems, such as fen meadows and quaking fens, are regarded as the Dutch crown jewels of biodiversity. On only a few square meters one may find many, often rare and endangered, plant species such as various orchids, *Cirsium dissectum* (meadow thistle), *Carex pulicaris* (flea sedge) and *Pinguicula vulgaris* (common butterwort) (Van Wirdum, 1991). Because of their intriguing high biodiversity, wet mesotrophic meadows have long attracted the interest of ecologists (Boyer and Wheeler, 1989; Grootjans, 1985; Jansen, 2000; Klijn and Witte, 1999; Van Wirdum, 1991; Wheeler, 1980).

Field observations led ecologists to conclude that these ecosystems are often confined to areas with upward seepage of groundwater. Among others the work of Van Wirdum (1991) contributed to the notion that they are tied primarily to the supply of unpolluted, base rich water either from groundwater or from surface water. This supply ensures a relatively high and stable groundwater level and leads, in combination with a limited amount of infiltrating precipitation water, to small scale (cm - dm) spatiotemporal water quality gradients from base rich, mesotrophic with a circumneutral pH to base poor oligotrophic and more acid conditions in the root environment of the plants. As a result, plant species with different environmental preferences can grow next to and interwoven with each other, resulting in high biodiversity.



**Figure 1.1.** *Pinguicula vulgaris*, one of the plants found in mesotrophic fen meadows

## Threatened ecosystem

Wet mesotrophic meadows have become very rare in most EU countries. For example in the Netherlands, the surface area of *Juncus-Molinion* meadows has declined from around 100.000 hectares in the early 20th century, to merely 50 hectares today. This decline was mainly caused by the intensification of agriculture, especially from the 1950's onwards, which resulted in increased fertilizer application and intensification of drainage. This strongly increased crop productivity, at the expense of biodiversity. Although originally a product of the agricultural system (i.e. of extensive hay farming), nowadays these low productive meadows are only found in scattered, often small, protected nature reserves. Most of these small remnants suffer from acidification, eutrophication and especially hydrological deterioration due to the lowered groundwater levels as a result of the deep and intensive drainage of their agricultural surroundings.

To protect the reserves from drought caused by the lowered groundwater levels, nature conservation organizations raised the water level in ditches and filled up shallow ditches. These measures protected the ecosystems from drought, but introduced a new problem. The raising of the water level within the reserve and the filling up of ditches, in combination with intensive drainage, and low water levels outside the reserves, resulted in reduction of the upward seepage flux to the reserve and diminished discharge of precipitation water (Van der Schaaf, 1998; Zeeman, 1986). This leads to the formation of a so called 'precipitation lens'; a pocket of groundwater with a chemical composition similar to recently infiltrated precipitation water that lies on top of the upwelling base rich groundwater. The concept of precipitation lenses is discussed in more detail later on in this chapter.

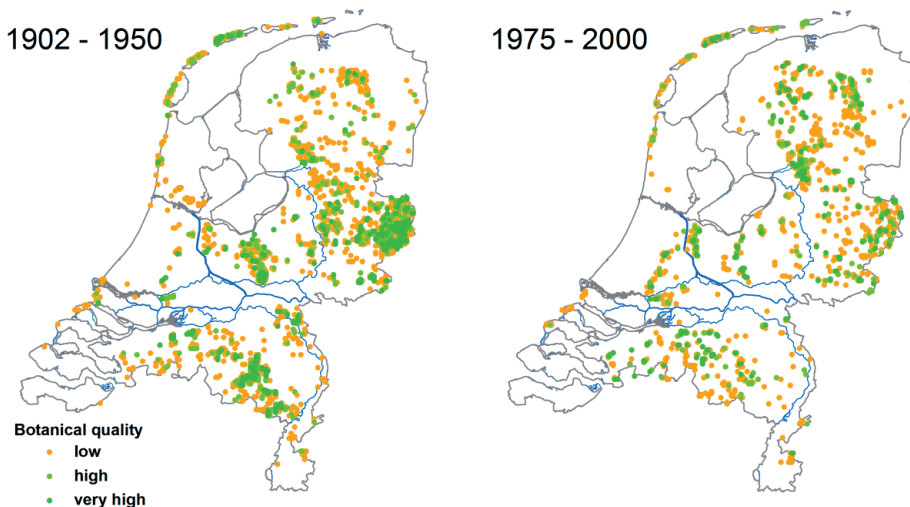


**Figure 1.2.** Strong decline in occurrence and botanical quality of ecosystems of wet, nutrient-poor and weakly acid sites over the 20th century (after: Witte (1998))

For many seepage dependant ecosystems the biggest threat is not drought, but changes in soil chemistry of the root zone, induced by the increased influence of infiltrated precipitation water (Jansen, 2000; Schot et al., 2004). Apart from the coastal dunes, nutrient-poor and wet habitats in the Netherlands are restricted to Pleistocene sandy soils and Holocene peat soils. These soils have typically a limited acid/base buffering capacity (little or no calcite in the topsoil) and are only able to neutralize acid to a certain amount. The increased influence of infiltrated slightly acidic, base poor rainwater compared to seepage water during the 20th century, resulted in a strong decrease of the buffering capacity of many Dutch fen meadow soils and disappearance of the small scale hydrochemical gradients. As a result plant species more adapted to moist, more acid conditions like *Molinia caerulea* (purple heath grass), *Eriophorum angustifolium* (common cotton grass) and *Sphagnum* species (bog moss) started to dominate and outcompete the plant species of neutral to calcareous conditions. Restoration measures have only been partly successful, not reaching the former levels of floral biodiversity (Van der Hoek, 2005) and have especially failed to restore high pH values in the top soil (Jansen, 2000).

In addition, intensive agricultural land use in upstream infiltration areas and air pollution has influenced the chemical composition of the groundwater flowing towards low lying seepage areas (Smolders et al., 2010; Van Beek et al., 2001). For instance nitrate and especially sulphate concentrations of the Dutch upper groundwater increased strongly over the last decades (Mendizabal et al., 2012). When this polluted groundwater reaches the reserves it may harm the species-rich vegetation. Due to the typically low velocity of groundwater flow, it can take decades to hundreds of years before a change in chemical composition of infiltrating groundwater becomes eminent in a seepage area. In smaller hydrological systems however, effects of nitrate and sulphate pollution are already noticeable in groundwater fed nature reserves and may pose a threat to the functioning and ultimately the survival of these ecosystems.

In order to restore seepage dependent meadow ecosystems to their full floristic glory, water management measures should aim at restoring seepage intensities and high groundwater levels, whilst preserving small-scaled gradients in abiotic conditions (e.g. soil moisture, soil acidity, redox conditions). However, hydrological and biogeochemical processes driving these small-scale abiotic gradients are complex and largely unknown, limiting restoration success. To develop effective restoration measures and to be able to assess the effects of changes in water management, pollution of inflowing groundwater and climatologic conditions, insight is needed in the spatiotemporal variation of both water flow and water quality patterns in wet mesotrophic meadows ecosystems.

## Upward seepage

As discussed, wet mesotrophic meadows are tied primarily to the supply of unpolluted, base rich water, either from groundwater or from surface water. The focus of this thesis is on processes occurring in meadows fed by upward seeping base rich, fresh groundwater (see Figure 1.3), although some of the results can be extrapolated to species-rich surface water fed ecosystems. When using the term ‘seepage water’, I refer to groundwater of (sub)regional origin that has undergone significant change in chemical composition due to interaction with the porous medium. The chemical composition of this water type largely depends on the reactivity of both the infiltrated water and the soil matrix, and the interaction time between soil matrix and groundwater, but seepage water generally has a circumneutral to alkaline pH and is enriched in base cations.

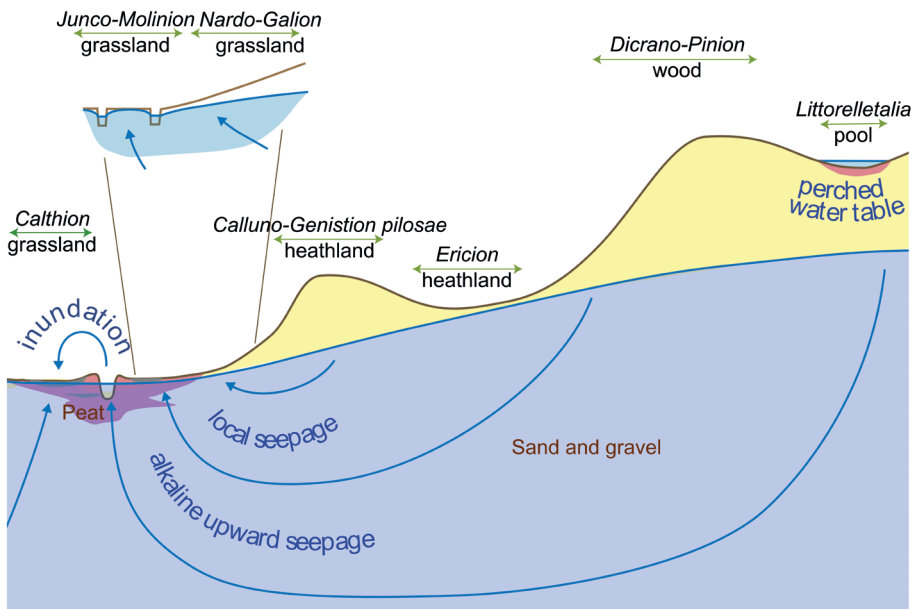


**Figure 1.3.** A typical (seminatural) landscape setting of seepage dependent nature types in the Netherlands (after Witte et al. (2012)). This thesis focusses on hydrological and biogeochemical processes occurring in the area of the inset.

Despite the acknowledged ecological importance of upward seepage, quantitative relationships between seepage fluxes and the occurrence of ‘seepage dependent’ plant communities appear hard to establish. One of the reasons is the lack of data at an appropriate spatial scale, with regard to both the quantity and the quality of upward seepage. Since in situ measuring of upward groundwater fluxes is virtually impossible, one has to derive these fluxes from water balance studies or infer them by calibrating hydrological models on directly measurable quantities such as groundwater and surface water levels. However, seepage data derived in such a way, generally lacks the spatial detail needed to explain biodiversity within nature reserves and can be subject to profound uncertainty and inaccuracy.

## Precipitation lenses

In most cases, upward flowing groundwater does not reach the root zone but is, depending on local conditions, diverted to ditches or shallow trenches in the upper meters of the soil. Related to the diversion of upward seeping groundwater to ditches and trenches is the development of ‘pockets’ of infiltrated precipitation water in the soil. The volume of such a ‘pocket’ of infiltrated precipitation usually has roughly the shape of a lens in a 2d cross section of the soil and is therefore called a ‘precipitation lens’. In well-drained areas with parallel ditches, the interface between infiltrated precipitation and upward seeping groundwater is deepest at the water divide in between two ditches and declines gradually in the direction of the draining ditches (Figure 1.4 A).

The concept of precipitation lenses was first described for large fresh water lenses on top of saline groundwater in dune area’s by Badon Ghyben (1888), Herzberg (1901) and the dynamics by Ribbius (1904). Later (since the end of the 1980’s) the importance of rainwater lenses for seepage dependent ecosystems was acknowledged by Grootjans et al. (1988); Wassen et al. (1988); Van Wirdum (1991) and Bootsma et al. (2002). Different methods have been developed to quantify the shape of field scale precipitation lenses, ranging from simple bucket models (Van Immerzeel et al., 1996) to complex multi-dimensional transient numerical calculations. Analytical solutions for the average (steady state) shape and thickness of a field scale precipitation lens are given by Dr. C. Maas (Poot and Schot, 2000). Quantifications of field scale precipitation lens dynamics are given by Cirkel (2003) and Schot et al. (2004) for freshwater ecosystems using two dimensional numerical calculations with the Hydrus 2D code (Šimůnek et al., 1999). More recently a (virtual) modelling exercise has been published by Frei et al. (2010) involving elaborate three dimensional modelling of a riparian wetland including surface runoff using the HydroGeoSphere code (Brunner and Simmons, 2012). The computational effort for such an analysis is however still very substantial.

Van Wirdum (1991) hypothesised that some degree of rainwater infiltration is beneficial for the species richness of a site. Too much infiltration however, can have a catastrophic effect on seepage dependent ecosystems, eliminating small scale gradients in water quality, gradually depleting the soil profile of base cations and ultimately leading to

acidification of the root zone (Hoogendoorn, 1990). Under Dutch climatologic conditions with an annual precipitation excess of roughly 200-300 mm, precipitation lenses will always form as long as the infiltration capacity of the soil is sufficient. The thickness of a precipitation lens is mainly determined by the dynamic balance between groundwater recharge and the intensity of upward seepage, and may well exceed the thickness of the root zone of fen meadow species (Cirkel, 2003; Schot et al., 2004). However, when groundwater levels are high during wet periods -as is the case in many wet mesotrophic meadows-, precipitation cannot infiltrate, but is discharged laterally as saturation excess overland flow. When groundwater levels raise above the soil surface, groundwater can even extrude from the lens and discharge over the soil surface to the ditches. As a result, the amount of groundwater recharge declines, resulting in a more neutral local water balance. Precipitation lenses can therefore be substantially thinner or even temporarily disappear in parts of a field where phreatic groundwater levels reach the soil surface during wet periods (Figure 1.4 B). Although the general field scale pattern is clear, much is unknown about the small-scale hydrological and biogeochemical processes occurring where the precipitation lens is very thin or even absent.

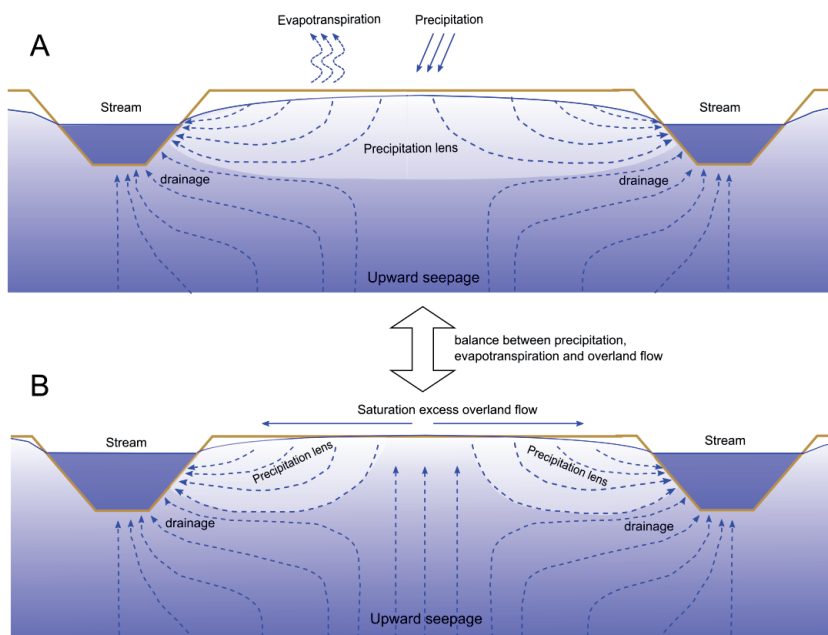


**Figure 1.4.** General shape of a precipitation lens in a field with draining parallel ditches (A) and (B) a situation in which part of the precipitation is temporarily diverted as overland flow during wet periods and upward seepage can reach the root zone or even extrude at the soil surface.

Since fresh water lenses in seepage dependent nature areas have a smaller volume than those found in intensively and deeply drained agricultural areas, they are more susceptible to meteorological variability, with especially spells of wet and dry years. Temporal variations in groundwater recharge result in oscillations of the interface between the precipitation lens and underlying groundwater. This oscillating movement of the interface leads to dispersive mixing of the upward seeping groundwater and the infiltrated precipitation water. Hoogendoorn (1990) and Van Diggelen (1998) already hypothesised in the 1990's that truly oscillating flow conditions (no net recharge on a yearly basis) can be a major factor in preventing solute loss to the subsoil and acidification of fen meadow. However, no detailed analysis of these oscillating mixing processes has been done in this context so far. Moreover, many of the solutes of interest (e.g.  $\text{Ca}^{2+}$ ,  $\text{Mg}^{2+}$ ,  $\text{Fe}^{2+}$ ) do not behave conservatively in the soil, but show strong non-linear behaviour (sorption, precipitation). Insight in this non-linear behaviour in relation with oscillating flow conditions may be crucial for understanding the biogeochemical dynamics of seepage fed ecosystems.

## Spatiotemporal variation of abiotic factors and biodiversity

In wet mesotrophic ecosystems, several factors may affect the local water balance and as such the thickness of a precipitation lens: evapotranspiration, diminished infiltration due to saturation excess and extruding groundwater when groundwater levels breach the soil surface. This allows seepage water to enter the root zone and even the surface (Figure 1.4 B). When slightly elevated parts within this seepage zone allow for the infiltration of precipitation water, small scale (cm – dm) water quality gradients may develop, superimposed on the field scale pattern. This zone, called poikilotrophic by Van Wirdum (1991) (combination from Greek *poikilos* = irregular, varied and *throphé* = nourishment) provides a high level of environmental heterogeneity and, according to Questad and Foster (2008), might therefore sustain the highest level of biodiversity if a functional diverse species pool is available.

Notwithstanding the potentially important role of small-scale environmental heterogeneity in seepage dependent wetlands, limited research has been done on this topic. An exception is the study of Vivian-Smith (1997) who showed experimentally that floristic diversity increases with an increase of micro-topographic heterogeneity in a wetland setting. Such a micro-topography affects a number of important site conditions such as soil redox conditions and soil pH, which in turn affects soil nutrient and oxygen availability and the occurrence of phytotoxic substances such as  $\text{H}_2\text{S}$  and  $\text{Fe}^{2+}$ . An explanation for the lack of information on small-scale environmental heterogeneity is the effort to collect samples of site factors and vegetation on such a fine scale. Small scale measurement are very laborious and can potentially disturb the small scaled patterns one is trying to measure (Figure 1.5). Moreover, it is not always clear what and where species respond to due to physiological adaptations, which can be manifold. For instance clonal species might integrate their resource use across patch types (Reynolds et al., 2007). Other

factors including unknown variation in rooting depth may further complicate such an analysis. Finally, especially at a fine spatial scale site conditions such as soil pH may be prone to substantial temporal variation as a result of meteorological variability.

In many studies spatial homogeneity of site factors i.e. soil pH is assumed within a small vegetation sampling plot (Schaminée et al., 1995a). Empirical relationships between site factors and vegetation are therefore often based on only one abiotic sample per plot, completely ignoring within plot variability in space and time. Such an approach is, given the above, at least questionable in areas where upward seepage meets infiltrating precipitation near the soil surface. An analysis of small scale hydrological and hydrochemical processes in these areas and the effect of these processes on empirical relations between seepage relates site factors, such as soil-pH and vegetation patterns is therefore urgently needed.

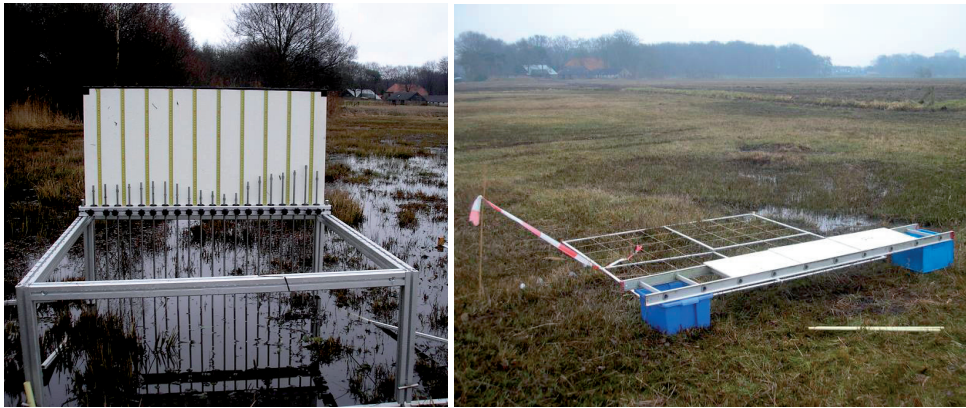


**Figure 1.5.** Detailed measurements of microtopography, hydrochemistry and vegetation composition in the Meeuwenkampje nature reserve provide data for this thesis (Chapter 3 & 4).

## Aims and outline of the thesis

The general aim of this thesis is to provide quantitative insights into the small scale, hydrological and biogeochemical relationships between upward seeping groundwater, infiltrating precipitation water and vegetation patterns. These insights may contribute to a sound management of wet mesotrophic meadow and may help to improve the applicability of ecohydrological modelling approaches. More specifically, I will :

- Develop a method to infer seepage intensities on an appropriate ecological scale from measured time series of ground and surface levels and quantify the accuracy and uncertainty associated with the estimation.
- Model the dispersive and chromatographic mixing behaviour at the interface between infiltrated rainwater and upwelling  $\text{Ca}^{2+}$  rich groundwater to gain insight in the influence of oscillating flow conditions on (vertical) transport of solutes in precipitation lenses.
- Measure and explain field scale spatial and temporal variation in groundwater- and soil water quality of mesotrophic meadows with upward seepage, surrounded by intensive agricultural land use.
- Determine the influence of small-scale spatiotemporal variation on empirical relationships between soil acidity and vegetation. Main objective is to gain insight in possible mechanistic relations between soil acidity, with special focus on seepage dependent ecosystems.
- Illustrate the influence of micro-topographical variation on ecohydrological and biogeochemical processes and vegetation patterns in wetlands.

To this end, I performed numerical and analytical calculations, analysed a national dataset consisting of several subsets of vegetation recordings taken in different years together with biogeochemical information and performed detailed hydrological, biogeochemical and surface level measurements and vegetation recordings in a relatively well preserved seepage dependent nature reserve.

Chapter 2 describes a computational method to derive point scale information on seepage intensities by using measurable hydrological quantities such as groundwater and surface water levels. Furthermore, I show how the accuracy and uncertainty of calibrated seepage fluxes depend on the measurement interval of input data and on the accuracy and uncertainty of inferred local geohydrological parameters and boundary conditions.

Chapter 3 theoretically describes the effect of oscillating flow on dispersive and chromatographic mixing using both analytical approximations and numerical calculations.

It is shown that oscillative mixing involving non-linear sorption, can be described with a (non-linear) diffusion equation with an effective diffusion coefficient based on the absolute average movement of the interface and the dispersivity of the porous medium.

Chapter 4 presents the results of field measurements in the groundwater fed Meeuwenkampje nature reserve. Hydrological and biogeochemical processes and patterns on both field and plot scale are described and quantified. This chapter focusses on the question whether upward seepage polluted with sulphate may lead to deterioration of the vegetation. It is shown that seepage dependent alkaline fen ecosystems can be remarkably resilient to groundwater quality changes.

In Chapter 5 vegetation recordings and pH measurements from the national dataset are combined with extremely detailed pH measurements and vegetation recordings in the seepage fed Meeuwenkampje nature reserve, in order to provide a structural analysis of residual variance of empirical relations between soil acidity and vegetation response. Although the strength of empirical relations between soil pH and vegetation is generally strong, these relations can be seriously biased by spatiotemporal variations of soil pH. Moreover, it is shown that adaptations of plants to wet conditions may result in indifference to soil pH.

Chapter 6 is based on a collaborative effort that describes the influence of microtopography on ecohydrological processes in wetlands. Special attention is given to the influence of microtopography on small scale flow patterns and water quality variation in seepage fed wetlands. Microtopography in such ecosystems is shown to have significant impact on micro scale distribution of plant species.

A synthesis of the research presented in this thesis is given in Chapter 7. Additionally implications and applications of the results for nature management and ecohydrological modelling and perspectives for further research regarding spatiotemporal patterns of water flow and quality in seepage fed nature reserves are discussed.



## CHAPTER

# 2

### Estimating seepage intensities from groundwater level time series by inverse modelling; a sensitivity analysis on wet meadow scenarios

This chapter is a slightly modified version of the published manuscript:

Cirkel, D.G., J.P.M. Witte & S.E.A.T.M. van der Zee (2010) Estimating seepage intensities from groundwater level time series by inverse modelling: A sensitivity analysis on wet meadow scenarios, *Journal of Hydrology* 385, 132–142

## Abstract

Mesotrophic wet meadows with an upward seepage of fresh, alkaline groundwater are famous for their high species richness. However, due to the lack of seepage data on an appropriate spatial scale, no quantitative relationships have been established as yet between seepage and the occurrence of seepage-dependent plant communities. Since there is no established method to directly measure upward seepage in the field, we investigated the possibility of inferring the seepage intensity by using measurable hydrological quantities such as ground and surface water levels.

To this end, we designed 16 representative plots of virtual hydrological situations, using known sets of geohydrological parameters. Then we applied the integrated soil-water-atmosphere-plant model SWAP to generate ‘measured’ time series of ground and surface water levels for these plots. Finally, using the SCEM-UA optimisation algorithm, we calibrated parameters that affect seepage onto these time series. We analysed how the accuracy and uncertainty of calibrated seepage fluxes depend on the measurement interval of input data and on the accuracy and uncertainty of inferred local geohydrological parameters and boundary conditions.

Our analysis shows that it is possible to make reliable estimates of seepage intensities from data provided by easy to place piezometers and water level gauges. For application on real datasets, the analysis gives insight into the limitations of both the approach and the data requirements. For example, data supplied every fortnight was found to be just as valuable for seepage estimation as modern high frequency measurements. When setting up a monitoring programme, our method can help to decide what and when to measure. Furthermore, our method can be used establish quantitative relationships between seepage and plant communities on an appropriate spatial scale.

## Introduction

Because of their intriguingly high biodiversity, mesotrophic wet meadows with an upward seepage of fresh, alkaline groundwater have long attracted the interest of ecologists (Boyer and Wheeler, 1989; Grootjans, 1985; Jansen et al., 2000; Klijn and Witte, 1999; Van Moorsel and Barendregt, 1993; Van Wirdum, 1991; Wheeler, 1980). There are various explanations for the richness of species and the relatively large number of rare and threatened species in these areas (Figure 2.1). One of them is that the inflow of seepage water contributes to a stable and high groundwater level and to a buffering of the pH in the root zone. Such a stable environment favours species that have very specific requirements, i.e. species with narrow ecological amplitudes. For soils that are low in calcium carbonate, the upward seepage of alkaline groundwater is the only mechanism for buffering of the pH. Another explanation for the high biodiversity is that upward seepage, combined with an excess of precipitation, may lead to steep vertical gradients in water quality across the upper part of the soil. This heterogeneous environment allows species

with different root depths, that would otherwise grow in completely different habitats, to grow next to, or interwoven with each other. Despite the acknowledged ecological meaning of upward seepage, a quantitative relationship between seepage and the occurrence of seepage dependent plant communities has not yet been established. One of the major reasons for this is the lack of seepage data on an appropriate spatial scale. Plant communities are described by means of sample stands (relevés). In mesotrophic wet meadows these relevés typically measure about 4 - 10 m<sup>2</sup>.



**Figure 2.1:** A seepage dependent mesotrophic meadow with meadow thistle (*Cirsium dissectum*) and heath spotted orchid (*Dactylorhiza maculata*) in full bloom. Photo: R. Knol

With the term upward seepage we refer to the upward flow of groundwater through the subsoil. Seepage intensities are usually derived from water balance studies or inferred by calibrating hydrological models on measurable quantities such as ground and surface water levels. Consequently, their quantification is subject to profound uncertainty. In regional groundwater models, seepage is often calculated as the vertical flux over a semi confining layer to the top system (De Lange, 1996; Vermulst et al., 1998). In reality, along with the local difference between the head of the phreatic aquifer and that of the underlying aquifer seepage may vary considerably within a computational element (Bruggeman, 1972; De Lange, 1996; Ernst, 1983; Wesseling and Wesseling, 1984). Because of this, the spatial detail of the computed seepage flux directly depends on the element size of the regional groundwater model applied. Computational elements of regional groundwater models usually measure from 10<sup>3</sup> to 10<sup>6</sup> m<sup>2</sup>, thus they are typically orders larger than relevés (which measure from 4 to 10 m<sup>2</sup>). Fitting the resolution of regional groundwater models onto plant communities is hardly ever feasible, due to the limited availability of geohydrological and soil hydraulic data and to limitations in computational power.

Direct non-invasive measurement of seepage at the spatial scale of relevés is not an option because such measurements are virtually impossible. Available ‘seepage meters’ are typically designed and used for measuring flow across the sediment water interface, for instance in limnology and oceanography (Lee, 1977; Rosenberry et al., 2008), and are not readily applicable to terrestrial soils. Estimating upward seepage from the vertical difference in hydraulic head between two points also offers no solution, since the soil samples needed to measure the hydrological conductivity between these points immediately affect local flow conditions.

Phreatic piezometers and water level gauges are easy to place, and are frequently available in wetland nature reserves. These provide valuable information about local hydrological and soil physical conditions. The idea of using phreatic groundwater level data to estimate seepage intensities was first published by Bloemen (1968). However, where Bloemen had to use graphical elaboration of the data to correct for storage changes, we will do so by calibrating a physically based, soil water balance model, SWAP (Kroes et al., 2008; Van Dam, 2000; Van Dam et al., 2008). Calibration will be done using an automatic procedure that not only produces the optimal parameter values, but their posterior probability density functions as well. Though SWAP computes water flow one dimensionally, its horizontal representative resolution is estimated to be in the order of a number of square metres (Kroes et al., 2008), and so it matches the spatial scale of relevés. Moreover, as phreatic heads hardly vary within a vegetation relevé, (Runhaar et al., 1997), it is reasonable to assume that upward seepage through the soil will also be reasonably uniform at this scale.

In this chapter, we investigate the possibility of inferring seepage intensities on an appropriate ecological scale by using measured time series of groundwater and surface water levels. Our main objective is to analyse how the accuracy and uncertainty of calibrated seepage fluxes are influenced by the time interval used for measuring the groundwater and surface water levels and the accuracy of inferred local geohydrological properties and boundary conditions. Since upward seepage is not a directly measurable quantity, we are bound to an inverse modelling approach on a virtual dataset. Therefore, our analysis does not as such focus on new ecological insights, but gives insight in the reliability of seepage estimates based on model calibration on measurable quantities such as groundwater and surface water levels.

## Material and methods

### General approach

To enable us to investigate whether it is possible to infer parameter values and seepage intensities correctly, we constructed a number of virtual plots. These plots are characteristic of seepage dependent ecosystems in the Netherlands (moderate climate, sedimentary sub-soils). For each plot, we generated, daily time series of the phreatic groundwater level, the surface water level, the hydraulic head in the underlying (semi-confined) aquifer and the seepage intensity (Figure 2.2, step 1). These time series served as ‘observations’ for the rest of the analysis. To investigate the effect of sampling frequency, we then resampled the time series on a fortnightly and monthly basis. After that (step 2), we used inverse modelling, by calibrating the geohydrological parameters on the ‘observed’ groundwater level time series, to infer the parameters of the plots. SCEM-UA (Vrugt et al., 2003) – a genetic algorithm combined with a Bayesian inference scheme – was used for the calibration. Next (step 3), the estimated parameter distributions were used to simulate time series of groundwater level and upward seepage. Finally, these predictions were validated on four years of ‘observations’ and the estimated parameter distributions were compared with the original parameter values in the synthetic dataset (step 4).

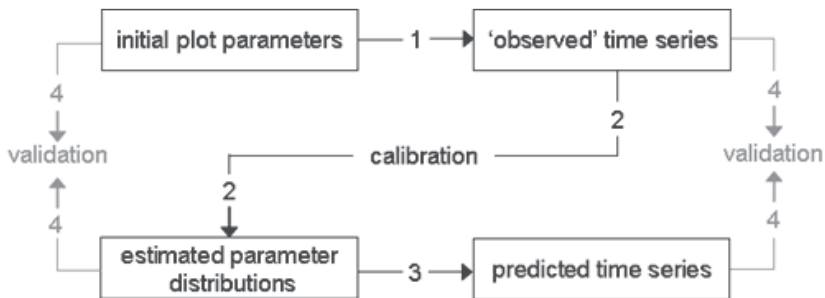


Figure 2.2: General approach

## The SWAP model

SWAP was developed for integrated modelling of Soil-Water-Atmosphere-Plant systems. Here, we describe only those features of SWAP that are relevant to our study (Figure 2.3). The domain of the model extends downwards from a plane just above the canopy to a plane in the phreatic aquifer. Only vertical water flow is assumed in this domain. Below groundwater level, lateral fluxes are included using analytical drainage equations (Ernst, 1956; Hooghoudt, 1940). The upper boundary condition is described using a grass crop model. The function of Feddes et al. (1978) is used to describe the reduction of potential transpiration due to water stress. Vertical soil water flow in the saturated and unsaturated zone is calculated by solving the Richard's equation, numerically. The soil hydraulic functions for water retention and hydraulic conductivity are specified using modified Mualem-Van Genuchten-function parameters (Mualem, 1976; Van Genuchten, 1980; Vogel et al., 2001):

For the water retention curve:

$$\theta(h) = \begin{cases} \theta_r + \frac{\theta_m - \theta_r}{[1 + |\alpha h|^n]^m} & h < h_s \\ \theta_s & h \geq h_s \end{cases} \quad (2.1)$$

For the hydraulic conductivity function:

$$K(h) = \begin{cases} K_0 (S_e)^l \left[ \frac{(1 - F(S_e))}{1 - F(1)} \right]^2 & h < h_s \\ K_0 & h \geq h_s \end{cases} \quad (2.2)$$

$$\text{With: } F(S_e) = (1 - S_e^{1/m})^m, \quad S_e(h) = \frac{\theta(h) - \theta_r}{\theta_m - \theta_r}, \quad m = 1 - 1/n$$

In which  $\theta_r$  ( $\text{cm}^3\text{cm}^{-3}$ ) and  $\theta_s$  ( $\text{cm}^3\text{cm}^{-3}$ ) are the residual and saturated water contents, respectively;  $\theta_m$  ( $\text{cm}^3\text{cm}^{-3}$ ) is an extrapolated parameter ( $\theta_m \geq \theta_s$ );  $n$  (-) and  $\alpha$  ( $\text{cm}^{-1}$ ) are empirical shape parameters; and  $l$  (-) is the pore connectivity parameter.  $K_0$  ( $\text{cmd}^{-1}$ ) is a matching point at saturation,  $b$  (cm) is the pressure head, and  $b_s$  (cm) a small minimum capillary height, often referred to as the air-entry value.

Because of the high groundwater levels that occur in seepage-dependent ecosystems, we adapted the SWAP code using Eq. (2.3) – the modification for hydraulic conductivity near saturation,  $K^*$  – as proposed by Schaap and van Genuchten (2006):

$$K^*(h) = \left[ \frac{K_s}{K(h)} \right]^{R(h)} K(h) \quad (2.3)$$

$$R(h) = \begin{cases} 0 & h < -40 \text{ cm} \\ 0.2778 + 0.00694h & -40 \leq h \leq -4 \text{ cm} \\ 1 + 0.1875h & -4 \leq h \leq 0 \text{ cm} \end{cases}$$

In which  $K_s$  (cm) is the saturated hydraulic conductivity.

Lateral fluxes in SWAP are described by overland flow (runoff) and drainage. When the groundwater level rises above the soil surface, or when the infiltration capacity is insufficient, the ponding reservoir will fill up until the threshold level,  $z_{\text{sill}}$  (cm), of the reservoir is exceeded. When this happens, the surface runoff  $q_{\text{runoff}}$  (cm d<sup>-1</sup>) is calculated as follows:

$$q_{\text{runoff}} = \frac{1}{\gamma_{\text{sill}}} (h_{\text{pond}} - z_{\text{sill}})^{\beta_{\text{sill}}} \quad | h_{\text{pond}} > z_{\text{sill}} \quad (2.4)$$

In which  $h_{\text{pond}}$  (cm) is the depth of water ponding on the soil surface,  $\gamma_{\text{sill}}$  (d) is the resistance to runoff, and  $\beta_{\text{sill}}$  (-) is an empirical exponent.

The interaction between phreatic groundwater and the surface water system is described by:

$$q_{\text{drain}} = \frac{\phi_{\text{phreatic}} - \phi_{\text{drain}}}{\gamma_{\text{drain}}} \quad (2.5)$$

Where  $q_{\text{drain}}$  (cm d<sup>-1</sup>) is the drainage flux (negative values: infiltration),  $\phi_{\text{drain}}$  (cm) is the level of the surface water,  $\gamma_{\text{drain}}$  (d) is the resistance to drainage.

A Cauchy condition is used to describe the bottom boundary of the SWAP model. The bottom flux is calculated using the difference between the hydraulic head in the underlying semi-confined aquifer ( $\phi_{\text{aquifer}}$ ) and the phreatic head ( $\phi_{\text{phreatic}}$ ), divided by the resistance of the semi-confining layer ( $\gamma_{\text{semi-conf}}$ ).

$$q_{\text{seep}} = \frac{\phi_{\text{aquifer}} - \phi_{\text{phreatic}}}{\gamma_{\text{semi-conf}}} \quad (2.6)$$

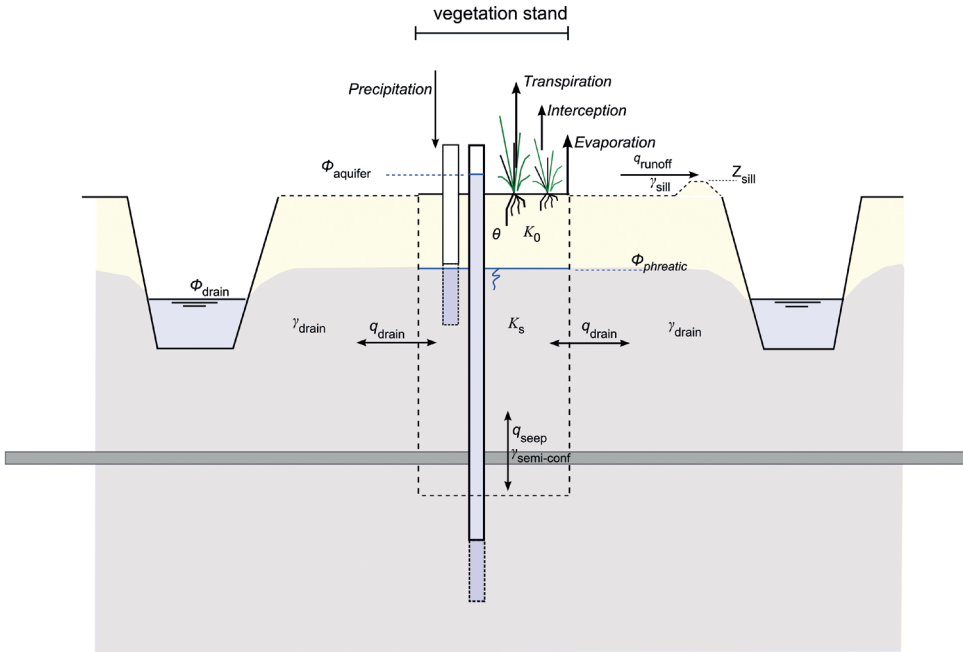


**Figure 2.3:** A schematised overview of the processes modelled with SWAP.

### Virtual plots and computational generation of time series (step 1)

To investigate whether it is feasible to infer parameter values and seepage intensities correctly, we constructed 16 virtual SWAP plots (Table 2.1). Each plot consists of a unique combination of different values for: weir-crest height ( $P$ ), drainage resistance ( $\gamma_{\text{drain}}$ ) (Stoppelenburg, 1999), saturated hydraulic conductivity ( $K_s$ ) (Schaap et al., 2001; Wösten et al., 2001), the mean hydraulic head in the underlying aquifer ( $\phi_{\text{aquifer}}$ ) (simulated as a sinusoidal wave with an amplitude of 50 cm, a period of 365 days and a maximum head at day 59) (Kroes et al., 2008) and the resistance of the semi-confining layer ( $\gamma_{\text{semi-conf}}$ ) (Stoppelenburg, 1999). For more information about the model structure we refer to Figure 2.3. The parameter ranges represent the variation of hydro-physical conditions in seepage dependent (semi-natural) meadow ecosystems with a fine loamy sand soil, that are typical of wet meadow ecosystems in the Pleistocene cover-sand landscape of the Netherlands (Beets et al., 2003; Runhaar, 1989; Van Delft, 1995). These fine loamy sand soils occur in up to 60% of the seepage dependant ecosystems in the Netherlands. Appropriate soil hydraulic parameters were taken from Schaap et al. (2001) and Wösten et al. (2001) and are listed in Table 2.2. To avoid complicating our numerical experiment, we assumed a homogeneous soil profile, which is, except for a thin humic top layer, reasonable for these types of soil. The meadow vegetation was modelled as a standard grass crop, with parameters adopted from Kroes et al. (2008). On the basis of a literature

survey (Eggelsman, 1981; Jansen, 1995; Koerselman and Beltman, 1988; Schouvenaars, 1993), potential evapotranspiration of the meadow was assumed as being equal to Makkink's reference crop evapotranspiration. Drain spacing ( $L$ ) was set to a value of 3,000 cm. Surface water levels were simulated with the SWAP extended-drainage package (Kroes et al., 2008), using a stage-discharge relation, based on the Dutch design discharge for seepage areas with high groundwater levels (1.67 l/s/ha) (Anonymous, 1988). Ponding and runoff were controlled by setting the ponding threshold ( $Z_{\text{sill}}$ ) and the resistance to runoff ( $\gamma_{\text{sill}}$ ) at 5 cm and 0.1 d, respectively.  $\beta_{\text{sill}}$  was set to 1.

Meteorological input was provided by the Royal Netherlands Meteorological Institute. It consisted of daily precipitation and Makkink reference evaporation (Makkink, 1957) data for the period 1971-1976 taken from the De Bilt weather station, located in the centre of the Netherlands. We chose this period because it contains moderate as well as extremely wet and dry years.

We used the 16 plots to simulate time series of groundwater levels, surface water levels and hydraulic heads in the underlying aquifers, on a daily basis (Appendix 2.A gives the range of the simulated time series). These time series served as 'observations' for further analyses. (In practice, however, levels are usually sampled less frequently than every day: a fortnightly interval is still common in the Netherlands, although with the increasing application of data loggers, higher frequencies are becoming more common.) To include the effect of sampling frequency in the analysis, we also derived time series with fortnightly and monthly intervals, by sampling day values every fortnight and month, respectively.

## Inverse modelling (step 2)

We used the Shuffled Complex Evolution Metropolis Algorithm (SCEM-UA) (Vrugt et al., 2003; Vrugt et al., 2004) to estimate the best set of parameters and the underlying posterior density functions of each of the plots and sample intervals. We did so by calibrating SWAP models on 'observations' of phreatic groundwater levels in 1971 and 1972 taken from the synthetic datasets (1973-1976 were used for the validation; see next section). During this calibration, the following quantities were varied: the ponding threshold ( $Z_{\text{sill}}$ ), the resistance to runoff ( $\gamma_{\text{sill}}$ ), soil hydraulic properties of the Mualem-van Genuchten model ( $K_0$ ,  $\alpha$ ,  $K_s$ ), the resistance of the semi-confining layer ( $\gamma_{\text{semi-conf}}$ ) and the drainage/infiltration resistance ( $\gamma_{\text{drain}}$ ).

**Table 2.1:** Varied parameters of the 16 synthetic plots (The first digit of the plot number reflects the value of P, the second digit the value of  $K_s$  and  $\gamma_{\text{drain}}$ , and the last digit the value of the seepage flux determined by  $\gamma_{\text{semi-conf}}$  and  $\bar{\phi}_{\text{aquifer}}$ .)

Plot no.	Weir-crest height	Drainage resistance	Saturated hydraulic conductivity	Resistance of the semi- confining layer	Mean hydraulic head underlying aquifer
	P (cm+ surf.lev.)	$\gamma_{\text{drain}}$ (d)	$K_s$ (cmd <sup>-1</sup> )	$\gamma_{\text{semi-conf}}$ (d)	$\bar{\phi}_{\text{aquifer}}$ (cm+ surf.lev.)
1a1	-25	201	23.53	10,000	75
1a2	-25	201	23.53	200	-25
1a3	-25	201	23.53	1,000	75
1a4	-25	201	23.53	20	-25
1b1	-25	41	120.00	10,000	75
1b2	-25	41	120.00	200	-25
1b3	-25	41	120.00	1,000	75
1b4	-25	41	120.00	20	-25
2a1	-50	201	23.53	10,000	75
2a2	-50	201	23.53	200	-25
2a3	-50	201	23.53	1,000	75
2a4	-50	201	23.53	20	-25
2b1	-50	41	120.00	10,000	75
2b2	-50	41	120.00	200	-25
2b3	-50	41	120.00	1,000	75
2b4	-50	41	120.00	20	-25

**Table 2.2:** Values of the Mualem-van Genuchten parameters for the soil hydraulic properties of loamy fine sand

Parameter	Unit	Value
$\theta_s$	cm <sup>3</sup> cm <sup>-3</sup>	0.01
$\theta_r$	cm <sup>3</sup> cm <sup>-3</sup>	0.34
$K_0$	cm d <sup>-1</sup>	10.87
$\alpha$	cm <sup>-1</sup>	0.017
n	-	1.717
l	-	0.00

Instead of considering all the Mualem-van Genuchten parameters as calibration parameters, the soil hydraulic functions of the virtual plots were estimated using calibrated (Miller) scaling factors  $\chi_{\text{vgm}}$  (Bakker and Nieber, 2004; Miller and Miller, 1956; Vogel et al., 1991).

$$K_0 = \chi_{\text{vgm}}^2 K_{0\text{ref}} \quad (2.7)$$

$$\alpha = \chi_{\text{vgm}} \alpha_{\text{ref}} \quad (2.8)$$

With  $K_{0\text{ref}} = 10.87 \text{ cm d}^{-1}$  and  $\alpha_{\text{ref}} = 0.017 \text{ cm}^{-1}$

Given the fact that  $K_s > K_0$ , we estimated the value of  $K_s$  as a function of  $K_0$  using a dimensionless calibrated adjustment factor,  $\chi_{K_{\text{sat}}}$ :

$$K_{\text{sat}} = \chi_{K_s} K_0 \quad (2.9)$$

The drainage resistance ( $\gamma_{\text{drain}}$ ) can be written as a function of  $K_s$ , the drain spacing ( $L$ ) and some other parameters, describing the shape of the flow problem (Aronovici and Donnan, 1946; Ernst, 1956; Hooghoudt, 1940). We lumped the shape parameters together, into one dimensionless calibrated adjustment factor,  $\chi_{\text{dr}}$ :

$$\gamma_{\text{drain}} = \frac{1}{LK_{\text{sat}}} \chi_{\text{dr}} \quad (2.10)$$

This leads to a set of 6 calibration parameters. For each of these parameters, a uniform distribution was assumed between the minimum and maximum values of the prior uncertainty ranges, as presented in Table 2.3. The prior uncertainty ranges of the soil hydraulic parameters were based on a large dataset with soil hydraulic descriptions of wet seepage dependant meadows (Beets et al., 2003; Runhaar, 1989). Transforming the scaling and adjustment factors back into the more physically identifiable quantities  $K_0$ ,  $\alpha$ ,  $K_s$  and  $\gamma_{\text{drain}}$  results in the parameter ranges given in Table 2.4. Some of these ranges are quite wide, because, normally the geohydrological parameters that correspond with them are not very accurately known. However, by sampling these parameters ( $\gamma_{\text{fill}}$ ,  $\gamma_{\text{semi-conf}}$ ) in log space, the search efficiency of the algorithm is enhanced.

The SCEM-UA algorithm was set to optimise the 6 parameters, using 5 parallel sequences, each containing 1200 samples. This resulted in 6000 SWAP runs per plot. The residual error between prediction and ‘observation’ was calculated using a simple least-square objective function. Convergence to a stationary posterior distribution was ascertained using the Gelman and Rubin (1992) scale-reduction criterion. Although the SCEM-UA algorithm is efficient compared with traditional Metropolis Hastings samplers (Vrugt et al., 2003), a considerable computational effort is still required. To complete the 6000 SWAP optimisation runs – with the computation of each plot taking on average 5 to 30 seconds (on a Pentium IV 2 GHz computer)– 8 to 16 hours of calculation time is needed.

**Table 2.3.** Calibration parameters

Calibration parameter	Description	Unit	Prior uncertainty range	
			min	max
$z_{\text{sill}}$	Max. depth of ponding	[cm]	1	10
$\gamma_{\text{sill}}$	Runoff resistance	[log(d)]	-2	0
$\gamma_{\text{vgm}}$	Miller scaling factor	[-]	0.3	1.5
$\gamma_{\text{ks}}$	$K_s$ adjustment factor	[-]	1	12
$\gamma_{\text{semi-conf}}$	Resistance of the semi-confining layer	[log(d)]	1	4301
$\gamma_{\text{dr}}$	Drainage/infiltration resistance adjustment factor	[-]	14.4	17.6

**Table 2.4.** Prior uncertainty ranges of:  $K_0$ ,  $\alpha$ ,  $K_s$  and  $\gamma_{\text{drain}}$ 

Parameter	Unit	min	max
$K_0$	cm d <sup>-1</sup>	0.98	24.45
$\alpha$	d <sup>-1</sup>	0.0005	0.0255
$K_s$	cm d <sup>-1</sup>	0.98	293.4
$\gamma_{\text{drain}}$	d	14.7	5388

For our analysis, we used non-perturbed synthetic data with different time intervals and assumed a small measurement error of 0.5 cm. This makes it possible to verify the ability of the SCEM-UA algorithm to infer the parameters used for generating the time series and to analyse the effect of the sampling frequency. Furthermore, it gives an indication of the minimal uncertainty and maximal accuracy of estimated model parameters (Raat et al., 2004). After each calibration, the parameter distribution intervals (95% confidence level) were calculated from the posterior probability distributions. These were based on 2000 samples taken after convergence had been achieved. These parameter sets were used to compute the uncertainty ranges related to the simulated groundwater levels and seepage fluxes for each of the plots.

### Prediction of groundwater level and seepage time series (step 3)

The parameters distributions estimated in step 2 were used to predict groundwater levels and seepage intensities for the four-year validation period 1973-1976. This validation period included 1976, an extremely dry year, with an average precipitation deficit repetition time of 73 years (Beersma and Buishand, 2007). The simulated time series were used to validate the inverse modelling procedure.

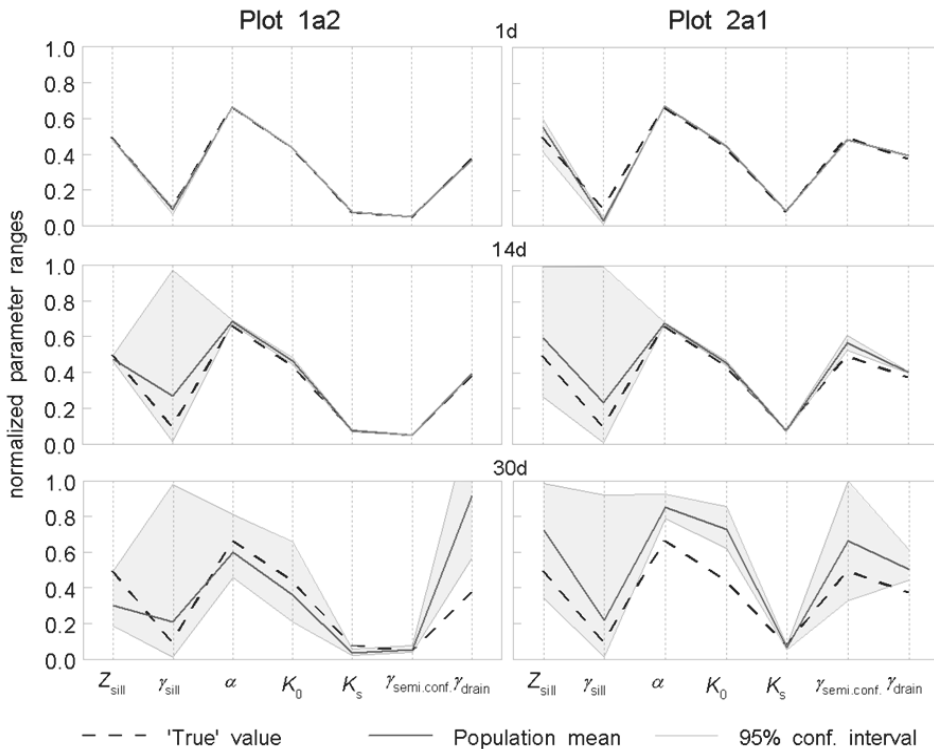


**Figure 2.4.** Effect of sampling frequency on parameter uncertainty and accuracy for two representative plots and three sampling frequencies: daily, fortnightly and monthly. The model parameters are listed on the x axis, while the y axis corresponds to the parameter values, scaled to their prior uncertainty ranges (Table 2.1).

## Results & discussion

### Validation

#### *Calibrated plot parameters (1971-1972)*

The sampling frequency of ‘observed’ data considerably affects both the uncertainty (the 95% confidence interval) and the accuracy (the absolute difference between the population mean and the ‘true value’) of the calibrated model parameters (Figure 2.4). The use of daily sampled data results in small uncertainties and high accuracies, except for the runoff parameters  $Z_{\text{sill}}$  and  $\gamma_{\text{sill}}$ , and particularly the latter (Table 2.5). The two years of daily groundwater level data clearly does not contain enough information to infer the parameter values of the runoff model properly for all of the plots. Although the daily data give insufficient information to infer parameter values, accounting for the prior uncertainty ranges shows that the calibrated values are good enough.

Decreasing the sampling frequency to fortnightly ‘observations’, still resulted in clearly identifiable parameters, except again for  $Z_{\text{sill}}$  and  $\gamma_{\text{sill}}$ . However, when monthly ‘observations’ were used, this resulted in poor descriptions of almost all parameters and equally acceptable calibrations for quite different combinations of parameter values (a phenomenon known as ‘equifinality’ (Beven and Binley, 1992; Beven and Freer, 2001; Raat et al., 2004). Hence, for systems such as the ones considered here, measuring once every two weeks appears to be a well-founded effort. An interesting feature is that the soil hydraulic properties for plots denoted by ‘b’ (Table 2.1) show wider parameter distribution intervals at a 95% confidence level and less accurate expected values than plots denoted by ‘a’. The difference between the ‘a’ and ‘b’ plots is de ratio between  $K_0$  and  $K_{\text{sat}}$ , where small ratios (‘b’), indicate that macro pore flow plays a more important role (Schaap and Leij, 2000; Schaap and van Genuchten, 2006). The steep slope and nonlinearity associated with the  $K(h)$  function near saturation, are known to complicate the estimation of soil hydraulic properties.

**Table 2.5.** Percentage of accuracy for three sampling frequencies, averaged over the 16 plots (small values indicate high accuracy).

Sampling Frequency	Plot Parameter						
	$Z_{\text{sill}}$	$\gamma_{\text{sill}}$	$\alpha$	$K_0$	$K_s$	$\gamma_{\text{semi-conf.}}$	$\gamma_{\text{drain}}$
Daily	25	116	2	5	12	12	14
Fortnightly	21	168	10	21	14	8	16
Monthly	20	122	28	66	55	61	62

**Table 2.6.** Percentage of accuracy for three sampling frequencies averaged according to the value of  $\gamma_{\text{semi-conf}}$ .

$\gamma_{\text{semi-conf}}$	Daily	Fortnightly	Monthly
10,000	39%	25%	28%
1000	3%	3%	85%
200	2%	1%	86%
20	6%	4%	45%

The parameter  $\gamma_{\text{semi-conf}}$  is well identifiable at daily, and fortnightly sampling frequencies, except for a value of 10,000 d, which yields small accuracies (see Table 2.6) and large uncertainties (see Figure 2.4). Such a large value of  $\gamma_{\text{semi-conf}}$  leads to a very small seepage flux and thus to insensitivity of the objective (Yapo et al., 1996). The results of this section therefore show that for the systems on which this thesis focuses, a dataset with a measuring frequency of once every 14 days is already sufficient, provided that the soils are not characterised by highly non-linear hydraulic properties or extremely small seepage fluxes due to a highly undulating semi-confining layer. The latter constraints do not occur often, or do not occur together, in the systems considered here.

#### *Validation on phreatic groundwater levels (1973-1976)*

Simulated groundwater levels (1973-1976) based on calibration on daily and fortnightly sampled data (1971-1972) give small RMSE values. The average values were 1.42 cm and 1.64 cm, respectively, for the 16 plots during the validation period (1973-1976). RMSE values for the monthly sampled data were significantly larger, with an average of 9.72 cm. Again, this result indicates that a fortnightly sampling spacing is adequate. From Figure 2.5, we also observe that the simulated groundwater levels show a slight under estimation for all sampling frequencies. This systematic error is caused by the underestimation of shallow groundwater levels during wet periods, due to erroneous runoff parameters. Thus, even high frequency daily observations do not, in themselves, ensure a correct estimation of runoff. This is not unexpected given the discrepancy in time scale between the runoff processes and measurements.

#### *Validation on seepage fluxes (1973-1976)*

Simulated seepage fluxes (1973-1976) based on daily and fortnightly sampled 'observations' (1971-1972) show narrow uncertainty ranges at the 95% confidence level. The uncertainty of the seepage fluxes for plots with a high value of  $\gamma_{\text{semi-conf}}$  is small. The uncertainty found, is predominantly determined by uncertainty in the estimated resistance of the semi-confined layer and to a lesser extent by uncertainty in groundwater levels.

Plots with lower values of  $\gamma_{\text{semi-conf}}$  show even narrower uncertainty ranges. In these plots, uncertainty is concentrated in the periods during which phreatic groundwater levels are high, and is caused by poorly constrained runoff parameters, as discussed in “Calibrated plot parameters (1971–1972)”. For monthly sampled observations, seepage flux uncertainty was considerable for all plots, and particularly large in plots with high values of  $\gamma_{\text{semi-conf}}$ . The accuracy of estimated seepage fluxes is high for calibrations on daily and fortnightly sampled data (Figure 2.6). The average simulated seepage fluxes are close to the average ‘observed’ seepage fluxes, and RMSEs were small, with an average over the 16 plots of 0.06 and 0.09 mm/d for daily and fortnightly ‘observations’ respectively. However, with an average of 1.10 mm/d over the 16 plots, the RMSEs of seepage fluxes based on monthly sampled data were found to be very large. In contrast to the calibrated groundwater levels, the simulated averages at this sampling frequency are completely out of line with the ‘true’ values. Hence, using a combination of erroneous parameters, it is possible to get reasonably accurate groundwater level simulations (Figure 2.5), but completely inaccurate seepage fluxes. This demonstrates the risk posed by equifinality when calibrating on groundwater level time series, measured at large intervals.

The Nash-Sutcliffe efficiency coefficient (Nash and Sutcliffe, 1970) is commonly used to describe the accuracy of hydrological model outputs quantitatively. The efficiency coefficients calculated for the simulated seepage fluxes (data not shown) confirmed our conclusions; e.g. that efficiency is poor in plots with a highly undulating semi-confined layer, impaired in plots where overland flow or highly non-linear soil hydraulic properties are predominant and very bad if the sampling interval is large, as with the monthly sampling.

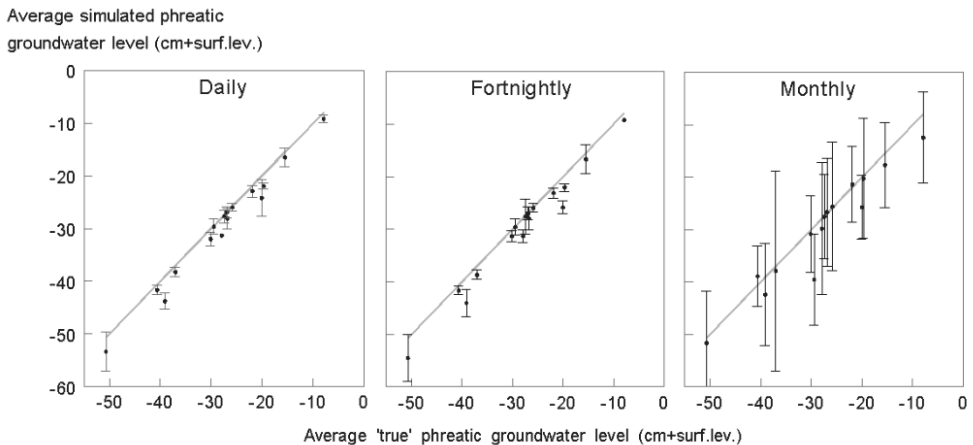


**Figure 2.5.** Effect of sampling frequency on the average phreatic groundwater levels (cm+surf.lev.) (black dots) calculated using the means of the individual parameter distributions. (The error bars denote the RMSE of the simulated phreatic groundwater level during the validation period.)

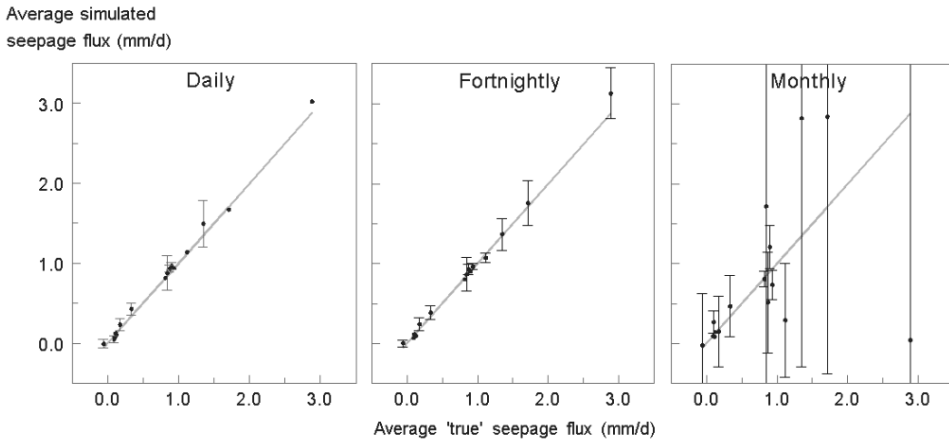


**Figure 2.6.** Effect of sampling frequency on the simulated seepage flux (average plus RMSE). The simulations were based on the means of the individual calibrated parameter distributions.

### Boundary conditions

So far, we have assumed the availability of accurate data on boundary conditions. In practice, however, such data is often missing. Measured surface water levels are particularly scarce. Often, the only information available is the height of a weir crest or data from a water level gauge further downstream. Although hydraulic heads are measured more frequently in nature reserves, these piezometers are often placed in other locations than where the phreatic observation wells are situated. Therefore, to test the effect of calibrated surface water levels on the estimated model parameters, we simulated surface water levels by assuming a fixed stage-discharge relation and a calibrated weir crest height ( $P$ ). Then, to test the effect of a calibrated Cauchy bottom boundary, we varied the mean of the time series ( $\bar{\phi}_{\text{aquifer}}$ ), assuming no change in amplitude. To reduce calculation time, we only tested on fortnightly sampled ‘observation’ data. We assumed a prior uncertainty range of -5 to 10 cm for  $P$  and -10 to 10 cm for  $\bar{\phi}_{\text{aquifer}}$ . Adding  $P$  to the set of calibration parameters gave overall better constrained parameters and well simulated phreatic groundwater levels and seepage fluxes (Figure 2.7). Varying the surface water levels was found to add information to the calibration, thus enhancing efficient exploration of the parameter space. Adding  $\bar{\phi}_{\text{aquifer}}$  to the calibration gave poorly constrained model parameters and thus profound equifinality. The uncertainty associated with  $\bar{\phi}_{\text{aquifer}}$  was considerable, and related to  $\gamma_{\text{semi conf}}$ . For plots with  $\gamma_{\text{semi conf}} = 10,000$  d, the 95% confidence level of the parameter space occupied almost the entire prior uncertainty range.

Average simulated  
seepage flux (mm/d)

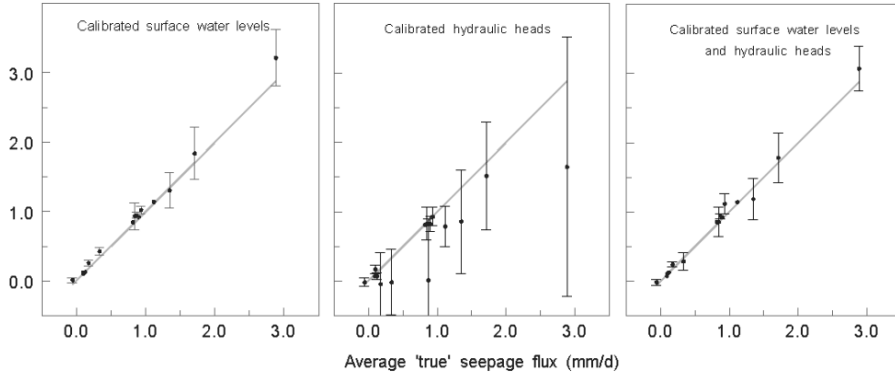


**Figure 2.7.** The effect of calibrated boundary conditions on the simulated seepage flux (mm/d) (average plus RMSE). The simulations were based on the mean of the individual calibrated parameter distributions.

A major part of the uncertainty found, originates from interaction between  $\bar{\phi}_{\text{aquifer}}$  and the drainage parameters (e.g. either a rise in  $\bar{\phi}_{\text{aquifer}}$  or an increase in  $\gamma_{\text{drain}}$  contributes to a higher phreatic groundwater level). In our previous analysis, the fit of the phreatic groundwater levels (calculated with the means of individual parameter distributions) was close to the optimal fit. In this case, however, the outcome was a poor fit, even for the phreatic groundwater level. This illustrates that where profound equifinality occurs, a single optimal parameter combination is no longer suitable, and the whole range of equally fitting parameter combinations needs to be assessed. Our final test was to add both  $P$  and  $\bar{\phi}_{\text{aquifer}}$  to the set of calibration parameters. The near perfect negative correlation between  $\bar{\phi}_{\text{aquifer}}$  and  $P$ , indicates that erroneous drainage fluxes (due to an erroneous  $P$ ) can be compensated by (erroneous) seepage fluxes. This results in relatively wide distribution intervals at 95% confidence level. However, varying the weir crest height results in better estimates of the drainage parameters, which, in turn, leads to good estimates of the drainage flux. Subsequently, this leads (assuming no meteorological forcing data error) to a good estimate of the seepage flux and thus in good estimates of both  $\bar{\phi}_{\text{aquifer}}$  and  $\gamma_{\text{semi-conf}}$ .

To conclude, uncertainty in the Cauchy bottom boundary significantly affects the identifiability of the model parameters and results in high levels of uncertainty and inaccurate seepage estimates. The use of a smooth sinusoidal wave, as in this study, is of course a simplification. In reality the hydraulic head will be more strongly correlated to the freatic groundwaterlevels, which probably makes it even harder to successfully identify the model parameters. Varying the surface water levels, improves the identifiability of the drainage and soil hydraulic parameters and, as a consequence, results in better constrained Cauchy bottom boundary parameters.

## Real world application

In this chapter, we neglected errors in forcing data and inadequacies in the model structure, which, of course, in a real world context, would affect the results. To study the effect of such errors, we also performed an analysis on perturbed data (Appendix 2.B.). The results demonstrate that the combination of measured groundwater and surface water level data and with an efficient calibration algorithm is a promising method for estimating local scale seepage fluxes. Prior analysis on virtual data (Raaijmakers et al., 2004; Van Dam, 2000), such as those presented in this chapter, serves as a useful tool preceding the application on real data or the design of a monitoring programme. Since seepage is not a directly measurable quantity, prior analysis gives insight into the processes influencing the level of accuracy and uncertainty of estimated seepage intensities. For example, our analysis showed that the quality of the seepage estimate is directly related to the contribution of the seepage flux to groundwater level fluctuations. Correct inference of small seepage fluxes, e.g.  $<0.1$  mm/d, will therefore be difficult. This will be especially true in a real world context, where input errors and model structural errors do occur. Our analysis shows that data provided by relatively easy to place piezometers and water level gauges, contain valuable information on local soil hydraulic and hydrologic properties. However, combined measurements of phreatic groundwater levels, hydraulic heads and surface water levels are often scarce. Unavailability of measured time series of especially hydraulic heads will result in less accurate estimates and high uncertainty. Nevertheless, by varying the surface water levels, we found that equifinality could be reduced. This resulted in less uncertainty and higher accuracy of seepage estimates. We expect rainfall input data to be an additional source of uncertainty, due to highly heterogeneous spatial rainfall patterns. Recently, however, by combining rain-gauge measurements with radar images (DeGaetano and Wilks, 2009; Leijnse et al., 2008; Schuurmans et al., 2007), the prediction of spatial rainfall patterns has improved. Moreover, much progress has been made in the treatment of rainfall forcing data error (Clark and Slater, 2006; Clark et al., 2008; Kavetski et al., 2006a; Kavetski et al., 2006b; Vrugt et al., 2008). Application of these methods will either improve the quality of meteorological input data, or will enhance our method by explicitly taken into account error in forcing data. In this study we used a 1D model. Expanding the approach to 2D or 3D is possible (see Vrugt et al. (2001)), but will strongly increase the computational and data demands. Future research will focus on the application on a real dataset of up to 200 relevés.

## Conclusions

Mesotrophic wet meadows with upward seepage of fresh, alkaline groundwater are famous for their intriguingly high diversity of plant species. However, a quantitative relationship, between seepage intensity and the occurrence of seepage dependent plant communities, still needs to be established. The main reason for this, is the fact that seepage is not a directly measurable quantity. In this chapter, we present a method for quantifying seepage intensities on an appropriate ecological scale, using measurable and commonly available quantities such as groundwater and surface water levels. The method

presented here provides insight into the maximum level of accuracy and the minimum level of uncertainty associated with it when estimating seepage intensities on the spatial scale of relevés, depending on the measurement time interval of ‘measured’ input data and on the accuracy of inferred local hydrological properties and boundary conditions.

Above all, our analysis shows that (1) it is possible to infer seepage intensities from data provided by relatively easy to place piezometers and water level gauges. For practical applications, it is important to know at which sampling frequency reliable estimates of first the model parameters and second the seepage intensity, can be made. (2) We showed that groundwater levels monitored at fortnightly intervals are adequate for producing reliable estimates, whereas monthly data do not contain enough information to successfully infer model parameter values and the seepage intensities. (3) Furthermore, we showed that existing manually measured data on a fortnightly basis are as valuable for the estimation of seepage intensities as modern high frequency measurements by data loggers. This makes it possible to apply our method on existing datasets of combined ecological and hydrological information (Beets et al., 2003; Ertsen, 1999; Runhaar, 1989), thus allowing us to derive quantitative relationships between seepage and plant communities.

## **Acknowledgments**

We would like to thank Jasper Vrugt for kindly providing SCEM-UA and for his help in applying the algorithm. This study was carried out within the framework of the Netherlands Organization for Scientific Research (NWO) CASIMIR programme (018.002.007) and the Dutch Water Utility Sector joint research programme (BTO).

## Appendix 2.A. Simulated ranges

Simulated ranges for the 16 synthetic SWAP plots of (A) phreatic groundwater level, (B) surface water level and (C) upward seepage, based on six years of daily values. Each range is characterised by box and whisker plot lines with lines at the lower quartile, median, and upper quartile values. Whiskers extend to the most extreme values within 1.5 times the interquartile; extreme values are displayed with a grey  $\times$  sign. Codes on the  $x$  axis refer to the plots described in Table 2.1.

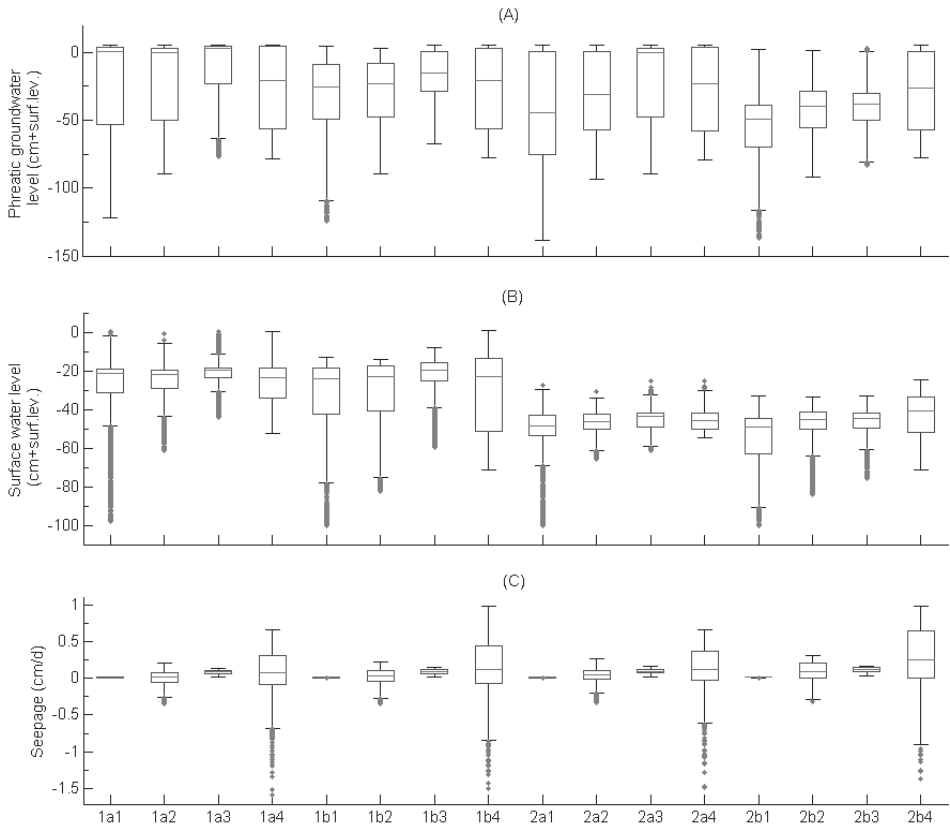


**Figure 2.A.1.** Ranges of the simulated time series of the 16 synthetic SWAP plots.

## Appendix 2.B. Perturbed ‘observations’

We assumed our model to be an exact representation of the system under consideration and assumed no error in forcing data such as precipitation and potential evaporation. This, of course, is unrealistic for real world applications. To gain some insight into the applicability of the model concept in real world situations, we perturbed our ‘observations’ by adding an error term (McIntyre and Wheeler, 2004; Van Dam, 2000; Vrugt et al., 2002). We created first order auto correlated error time series with  $E[X] = 0$  cm and  $VAR[X] = 4$  cm, by feeding normalised white noise into an AR(1) model, and then added this error term to the time dependent ‘observations’ of the different plots. During calibration, we assumed a measurement error of 2 cm, which is considered as a reasonable upper boundary for groundwater level observations.

As to be expected, the estimated parameter distributions are wider and the expected value of the estimated parameters show larger deviations from the ‘observed’ values (Figure 2.B.1) compared to the non-perturbed case. Nonetheless, we can state that the model parameters except  $Z_{sill}$  and  $\gamma_{sill}$ , are still reasonably well identifiable at daily and fortnightly sampling frequencies for most of the plots. In line with the non-perturbed case, a further decrease of the sampling frequency to monthly ‘observations’, resulted in a poor description of almost all parameters. Similarly to the non-perturbed case, high values of  $\gamma_{semi\ conf}$  are hard to estimate (Figure 2.B.1, plot 2a1). However, even with perturbed ‘observation’ data, seepage fluxes could be estimated with acceptable accuracy for most of the plots (Figure 2.B.2). The largest deviations were found for plots with a small value of  $K_o / K_s$  combined with a low value of  $\gamma_{semi\ conf}$ .

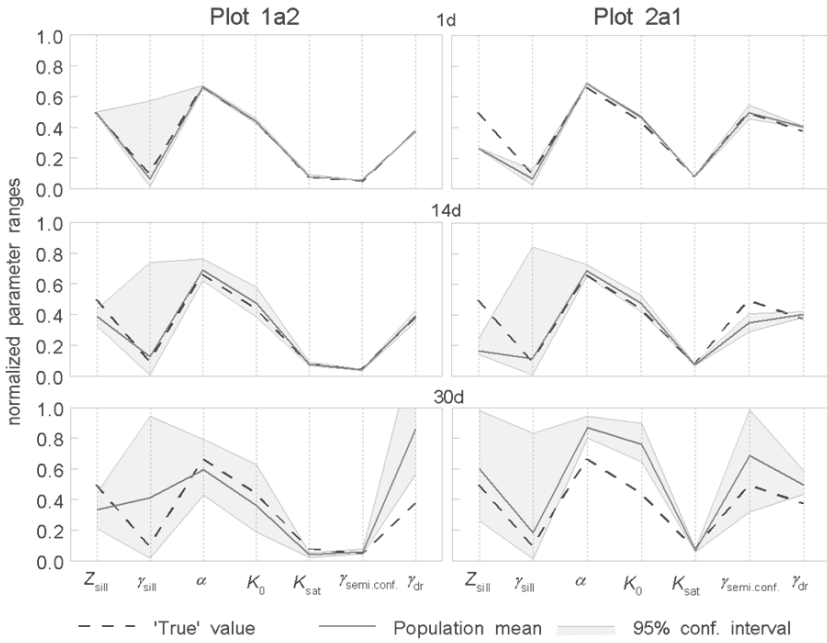


**Figure 2.B.1.** The effect of perturbed 'observations' on the estimated parameter distributions. The model parameters are listed on the x axis, while the y axis corresponds to the parameter values scaled according to their prior uncertainty ranges.

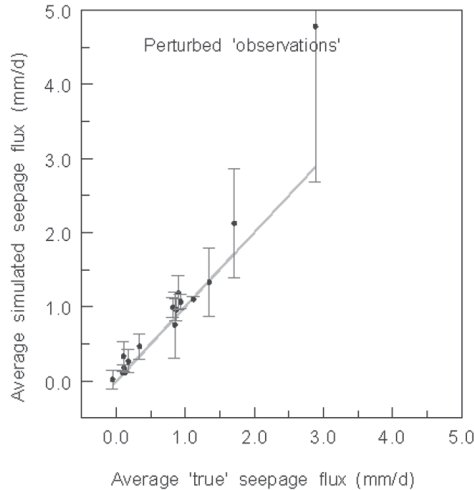


**Figure 2.B.2.** The effect of fortnightly sampled perturbed 'observations' on the average seepage flux (mm/d) (black dots), calculated with the mean of the individual parameter distributions. (The error bars denote the RMSE of the simulated seepage flux during the validation period.)



CHAPTER

# 3

## Mixing behaviour at oscillating fronts

This chapter is a slightly modified version of the manuscript:

**Cirkel, D.G., S.E.A.T.M. van der Zee & J.C.L. Meeussen (*Submitted*) Mixing Behaviour at Oscillating Fronts.**

## Abstract

Dispersive mixing at interfaces that oscillate position as a function of time is of interest in many hydrological and engineering situations. We consider dispersive and chromatographic mixing at an interface, of which the mean position varies periodically as a function of time. For the case of a non-reactive or linearly sorbing solute, the width (standard deviation) of the mixing zone may be approximated with  $\sigma = \sqrt{2\alpha \langle |v| \rangle t}$ , if  $\langle |v| \rangle$  is equal to the absolute travelled distance of the interface over time, in complete analogy with classical dispersion theory. For nonlinear exchange at constant total concentration, oscillating flow leads to an alternation of sharpening (Traveling Wave TW) and spreading (Rarefaction Wave RW) type of transport. As the limiting TW form is never really accomplished at the end of the TW half cycle, the nonlinear oscillating fronts reveal a gradual continuous spreading that converges to a zero-convection nonlinear pure diffusion spreading. This behaviour of the concentration fractions is maintained in case the total concentration changes over the front. Whereas the total concentration front spreads in a purely Fickian way of a non-reactive solute and thus extends over a broader distance than the nonlinearly exchanging chemical fractions, that change only over the position interval where exchange occurs.

## Introduction

Mixing processes at solute fronts have received considerable attention over the past decades, after the foundation has been given for convective-dispersive transport (Bear, 1972; De Josselin de Jong, 1958). Particularly for non-reacting solutes, solutions have been provided for a range of initial and boundary conditions, as well as domain dimensionality, such as 1D (Van Genuchten and Alves, 1982), and 2 and 3 D (Bear, 1972; Bruggeman, 1999). With the recognition that porous formations are spatially variable, solute transport theory made a profound conceptual leap, with both analytical (Dagan, 1989) and numerical advances (Cirpka et al., 1999). Reactive transport is mathematically more complicated if the reactions are nonlinear in concentration. The diversity of biogeochemical interactions has been an inspiration for theoretical research, from the perspectives of physics, petroleum and chemical engineering, and geosciences (Bolt, 1982; Levenspiel, 1972). Originally, that work was often focused on 1D situations (chemical reactors in industry, vertical displacement in the vadose zone) but multi-D and heterogeneous systems were also considered (Bellin et al., 1993; Cirpka and Kitanidis, 2000; Janssen et al., 2006; Prommer et al., 2003; Tang et al., 1981).

Modest attention has been given to situations where a concentration front position fluctuates as a function of time, instead of having a monotonous displacement in one direction. Such types of problems are, however, of interest. At well screens, extraction and injection phases may occur alternatively, e.g. aquifer storage and recovery (Antoniou et al., 2012; Bakker, 2010; Dillon et al., 2006; Pyne, 2005; Wallis et al., 2011), aquifer

thermal energy storage (Bonte et al., 2011; Gao et al., 2009; Zuurbier et al., 2013b) or to avoid clogging of wells by iron oxide precipitates (Appelo et al., 1999; Van Beek, 1980). Also near the soil surface, slightly acid fresh water lenses may form on groundwater that may be either saline (de Louw et al., 2011; Eeman et al., 2011; Vandenbohede et al., 2008) or calcareous (Cirkel et al., 2013; Cirkel et al., 2014; Peach and Zedler, 2006; Schot et al., 2004; Van der Ploeg et al., 2012). These fresh water lenses have a much smaller volume than fresh water bodies in dunes (Bakker, 2000; De Josselin de Jong and Van Duijn, 1986; Maas, 2007), and are therefore more susceptible to a fluctuating thickness due to rainfall and evapotranspiration variability, hence a fluctuating depth of the interface between water in the lens and underlying groundwater.

The effect of such fluctuating, or oscillating, concentration fronts has received relatively little attention to our knowledge. In the 1960's Raats and co-workers (e.g. Raats (1969); Raats (1973)), investigated oscillating boundary flow and transport of gasses in a porous medium as a result of barometric pumping. Of particular interest is the work of Scotter and Raats (1968) and Raats and Scotter (1968), who investigated dispersive mixing as a result of oscillating flow. Reactive transport however, was not considered in these studies. More recently, Neeper and Stauffer (2012) and Neeper (2001) investigated the effect of sinusoidal barometric pumping on transport of vapours in a medium with a mobile and immobile fluid phase. Scotter and Raats (1968) already pointed at the similarities between dispersion of gasses and dispersion of solutes in aqueous solutions, which was implemented by Neeper (2001) for mixing as a result of tidal forcing. Ecohydrologists hypothesised already in the 1990's (Hoogendoorn, 1990; Van Diggelen, 1998) that oscillating flow conditions (no net recharge) could be a major factor in preventing solute loss to the subsoil and acidification of fen meadows in slightly drained flatlands. However, no detailed analysis of oscillating mixing processes including non-linear adsorption has been done in this context.

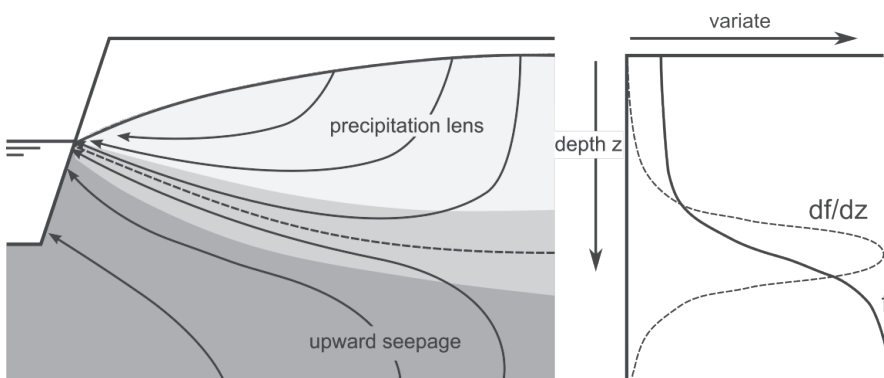


**Figure 3.1.** Mixing behaviour at the oscillating solute front of a precipitation lens.

In this chapter, we consider dispersive and chromatographic mixing at an interface, of which the mean depth varies periodically as a function of time. We consider the non-reactive case, as well as Gapon cation exchange, as an example of nonlinear chemical interactions, for the case that the total salt concentration is either constant or not. The resulting alternating Rarefied and Traveling behaviour of the solute fronts can be seen as a proxy for different ecologically relevant soil chemical processes such as adsorption and desorption of base cations, but also for mixing of aerobic meteoric water with upward seeping reduced iron rich groundwater.

## List of symbols

Symbol	Unit	Description	Symbol	Unit	Description
$q$	mol <sub>e</sub> /dm <sup>3</sup>	adsorbed amount of an ion species	$\omega$	d	angular frequency of oscillations
$q_i$	mol <sub>e</sub> /dm <sup>3</sup>	same, initially present	$T$	d	period of a full cosine-cycle
$q_f$	mol <sub>e</sub> /dm <sup>3</sup>	same, finally present after passage of a feed solution	$t$	d	time
$\bar{q}$	-	$= (q - q_i)/(q_f - q_i)$ normalised amount of an adsorbed ion species	$\sigma$	m	standard deviation
$c$	mol <sub>e</sub> /dm <sup>3</sup>	(equivalent) concentration in solution of an ion species	$n$	-	water filled porosity
$c_i$	mol <sub>e</sub> /dm <sup>3</sup>	same, initially present	$\delta_f$	m	correction factor for diffusion/dispersion of a solute front
$c_f$	mol <sub>e</sub> /dm <sup>3</sup>	same, of the feed solution	$\tilde{x}$	m	$= (x - v^* t + u)$ , moving (wave) coordinate
$\bar{c}$	-	$= (c - c_i)/(c_f - c_i)$ , scaled concentration	$v^*$	m/d	$= J^v / (n + \Delta q / \Delta c)$ , mean rate of propagation of a solute front
$N$	-	equivalent fraction of an adsorbed divalent ion species	$\Delta x$	m	node distance
$f$	-	equivalent fraction of a divalent ion species in a mixture of mono and divalent ions	$\rho$		density
$C$	mol <sub>e</sub> /dm <sup>3</sup>	total concentration	$\mu$	m	mean position of a solute front
$K_G$	(mol/dm <sup>3</sup> ) <sup>-1/2</sup>	Gapon exchange 'constant'	$\sigma^2$	m <sup>2</sup>	variance of a solute front
$J^v$	m/d	specific discharge	$\gamma_1$	-	skewness of a solute front
$v$	m/d	$= J^v / n$ , interstitial velocity	$\gamma_2$	-	kurtosis of a solute front
$D$	m <sup>2</sup> /d	dispersion coefficient	$D_e$	m <sup>2</sup> /d	effective diffusion coefficient
$x$	m	position coordinate	$\chi$	-	$= K_G \sqrt{2C}$ , dimensionless exchange constant
$\mathcal{E}_c$	mol <sub>e</sub> /dm <sup>3</sup>	adsorption (exchange) capacity	$\tilde{x}_c$	m	position of a solute front relative to the position of an arbitrary chosen reference value $f_s$
$\mathcal{E}_c^*$	-	ratio of dissolved and adsorbed pool sizes	$C_{\max}$	mol <sub>e</sub> /dm <sup>3</sup>	maximum concentration of an ion in the system
$v_A$	m/d	amplitude of a cosine-velocity cycle	$u$	-	integration constant
$\alpha$	m	dispersivity	$S$	-	system constant

## Theory

### Basic equations

We consider two major cases to illustrate mixing processes of oscillating fronts: a non-reactive case and a case involving a simple non-linear exchange equation (Gapon). Because we want to arrive at a transport equation that is suitable for both situations, we first scale to exchange equations. Gapon type of cation exchange between a monovalent cation, sodium (Na) and a divalent cation, calcium (Ca), is described by

$$\frac{q_{Na}}{q_{Ca}} = K_G \cdot \frac{c_{Na}}{\sqrt{c_{Ca}/2}}, \quad (3.1)$$

where concentrations in solution  $c$ , are conventionally in  $\text{mol}_e/\text{dm}^3$ .  $\text{mol}_e$  stands for mol charge (former equivalent). The adsorbed concentrations,  $q$ , are on a volumetric basis (see list of symbols). Using normalized concentrations:

$$\bar{c} = \frac{c - c_i}{c_f - c_i} = \frac{f - f_i}{f_f - f_i}, \bar{q} = \frac{q - q_i}{q_f - q_i} = \frac{N - N_i}{N_f - N_i} \text{ we rewrite Eq. (3.1) as:}$$

$$\frac{1 - N}{N} = K_G \sqrt{2C} \cdot \frac{1 - f}{\sqrt{f}}, \quad (3.2)$$

where the fractions in solution and exchange complex are given by:

$$f = \frac{c_{Ca}}{C}; 1 - f = \frac{c_{Na}}{C}; N = \frac{q_{Ca}}{\varepsilon_c}; 1 - N = \frac{q_{Na}}{\varepsilon_c} \text{ and } C = c_{Na} + c_{Ca}. \quad (3.3)$$

In which (capital)  $C$  is the total concentration (sum of all cations or of all anions) and  $\varepsilon_c$  is the cation exchange capacity, CEC. Assuming only two cations, we can eliminate one (sodium Na) and rewrite as  $N$  as function of  $f$ :  $N(f)$ .

We obtain the mass balance equation in terms of  $f$ , for 1D transport as:

$$\frac{\partial}{\partial t} [\varepsilon_c N(f) + nCf] + \frac{\partial}{\partial x} [J^v Cf] = \frac{\partial}{\partial x} nD \left[ \frac{\partial Cf}{\partial x} \right], \quad (3.4)$$

where  $J^v$  is the Darcy velocity (specific discharge;  $J^v = \mathbf{v} \cdot \mathbf{n}$  if  $n$  = water filled porosity) and  $D$  is the dispersion coefficient, if we assume that molecular diffusion can be neglected. Using common assumptions as made by e.g. Bear (1972), we have:

$$D = \alpha |v|. \quad (3.5)$$

Combining Eq. (3.4) and Eq. (3.5) and dividing by  $n$  and  $C$ , yields:

$$\frac{\partial}{\partial t} [\varepsilon_c^* \cdot N(f) + f] + \frac{\partial}{\partial x} [vf] = \frac{\partial}{\partial x} D \left[ \frac{\partial f}{\partial x} \right], \quad (3.6)$$

with  $\varepsilon_c^* = \frac{\varepsilon_c}{nC}$ , which serves as a ratio of (adsorbed and dissolved) pool sizes.

For the interstitial velocity,  $v$ , we first assume:

$$v = v_A \cos(\omega t). \quad (3.7)$$

We consider alternative ways for fluctuating  $v$ -values, see Figure 3.3, for the non-reactive solute. For  $t=T$  we have a full cycle ( $T = 2\pi/\omega$ ). We have an average velocity for a complete cycle given by

$$\langle v \rangle = \frac{1}{T} \int_0^T v(s) ds = \frac{v_A}{T} \int_0^T \cos(\omega s) ds = 0 \quad (3.8)$$

and the average absolute velocity given by:

$$\langle |v| \rangle = \frac{1}{T} \int_0^T |v(s)| ds = \frac{v_A}{T} \int_0^T |\cos(\omega s)| ds = \frac{2v_A}{T}. \quad (3.9)$$

### Non-reactive solute transport

For a solute that does not react chemically ( $K_G = 0$ ), we have from Eq. (3.6)

$$\frac{\partial}{\partial t} [f] + \frac{\partial}{\partial x} [vf] = \frac{\partial}{\partial x} D \left[ \frac{\partial f}{\partial x} \right] \quad (3.10)$$

The dispersion term contains the absolute velocity (Eq. (3.5)) which leads to a complex term, as both  $v$  and the gradient change continuously with time. To assess the dominant feature, we average over one complete cycle and find for the dispersion term that analogous to Raats and Scotter (1968):

$$\left\langle \frac{\partial}{\partial x} D \left[ \frac{\partial f}{\partial x} \right] \right\rangle = \frac{1}{T} \int_0^T \frac{\partial}{\partial x} \left[ \alpha |v_A \cos(\omega s)| \frac{\partial f}{\partial x} \right] ds = \frac{\alpha v_A}{T} \int_0^T |\cos(\omega s)| ds \frac{\partial^2 f}{\partial x^2} = \alpha \langle |v| \rangle \frac{\partial^2 f}{\partial x^2}, \quad (3.11)$$

provided that the time dependency of the derivative term (the gradient) may be neglected. To illustrate that this is the case, we calculated the two terms that account for both the time dependency of flow velocity and of gradient (the total time dependence,  $T$ ) and the case where the variation of the gradient with time is ignored and only velocity varies as a function of time. Hence for given  $f = f_0$ ,

$$B^{(T)} = \frac{1}{T} \int_i^{i+1} |v(t)| \frac{df}{dx}(f_0, s) ds \quad (3.12)$$

$$B^{(v)} = \frac{1}{T} \int_i^{i+1} |v(t)| \frac{df}{dx}(f_0, s_i) ds \quad (3.13)$$

As Figure 3.2 reveals, the contribution of the time dependency of the gradient is already minor after the first few cycles, and rapidly decreasing, which warrants the approximation in Eq. (3.11).

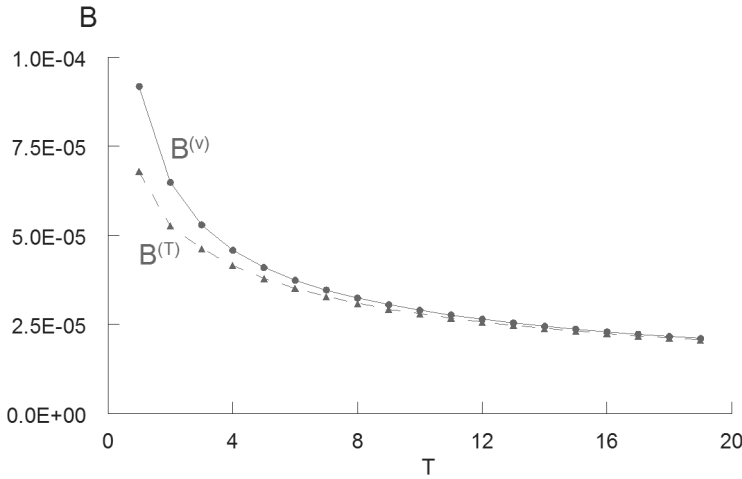


**Figure 3.2.** Comparison of the integrals  $B^{(T)}$  and  $B^{(v)}$ , as a function of cosine cycle number ( $T$ ), where initial condition is a step front.

For the non-reactive case, the width of the mixing zone in the Fickian regime, can be parameterized by the standard deviation,  $\sigma$ , (or variance,  $\sigma^2$ ) of this zone. Then,

$$\sigma = \sqrt{2\alpha \langle |v| \rangle t}. \quad (3.14)$$

Over many cycles, the mean absolute velocity in Eq. (3.8) corresponds with the distance that was travelled by the interface divided by the total time (i.e., not the ‘effective’ distance, which is zero). For a velocity that is spatiotemporally constant, replacing time by travelled distance ( $x = v \cdot t$ ), vice versa, is quite common and trivial. Hence, for a non-reacting solute and oscillating flow, we have for  $D$  and for  $\sigma$  a full analogy with the case of a constant flow velocity of e.g. Bear (1972), Dagan (1989) and many others. The perfect agreement, expressed in increase of the mixing zone width, is shown for two

cosine shaped flow rates with different amplitude and an irregular shaped flow rate in Figure 3.3. Similar results for cosine shaped flow rates, were obtained experimentally by Scotter and Raats (1968) measuring the displacement of inert gasses. To relate  $\langle |v| \rangle$  with the total distance that the interface has travelled is meaningful, as it illustrates that it does not matter how the velocity fluctuates. For instance for even more erratic fluctuations than that of the triangles in Figure 3.3, we obtained identical mixing results. Based on our results, Eeman et al. (2012) showed the agreement for variations in precipitation lens interface velocity derived from real rainfall records

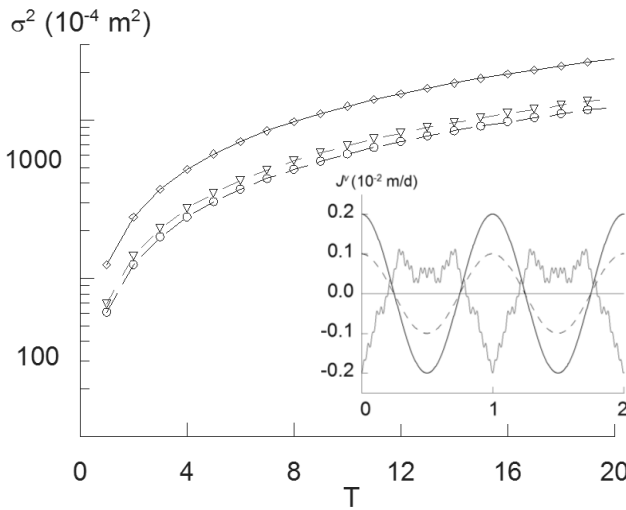


**Figure 3.3.** Increase of the mixing zone width (second central moment of the concentration gradient) as a function of time for a numerically derived oscillating front (lines) and the analytical approximation assuming unidirectional steady flow with  $v = \langle |v| \rangle$  (Eq. (3.14)). Data shown for two cosine shaped flow rates with amplitude ( $J^v = v \cdot n$ ) of respectively  $0.1 \times 10^{-2}$  (circles) and  $0.2 \times 10^{-2}$  m/d (diamonds) and an irregular shaped flow rate (triangles).

### Reactive solute transport

As a next step we consider the effects of chemical sorption non-linearity on the shape and behaviour of the solute front. The concentration (or, for constant total concentration, the concentration fraction  $f$ ) front can interact in two ways on the transport in flowing water. If the constraint mentioned by Van der Zee (1990); Bolt (1982); Van Duijn and Knabner (1992) is met, dispersion of the front is countered by chemical sorption non-linearity. If the constraint is not met, spreading of the front is enhanced by both this nonlinearity and dispersion. In the first case, a traveling wave (TW) is the limiting front, in the second case, a rarefied/rarefaction wave (RW) develops. For the latter case, an

analytical solution is not available for the case  $D > 0$ , but a reasonable approximation is possible. We give this analytical approximation for the RW case first. For the TW case, an analytical solution is available for the limiting front ( $t$  approaching  $\infty$ ) for Gapon exchange  $N(f)$  (Bolt, 1982; Reiniger and Bolt, 1972).

### Pure convection

We consider a solute that is chemically reactive, but first assume that  $D=0$ . The convective mass balance equation is

$$\frac{\partial}{\partial t} [\varepsilon_c^* N(f) + f] + \frac{\partial}{\partial x} [vf] = 0 \tag{3.15}$$

and for concave  $N(f)$  leads to a Rarefaction Wave (RW), if  $f$  increases in the direction of flow. If  $f$  decreases in the direction of flow, a Shock develops, with a trivial solution that follows from mass balance considerations. The hyperbolic equations for the RW can be described with the Method of Characteristics, MC. We start with a step front at some  $x = 0$ . Using the chain rule, we obtain:

$$\frac{\partial}{\partial t} [N(f) + f] = \left( 1 + \varepsilon_c^* \frac{dN(f)}{df} \right) \frac{\partial f}{\partial t} \tag{3.16}$$

In Eq.(3.16), the derivative  $N'$ , of  $N$  with respect to  $f$ , is

$$\frac{dN}{df} = \frac{\sqrt{C}(f+1)K_G}{\sqrt{2}\sqrt{f}(-\sqrt{2}\sqrt{C}fK_G + \sqrt{2}\sqrt{C}K_G + \sqrt{f})} \tag{3.17}$$

This derivative  $N'$  leads to a concentration dependent retardation factor, hence, for a designated concentration fraction, its position is equal to

$$x_c = \frac{vt}{1 + \frac{\varepsilon_c \sqrt{C}(f+1)K_G}{Cn\sqrt{2}\sqrt{f}(-\sqrt{2}\sqrt{C}fK_G + \sqrt{2}\sqrt{C}K_G + \sqrt{f})^2}} \tag{3.18}$$

if all concentrations start at position  $x = 0$  at  $t = 0$ .

## Convection and dispersion

In case  $D > 0$ , the RW case can be corrected according to Bolt (1982), using:

$$\delta_f = 2\sqrt{(\alpha v t) \operatorname{inverfc}(2f)} \quad (3.19)$$

where the position of each  $f$ -value is corrected with a factor that follows from the nonreactive transport solution. If the concentration fraction  $f$  decreases in the direction of flow, the criteria are met for the development of a Traveling Wave (TW) as formulated by Van Duijn and Knabner (1992) and Van der Zee (1990). The limiting Traveling Wave behaviour has been considered analytically by Reiniger and Bolt (1972), Bolt (1982), Van der Zee (1990) and Van Duijn and Knabner (1992), but differ with regard to the functional relationship of  $N(f)$ . If this relationship obeys Gapon exchange, the most versatile solution is that of Bolt (1982), which is of the type:

$$\tilde{x} = x - v^* t + u \quad \Delta \tilde{x} / \alpha = F(f), \quad (3.20)$$

where we assumed that molecular diffusion can be ignored. We give the full solution in Appendix 3.A., as we arrive at a somewhat different function  $F(f)$  than Bolt (1982).

## Results

### Comparison of analytical approximations for uni-directional flow with numerical results

To be able to study the non-linear behaviour of the oscillating fronts, we constructed a 1D numerical model, using the Orchestra modelling environment (Meeussen, 2003). For parameterization of the model see Table 3.1. As a first check of our numerical model, we compare the numerical results for constant flow velocity (i.e., uni-directional flow) with the analytical TW and RW approximations. On the left side of Figure 3.4, we compare the numerical RW results with the analytical RW approximations, where the ad hoc correction for dispersion either is (dashed lines), or is not (solid lines) taken into account. If dispersion is completely ignored, the analytical approximation obviously disagrees with the numerical solution at large  $f$ -values, but the agreement is still quite reasonable for smaller fractions. If dispersion is accounted for using Eq. (3.19), the agreement is remarkably good. On the right side of Figure 3.4, we compare the numerical and analytical Traveling Wave solutions. Agreement between numerical TW fronts and the analytical solutions is very good. Notice that to obtain a good agreement, very careful discretisation of the numerical model was required. As shown for Freundlich adsorption by Bosma and van der Zee (1993) a wrong (to coarse) discretisation can result in deviations between numerical and analytical TW shape at  $t \rightarrow \infty$ . The node distance  $\Delta x$  was therefore chosen to be  $1.0 \times 10^{-3}$  m. See Table 3.1 for other constant model parameters.

**Table 3.1.** Constant parameter values

Parameter		Value
$\Delta x$ , m	Node distance	$1 \times 10^{-3}$
$n$ , -	Water filled porosity	0.38
$\rho$ , $\text{kg m}^{-3}$	Density	1650
$\alpha$ , m	Dispersivity	0.005
$K_G$ , $(\text{mol dm}^{-3})^{0.5}$	Gapon constant	0.5
$\varepsilon_c$ , $\text{mol}_c \text{kg}^{-1}$	Cation Exchange Capacity	0.0125
$C$ , $\text{mol}_c \text{dm}^{-3}$	Total concentration	$2.002 \times 10^{-2}$
$c_i$ , $\text{mol}_c \text{dm}^{-3}$	Initial concentration of bivalent ions in solution	$2.000 \times 10^{-5}$
$c_f$ , $\text{mol}_c \text{dm}^{-3}$	Concentration of bivalent ions in the feed solution	$2.001 \times 10^{-2}$

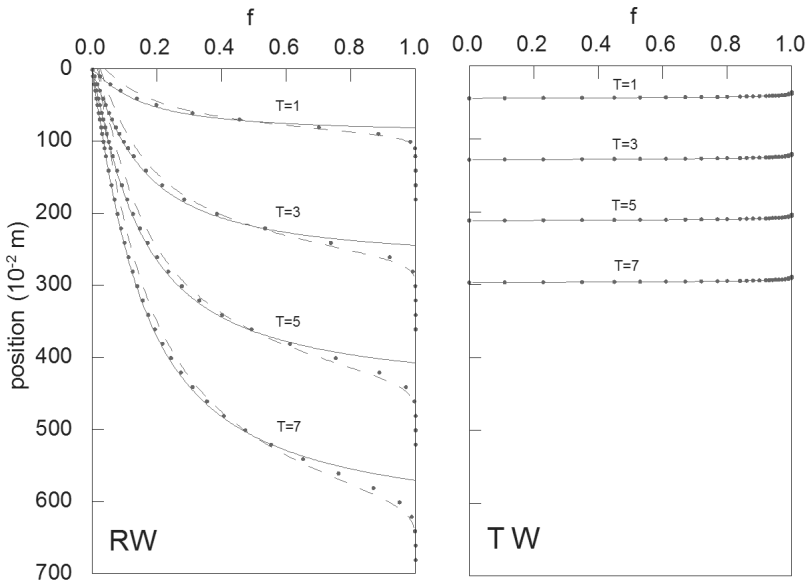


**Figure 3.4.** Agreement between numerical and analytical results for constant flow velocity. Left: numerical fronts for RW case (dots) and the analytical RW approximations without (solid lines; Eq. (3.18)) and with correction factor for dispersion (Eq. (3.19)) (dashed line). Right: numerical front for TW case (dots) and analytical TW solution (solid lines). Both with  $J^v = 0.1 \times 10^{-2} \text{ m d}^{-1}$ .

### Mixing behaviour of non-linear exchanging oscillating fronts

To examine oscillating fronts, we assume a cosine shaped Darcian flow rate,  $J^v$  with amplitude of  $0.1 \times 10^{-2} \text{ m d}^{-1}$  and a period  $T$  of one year. As initial condition, we consider a step front at  $x = 200 \text{ cm}$ , with the initial calcium concentration  $c_i$  equal to  $2.000 \times 10^{-5}$  and  $2.001 \times 10^{-2} \text{ mol}_c \text{ dm}^{-3}$  for, respectively smaller and larger  $x$ -values. As Gapon exchange depends on the total cation concentration,  $C$ , (Eq. (1)), the total concentration was kept constant throughout the column at  $2.002 \times 10^{-2} \text{ mol}_c \text{ dm}^{-3}$ . This implies that exchange is incomplete over the front. We provide numerical results for the concentration fraction fronts  $f(x, t^*)$  (Eq. (3.3)), at specific times where the front has dispersed for different numbers of cosine-velocity cycles. The times are chosen such that the initial position (beginning of cycle, front moving downward), the lowest position, the highest position, and the intermediate one (front moving upward or downward) of each of the provided cosine-velocity cycles are represented (Figure 3.5).

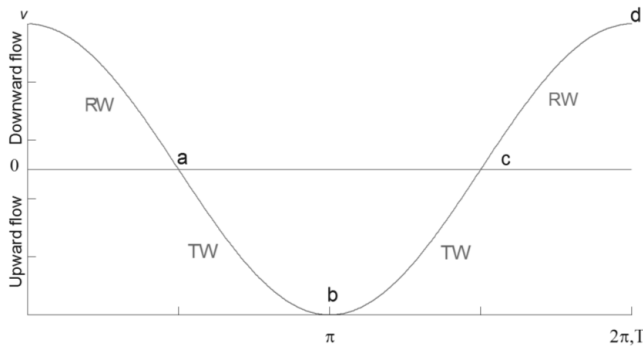


**Figure 3.5.** Cosine shaped pore water velocity, where positive velocity is in the downward direction, and with (a) lowest position of the solute front, (c) upper position of the solute front and (b) and (d) intermediate positions of the solute front.

We observe that the front shapes (Figure 3.6, left figure) at the highest and lowest positions are different. As the front moves from the initial step front to the lowest position (a), a rather sigmoid front results, where adsorption and dispersion enhance front spreading in the RW regime. For the highest position (c), conversely, a steep front is found, which, in view of the nonlinearity and initial/boundary conditions, shows TW behaviour. When we shift the flow cycle by half a period, moving first from the initial step front upward (Figure 3.6, right figure), the cycle starts with TW behaviour (a'), changes to RW behaviour (b', c') and ends with TW behaviour (d').

The front shape at position c, that follows after a RW phase is less sharp than the shape at a' that follows from a step front. The sharpening behaviour is also visible in the transition from the front at position b to position c (Figure 3.6, left figure). Being aware

that the analytical solution for the TW shape concerns a limiting front, the differences in Figure 3.6 emphasize that the self-sharpening takes time. As the number of cosine-cycles grows, the numerical fronts continue to flatten and cover an increasingly larger  $x$ -range. Interestingly the front shapes of the ‘intermediate positions’ (b, d) are rapidly becoming identical for the moving upward and for the moving downward phase of the cosine shaped velocity cycle (Figure 3.7).

We interpret these observations as follows. The convergence of the front (moving upward for our parameter choice) towards a limiting TW, takes time. As the deviation of the starting front (e.g. our initial step front, or, after some cycles, a RW front) from the limiting TW becomes larger, the time to attain the limiting front closely enough also becomes larger. Our results indicate that for our cases, the convergence rate is too slow to attain the limiting TW. In each following RW phase we observe rapid further spreading due to nonlinearity and hydrodynamic dispersion, and the starting front at the moment that the RW phase sets in. Therefore, with each next cycle, the limiting TW is approached less well and the front continues to spread as a function of increasing time. We postulate, that the discrepancy between RW spreading rate and TW sharpening rate is typical, and not incidental and due to our parameter choice.

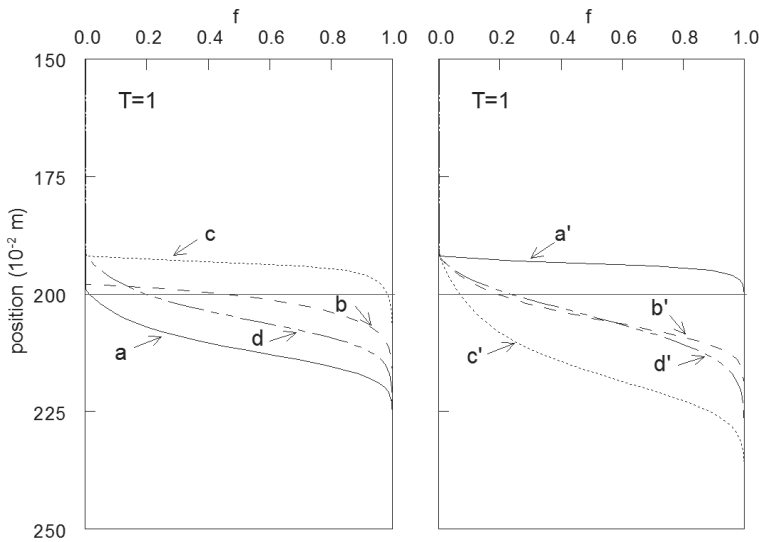


**Figure 3.6.** Solute fronts during the first cosine velocity cycle. Left: solute fronts (bivalent ions) at positions a, b, c and d if starting at  $t=0$  in downward direction. Right figure: same but starting in upward direction.

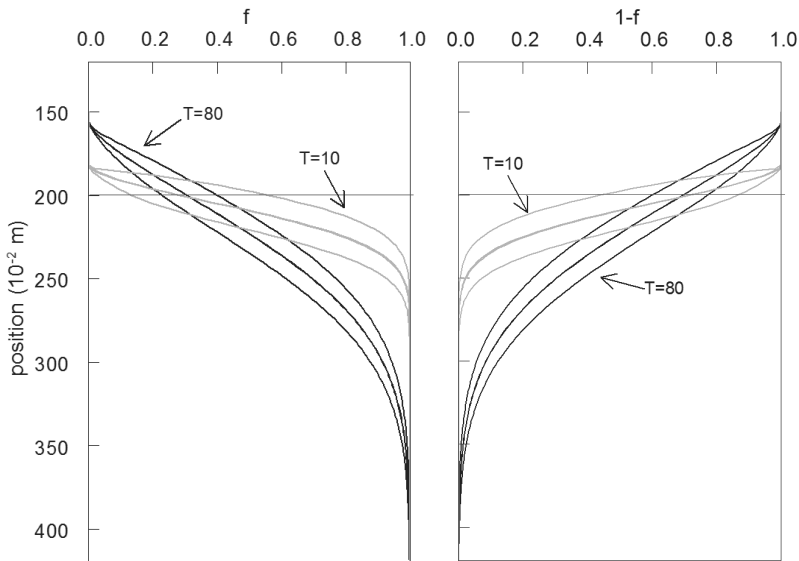


**Figure 3.7.** Position and shape of the solute fronts for velocity cycle  $T = 10$  and  $T = 80$ . Left: divalent cations (Ca), right monovalent cations (Na). The front shapes in terms of  $f$  and  $1-f$  of the mono- and bivalent cations are complementary (mirror image), in view of Eq.(3.3) and the assumed constant total concentration

### Comparison with non-linear diffusive mixing

For constant velocity (in one direction), the analytical (TW and RW) solutions provided a good approximation. For both cases it is essential that convective transport occurs. This implies that purely diffusive transport in case of nonlinear exchange is essentially different from the convective dispersive transport involving interface oscillations. However, we observed that with an increasing number of cosine-cycles, the fronts deviate from both TW and RW solutions and behaviour. In view of the different spreading behaviour during the TW and RW phases, respectively, it is conceivable that on the longer term (many cycles), the overall spreading of the front is comparable to pure (non-linear) diffusion, e.g. as analysed by Van Duijn and Peletier (1977). For this reason, we compared a pure nonlinear diffusion front with adjusted diffusion coefficient, with a long term front with oscillating flow in Figure 3.8. The front with zero convection, corresponds well with the positions b and d of the oscillating convective-dispersive case.

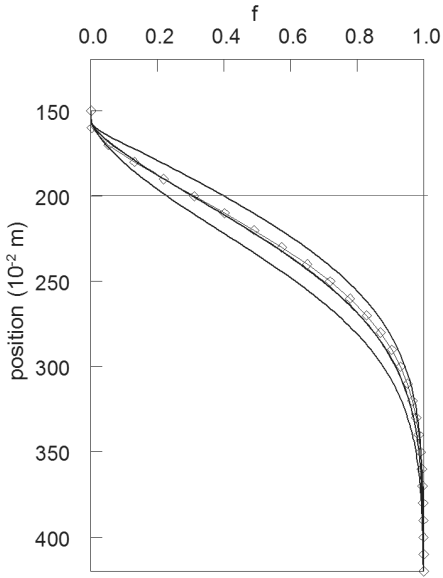


**Figure 3.8.** Comparison of front shapes at cycle  $T=80$  (lines) for oscillating flow with front shape at  $T=80$  calculated with diffusion only (diamonds).

To test how well the observed numerical results can be approximated with non-linear (pure) diffusion, with adjusted value of  $D$ , we compared spatial moments rather than a quite coarse visual inspection of front shapes (Bosma and van der Zee, 1993). The spatial moments mean ( $\mu$ ), variance ( $\sigma^2$ ), skewness ( $\gamma_1$ ) and kurtosis ( $\gamma_2$ ) were calculated for each of the four positions of the oscillating case and for the diffusive case according to:

$$\mu = M1 = \int_{-\infty}^{\infty} x f(x) dx \quad (3.21)$$

$$\sigma^2 = M2 = \int_{-\infty}^{\infty} (x - \mu)^2 f(x) dx \quad (3.22)$$

$$\gamma_1 = \frac{M3}{((\sigma^2)^{1/2})^3} = \frac{M3}{(\sigma^2)^{3/2}} \quad (3.23)$$

$$\gamma_2 = \frac{M4}{(\sigma^2)^2} - 3 \quad (3.24)$$

$$\text{With: } M3 = \int_{-\infty}^{\infty} (x - \mu)^3 f(x) dx \text{ and } M4 = \int_{-\infty}^{\infty} (x - \mu)^4 f(x) dx$$

For convenience, we use the concentration fraction ( $f$ ) instead of mass in the above equations, which is valid because the water content is kept constant during our analysis. In agreement with the non-reactive case we approximate the effective diffusion coefficient  $D_e$  in the pure diffusion case by:  $D_e \approx \langle |v| \rangle \alpha$ , in which  $\langle |v| \rangle$  is the mean absolute velocity and  $\alpha$  is the (longitudinal) dispersivity. Both  $\langle |v| \rangle$  and  $\alpha$  are taken from the oscillating flow case. The mean position of the diffusion front (solid line) agrees well with the mean position of the intermediate fronts (b and d) (circles, diamonds) of oscillating flow (Figure 3.9). The slight deviation in mean position can be attributed to the TW flow during the first cosine cycle of the oscillating flow case (Figure 3.6). Moreover, kurtosis and skewness of the intermediate fronts (b and d) also converge to the values of the pure diffusive front after approximately 20 cosine-cycles. The variance of the diffusion front shape slightly deviates from the intermediate positions (b and d), but reflects the ‘upper’ position (c) very well. After many cosine-cycles, the relative deviations between oscillating convective dispersive mixing and non-linear diffusion are small. Based on our analysis, it thus appears that mixing as a result of oscillating flow approaches a non-linear diffusion equation, with an effective diffusion coefficient  $D_e$  based on the product of the absolute average movement of the interface  $\langle |v| \rangle$  and the dispersivity  $\alpha$ .

The (diffusive) spreading behaviour of oscillating fronts is maintained at different amplitudes of the cosine-velocity cycles, different values for the  $\epsilon_c$ , and different values for  $K_G$ . The spreading of the fronts is linearly related to travelled distance over time and thus to amplitude  $J_A^v$  of the cosine velocity cycle (Figure 3.10). Front spreading is much less sensitive to  $K_G$  and  $\epsilon_c$  (Figure 3.10) and decreases with larger values for  $K_G$  and  $\epsilon_c$ . A decrease of the total concentration  $C$ , leads to stronger affinity of  $\text{Ca}^{2+}$  for the adsorption complex and thus to increased non-linear behaviour and decreased spreading of the front.

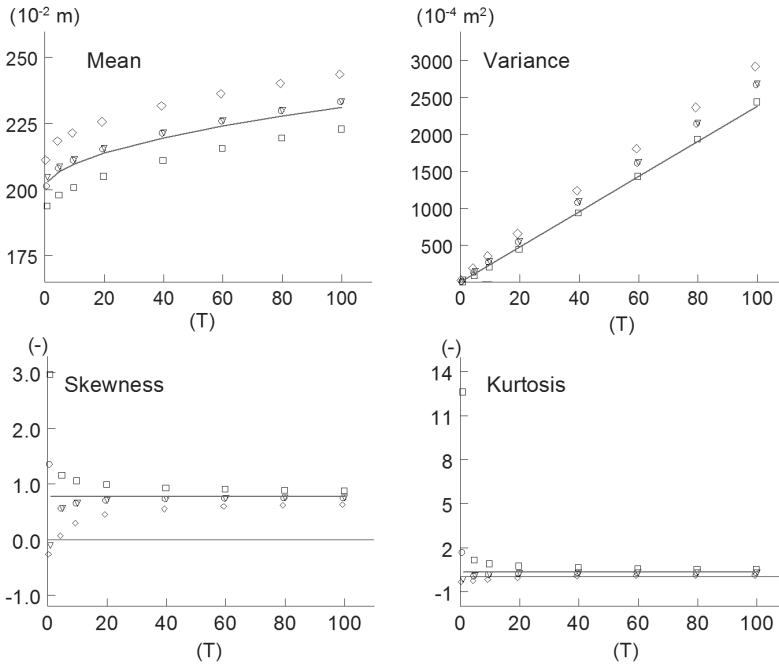


**Figure 3.9.** Spatial moments for oscillating convective-dispersive and pure diffusion front shapes for divalent cations. Symbols: values for positions a (diamonds), b (circles), c (squares) and d (triangles) for oscillating convective-dispersive front shape behaviour. Lines: values for pure diffusive front shape behaviour. For Fickian behaviour (normal  $f$ -distribution) skewness and kurtosis are both zero.

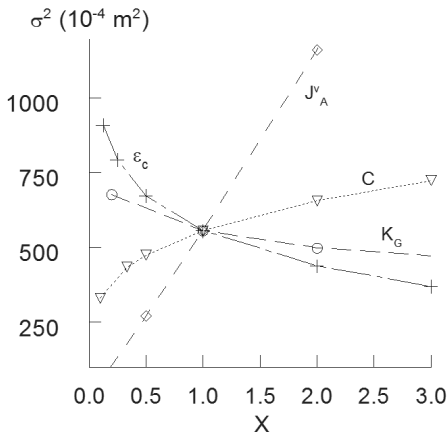


**Figure 3.10.** Sensitivity of the front spreading for different values (multiplications of the original value by  $X$ ) of the Gapon constant,  $K_G$ , the CEC,  $\epsilon_c$  (for convenience expressed in  $\text{mol}_e/\text{kg}$ ), the amplitude of the cosine velocity cycle,  $J_A^v$  and the total concentration  $C$ . Variances shown for  $T=20$ .

### Effect of a salt shock

In the previous paragraphs, we assumed a constant total concentration ( $C$ ) throughout the domain. In practice, situations with a change in total concentration over an interface are more common. For instance, water within a shallow rainwater lens in Dutch coastal areas can deviate more than  $0.4 \text{ mol}_e \text{ dm}^{-3}$  from the (saline) groundwater below (de Louw et al., 2011). Similar differences in total ion concentration can be found during aquifer storage of fresh (sometimes demineralised) water in brackish or saline aquifers (Zuurbier et al., 2013a). Although less pronounced, differences in total concentration certainly occur in seepage dependent nature reserves, with rainwater lenses on upwelling, fresh, alkaline groundwater. Cirkel et al. (2013) (see chapter 4), for instance observed a factor 5 difference in total concentration between lens and alkaline groundwater. For brevity, we refer to a change in total concentration as a salt shock. Such a salt shock, e.g. of inert anions as chloride, propagates with the rate of water flow (no retardation), which is significantly faster than most exchange fronts as considered so far in this chapter. To test the effect of a salt shock, we reduced the total concentration  $C$  above the step front with a factor 10 from  $2.002 \times 10^{-2}$  to  $2.002 \times 10^{-3} \text{ mol}_e \text{ dm}^{-3}$ , reminiscent of the concentration change between a rainwater lens and underlying groundwater as just discussed. Concentrations of the bivalent and monovalent cations are scaled accordingly.

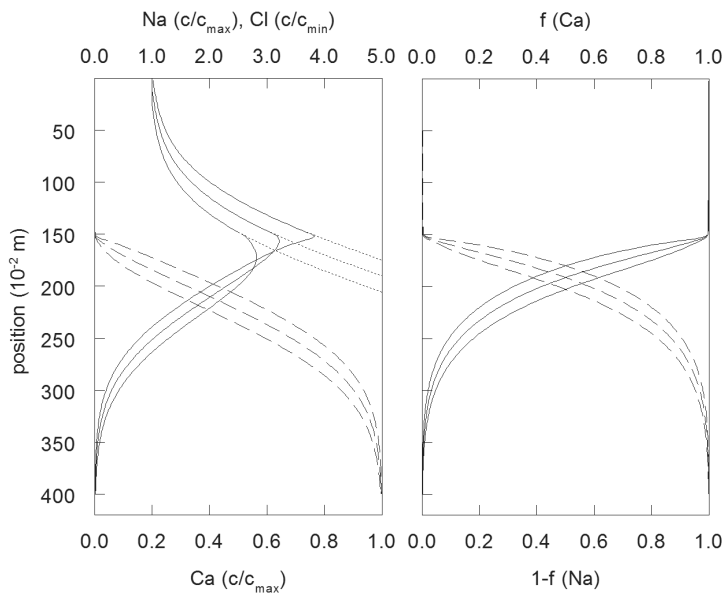


**Figure 3.11.** Concentration profiles for the case of a change in total concentration. Left: concentration profiles, presented as  $c/c_{\max}$  for Na (solid line) and Ca (dashed line) and as  $c/c_{\min}$  for Cl (dotted line) in case of a change in total concentration  $C$  (salt shock). Right: Position and shape of the solute fronts, expressed as concentration fractions  $f$  (Ca) (dashed line) and  $1-f$  (Na) (solid line). Data presented for positions a, b, c and d during cosine velocity cycle  $T=80$ .

The basic concentration fronts for total concentration or Cl, Ca, and Na, are shown in Figure 3.11, left figure. In this figure, the Na and Ca concentration fronts are normalised by the maximum concentration in the system. The total concentration or Cl fronts are normalised using  $c/c_{\min}$ , for easy comparison with the shape of the Na concentration fronts. Also shown are Ca and Na expressed as concentration fractions  $f$  and  $1-f$ . Compared to the previously shown Ca fronts the current normalized Ca fronts are only slightly influenced by the salt shock, but show enhanced spreading. Expressed as dimensionless fraction  $f$  of the total concentration  $C$ , these differences become more apparent (Figure 3.12). The fronts in case of a salt shock are sharper and move slightly faster in the direction of lower total concentration. The sharpness of the front is in accordance with the higher affinity of the cation exchange complex (hence, stronger nonlinearity) for Ca at lower total concentrations. The faster movement of the front is perhaps a bit counter intuitive at first glance, in view of the higher affinity. However, exactly because of this higher affinity for Ca, the initial amount of adsorbed Ca for smaller  $z$ -values is larger in case the total concentration there is smaller:  $N = 0.5$  instead of 0.23. This implies, on the basis of a simple mass balance consideration, that the front moves faster if the upper total concentration is decreased, as is the case here.

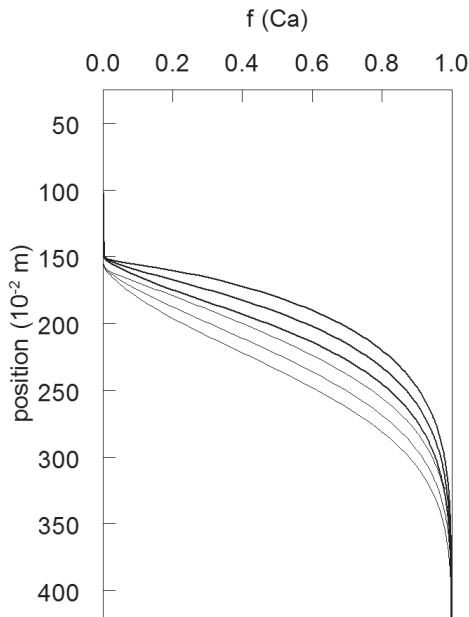


**Figure 3.12.** Comparison of front shapes for  $f$  with (thick lines) and without (thin lines) a change in total concentration  $C$  (salt shock). Data shown for velocity cycle  $T=80$ .

The total concentration (expressed by chloride) front agrees with a classical (symmetric) Fickian spreading. The distance over which this front extends is larger than for the calcium front and equal to that of sodium. With the front variances, shown in Figure 3.13, the differences between the fronts of Figure 3.11 can be quantified. For sodium, though, a concentration peak occurs that is larger than the initial concentration on either side of the initial shock front. Such peaks are due to the combination of change in total concentration and nonlinear exchange between calcium and sodium. The peak concentration for sodium coincides with the maximum position of the calcium front (around position 150 in the system). As can be seen from Figure 3.11, the concentration from this position to smaller numbers is controlled completely by the Fickian spreading of the total concentration front. The sodium concentration from position 150 to higher numbers is controlled by both spreading of the total concentration front and (non-linear) exchange depending on the shape of the exchange isotherm and the direction of flow.

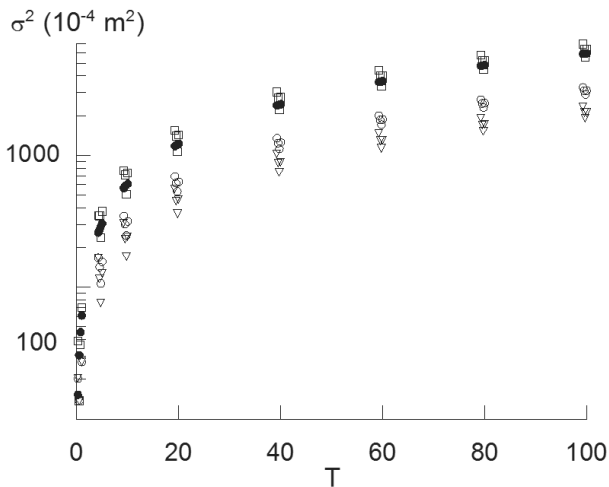


**Figure 3.13.** Development of the variance over time of  $c/c_{\max}$ , for respectively Cl (dots), Ca (triangles), Na (squares) and of  $f$  for Ca (circles). Note the log scale of the y-axis.

## Synthesis and conclusions

In this contribution, we investigated dispersive and chromatographic mixing at an interface, of which the mean depth varies periodically as a function of time. We first analysed the non-reactive (Fickian) case and showed that the time dependency of the concentration gradient in the dispersion term has a rapidly decaying effect and may therefore be neglected in a first approach. In that case, the width of the mixing zone of an oscillating interface (expressed as a standard deviation), may be described with  $\sigma = \sqrt{2\alpha \langle |v| \rangle t}$ , in which the mean absolute velocity,  $\langle |v| \rangle$ , is the travelled distance of the interface divided by the total time. To relate  $\langle |v| \rangle$  with the total distance that the interface has travelled is meaningful, as it illustrates that it does not matter how the velocity fluctuates. The above will thus also hold for arbitrary moving fronts, e.g. if  $v$  depends on highly erratic atmospheric forcing, as has been considered by Eeman et al. (2012), inspired by our analysis.

Next, we analysed the effects of nonlinear sorption assuming Gapon type of cation exchange. This non-linear exchange leads to TW or RW behaviour, depending on the flow direction in relation with the concentration gradient of the front and the nonlinearity (concave, convex) of exchange, i.e., the boundary conditions. We validated our numerical model by comparing the numerical results for steady flow in one direction with analytical approximations. The agreement between the numerical results and the analytical was found to be very good. For oscillating flow, TW and RW type of transport alternate. Although this alternate behaviour is still visible during the first cosine cycle, the front shape does not shift between the extremes that agree with the analytical approximations. Rather, the RW spreading occurs rapidly, but the TW self-sharpening requires time. As a result of this asymmetry in spreading/sharpening, oscillating fronts show a gradual spreading, which looks comparable to Fickian diffusion. However, as is shown by higher order front spatial moments that indicate non-Gaussian behaviour, spreading is not really Fickian, but converges to a pure diffusion, non-linear exchange transport case (i.e. with zero convection). For practical applications, it is thus possible to account for larger time spreading as a result of oscillating flow, by introducing an effective diffusion coefficient  $D_e$ , based on the product of the absolute average movement of an interface  $\langle |v| \rangle$  and the dispersivity  $\alpha$ , yet ignoring the convective transport.

We also considered a change in total concentration, by decreasing its value in the upper part of the domain. The fronts of the concentration fractions behave the same in case of a change in total concentration, despite that the total concentration front itself is spreading in a pure Fickian way, and extends over a broader (unretarded) interval than the concentration fractions. As a result of the spreading of the change in total concentration, affinity for calcium increases in the direction of lower concentrations, which results in a sharper front than if total concentration is constant with depth and large. However, the spreading of the calcium front in this direction is still enhanced slightly, due to the higher

amount of initially adsorbed calcium at lower total concentrations. For the sodium concentration fronts, the influence of the salt shock is much stronger and determines the spreading and maximum concentrations to a large extent.

## Acknowledgements

This study was carried out within the framework of the Netherlands Organisation for Scientific Research (NWO) CASIMIR programme (018.002.007), the Dutch Water Utility Sector joint research programme (BTO) and the Knowledge for Climate programme (Theme 2 & 3, Fresh water supply). We appreciated discussions in the NUPUS network (<http://www.nupus.uni-stuttgart.de/>) and good suggestions of A. (Toon) Leijnse of Wageningen University.

## Appendix 3.A.: Traveling Wave solution (Bolt, 1982)

Transport equation:

$$\frac{\partial q(c) + nc}{\partial t} = nD \frac{\partial^2 c}{\partial x^2} - nv \frac{\partial c}{\partial x} \quad (3.A.1)$$

Where  $q(c)$  stands for the non-linear relation between adsorbed and dissolved, i.e.  $q$  is a function of the concentration in solution  $c$ . Eq. (3.A.1) can be integrated for a generic solution without specifying the exact function of  $q(c)$ . This results in a traveling wave (TW) solution i.e. the position and shape of the front does not change while moving along with the front. To be able to move along with the front a new (wave) coordinate is introduced:

$$\tilde{x} = x - v^*t + u. \quad (3.A.2)$$

Transforming and integrating (3.A.1) yields:

$$\frac{S\tilde{x}}{\alpha} = -\int \frac{d\bar{c}}{(\bar{q}(\bar{c}) - \bar{c})} = F(\bar{c}, \bar{c}_u). \quad (3.A.3)$$

Where  $u$  is an unknown integration constant and  $F(\dots)$  an integral of a function of  $q$  and  $c$  and

$$S = \frac{(\Delta q / \Delta c)}{(n + (\Delta q / \Delta c))}. \quad (3.A.4)$$

Using normalized concentrations:

$$\bar{c} = \frac{c - c_i}{c_f - c_i}, \bar{q} = \frac{q - q_i}{q_f - q_i} \quad (3.A.5)$$

Normalize concentration to total concentration ( $C$ ) and adsorbed amount per volume soil to CEC ( $\varepsilon_c$ ):

$$\frac{c}{C} = f, \frac{q}{\varepsilon_c} = N \quad (3.A.6)$$

Gapon equation:

$$\frac{1-N}{N} K_G \sqrt{2C} \frac{1-f}{\sqrt{f}} \quad (3.A.7)$$

(3.A.3) can be rewritten using (3.A.6) and (3.A.7):

$$\bar{q} = \frac{(N - N_i)}{(1 - N_i)} \quad (3.A.8)$$

$$= \frac{\sqrt{f}}{\chi(1-f) + \sqrt{f}} \frac{\chi(1-f_i) + \sqrt{f_i}}{\chi(1-f_i)} - \frac{\sqrt{f_i}}{\chi(1-f_i)} \quad (3.A.9)$$

Where:

$$\chi = K_G \sqrt{2C} \quad (3.A.10)$$

$$\bar{c} = \frac{f - f_i}{(1 - f_i)} \quad (3.A.11)$$

$$d\bar{c} = \frac{df}{(1 - f_i)} \quad (3.A.12)$$

Equation (3.A.3) then becomes:

$$S\bar{x} / \alpha = - \int \frac{\{\chi(1-f) + \sqrt{f}\} df}{(\sqrt{f} - \sqrt{f_i})(1-f)\{1 - \chi(\sqrt{f} + \sqrt{f_i})\}} \quad (3.A.13)$$

Which yields a solution of the type:

$$\begin{aligned} S\bar{x} / \alpha &= -a \ln(\sqrt{f} - \sqrt{f_i}) - b \ln\{1 - \chi(\sqrt{f} - \sqrt{f_i})\} + c \ln(1 + \sqrt{f}) + d \ln(1 - \sqrt{f}) \\ &= \quad \text{I} \quad + \quad \text{II} \quad + \quad \text{III} \quad + \quad \text{IV} \end{aligned} \quad (3.A.14)$$

With:

$$a = \frac{2\sqrt{f_i}(\chi + \sqrt{f_i})}{(1 - f_i)(1 - 2\chi\sqrt{f_i})} \quad (3.A.15)$$

$$b = \frac{2\chi[\chi + \sqrt{f_i}\{(1 - \chi\sqrt{f_i})^2 - \chi^2\}]}{(1 - 2\chi\sqrt{f_i})\{(1 - \chi\sqrt{f_i})^2 - \chi^2\}} \quad (3.A.16)$$

$$c = 1/(1 + \chi - \chi\sqrt{f_i}) \quad (3.A.17)$$

$$d = 1/(1 - \chi - \chi\sqrt{f_i}) \quad (3.A.18)$$

In order to determine  $\langle \tilde{x}_c \rangle$  each of the four terms of Eq. (3.A.14) is integrated over  $f$  from  $f_i$  to 1 and divided by  $(1 - f_i)$ . Indicating these integrals after division, by  $\langle I \rangle$ ,  $\langle II \rangle$  etc. one finds:

$$\langle I \rangle / a = -\ln(1 - \sqrt{f_i}) + 1 + 3\sqrt{f_i} / 2(1 + \sqrt{f_i}) \quad (3.A.19)$$

$$(1 - f_i)\langle II \rangle / b = \dots$$

$$\begin{aligned} & \frac{1}{2}(-2\chi\sqrt{f_i} - 2\ln(-2\chi\sqrt{f_i} + 1) + \chi^2 f_i + 4\ln(-2\chi\sqrt{f_i} + 1)\sqrt{f_i}\chi - 2\sqrt{f_i}\chi^2 - \\ & 2\ln(-\chi + 1 - \chi\sqrt{f_i})\chi^2 + 2\ln(-\chi + 1 - \chi\sqrt{f_i}) - 4\ln(-\chi + 1 - \chi\sqrt{f_i})\sqrt{f_i}\chi + \chi^2 + \\ & 2f_i \ln(-\chi + 1 - \chi\sqrt{f_i})\chi^2 + 2\chi) / \chi^2 \end{aligned}$$

(3.A.20)\*

\*correction on solution by Bolt (1982) p 318)

$$\langle III \rangle / c = \ln(1 + \sqrt{f_i}) + (1 - \sqrt{f_i}) / 2(1 + \sqrt{f_i}) \quad (3.A.21)$$

$$\langle IV \rangle / d = \ln(1 - \sqrt{f_i}) - (3 + \sqrt{f_i}) / 2(1 + \sqrt{f_i}) \quad (3.A.22)$$

The mean location of the solution front relative to the location of an arbitrarily chosen reference value  $f_s$  is then found as:

$$S\langle \tilde{x}_c \rangle / \alpha = \langle I \rangle - I(f_s) + \langle II \rangle - II(f_s) + \langle III \rangle - III(f_s) + \langle IV \rangle - IV(f_s) \quad (3.A.23)$$





## CHAPTER

# 4

### Sulphate reduction and calcite precipitation in relation to internal eutrophication of groundwater fed alkaline fens

This chapter is a slightly modified version of the published manuscript:

**Cirkel, D.G., C.G.E.M. van Beek, J.P.M. Witte & S.E.A.T.M. van der Zee (2013) Sulphate reduction and calcite precipitation in relation to internal eutrophication of groundwater fed alkaline fens. *Biogeochemistry* doi 10.1007/s10533-013-9879-4**

## Abstract

Although in Europe atmospheric deposition of sulphur has decreased considerably over the last decades, groundwater pollution by sulphate may still continue due to pyrite oxidation in the soil as a result of excessive fertilisation. Inflowing groundwater rich in sulphate can change biogeochemical cycling in nutrient-poor wetland ecosystems. Incoming sulphate loads may induce internal eutrophication as well as the accumulation of dissolved sulphide, which is phytotoxic. We, however, argue that upwelling sulphate rich groundwater may also promote the conservation of rare and threatened alkaline fens, since excessive fertilisation and pyrite oxidation also produces acidity, which invokes calcite dissolution, and increased alkalinity and hardness ( $\text{Ca}^{2+} + \text{Mg}^{2+}$ ) of the inflowing groundwater.

Our observations in a very species-rich wetland nature reserve show that sulphate is reduced and effectively precipitates as iron sulphides when this calcareous and sulphate rich groundwater flows upward through the organic soil of the investigated nature reserve. Furthermore, we show that sulphate reduction coincides with an increase in alkalinity production, which in our case results in active calcite precipitation in the soil. In spite of the occurring sulphate reduction we found no evidence for internal eutrophication. Extremely low phosphorous concentration in the pore water could be attributed to a high C:P ratio of soil organic matter and co-precipitation with calcite. Our study shows that seepage dependent alkaline fen ecosystems can be remarkably resilient to fertilisation and pyrite oxidation induced groundwater quality changes.

## Introduction

Atmospheric deposition of sulphur oxides in Europe was very high in especially the 1960s and early 1970s (Lefohn et al., 1999; Stern, 2005), but decreased considerably in the last three decades due to effective policy (Fowler et al., 2007; van der Swaluw et al., 2011). In the Netherlands for instance, annual atmospheric deposition of sulphur decreased from more than 60 kg S/ha in the 1980s to current values of below 10 kg S/ha ([www.RIVM.nl](http://www.RIVM.nl)). Still, it is well known that groundwater sulphate concentrations in many Dutch aquifers are still increasing (Mendizabal et al., 2012). This continuing increase has been attributed to oxidation of pyrite by atmospheric oxygen in the subsoil, as a result of lowering groundwater levels (Boman et al., 2010; Smolders et al., 2006) and oxidation of pyrite by nitrate as a result of excessive fertilisation (Appelo and Postma, 2005; Juncher Jørgensen et al., 2009; Zhang et al., 2009). As a result, large amounts of sulphate are transported along the hydrological pathway to seepage areas, a process likely to continue for the coming decades (Mendizabal et al., 2012; Van Beek et al., 2001).

This redistribution of sulphur is commonly regarded as a threat to downstream wetland ecosystems that depend on upward seepage (Smolders et al., 2010). The inflow of sulphate rich groundwater stimulates decomposition of organic matter and release of phosphate and ammonium, a process called ‘internal eutrophication’ (Jørgensen, 1982). In

addition, reduction of iron(hydr)oxides may result in decreased P-binding capacity of the soil (Lamers et al., 2001; Smolders et al., 2006). Also, sulphate reduction may lead to the accumulation of dissolved sulphide ( $\text{H}_2\text{S}$ ,  $\text{HS}^-$ ) in the soil, which has a (phyto)toxic effect, even at low concentrations (Koch et al., 1990; van der Welle et al., 2008). Thus, due to internal eutrophication and sulphide toxicity, the inflow of sulphate-rich groundwater may result in deterioration of natural vegetation characteristic of wet, nutrient poor conditions.

However, oxidation of pyrite by excessive fertilisation and concomitant production of acidity also can dissolve calcite, if available, along the flow path (Mendizabal, 2011). As a consequence, alkalinity ( $\text{HCO}_3^-$ ) and hardness ( $\text{Ca}^{2+} + \text{Mg}^{2+}$ ) of the groundwater strongly increase, which is beneficial for the conservation and development of specific fen ecosystems that, according to (Boyer and Wheeler, 1989; Grootjans et al., 2006), depend on continuous supply of base-rich groundwater to maintain circumneutral pH and nutrient poor conditions. These low productive ecosystems (e.g. *Junco-Molinion* and *Caricion davallianae* communities) have become very rare in most EU countries and have high conservation value because they harbour many rare and endangered plant species (ŠeffEROVÁ StanOVÁ et al., 2008). The nutrient poor conditions in these ecosystems are often achieved by P (co-) limitation (Olde Venterink et al., 2003), which can be maintained under neutral to alkaline conditions by  $\text{Ca}^{2+}$  enhanced adsorption to metal oxides (Devau et al., 2009; Hinsinger, 2001; Weng et al., 2011), by adsorption to and co-precipitation with calcite (Boyer and Wheeler, 1989; Karageorgiou et al., 2007; Plant and House, 2002; Wang and Tzou, 1995) and by precipitation of calcium phosphate minerals (Alvarez et al., 2004). As is shown by various authors (Boeye et al., 1995; Glaser et al., 1990; HájkOVÁ et al., 2011; Nicholson and Vitt, 1990), increased hardness and alkalinity of inflowing groundwater can result in rapid changes in vegetation composition and transitions from poor fen or even bog to rich fen.

Our working hypothesis is that upstream excessive fertilisation and pyrite oxidation in calcium carbonate rich soils leads to increased hardness and alkalinity of groundwater, which might lead to increased pH buffering and amelioration of internal eutrophication in downstream groundwater fed wetlands. To test this hypothesis, we investigated the hydrogeochemical patterns in groundwater and soil moisture of the Meeuwenkampje nature reserve. This reserve harbours a rare and highly endangered calcareous rich fen vegetation and is surrounded by intensive agriculture. The fen is known to have received upward seepage of sulphate rich groundwater for at least the last 20 years (Jansen and Kemmers, 1995). Despite this legacy, the fen does not show significant signs of deterioration. Detailed vegetation recordings since the 1970s show that it has a very stable plant species composition and stable vegetation patterns, and it still harbours many rare and endangered species typical of wet, alkaline and nutrient poor conditions. In this contribution we specifically focus on the biogeochemical processes occurring in a seepage face within the reserve, which harbours the highest biodiversity of the field, but also receives groundwater with the highest sulphate concentrations.

## Materials and Methods

### Field site

The Meeuwenkampje nature reserve is located in the centre of the Gelderse Vallei, a valley of Saalian glacial origin near the Dutch town of Veenendaal (52°02'57.29"N – 5°32'53.50"E, 7 m +MSL) (Figure 4.1). The glacial valley is filled up with Late Pleistocene and Holocene deposits and is bordered by sandy moraines that have an altitude of up to 50 m +MSL (Jelgersma and Breeuwer, 1975). Regional groundwater flow is dominated by the hydraulic gradient from the moraines to the valley, resulting in strong upward seepage. The morphology of the valley is dominated by an up to 15 m thick eolian sand sheet or cover sand deposit, originating from the last major ice advance (Koster, 2005). The cover sand deposits to the east of the reserve are calcite rich (> 1-2% CaCO<sub>3</sub>), except for the (younger) upper 2.5 - 4 meter and are underlain by an Eemian marine clay layer.

In the Holocene, peat started to grow in local depressions, eventually resulting in raised bogs to the east and south of the Meeuwenkampje reserve. From the 16th century to the early 20th century these bogs were excavated and transformed into extensively farmed and poorly drained hay meadows. From the 1930s onwards, drainage of the valley intensified with the aid of ditches and drain pipes and the area became one of the most intensive agricultural areas of the Netherlands. The drainage of the valley had drastic implications for groundwater flow patterns: upward seepage areas to the east of the current reserve turned into infiltration areas. Combined with the intensification of agriculture, this led to a strong deterioration of the very species rich fen meadow vegetation found throughout the valley. At present, only a few hectares of such fen meadows remain, among which the Meeuwenkampje reserve. The reserve is located in a local depression in the cover sand deposits, which is filled up with calcareous gyttja, reed-sedge peat and sphagnum peat. Groundwater is flowing to the reserve from the former bog areas in the north-east and is forced upward by the hydraulic gradient imposed by the underlying regional groundwater flow system (Jansen and Kemmers, 1995).

The reserve houses a large number of species typical for alkaline fen meadow and rich fen vegetation such as: brown mosses including *Campylium stellatum*, *Caliergonella cuspidata*, *Fissidens adiantoides*; sedges including *Carex hostiana*, *C. pulicaris* and herbs including *Pinguicula vulgaris*, *Gymnadenia conopsea*, *Cirsium dissectum*, *Dactylorhiza maculata* and *Platanthera bifolia*. The vegetation shows a distinctive gradient, which largely coincides with the local elevation (dm) within the field, from *Cirsium dissecti-molinietum nardetosum* communities on the relatively highest parts, via a very species rich small sedge community at intermediate levels, to more productive marsh vegetation with large sedges in the lowest and most frequently inundated part of the field (Figure 4.2).

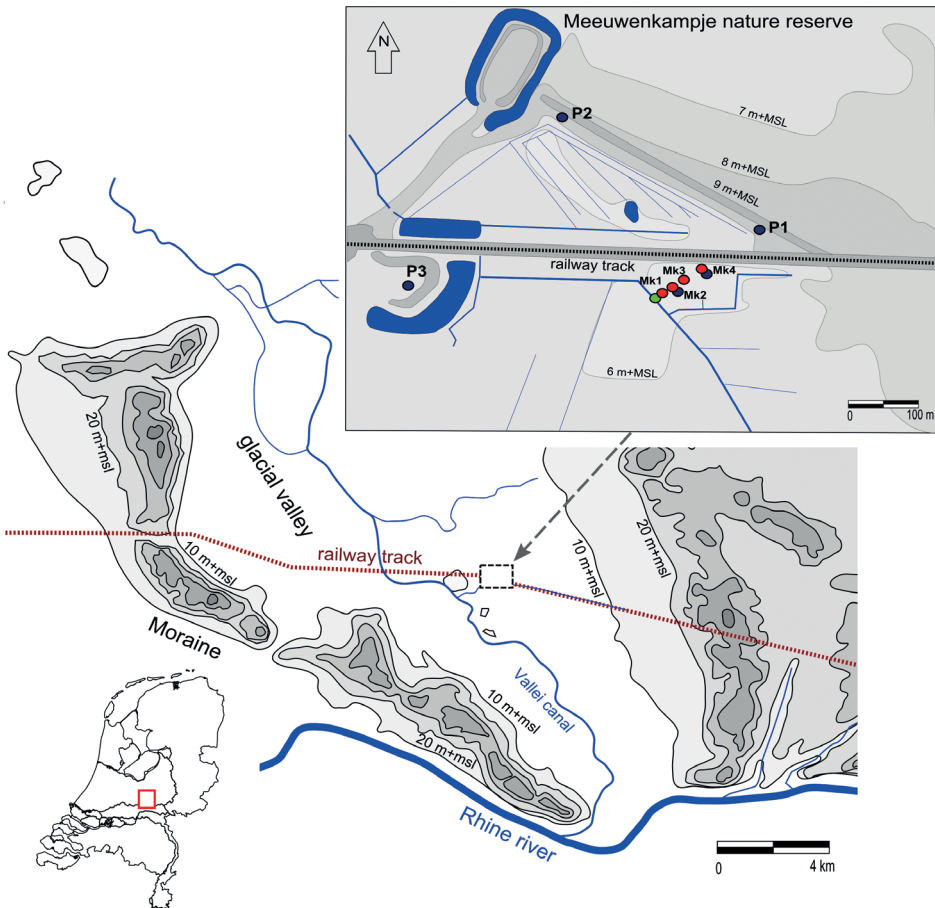


**Figure 4.1.** Topography of the Gelderse Vallei glacial valley and location of the study area. Red dots: location of Macro-Rhizons, dark blue dots piezometers and mini-filters, green dot: surface water sampling point.

### Sampling and analytical methods

Fieldwork for this study was carried out from spring 2008 to summer 2009. Groundwater and surface water levels within the field transect (Figure 4.1) were monitored using 2 piezometers equipped with Diver<sup>®</sup> dataloggers at Mk2 and Mk4. The measuring interval of the dataloggers was set to 15 minutes to be able to measure hydrological events, with a relatively small duration such as overland flow. Three existing piezometer nests at the edges of the reserve at P1, P2 and P3 (see Figure 4.1) were monitored manually every two weeks since 1996.

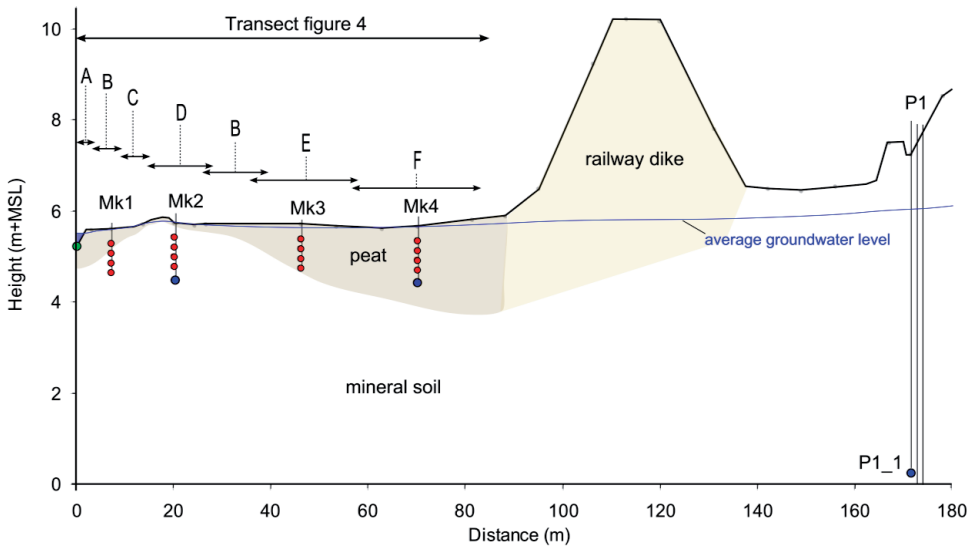


**Figure 4.2.** Depth of the macro-rhizons (red dots), the mini-filters and piezometers (blue dots), and the surface water sampling point (green dot) along the transect depicted in Figure 4.1. Vegetation types denoted as: A: *Typho-Phragmitetum*, B: *Cirsio-molinietum typicum*, C: *Ericetum teraliciis sphagnetosum*, D: *Cirsio-molinietum nardetosum*, E: *Cirsio-molinietum orbietosum*, F: *Caricetum elatae*. Nomenclature according to Schaminée et al. (1995b).

Water quality of shallow groundwater, surface water and soil moisture was sampled using MacroRhizons (Meijboom and Van Noordwijk, 1996) and mini-filters along the transect within the reserve (see Figure 4.1 and Figure 4.2 for the sampling locations and depths). MacroRhizons were placed at four locations: Mk1 (near the ditch), Mk2 (highest point, sandy subsoil), Mk3 (seepage face, highest biodiversity) and Mk4 (lowest point, thick peat layer). For each location, MacroRhizons were inserted at four depths (25-35, 50-60, 75-85 and 100-110 cm depth) and placed at an angle of 45° to prevent infiltration of rainwater or runoff along the sampler. Minifilters were placed at 125 cm depth. Deep groundwater was sampled at relevant depths using the piezometers located at P1, P2 and P2 (see Table 4.1 for measuring depths). Samples were taken 9 times during the measuring period, except for the deep groundwater which was only sampled in July and October 2008.

All samples were divided in the field into three portions: (1) a small portion (ca 2.5 ml) for direct in-field pH, temperature and EGV measurements; (2) a standard ICP tube filled to the brim, for element analysis; (3) a 50 ml tube for chloride, carbon and nutrient analysis. Samples taken from the MacroRhizons were filtrated by the 0.2 µm porous membrane of the sampler. All other samples were filtered through 0.45 µm Millipore filters. Sample bottles were placed in melting ice during sampling and transport. Samples

were taken directly to the lab after sampling and analysed directly after arrival. Chloride was analyzed on a flow injection analyser (FOSS, FIAstar 5000). Element content (Al, As, Ca, Cu, Fe, K, Mg, Mn, Na, Ni, P<sub>tot</sub>, S<sub>tot</sub>, Zn) was determined with ICP-AES (Varian, Vista pro). Total carbon (TC) and total inorganic carbon (TIC) were measured on a TOC analyser (Shimadzu 5050). Dissolved organic carbon (DOC) and nutrients (N-NH<sub>4</sub>, N-(NO<sub>3</sub>+NO<sub>2</sub>), N<sub>tot</sub>, P-PO<sub>4</sub>) were analysed by segmented flow analysis (Skalar SK12).

The hydrochemical computer program PHREEQC 2.1 (Parkhurst and Appelo, 1999) was used to calculate carbonate speciation based on measured pH and TIC and saturation indexes for calcite, siderite, rhodochrosite, gypsum and hydroxyapatite. Using the standard database of Phreeqc, we tested whether the chemical process interpretation that was based on the field observations was in agreement with modelling these processes.

Soil cores were taken at Mk2 and Mk3, at the end of the monitoring campaign. The cores were taken at the same depth and closely adjacent to the macrorhizon probes. In addition we took a sample of the root zone (0-10 cm depth) and a sample below the deepest macrorhizon (120-130 cm depth). After collection, the cores were placed under N<sub>2</sub> gas in glass jars and refrigerated. At the laboratory, the glass jars were opened in a glove box under anoxic conditions, to take a subsample from each depth for analysis of oxalate extractable iron, aluminium, manganese and phosphate according to Houba et al. (1989). The remainder of the soil was dried in an oxygen free desiccator as described by Begg et al. (1994) and grinded to 5 mm, homogenized and divided into subsamples for further analysis. Water content of the soil samples was measured by weight loss during drying. Bulk density was calculated using the core volume and material dry weight. Total element content (Al, Ca, Cu, Fe, K, Mg, Mn, Na, P, S, Zn, Ni, As) after destruction with HNO<sub>3</sub>-HCl (Aqua Regia) was determined by analysis with ICP-AES (Varian, Vista pro). Organic matter and calcite content were determined by a four step Thermogravimetric Analysis (TGA) at 105, 330, 550 and 1000 °C. Total carbon and nitrogen content were determined using pyrolysis with a CNS analyser (Thermo Finnegan Flash EA-1112 NC). Clay content and grain size distribution of the mineral parts were determined by laser-diffraction (Konert and Vandenberghe, 1997). An exploratory SEM-EDS analysis was performed on dried soil samples to identify minerals in the soil.

## Chemical Processes

Calcite dissolution and the consequent increase of alkalinity and hardness are closely related to proton release by pyrite oxidation. A simplified overview of the primary reaction equations related to pyrite oxidation, sulphate reduction and dissolution of calcite are presented below.

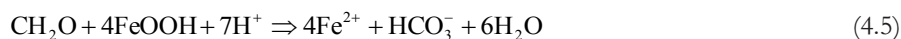
Oxidation of pyrite by oxygen (due to drainage) and/or nitrate (from fertilisation):



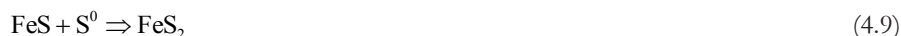
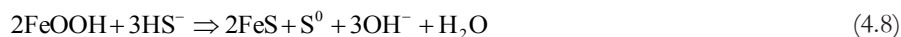
Dissolution of calcite by CO<sub>2</sub> and strong acid (protons):



Reduction of iron(hydr)oxides, nitrate and sulphate by organic matter (represented as CH<sub>2</sub>O<sup>1</sup>):



Precipitation of iron sulphides, assuming alkaline conditions:



## Results

### Meteorology and hydrology

Annual precipitation in 2008 and 2009 (941 and 755 mm) was near the long term average value of 832 mm. Potential annual Makkink evapotranspiration was 576 mm and 612 mm respectively. Shallow groundwater levels within the reserve at Mk4 were very stable and fluctuated between 12 cm above and 31 cm below land surface. Groundwater levels below 20 cm below land surface only occurred briefly in July 2008 and June 2009. Inundation of the lowest parts of the field occurred from November 2008 to April 2009. Inundation with short duration also occurred during storm events out of this period. Inundation did not occur at the slightly elevated location Mk2. Observed piezometric heads at P1, P2 and P3 (Figure 4.3) show that groundwater above the Eemian clay layer flows towards the reserve and is forced upward by higher piezometric heads in the underlying aquifers.

<sup>1</sup> Describing organic matter as CH<sub>2</sub>O is of course a simplification, it contains for instance significant amounts of nitrogen and phosphorous, which will be released when organic matter is oxidized.

## Groundwater quality measured in the deep piezometers

Based on a hydrochemical facies analysis of the region by Beemster et al. (2002) and water samples collected from the deep piezometers (Table 4.1) surrounding the reserve, two major groundwater types can be distinguished. Water samples containing substantial amounts of sulphate (P1\_1<sup>2</sup> (1.19 mmol/l), P3\_2 (1.72 mmol/l) respectively) represent groundwater above the Eemian clay layer. Water samples below the Eemian clay layer originates from the moraines to the east of the valley (Figure 4.1) and contains almost no sulphate. At the edge of the Eemian clay layer this 'pristine groundwater' is forced upward (Figure 4.3), which is reflected in the groundwater composition at P2\_1 (Table 4.1). Of specific interest to this study is piezometer P1\_1 because it is positioned upstream of the Meeuwenkampje. Samples taken from this piezometer confirm the inflow of sulphate rich groundwater to the reserve, from the north-eastern direction. Also high chloride and ammonium concentrations (0.89 and 0.1 mmol/l, respectively) reflect the influence of intensive agriculture in the recharge area. In comparison, the groundwater below the Eemian clay (i.e. P2\_2) has a chloride concentration of only 0.23 mmol/l, which is a level typical for pristine infiltrated rainwater originating from the moraines (Beemster et al., 2002). Water samples containing high concentrations of sulphate also contain high levels of calcium and bicarbonate alkalinity and are supersaturated with respect to calcite and siderite. All groundwater samples were undersaturated with respect to gypsum.

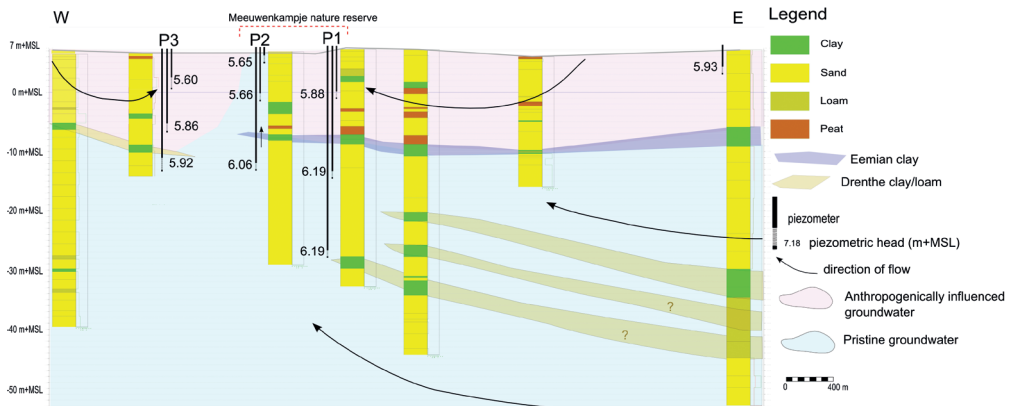


**Figure 4.3.** Regional geohydrological schematisation based on drilling logs and piezometric heads. Numbers denote average ( $n > 250$ ) hydraulic heads. The division in pristine and anthropogenically influenced groundwater is based on Beemster et al. (2002) and is supported by our measurements.

<sup>2</sup> To be read as: piezometer P1, filter 1

**Table 4.1.** Average groundwater quality and relevant saturation indexes deep piezometers

Piezometer		P1_1	P1_2	P2_2	P2_3	P3_2
filter depth (m-MSL)	from	0.22	-12.37	-0.12	-13.55	-6.44
	to	-0.78	-13.37	-1.12	-14.55	-7.44
pH	(-)	7.15	7.5	7.65	7.2	6.9
EGV	µS/cm	1155	251	185	197	1320
T	°C	11.5	11.0	13	13.5	13.5
Cl	mmol/l	0.89	0.28	0.23	0.27	1.71
Na	mmol/l	0.83	0.30	0.27	0.27	1.25
K	mmol/l	0.02	0.02	0.01	0.06	0.02
Ca	mmol/l	5.74	1.05	0.77	0.72	5.45
Mg	mmol/l	0.9	0.10	0.08	0.09	0.26
Fe	mmol/l	0.198	0.01	0.004	0.006	0.343
Mn	mmol/l	0.011	0.002	0.001	0.001	0.016
DOC	mmol/l	1	0.19	0.07	0.12	0.76
TIC	mmol/l	13.57	2.68	1.75	1.86	11.82
HCO3	mmol/l	11.49	2.46	1.65	1.57	8.94
N-NH4	mmol/l	0.1	0.13	0.02	0.01	0.34
N-NO3	mmol/l	< 0.002	< 0.002	< 0.002	< 0.002	< 0.002
Nts	mmol/l	0.1	0.1	0.05	0.09	0.39
P-PO4	mmol/l	0.003	0.008	0.002	0.002	0.007
S <sub>tot</sub>	mmol/l	1.19	0.02	0.1	0.1	1.72
Ni	umol/l	< 0.03	< 0.03	< 0.03	2.8	< 0.03
Zn	umol/l	< 0.08	< 0.08	< 0.08	4.1	-
Cu	umol/l	0.05	< 0.05	< 0.05	< 0.05	< 0.05
Al	umol/l	< 1.1	< 1.1	< 1.1	< 1.1	< 1.1
As	umol/l	< 0.07	< 0.07	< 0.07	< 0.07	< 0.07
Saturation index:						
Calcite		0.6	-0.3	-0.4	-0.9	0.2
Siderite		1.3	-0.2	-0.8	-0.7	1.2
Rhodochrosite		0.3	-0.4	-0.7	-1.1	0.2
Gypsum		-1.2	-3.3	-2.9	-2.9	-1.1
Hydroxyapatite		-7.6	-8.1	-7.8	-3.9	-8.9

## Water quality patterns along the field transect

### *Chloride*

Because chloride is inert, it is a suitable component to trace the local spatial distribution of infiltrating rainwater and upward seeping sulphate rich groundwater (Figure 4.4) within the nature reserve. Local rainwater has an average chloride concentration of 0.07 mmol/l ([www.lml.rivm.nl](http://www.lml.rivm.nl)), which is concentrated roughly three times after infiltration due to evapotranspirative water loss. Chloride concentrations of the upward seeping groundwater are much higher, with values of up to 2.88 mmol/l. The low chloride concentrations at Mk2 thus indicate infiltration of rainwater and the formation of a rain water lens (dashed blue line in Figure 4.4). Formation of a rainwater lens is in agreement with conditions described by Schot et al. (2004), given the slightly higher elevation (2-3 dm) of this part of the field and the presence of a sandy subsoil. The higher values at the top of the profile at Mk2 indicate the concentrating effect of evapotranspiration, while the slightly raised values at the bottom of the lens point to dispersive mixing.

Substantial shrinkage of the lens, by evapotranspirative water loss, occurred only in the summer of 2009. The upward movement of the bottom boundary layer of the lens, resulted in a chloride concentration of 2.25 mmol/l at a depth of 125 cm at Mk2. At the lower sampling locations Mk1, Mk3, and Mk4, infiltration of rainwater is very limited due to the high groundwater levels, resulting in saturation excess overland flow. Highest chloride concentrations are found at Mk3. The slight upward decrease of the chloride concentration here, was caused by very limited dilution with rainwater (<2%). The absence of significant thickening or dilution at Mk3 points to flushing of the profile by upward seeping groundwater.

### *Sulphate*

Sulphate concentrations in the rainwater lens (Mk2) were very low (Figure 4.4), and consistent with (recently) infiltrated rainwater concentrated by evapotranspiration. In the upward seeping groundwater, however, sulphate concentrations were very high. The highest sulphate concentrations, ranging up to 2.3 mmol/l, were observed in the lowest MacroRhizon of Mk3. Sulphate concentrations were rapidly declining in the upward (flow) direction at Mk3 and Mk4. At Mk3 for instance, the time averaged sulphate concentration declines from 2.07 at a depth of 95 cm to 0.12 mmol/l at 25 cm depth. Samples taken from the mineral subsoil at Mk1 did not show significant decline in sulphate concentration. High sulphate concentrations at Mk3 and the minifilters at Mk2 and Mk4 coincide with trace amounts of nickel (see appendix 4.A).

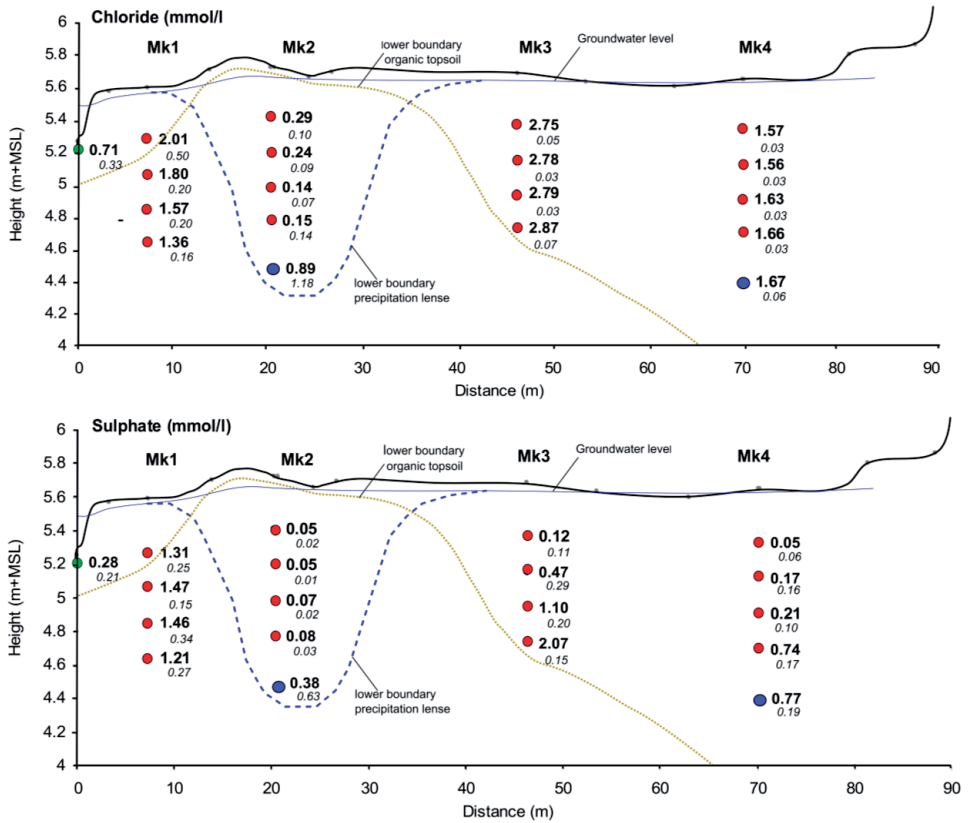


**Figure 4.4** Time averaged ( $n=7-9$ ) chloride and sulphate concentrations (mmol/l) as observed along the field transect from ditch to railway dike, standard deviations presented as subscript. Red dots: macro-rhizons, blue dots minifilters, green dot: surface water sampling point.

### Spatiotemporal patterns

The observed hydrochemical patterns along the transect were very stable over time, for most parameters, especially at the bottom of the profile (see error bars Figure 4.6). Observed temporal dynamics at Mk3 appear to be associated with summer and winter periods. Figure 4.5 gives an overview of the major changes in water chemistry during upward seepage through the soil as observed at Mk3: Figure 5a is representative for the situation after the wet winter period of 2008/2009; Figure 5b for the situation after the warm and relatively dry summer period of 2008. Compared to the winter measurements, summer measurements show a more rapid decline of sulphate and stronger increase of DOC and  $\text{HCO}_3^-$  in the direction of flow.

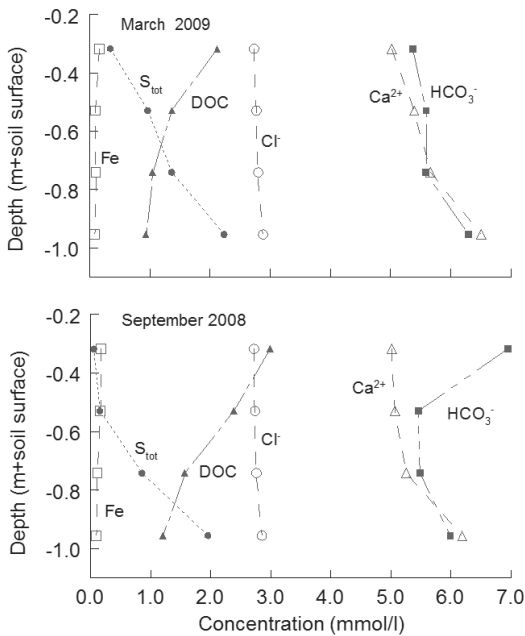


**Figure 4.5.** Soil water quality profiles at Mk3 as observed at March 2009 and September 2008.

More detailed information on the water chemistry at Mk3, which is located in the most species rich part of the field, is presented in Figure 4.6. This figure confirms that sulphate strongly decreases in the direction of flow. DOC concentrations show a reciprocal trend: they strongly increase in the upward flow direction (Figure 4.6A), which points to decomposition of soil organic matter as a source.

The profile at Mk3 can be divided into two distinct zones with respect to  $\text{Ca}^{2+}$  and  $\text{HCO}_3^-$  (Figure 4.6B). In the lower part of the profile (75–100 cm depth)  $\text{HCO}_3^-$  is slightly lower than  $\text{Ca}^{2+}$  and a strong decline of  $\text{Ca}^{2+}$  concentration in the upward flow direction occurs, which points to calcite precipitation (equation 4).  $\text{HCO}_3^-$  however declines less than proportionally with  $\text{Ca}^{2+}$ , which indicates production of  $\text{HCO}_3^-$ . At 75 cm depth  $\text{Ca}^{2+}$  and  $\text{HCO}_3^-$  concentrations are comparable. In the upper part of the profile (above the gyttja layer), the  $\text{Ca}^{2+}$  decline is less steep and  $\text{HCO}_3^-$  concentrations show a strong increase in the direction of flow. The pH (Figure 4.6D) shows a decrease in the direction of flow, and is rather stable over time up to a depth of 25 cm below soil surface. Above this depth, pH increases and shows much more variation over time. Soil water at Mk3 is supersaturated with respect to siderite and at equilibrium ( $-0.1 < \text{SI}_{\text{calcite}} < 0.1$ ) with, or slightly saturated with respect to calcite (Figure 4.6C). All samples were undersaturated with respect to Gypsum and Hydroxyapatite. Iron concentrations (Figure 4.6E) were in the range of 0.1–0.2 mmol/l. Manganese concentrations were stable at 0.01 mmol/l. Although organic matter is clearly decomposed at Mk3, phosphate levels remain very low in soil solution (Figure 4.6F). The highest P- $\text{PO}_4$  level measured in the profile at Mk3 was

0.90  $\mu\text{mol/l}$ , but most of the observed concentrations were below the detection limit of 0.65  $\mu\text{mol/l}$ . The highest  $\text{P}_{\text{tot}}$  observed in the profile was 1.58  $\mu\text{mol/l}$ , however most of the observations for this parameter were below detection limit. Although  $\text{NH}_4^+$  is likely to be released during (anaerobic) decomposition, we observed a steady decline in the concentration of this nutrient in the direction of flow (Figure 4.6F). Nitrate ( $\text{N}-(\text{NO}_3+\text{NO}_2)$ ) concentrations were below detection limit (2.14  $\mu\text{mol/l}$ ) in all samples taken at Mk3. Redox conditions were considered anoxic, based on the absence of nitrate and observed iron concentrations.

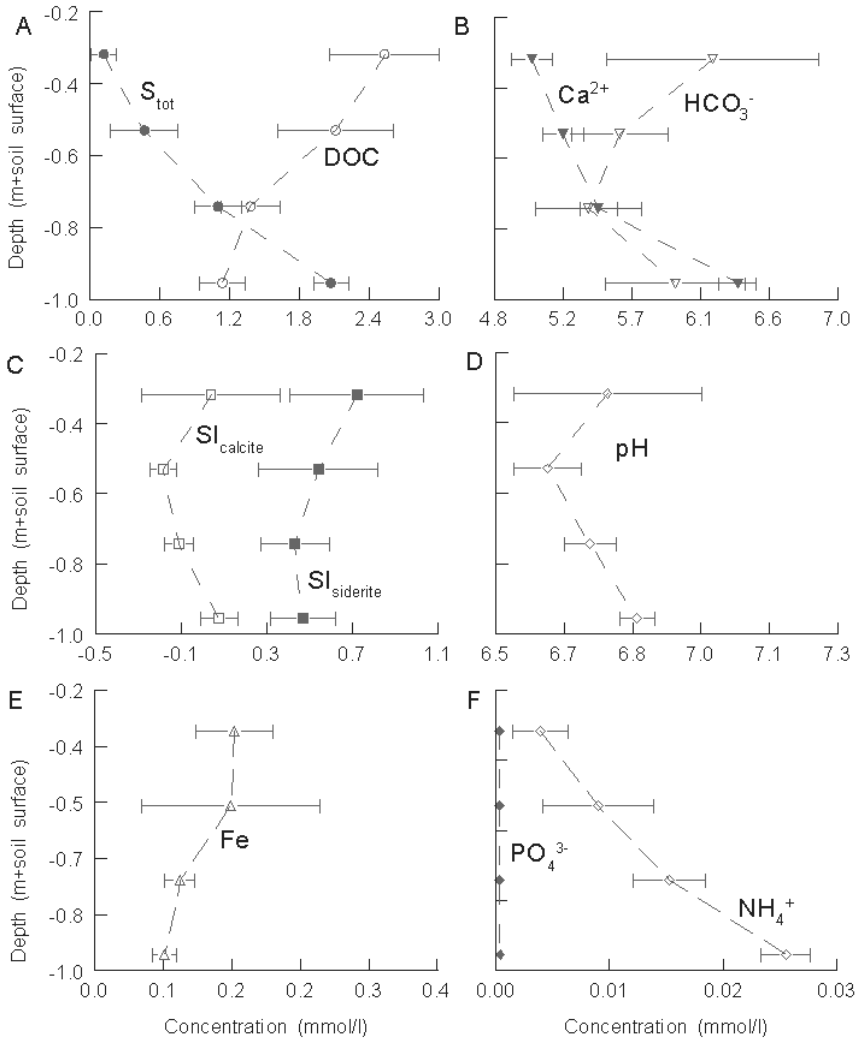


**Figure 4.6.** Time averaged soil water quality profiles at Mk3. Horizontal bars represent standard errors ( $n = 7 - 9$ ), which indicate the temporal variation.

## Analysis of soil cores

Results of the soil core analyses are presented in Table 4.2 and Figure 4.7. Clay, silt and sand content is highest at 45 – 60 cm depth. Organic matter content is relatively low (around 13%) in the gyttja layer (95 -130 cm depth) and high in the overlying peat layer (45-86%). The early Holocene gyttja has an extremely high calcite content of 60-70% on dry weight basis. The remainder of the soil profile has a much lower calcite content, but is still calcite rich, with a peak of more than 5% at 25-35 cm depth (Figure 4.7B). Similar calcite profiles were observed by Almendinger and Leete (1998) in calcareous fens in Minnesota.

Commonly, a large part of sulphur in peat soils is carbon bound, especially in humin and humic acids (Casagrande et al., 1980). To get indicative information of the location and amount of mineral S ( $S_{\min}$ ) accumulated in the profile, the total S content ( $S_{\text{tot}}$ ) of the soil samples (Table 4.2, Figure 4.7C) has to be corrected for organically bound S ( $S_{\text{org}}$ ). The C:S ratio of organic matter is largely dependent on the S content of fresh plant material and the level of decomposition. Based on Kirkby et al. (2011) and Parton et al. (1988) we assumed a C: $S_{\text{org}}$  ratio of 200:1 for non-decomposed peat in the profile and a C: $S_{\text{org}}$  ratio of around 100:1 for the upper 30 cm of the soil, which is slightly more decomposed. The value of 100:1 is consistent with the C:S ratio found in the topsoil of the precipitation lens at Mk2. When applied, this results in the  $S_{\min}$  profile as depicted in Figure 4.7C. The estimated  $S_{\min}$  profile is in line with the observed soil water chemistry and visual observations in the field, where a change from brown to black coloured sediment occurred at a depth of 45 cm. SEM-EDS analysis confirmed the presence of iron sulphide minerals in this part of the soil profile. Moreover, the difference between total iron  $Fe_{\text{tot}}$  and  $Fe_{\text{ox}}$  content, as a proxy for reducible iron (van Bodegom et al., 2003) (Figure 4.7A) is of the same order of magnitude as the estimated mineral sulphur content. In addition, the concentration of the trace elements nickel, zinc and arsenic (Figure 4.7D and Figure 4.7F), which are common constituents of iron sulphides, are in comparison with the lutum content (mineral particles < 2  $\mu\text{m}$ ) clearly elevated at 75-85 cm depth. This is in line with the estimated mineral sulphur profile and direction of flow.

Except for the gyttja layer and the topsoil, oxalate extractable phosphorous was below detection limit. Assuming all non-oxalate extractable P to be organic results in high C: $P_{\text{org}}$  ratios of 685:1 for the topsoil and values of around 1500:1 for the subsoil. The C: $P_{\text{org}}$  ratios of the soil correspond well with C:P ratios of fresh plant material as reported by Kemmers and Van Delft (2008) for the Meeuwenkampje reserve. Comparable C:P ratios were observed by Boyer and Wheeler (1989) in British spring fed calcareous fen soils with active calcite precipitation. The low phosphorous content of the peat can be explained by the absence of fertilisation and strong upward seepage of extremely phosphorous poor groundwater, together with a highly reactive calcareous gyttja layer at the base of the peat.

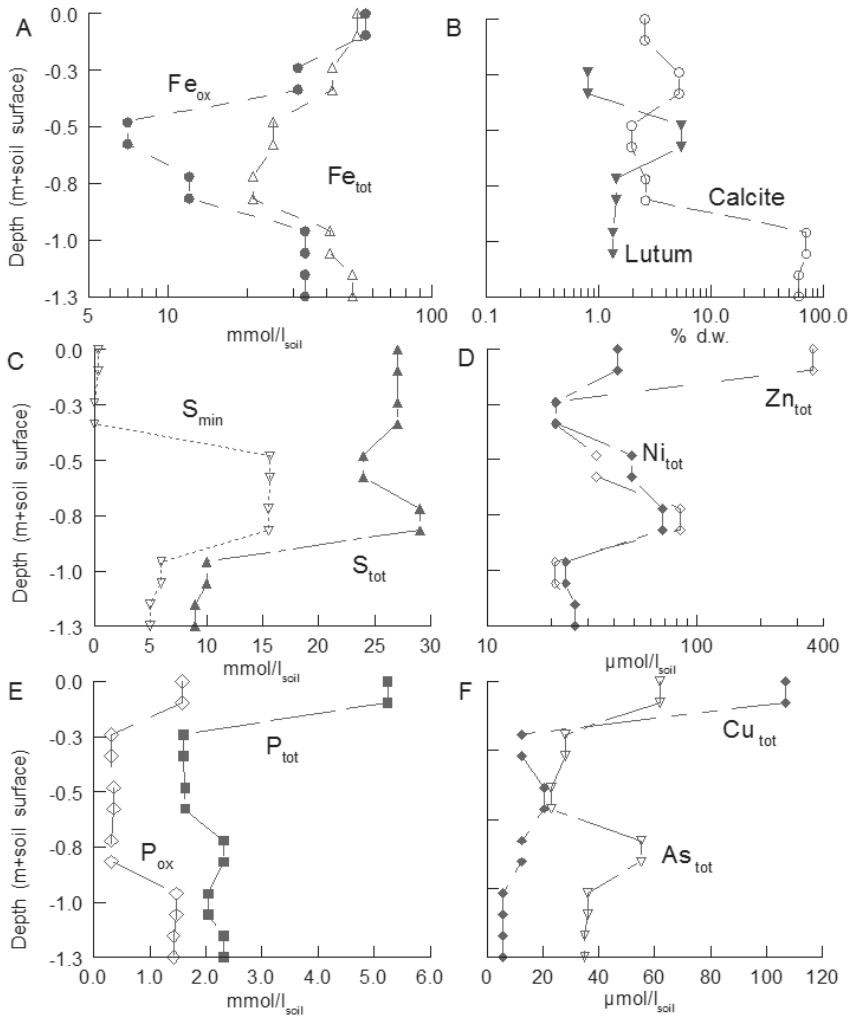


Figure 4.7. Soil quality profiles at Mk3.

**Table 4.2.** Characteristics of soil cores collected at Mk2 (precipitation lens) and Mk3 (seepage face).

	unit	depth (cm-soil surface)					
		0-10		25-35		50-60	
		Mk2	Mk3	Mk2	Mk3	Mk2	Mk3
CaCO <sub>3</sub>	(% d.w.)	0.9	2.6	0.9	5.2	0.3	2.0
Clay	(% d.w.)		2.4	2.4	0.8	1.7	5.5
Silt	(% d.w.)		11.8	14.8	4.4	8.8	23.3
Sand	(% d.w.)		11.7	60.1	3.6	82.8	24.4
Org. mat.	(% d.w.)	42.9	71.5	21.7	86.0	6.3	44.8
Dry bulk density	(kg/l)	0.381	0.212	0.313	0.195	0.728	0.217
Al <sub>ox</sub>	mg/kg	3420	3470	1400	2340	570	1660
Fe <sub>ox</sub>	mg/kg	10450	8995	3060	14795	335	1800
Mn <sub>ox</sub>	mg/kg	125	125	19	115	2.9	43
P <sub>ox</sub>	mg/kg		228		< 100		< 100
Al <sub>tot</sub>	mg/kg	7908	6949	3570	1782	4225	7314
Ca <sub>tot</sub>	mg/kg	9587	21626	7647	32632	2108	17414
Mg <sub>tot</sub>	mg/kg	655	694	299	251	504	1206
Mn <sub>tot</sub>	mg/kg	164	163	42	151	33.6	96
Fe <sub>tot</sub>	mg/kg	13579	13711	3143	11905	2364	6397
K <sub>tot</sub>	mg/kg	560	347	332	57	587	708
Na <sub>tot</sub>	mg/kg	126	298	70	280	30	217
Cu <sub>tot</sub>	mg/kg	19	32	3	4	2	6
Ni <sub>tot</sub>	mg/kg	15.3	12	6.7	6	3.4	13
Zn <sub>tot</sub>	mg/kg	62	110	7	7	3	10
As <sub>tot</sub>	mg/kg	15.8	22	3.79	11	1.22	8
P <sub>tot</sub>	mg/kg	452	764	91	255	65	232
S <sub>tot</sub>	mg/kg	2003	4233	894	4536	278	3628

Table 4.2 continued:

unit		depth (cm-soil surface)				
		75-85		100-110		120-130
		Mk2	Mk3	Mk2	Mk3	Mk3
CaCO <sub>3</sub>	(% d.w.)	0.2	2.6	0.2	70.8	60.8
Clay	(% d.w.)	0.8	1.4	0.9	1.3	2.5
Silt	(% d.w.)	1.8	6.9	2.5	7.2	12.0
Sand	(% d.w.)	96.1	7.3	95.9	7.5	11.9
Org. mat.	(% d.w.)	1.1	81.8	0.5	13.2	12.8
Dry bulk density	(kg/l)	1.240	0.193	1.563	0.346	NA
Al <sub>ox</sub>	mg/kg	175	1550	180	435	435
Fe <sub>ox</sub>	mg/kg	61	3480	61	5340	5365
Mn <sub>ox</sub>	mg/kg	2.4	69	2.2	150	140
P <sub>ox</sub>	mg/kg		< 100		131	127
Al <sub>tot</sub>	mg/kg	2139	3406	2188	1308	1592
Ca <sub>tot</sub>	mg/kg	771	21128	736	285122	250493
Mg <sub>tot</sub>	mg/kg	402	640	429	1715	1708
Mn <sub>tot</sub>	mg/kg	25.5	104	26.2	450	438
Fe <sub>tot</sub>	mg/kg	1640	5934	1610	6561	8010
K <sub>tot</sub>	mg/kg	320	223	322	165	195
Na <sub>tot</sub>	mg/kg	19	389	25	178	159
Cu <sub>tot</sub>	mg/kg	1	4	1	1	1
Ni <sub>tot</sub>	mg/kg	2.7	21	2.4	4	4
Zn <sub>tot</sub>	mg/kg	3	28	3	4	5
As <sub>tot</sub>	mg/kg	0.9	22	0.89	8	8
P <sub>tot</sub>	mg/kg	55	371	59	182	207
S <sub>tot</sub>	mg/kg	128	5190	84	1047	954

## Discussion

### Redistribution of sulphur and carbonate on a regional scale

Based on the hydrochemical facies analysis of the area by Beemster et al. (2002) the observed water quality in the observation wells P1\_1 and P3\_2, can be regarded as representative for anthropogenically influenced groundwater above the Eemian clay layer. We used the Eq. (4.1) to (4.7) in combination with our observations to discuss possible sources of the elevated sulphate concentrations, hardness and alkalinity and test whether our findings are in agreement with the literature.

An important source of sulphate in Dutch groundwater used to be atmospheric deposition. Peak atmospheric deposition in the 1970s and 1980s in combination with fertilisers containing sulphur can account for an average  $\text{SO}_4^{2-}$  concentration of up to 0.6 mmol/l in shallow groundwater under Dutch agricultural fields (Oenema, 1999). However, the observed average sulphate concentration at P1\_1 is about twice as high (1.2 mmol/l) and even higher at P3\_2 (1.72 mmol/l) and at Mk3 ( $> 2$  mmol/l). Such high sulphate concentrations cannot be explained by air pollutant deposition and fertilization alone, indicating an additional source (Van Beek et al., 2001). Dissolution of gypsum can be ruled out, as this mineral is not present in Dutch soils. The actual occurrence of pyrite rich sand in the subsoil of the former bog area however, is confirmed by observations of Poelman (1972). Moreover, samples with high sulphate concentrations taken at Mk3 and Mk4, also contain nickel which is a common constituent of pyrite.

In line with Beemster et al. (2002), Mendizabal et al. (2012), Smolders et al. (2010), Van Beek et al. (2001) and Zhang et al. (2009) we therefore hypothesize that oxidation of pyrite by oxygen and nitrate (Eq. (4.1) and (4.2)) can be indeed an additional, and presumably major, source of sulphate in our field setting. For example, oxygen dissolved in infiltrating rainwater (0.35 mmol/l at 10 °C,  $P_{\text{O}_2}=0.2$  atm) can in theory be accountable for a maximum of 0.19 mmol/l  $\text{SO}_4^{2-}$  (Eq. (4.1)). Infiltrating nitrate can even 'produce' up to 2.7 mmol/l  $\text{SO}_4^{2-}$  (Eq. (4.2)), assuming a representative nitrate concentration between 0.3 and 4.0 mmol/l for infiltrating shallow groundwater under Dutch agricultural fields (Oenema, 1999).

Oxidation of pyrite results, as mentioned, in the production of protons, which in turn may lead to dissolution of calcite (if present). The plausibility of the dissolution by strong acid can be assessed qualitatively using index parameters as proposed by van Helvoort et al. (2007). For instance the ratio between  $(\text{Ca}^{2+} + \text{Mg}^{2+})$  and  $\text{HCO}_3^-$  may indicate whether calcite is dissolved by  $\text{CO}_2$  (produced by root respiration and/or mineralisation) or by a strong acid. Dissolution by  $\text{CO}_2$  will result in a  $(\text{Ca}^{2+} + \text{Mg}^{2+})/\text{HCO}_3^-$  ratio of 0.5 (Eq. (4.3)); dissolution by a strong acid in a 1:1 ratio (Eq. (4.4)). For piezometer P1\_1, we found an average ratio of 0.6 which is slightly higher than expected when assuming dissolution by  $\text{CO}_2$ . However, reduction processes (i.e. Eq. (4.5), (4.6) and (4.7)) produce additional  $\text{HCO}_3^-$ , which influences this ratio and makes dissolution by  $\text{CO}_2$  only, less

likely. Moreover, the average  $\text{Ca}^{2+}$  concentration observed at P1\_1 (5.74 mmol/l) and P3\_2 (5.45 mmol/l) is about 2.5 times higher than expected from Eq. (4.10), even when assuming a  $P_{\text{CO}_2}$  of  $10^{-1.5}$  atm in the soil of the infiltration area, which is near the upper limit for respiration and organic matter degradation (Appelo and Postma, 2005). The observed elevated  $\text{Ca}^{2+}$  concentration of the anthropogenically-influenced groundwater can thus be attributed to dissolution of calcite by strong acid.

$$m_{\text{Ca}^{2+}} = \sqrt[3]{10^{-5.8} * (P_{\text{CO}_2} / 4)} \quad 4.10$$

Our observations at P1\_1 and P3\_2 show a rather low  $\text{SO}_4^{2-}/(\text{Ca}^{2+}+\text{Mg}^{2+})$  ratio compared to the stoichiometry of Eq. (4.1) and (4.2) in combination with Eq. (4.4) (pyrite oxidation and dissolution of calcite). This excess hardness may be explained by contributions of calcite dissolved by  $\text{CO}_2$ , fertilisation related strong acid (e.g. calcium ammonium nitrate) or acid related to atmospheric deposition of nitrous oxides. However, it may also point to partial  $\text{SO}_4^{2-}$  reduction along the hydrological pathway and thus to originally even higher  $\text{SO}_4^{2-}$  levels. Given the even higher sulphate concentrations measured in the field transect, the occurrence of peat layers in the cover sand deposits upstream of P1\_1 (Figure 4.3) and the observed high alkalinity in relation to hardness, we consider the latter a plausible explanation.

Our hypothesis for the chemical evolution of the groundwater flowing towards the reserve is summarized in Figure 4.8: pyrite is oxidized by oxygen and/or nitrate infiltrated in the agricultural recharge area to the northeast of the reserve, resulting in strongly elevated sulphate concentrations in the groundwater (zone 1). Acid produced in this processes dissolves calcite, resulting in high calcium and bicarbonate levels. During transport, part of the sulphate may be reduced in local peat layers, producing extra alkalinity, which may result in super saturation with respect to calcite (zone 2). The hydraulic gradient of the regional groundwater system forces the sulphate rich, calcareous groundwater upward to the nature reserve (zone 3).

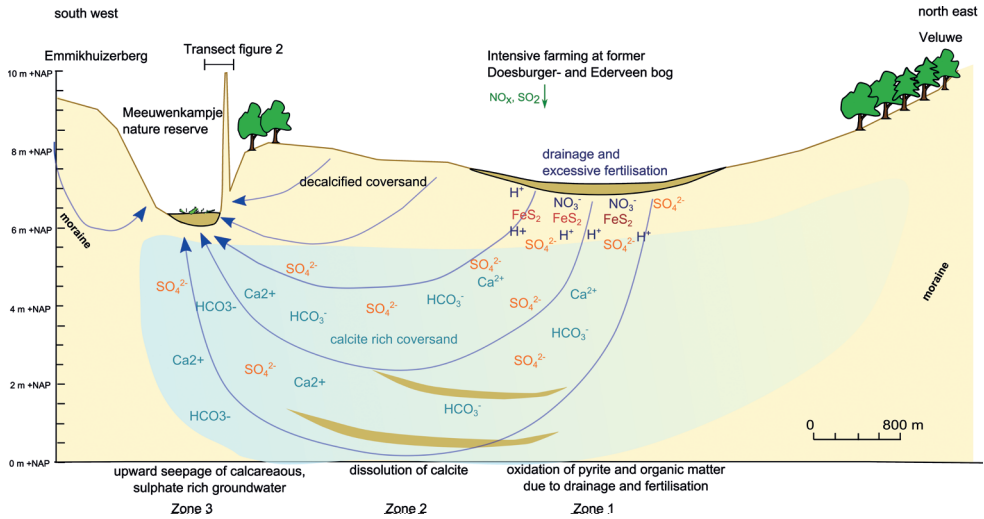


**Figure 4.8.** Conceptual model of redistribution of sulphur and carbonate minerals along the hydrological pathway. Distribution of the calcite rich sand is based on drilling records abstracted from the database on the Dutch subsurface ([www.dinoloket.nl](http://www.dinoloket.nl)). The indicative location of the pyrite in the recharge area is based on Poelman (1972).

### Water quality changes during passage of the organic top layer.

When seeping upward through the organic top-layer in the reserve, the chemical composition of the sulphate rich, calcareous groundwater changes significantly. Since Mk1 is regularly influenced by inundation from an adjacent agricultural ditch, and Mk2 contains a small rainwater lens, we focus on Mk4 and especially Mk3 to illustrate this chemical transformation.

Sulphate concentrations were observed to decline strongly in the direction of flow at Mk3 and Mk4 (Figure 4.4). The decline at Mk4 and especially Mk3 (see Figure 4.6A) is most conveniently explained by the occurrence of sulphate reduction and subsequent formation of iron sulphides (Eq. (4.7), (4.8) and (4.9)), which are common processes in wet organic rich soils. Precipitation of gypsum, as an alternative process, could be ruled out due to undersaturation of all samples with respect to this mineral. Adsorption of sulphate to metal oxides surfaces is possible, but very limited at near neutral pH conditions (Ali and Dzombak, 1996; Appelo, 2000; Geelhoed et al., 1997). Adsorption to metal oxide surfaces is therefore not considered a plausible alternative explanation for the observed decline of sulphate. Moreover the almost complete reduction of sulphate from soil solution is consistent with the observed reducible iron profile (Figure 4.7A), the estimated inorganic S profile (Figure 4.7C) and the profiles of trace elements Ni, As and Zn (Figure 4.7D and Figure 4.7F). The occurrence of iron sulphides in this part of the profile was confirmed by a SEM-EDS analysis. The Fe concentrations (Figure 4.6E) in

the range of 0.1-0.2 mmol/l can be explained by simultaneous reduction of iron oxides and sulphate, which is possible in an environment rich in iron oxides (Postma and Jakobsen, 1996). Our measurements of reducible iron content in the soil cores (Figure 4.7A), confirm such an environment.

Reduction of sulphate is strongly dependent on anaerobic decomposition of organic matter, because low molecular weight organic compounds produced during fermentation, are crucial as an energy source for sulphate reducing bacteria (Wiebe, 1981). Anaerobic decomposition of organic material and reduction processes, will not only result in the production of alkalinity (Eq. (4.5)-(4.7)) (Figure 4.6B), but in the formation of  $\text{NH}_4^+$ ,  $\text{HPO}_4^{2-}$  and dissolved organic carbon (DOC) as well. The observed increase in soil water DOC and simultaneous decrease of sulphate in the (upward) flow direction (Figure 4.6A) support these decomposition and reduction processes. Based on Eq. (4.5)-(4.7) also an increase is to be expected for  $\text{HCO}_3^-$ , but the early March 2009 observations (Figure 4.5) show a decline in  $\text{HCO}_3^-$  over the profile and the September 2008 observations, first show a decline, followed by an increase in  $\text{HCO}_3^-$  in the direction of flow.  $\text{HCO}_3^-$  concentrations dynamics are thus not only controlled by the processes discussed here, but by some other factors as well.

The profile at Mk3 can be divided into two distinct zones with respect to  $\text{Ca}^{2+}$  and  $\text{HCO}_3^-$  (Figure 4.6B). The steep decline of both  $\text{Ca}^{2+}$  and  $\text{HCO}_3^-$  in the lower part of the profile (75 -100 cm depth) can be explained by over-saturation with respect to calcite of the inflowing water (Figure 4.6C) and rapid equilibration due to calcite precipitation. This is promoted by the very high calcite content (up to 71 % of dry weight, Figure 4.7B) of the gytija deposits in this part of the profile. Precipitation of calcite will occur when a critical (super)saturation level is exceeded. However, if crystallization surfaces are available, nucleation will occur at lower saturation levels (Stumm and Morgan, 1996). The large amount of calcite in the gytija at MK3 provides a large reactive surface area, kinetically enhancing calcite precipitation.

Above the gytija layer, soil moisture is at equilibrium with calcite ( $-0.1 < \text{SI}_{\text{calcite}} < 0.1$ ). In this part of the profile, alkalinity is produced due to anaerobic decomposition of organic matter (Eq. (4.5)-(4.7)). The continuing addition of carbon to the water phase due to decomposition of organic matter, explains the increase of  $\text{HCO}_3^-$  and a decrease of  $\text{Ca}^{2+}$  due to precipitation of calcite when over saturation occurs. The occurrence of substantial amounts of calcite in the peat overlying the gytija layer (Figure 4.7B) provides evidence that active calcite precipitation has taken place. In addition, the observed pH values (Figure 4.6B) show a slight decrease in the direction of flow, which is consistent with calcite precipitation (see Eq. (4.4)). As calcite precipitation here is governed by the production of alkalinity, the calcite precipitation rate is governed by the sulphate reduction rate and ultimately by the fermentation rate of organic matter. Observed pH values are very stable over time up to 25 cm depth. At this depth, the time averaged pH value increases and shows more variation over time. Highest pH and related rise of  $\text{HCO}_3^-$  and  $\text{SI}_{\text{calcite}}$  at the upper sampling point appeared to occur during summer.

Possibly, outgassing of  $\text{CO}_2$ , as observed by Almendinger and Leete (1998) in similar fens, causes this pH increase.

The hypothesis of organic matter fermentation constraining the observed processes was tested by modelling sulphate reduction and calcite and iron sulphide precipitation in the upper (mainly organic) part of the profile with PhreeqC (Parkhurst and Appelo, 1999). We stepwise added organic carbon ( $\text{CH}_2\text{O}$ ) to the time averaged water composition as observed right above the gyttja layer at 75 cm depth. In the model setup, a large amount of iron oxides (goethite) was assumed to be present and  $\text{FeS}$  and calcite were able to precipitate. Our analysis showed that this simple system and the addition of  $\text{CH}_2\text{O}$  to the water phase were able to explain the evolution of the upward flowing groundwater in the peat layer at MK3. Considering the use of standard database constants, modelled and observed concentrations of sulphate,  $\text{Ca}^{2+}$  and  $\text{HCO}_3^-$  match very well (Figure 4.9). Results indicated the likeliness of simultaneous iron oxide and sulphate reduction, the precipitation of iron sulphides and the precipitation of calcite. Modelled hydrogen sulphide appears only at very low concentrations in the water phase because of excess iron and precipitation of iron sulphides.

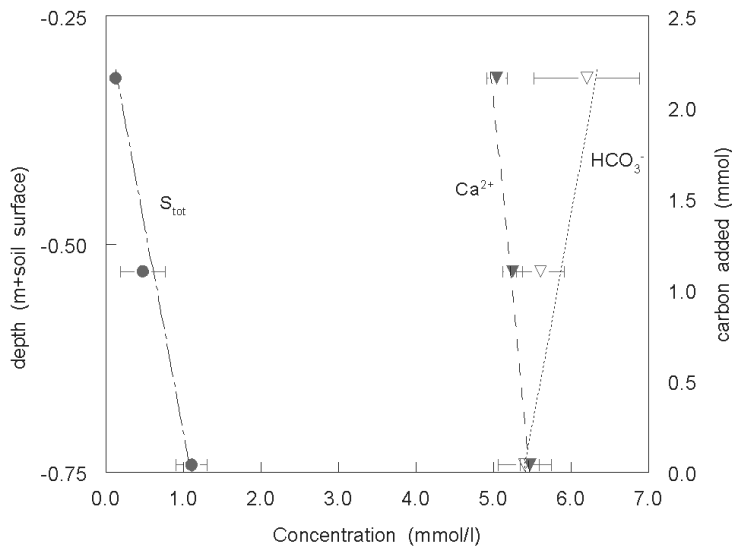


**Figure 4.9.** Development of Sulphate,  $\text{Ca}^{2+}$  and  $\text{HCO}_3^-$  concentrations in the Mk3 profile as modelled with PhreeqC (standard database) using stepwise addition of organic carbon ( $\text{C}_{\text{org}}$ ) in a system closed to with respect to  $\text{CO}_2$ . Symbols and error bars denote time averaged observed concentrations and temporal variation, lines denote concentrations modelled with PhreeqC.

## Internal eutrophication

Sulphate reducing bacteria are dependent on intermediate products of organic matter fermentation, such as lactate, as a source of energy. The process of fermentation of organic matter not only releases inorganic carbon, but also DOC and nutrients like  $\text{NH}_4^+$  and  $\text{PO}_4^{3-}$ . This release of nutrients is commonly referred to as ‘internal eutrophication’, and may lead to deterioration of natural vegetation of nutrient-poor sites. Although organic matter decomposition and iron oxide reduction was apparent at Mk3, no elevated phosphate concentrations were observed. Both  $\text{P}_{\text{tot}}$  and  $\text{P-PO}_4$  concentrations were low, with maximum observed values of 1.58 and 0.9  $\mu\text{mol/l}$  respectively, especially when compared to adequate P concentrations for optimal plant growth (Hinsinger, 2001). The observed values were in line with the findings of Kemmers and Van Delft (2008), who identified phosphorous as growth limiting nutrient for the vegetation of the Meeuwenkampje.

Several processes may be responsible for the low phosphate concentration found in soil solution at MK3. Phosphate, for instance, can co-precipitate with calcite. According to Plant and House (2002), calcite precipitation is not hampered by phosphate incorporation as long as the phosphate concentration in solution is less than 20  $\mu\text{mol/l}$ , which is the case in our soil. Use of regression data on co-precipitation rate and phosphate concentration data from several laboratory and field studies (Danen-Louwerse et al., 1995), yields an incorporation rate of 2.36  $\mu\text{mol P-PO}_4^{2-}$  per mmol Ca precipitated for the highest observed  $\text{P-PO}_4^{2-}$  concentration of 0.9  $\mu\text{mol/l}$ . Besides incorporation in freshly precipitated calcite minerals, phosphate can adsorb both electrostatically and chemically to calcite surfaces already present in the soil (Karageorgiou et al., 2007). Given the very low saturation indexes ( $< -5$ ), direct precipitation of phosphate as hydroxyapatite is not likely.

Another important sink for phosphate is adsorption to clay or metal oxides. As shown by Weng et al. (2011), adsorption of phosphate to metal oxide surfaces, in presence of organic acids and  $\text{Ca}^{2+}$ , is strongest at neutral pH. Weng et al. (2011) attributed this to the synergistic effect of  $\text{Ca}^{2+}$  adsorption, which strongly increases phosphate adsorption and governs to a large extent the pH dependency. Another perhaps more likely explanation for the low phosphate concentrations is simply an extremely low phosphate content of the deposited organic matter. Boyer and Wheeler (1989) found an extremely low P content in plant material from fen sites with a calcite rich soil. Given the range of our observed C:P ratios (685:1 to even 1500:1) and the low values for oxalate extractable P, this is the most likely explanation for the low phosphate concentrations in our soil solution at Mk3. Since the phosphorous content of the soil samples is extremely low (Figure 4.7E), only small amounts of phosphorous can be released during decomposition of organic material or reduction of metal oxides. Based on the results of the PhreeqC model (Figure 4.9), 2.26 mmol C is needed for reduction of sulphate and iron oxides and precipitation of FeS. Taking this amount of carbon and the observed (weight) C:P ratio of 1500:1 results in the release of only 0.6  $\mu\text{mol P}$ . Combined with active precipitation of

calcite and large amounts of reducible iron, this implies very low availability of phosphorous in the profile. Decomposition of organic matter will, in our case, thus not lead to internal eutrophication due to release of phosphate.

Ammonium, another nutrient linked to internal eutrophication, was counter intuitively observed to decline in the direction of flow (Figure 4.6F). As there is active sulphate reduction, this decrease cannot be caused by nitrification, because nitrification needs the presence of oxygen (Goreau et al., 1980; Regina et al., 1996). Moreover nitrite and nitrate concentrations measured as N-(NO<sub>3</sub>+NO<sub>2</sub>) remained below detection limit. We presume that physical adsorption to organic matter or clay as proposed by Triska et al. (1994) is, given the above, a more likely explanation.

### **Sustainability of the Meeuwenkampje alkaline fen**

Sulphate reduction will continue as long as sulphate rich groundwater enters the soil profile. Given the very low phosphate content of the soil and the occurrence of active precipitation of calcite, internal eutrophication is not likely to become a problem. For now, the reduction of sulphate did not result in phytotoxic levels of sulphides, due to the presence of a large amount of reducible iron in the soil. However, without further supply the amount of reducible iron in the soil is limited (Figure 4.7A), and iron oxides present in the soil will eventually be transformed into iron sulphides. An important question for the conservation of the fen is for how long sulphide levels will remain low. A rough estimate can be obtained by comparing the amount of reducible iron and the influx of sulphate rich groundwater according to the stoichiometry of Eq. (4.8). The amount of reducible iron left in the zone where sulphate reduction takes place (45 - 90 cm – soil surface), equals on average 10 mmol/l soil. Although groundwater sulphate concentrations might vary on longer timescales, we assume the sulphate concentration of the inflowing groundwater to be stable at a concentration of 2 mmol/l, which we consider a conservative estimate. Based on regional geohydrological model calculations with SIMGRO according to Cirkel (2010) and calculations by Jansen and Kemmers (1995) the average upward flux at Mk3 can range between 1 and 3 mm/d. Based on these values, the amount of reducible iron in the sulphate reduction zone is estimated to last for the next 15 – 40 years. In addition, above 45 cm depth, large amounts of reducible iron are present in the soil, providing an extra buffer against sulphide toxicity. Sulphide toxicity is thus not likely to be of concern in the near future.

Due to accumulation of sulphides in the soil, the system will become increasingly vulnerable to hydrological changes (Schiff et al., 2005). Decline of local groundwater levels due to drainage, groundwater abstraction or climate change, will result in oxidation of organically bound sulphur and of accumulated iron sulphides, which result in elevated sulphate concentrations and acidification, and by consequence in dissolution of calcite. This stresses the importance of fine-tuned water management in this fen ecosystem. However, to gain better quantitative insight to the vulnerability of the system, a more detailed analysis of different sulphide species in the soil is needed.

## Synthesis and conclusions

In this chapter, we discussed the biogeochemical effects of upward seepage of calcite saturated and sulphate rich groundwater through an organic fen soil. Inflow of sulphate rich groundwater into the organic wetland soil of the studied fen resulted in decomposition of organic matter and reduction of sulphate. These observations are consistent with those of others e.g. Jørgensen (1977), Lamers et al. (2001), as well as with a recent scheme proposed by Smolders et al. (2010) that illustrates the eutrophying and phytotoxic effects of sulphate originating from upstream pyrite oxidation, on downstream wetland nature reserves.

However, we hypothesised that upstream excessive fertilisation and pyrite oxidation as a source of sulphate, not only leads to elevated sulphate concentrations as proposed by Smolders et al. (2010), but to acid production and dissolution of carbonate minerals as well. Dissolution of calcite is reflected in the observed high calcium and bicarbonate concentrations accompanying the high sulphate concentration in upward seeping groundwater. When this upwelling groundwater enters the organic topsoil of the Meeuwenkampje fen, a reversal of chemical processes occurs: sulphate reduction with accompanying production of hydrogen sulphide and alkalinity. The produced hydrogen sulphide precipitates as iron sulphides (pyrite), while the produced alkalinity results in the precipitation of calcite. The resulting calcareous conditions in combination with high and stable groundwater levels are beneficial for a wide range of rare and endangered plant species (ŠefferoVá Stanová et al., 2008; Wheeler, 1980).

We also showed, that the degree of internal eutrophication by phosphorous is highly dependent on the C:P ratio of the organic material present in the soil and the amount of phosphorous adsorbed to oxide surfaces. Supply of dissolved phosphorous by upward seeping groundwater is generally small due to the low mobility of inorganic phosphorous (Hinsinger, 2001). For this reason, the soil phosphorous content is generally minimal in unfertilized groundwater fed areas. This reduces the risk of internal eutrophication due to sulphate-reduction induced decomposition of organic matter and/or reduction of iron(hydr)oxides. For conditions resembling the Meeuwenkampje, where active calcite precipitation occurs, co-precipitation with phosphate, and phosphate adsorption by calcite further inhibits the bioavailability of released phosphate (Boyer and Wheeler, 1989) and reduces the risk of internal eutrophication.

The reduction of sulphate produces sulphide which, as has been shown in various studies, is phytotoxic. Mostly, however, these studies concern peat soils that receive water from adjacent streams or ditches. The content of iron(hydr)oxides of these soils is therefore often low and insufficient to immobilize sulphides as iron sulphide minerals. However, organic soils in groundwater fed areas with a mineral subsoil, can contain large amounts of iron(hydr)oxides reducing the risk of phytotoxic sulphide levels. The analysed soil profile in the Meeuwenkampje site, for instance, contains enough iron(hydr)oxides to effectively immobilize sulphides.

In this chapter, we have explained the underlying biochemical processes maintaining the wet, calcareous and nutrient poor conditions and consequently high conservation values of the Meeuwenkampje site. In the literature, sites resembling the Meeuwenkampje reserve are mentioned for which our findings may be of interest. Our observations might for instance provide an (additional) explanation for active calcite precipitation as observed in pristine alkaline fens in Slovakia (Grootjans et al., 2005), Minnesota (Almendinger and Leete, 1998) or fossil pyrite-calcite stratifications in former seepage fed alkaline fens in the Netherlands (Van Delft et al., 2010). Moreover, our observations stress the importance of fine-tuned water management in these precious, but globally rare and threatened ecosystems. Since it is very likely that climate change will alter the diversity of plant species and plant communities through changes in the water cycle (Witte et al., 2012), knowledge of the hydro chemical functioning of these ecosystems will become increasingly important.

### **Acknowledgements**

This manuscript benefited significantly from the valuable comments of three anonymous reviewers. The study was carried out within the framework of the Netherlands Organisation for Scientific Research (NWO) CASIMIR programme (018.002.007), the Dutch Water Utility Sector joint research programme (BTO) and the Knowledge for Climate programme theme 2.

## Appendix 4.A. Time averaged soil water quality Meeuwenkampje

MR = MacroRhizon

MF = Minifilter

	type	depth	pH	EGV	Cl mmol/l	Na mmol/l	K mmol/l	Ca mmol/l	Mg mmol/l	Fe mmol/l	Mn mmol/l	DOC mmol/l	TIC mmol/l
surf. water	MR	-	7.08	431	0.71	0.59	0.09	2.19	0.23	0.033	0.006	1.65	4.69
Mk1	MR	25-35	6.43	700	2.01	1.26	< 0.015	3.68	0.22	0.004	0.000	1.01	5.05
	MR	50-60	6.45	688	1.80	1.27	< 0.015	3.65	0.22	0.005	0.003	0.73	4.90
	MR	75-85	6.45	651	1.57	1.23	< 0.015	3.35	0.22	0.017	0.008	0.61	4.61
	MR	100-110	6.54	595	1.36	1.16	< 0.015	3.07	0.20	0.006	0.006	0.58	4.40
Mk2	MR	25-35	6.14	167	0.29	0.07	< 0.015	1.16	0.01	0.063	0.001	4.45	2.12
	MR	50-60	6.12	151	0.24	0.05	< 0.015	1.04	0.02	0.091	0.001	3.54	2.30
	MR	75-85	5.90	143	0.14	0.02	< 0.015	0.94	0.02	0.031	0.001	3.18	2.28
	MR	100-110	5.96	147	0.15	0.02	< 0.015	0.94	0.02	0.034	0.001	2.94	2.27
Mk3	MF	120-125	7.26	277	0.89	0.24	< 0.015	1.49	0.06	0.022	0.003	2.12	1.33
	MR	25-35	6.90	854	2.78	1.21	< 0.015	5.04	0.14	0.163	0.012	2.53	8.85
	MR	50-60	6.62	907	2.79	1.31	< 0.015	5.24	0.17	0.159	0.011	2.11	8.88
	MR	75-85	6.72	951	2.87	1.41	< 0.015	5.46	0.20	0.099	0.009	1.38	8.07
Mk4	MR	100-110	6.83	1073	1.57	1.74	< 0.015	6.36	0.28	0.081	0.010	1.14	8.23
	MR	25-35	6.60	623	1.56	1.51	< 0.015	3.20	0.23	0.110	0.006	1.29	7.12
	MR	50-60	6.79	664	1.63	1.54	< 0.015	3.49	0.28	0.038	0.004	1.06	7.28
	MR	75-85	6.90	685	1.66	1.58	< 0.015	3.57	0.33	0.040	0.004	1.34	7.20
	MR	100-110	7.05	714	0.91	1.52	< 0.015	3.74	0.48	0.055	0.005	1.03	6.74
	MF	120-125	7.48	656	1.67	1.59	< 0.015	3.58	0.34	0.013	0.005	1.03	5.87

	type	depth	pH	EGV	Cl mmol/l	Na mmol/l	K mmol/l	Ca mmol/l	Mg mmol/l	Fe mmol/l	Mn mmol/l	DOC mmol/l	TIC mmol/l
surf. water	MR	-	7.08	431	0.71	0.59	0.09	2.19	0.23	0.033	0.006	1.65	4.69
Mk1	MR	25-35	6.43	700	2.01	1.26	< 0.015	3.68	0.22	0.004	0.000	1.01	5.05
	MR	50-60	6.45	688	1.80	1.27	< 0.015	3.65	0.22	0.005	0.003	0.73	4.90
	MR	75-85	6.45	651	1.57	1.23	< 0.015	3.35	0.22	0.017	0.008	0.61	4.61
	MR	100-110	6.54	595	1.36	1.16	< 0.015	3.07	0.20	0.006	0.006	0.58	4.40
Mk2	MR	25-35	6.14	167	0.29	0.07	< 0.015	1.16	0.01	0.063	0.001	4.45	2.12
	MR	50-60	6.12	151	0.24	0.05	< 0.015	1.04	0.02	0.091	0.001	3.54	2.30
	MR	75-85	5.90	143	0.14	0.02	< 0.015	0.94	0.02	0.031	0.001	3.18	2.28
	MR	100-110	5.96	147	0.15	0.02	< 0.015	0.94	0.02	0.034	0.001	2.94	2.27
Mk3	MF	120-125	7.26	277	0.89	0.24	< 0.015	1.49	0.06	0.022	0.003	2.12	1.33
	MR	25-35	6.90	854	2.78	1.21	< 0.015	5.04	0.14	0.163	0.012	2.53	8.85
	MR	50-60	6.62	907	2.79	1.31	< 0.015	5.24	0.17	0.159	0.011	2.11	8.88
	MR	75-85	6.72	951	2.87	1.41	< 0.015	5.46	0.20	0.099	0.009	1.38	8.07
Mk4	MR	100-110	6.83	1073	1.57	1.74	< 0.015	6.36	0.28	0.081	0.010	1.14	8.23
	MR	25-35	6.60	623	1.56	1.51	< 0.015	3.20	0.23	0.110	0.006	1.29	7.12
	MR	50-60	6.79	664	1.63	1.54	< 0.015	3.49	0.28	0.038	0.004	1.06	7.28
	MR	75-85	6.90	685	1.66	1.58	< 0.015	3.57	0.33	0.040	0.004	1.34	7.20
	MR	100-110	7.05	714	0.91	1.52	< 0.015	3.74	0.48	0.055	0.005	1.03	6.74
	MF	120-125	7.48	656	1.67	1.59	< 0.015	3.58	0.34	0.013	0.005	1.03	5.87





## CHAPTER

# 5

### **The influence of spatiotemporal variability and adaptations to hypoxia on empirical relationships between soil acidity and vegetation**

This chapter is a slightly modified version of the published manuscript:

**Cirkel, D.G., J.P.M. Witte, P.M. van Bodegom, J.J. Nijp & S.E.A.T.M. van der Zee (2014) How moisture regime and spatiotemporal variability shape empirical relationships between soil acidity and vegetation. *Ecohydrology* 7(1) 21-32 doi: 10.1002/eco.1312**

## Abstract

Soil acidity is well known to affect the species composition of natural vegetation. The physiological adaptations of plants to soil acidity and related toxicity effects and nutrient deficiencies are, however, complex, manifold and hard to measure. Therefore, generally applicable quantifications of mechanistic plant responses to soil acidity are still not available. An alternative is the semi-quantitative and integrated response variable 'indicator value for soil acidity' ( $R_m$ ). Although relationships between measured soil pH and  $R_m$  from various studies are usually strong, they often show systematic bias and still contain high residual variances. On the basis of a well-documented national dataset consisting of 91 vegetation plots and a dataset with detailed, within plot, pH measurements taken at three periods during the growing season, it is shown that strong spatiotemporal variation of soil pH can be a critical source of systematic errors and statistical noise. The larger part of variation however, could be explained by the moisture status of plots. For instance Spearman's rho's decreased from 93% for dry plots and 87% for moist plots, to 59% for wet plots. The loss of relation between soil pH and  $R_m$  in the moderately acid to alkaline range at increasingly wetter plots is probably due to the establishment of aerenchyma containing species, which are able to control their rhizosphere acidity. Adaptation to one site factor (oxygen deficit), apparently may induce indifference for other environmental factors ( $Fe^{2+}$ , soil pH). For predictions of vegetation response to soil acidity, it is thus important to take the wetness of plots into account.

## Introduction

Soil acidity is well known to affect vegetation composition (Ellenberg et al., 1991; Roem and Berendse, 2000; Witte et al., 2007). As early as the 1920s it was, after some dispute, recognized that soil acidity is of fundamental importance in controlling the distribution of plant species (Atkins, 1921; Wherry, 1922). However, relations between soil acidity and plants have for long remained descriptive, distinguishing for instance calcifuge and calcicolous plant communities (e.g. Fitter and Hay (2001)). Some first attempts to systematically unravel the complex response of plants to soil acidity were made in the 1960s for instance by Clymo (1962) and Grime (1963), yielding interesting findings on pH-controlled availability of toxic dissolved aluminium (Al) and deficiencies of phosphorus (P) and ferric iron ( $Fe^{3+}$ ). Over the last decades, the knowledge of soil chemistry and plant physiology increased substantially, which yielded insights in direct and indirect effects of soil acidity on plants. Although low pH is by itself toxic to plants, direct plant responses to protons ( $H^+$ ) are probably limited to organic soils lacking buffering by feldspar weathering (Kidd and Proctor, 2001). In mineral soils indirect effects prevail, such as Al, manganese (Mn) and Fe toxicity and P, calcium (Ca), magnesium (Mg) and potassium (K) deficiencies (Poozesh et al., 2007).

Adaptations of plants to high and low soil pH involve complex biochemical, physiological and mutualistic pathways, allowing adapted species to survive harsh chemical environments. Adaptations to acid mineral soils include root-induced changes in the rhizosphere, such as pH increase, release of chelators for Al, higher activity of ectoenzymes (acid phosphatases), and increase in root surface area via mycorrhiza (Marschner, 1991). Adaptations to alkaline conditions include pH decrease by excretion of protons to acidify the surrounding solution, reduction of  $\text{Fe}^{3+}$  to  $\text{Fe}^{2+}$  by  $\text{Fe}^{3+}$ -chelate reductase, changes in root morphology, increase of citrate concentrations in the phloem and alkaline phosphatases. Grasses release phytosiderophores (PS) to chelate  $\text{Fe}^{3+}$  in the rhizosphere and import the  $\text{Fe}^{3+}$ -PS complexes (Duff et al., 1994; Guerinot, 2001; Hell and Stephan, 2003; Römheld, 1991).

The last two decades have seen a movement towards quantifying and predicting plant strategies and the role of functional characteristics, or traits, therein. Conceptualizations of plant strategy schemes are manifold (e.g. Diaz et al. (2004), Grime (1977), Westoby (1998)) However, most only identify resource supply (water, light and nutrients) and disturbance as the main forces driving plant strategy selection in space and time. Generally applicable quantifications of plant responses to soil acidity are currently lacking, but urgently needed to allow full inclusion of soil acidity in plant strategy schemes. However, physiological adaptations of plants to soil acidity are often hard to measure or unclear. An alternative is the use of a semi-quantitative species based 'indicator value' (Ellenberg et al., 1991; Landolt, 1977). The use of indicator values is often criticized because they are based on experience rather than systematically derived from precise measurements (Dierschke, 1994; Økland, 1990). Nonetheless indicator values enjoy great popularity simply because they appear to reflect habitat quality so surprisingly well (Diekmann, 2003). Species based indicator values (i.e. the environmental preferences of species) can be aggregated for many species (whole communities) and therefore are likely to be more robust than the attributes of single species (Scherrer and Körner, 2011). The 'indicator value for acidity' ( $R_m$ ) can be seen as an integrated variable for the coordinated response of multiple traits to soil acidity controlled biogeochemical processes (Violle et al., 2007) and scales species responses to acidity based on expert knowledge.

Although the exact meaning of  $R_m$  is unclear, relating  $R_m$  to soil pH generally results in strong relationships (Diekmann, 1995; Dzwonko, 2001; Schaffers and Sýkora, 2000). However, also these relations contain a high residual variance (Diekmann, 2003). Three possible sources of uncertainty may explain this variance: (1) plants are indifferent to direct and indirect effects of soil pH for a wide range of soil pH values (2) large spatial heterogeneity in soil pH and (3) large temporal variation of soil pH occurs within plots. Although these explanations have been partly mentioned in literature, a structural analysis of the causes of variation is lacking. The aim of this chapter is to provide such an analysis. Specifically, we investigate (a) soil moisture status as a driver for indifference of plants to a wide range of soil pH values, which has been suggested by some authors (Schaffers and Sýkora, 2000; Wamelink et al., 2004) but never analysed, (b) the effect of strong vertical gradients in soil pH, (c) the effect of spatial heterogeneity in the horizontal plane

(evaluating pH- $R_m$  relationships at different scales) and (d) the effect of temporal pH variation (do plants respond to average conditions, or to extremes in pH). We discuss these sources of variation in the context of how soil pH controls biogeochemical processes in the rhizosphere and thus acts as a filter constraining the occurrence of species bearing specific response traits.

## Materials and methods

### Data

To quantify plant responses to soil acidity and to investigate causes of variation affecting this relationship, we analysed two datasets with pH measurements and vegetation recordings. Firstly a well-documented national dataset (Beets et al., 2003) consisting of well documented vegetation plots distributed over the Netherlands and secondly a local dataset with detailed, within plot, pH measurements. The national dataset was used to construct a relationship between soil pH and plant responses for 91 grassland habitats and to analyse the influence of soil moisture status and vertical pH gradients on the relationship. The local dataset was used to study the effect of spatial and temporal variability in soil pH on vegetation composition in more detail. None of the investigated plots had been under influence of a major change in hydrological conditions or in vegetation management. Within The Netherlands, there is little spatial variation in climate, with a mean annual precipitation of 769 mm and a mean annual temperature of 9.7°C (data from the Royal Netherlands Meteorological Institute: <http://www.knmi.nl/klimatologie>).

The plots of the national dataset were chosen to span a wide range of nutrient and water availability conditions in the soil. Dominant soil types in the dataset are: Endogleyic Arenosols (34 plots), Histosols (18), (Gleyic) Fluvisols (17), (Histic) Gleysols (11), Gleyic Podzols (6) and Protic Arenosols (5) (thus mostly relatively young soils with no distinct soil horizons other than O, H or Ah horizons). Phytosociological alliances dominant in the dataset are: *Arrhenatherion elatioris* (10 plots), *Calthion palustris* (9), *Caricion davallianae* (9), *Nardo-Galium saxatilis* (6), *Magnocaricion* (6) and *Lolio-Potentillion anserinae* (5). Within each of the 91 plots, at least one pH<sub>KCl</sub>-measurement had been taken from the upper soil layer (< 10 cm below soil surface), where root density usually is highest. 80 plots had paired soil samples taken at 0-5 and 5-25 cm, which enabled us to investigate the effect of vertical acidity gradients in the upper soil layer. Soil samples of the national dataset were collected from May till early September in the period 1999-2004. To check for pH changes during handling and lab analysis we compared the measured pH<sub>KCl</sub> values with indicative measurements of pH gradients (using Merck paper) taken in the field. The indicative pH gradient measurements were also used to verify whether the fixed depth sampling captured the pH gradient in the topsoil.

The local dataset was collected in a species-rich *Cirsio-Molinietum* dominated fen meadow nature reserve ‘Het Meeuwenkampje’, located in the centre of the Netherlands. This reserve has a substantial upward seepage of alkaline groundwater (2-3 mm/d), a shallow groundwater table and nutrient poor and peaty or fine sandy soils. Four plots of 4 m<sup>2</sup> were investigated that are positioned along a vegetation gradient with spatial variation in: (1) the thickness of the organic topsoil (ranging from 20 cm to 250 cm), (2) the moisture regime (ranging from moist to wet) and (3) the influence of alkaline seepage water (Figure 5.1). Each plot was divided into 64 grid cells of 25 by 25 cm for which vascular plants, mosses and liverworts were recorded in May 2009. On three dates in 2009 (7 March, 23 May and 2 September), soil acidity was measured in-situ in each grid cell at a depth of 5 -7.5 cm, using a Hanna Instruments HI99121 pH electrode. To enable adequate statistical description of short distance variation of soil acidity (Huisman et al., 2002), nested measurements were added randomly and in transects with a small lag distance (5 cm). This makes a total of 100 measurements per plot, which is adequate for geostatistical analysis (Webster and Oliver, 1992). No precipitation occurred 4 days preceding each of the three measurement dates.

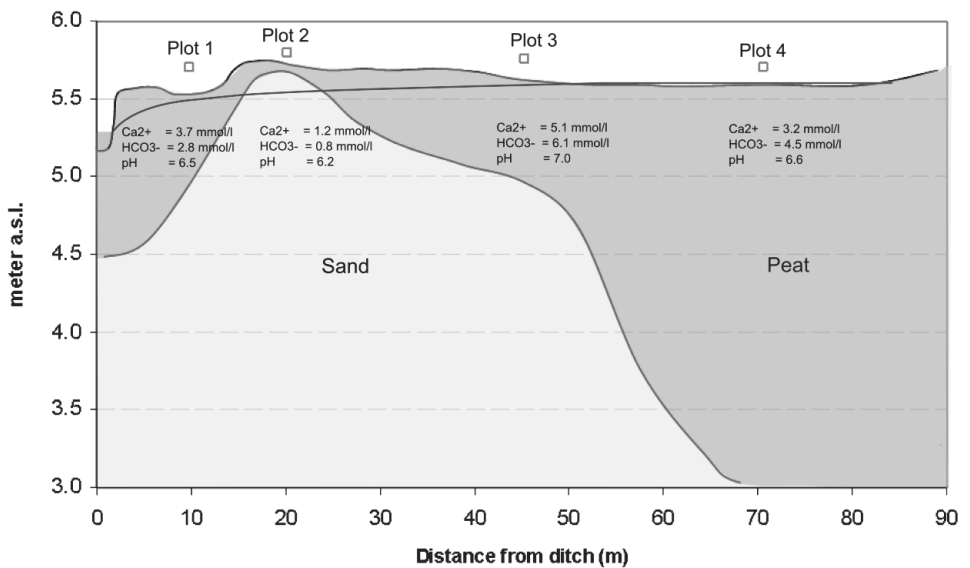


**Figure 5.1.** Location of the four local plots relative to a ditch. Figures represent average soil water quality at 25 cm depth, for more detailed water quality and soil profiles see Chapter 4. The blue line denotes the groundwater level in early spring.

## Data Analysis

### Indicator values

The first quantitative indicator system was developed for central Europe by Ellenberg (Ellenberg et al., 1991). The response of species may however vary across large geographical gradients and therefore the use of indicator value systems outside the region for which they were developed is a subject of considerable debate (Hill et al., 2000). To this end we used a list of acidity and moisture indicator values for plant species (vascular plants, mosses and liverworts) tailored to the Netherlands (Witte et al., 2007), which closely resembles the internationally accepted indicator values of Ellenberg. A major difference, however, is that non-existent combinations of classes have been omitted in the Dutch system (for instance the combination saline and nutrient-poor) and that many species have been ascribed to two or more ecological groups, thus taking into account the ecological amplitude of species (Ellenbergs list only mentions the optimum).

We computed arithmetic mean acidity ( $R_m$ ) and moisture ( $F_m$ ) indicator values (Bartholomeus et al., 2012) for each plot of the national dataset and each grid cell within the plots of the local dataset. Following Käfer and Witte (2004), no weight was given to species cover. The moisture indicator value ranges continuously from 1.0, for species from aquatic systems, to 4.0, for species from extremely dry systems. The acidity indicator value ranges continuously from 1.0, for species of extremely acid environments to 3.0, for species of alkaline conditions.

### Relating $R_m$ to $\text{pH}_{\text{KCl}}$ : non-linearity

In literature, linear regression is commonly used to relate pH to  $R_m$  (Diekmann, 1995; Dzwonko, 2001; Wamelink et al., 2002). The distribution of data points in several studies (e.g. Diekmann (2003); Ertsen et al. (1998); Schaffers and Sýkora (2000)) however, raises questions to the validity of assuming a linear relationship. We, as a first step, analysed whether there was evidence for nonlinearity, first by graphical inspection of the residuals of a linear model fitted on the national dataset and then by testing for a significant change in slope, using segmented linear regression with unknown breakpoints ((Muggeo, 2003). Davies test was used to test whether the assumption of a change in slope is valid (Davies, 1987). Segmented models were fitted in R 2.0.1 (Davies, 1987; R Development Core Team, 2008) statistical program using the segmented package (Muggeo, 2004). Coefficients of determination,  $R^2$ , were calculated for the total regression and for each of the segments according to Oosterbaan et al. (1990).

## The influence of wetness

Schaffers and Sýkora (2000) identified species from wet locations with high  $R_m$  values as a group of outliers. This might imply that species adapted to wet conditions are indifferent to a wide pH range. To investigate possible effects of moisture status on the  $\text{pH}_{\text{KCl}}-R_m$  relation, we divided the national dataset into three groups according to the site-means moisture indicator value  $F_m$ : (1) wet sites ( $F_m \leq 2$ ,  $n = 21$ ), (2) moist sites ( $2 < F_m \leq 3$ ,  $n = 48$ ) and (3) dry sites ( $F_m > 3$ ,  $n = 22$ ). Segmented relations were then fitted through the data to test whether the strength of the  $\text{pH}_{\text{KCl}}-R_m$  relationship is affected by wetness. Moreover, differences in Spearman rank correlations between pH and  $R_m$  of the three groups were analysed using the Fisher's  $z$  transformation (Myers and Sirois, 2004).

## Spatial and temporal heterogeneity as sources of variation

A wide amplitude in plant response to soil acidity may, as mentioned earlier, indicate indifference to a wide range of pH values. However, it may also represent strong spatial variation within a plot, in which case the measured pH (often a single measurement) may not be representative for the species composition of the entire plot. Moreover the pH may also vary over the growing season, which might indicate that the pH measured at a certain time does not reflect the value limiting plant growth. Both aspects may add noise or even bias the  $\text{pH}-R_m$  relationship. To assess whether the  $\text{pH}-R_m$  relation is significantly affected by vertical heterogeneity of soil acidity, and thus by sampling depth, we used the 80 paired measurements of  $\text{pH}_{\text{KCl}}$  from the nationwide dataset to test the null hypothesis that the population means at 5 cm and at 25 cm depth are equal, using a paired t-test. Furthermore we tested, by comparing Spearman rank correlations of  $\text{pH}_{5\text{ cm}}-R_m$  and  $\text{pH}_{25\text{ cm}}-R_m$ , whether the strength of the  $\text{pH}-R_m$  relationship is influenced by sampling depth.

The within-plot measurements of the local 'Meeuwenkampje' dataset enabled us to investigate the effect of small scale horizontal spatial variability, in both vegetation and soil acidity, on the breakdown of the  $\text{pH}-R_m$  relation in wet sites found for the national dataset (see 'results'). We did so by calculating  $R_m$  values for each 25\*25 cm grid cell, (denoted as  $R_{m,25}$ ) and related it to the measured pH per grid cell. Since the pH measurements were performed at three times during the growing season, the dataset also gives information on the scale of temporal variation. To quantitatively describe the spatial variation of soil pH within the plots, we applied geostatistical analysis (for details see Appendix 5.B). The spatial structure of the data was described by (1) the relative structural variance expressed as  $C/(C + C_0)$ , in which  $C$  = partial sill and  $C_0$  = nugget variance, which indicates whether or not the data are predominantly spatially structured, and (2) the (practical) correlation range,  $r$  (m), which represents the distance where spatial dependence has decayed (Webster and Oliver, 2001). Confidence intervals of fitted practical correlation ranges were obtained by parametric bootstrapping (Efron, 1979).

## Results

### Non-linearity

Linear regression of  $R_m$  as a function of  $\text{pH}_{\text{KCl}}$  resulted in a relationship with an  $R^2$  of 0.62. However, the residuals indicated that a linear model was not appropriate. Segmented linear regression on the national database identified a breakpoint at  $\text{pH}$  5.05 with a 95% confidence interval of  $\text{pH}_{\text{KCl}}$  4.37 to 5.63 (Figure 5.2). Davies test confirmed the location of the breakpoint ( $p < 0.001$ ). Slopes of both segments were significantly different, with a relatively steep left slope and a more flat right slope that still significantly differed from zero (Figure 5.2). The  $R^2$  values indicate that  $R_m$  becomes less dependent on  $\text{pH}_{\text{KCl}}$  at higher values.

### Effects of wetness on the $\text{pH}$ - $R_m$ relationship

Dividing the national dataset into three groups according to the site-means soil moisture indicator value revealed a significant decline in the strength of the relation with an increase in wetness (Figure 5.3). At  $R_m = 2.5$ , for instance, the variation in  $\text{pH}_{\text{KCl}}$  at dry plots is about 1  $\text{pH}$  unit, whereas this variation can span a  $\text{pH}$  range of up to 5  $\text{pH}$  units at wet plots. The segment right of the breakpoint was virtually horizontal for the 'wet' plots (Figure 5.3), pointing at almost complete loss of relation in the moderately acid to alkaline range. The right segments of the 'moist' and 'dry' plots had a comparable slope, but the  $R^2$  value of the 'dry' plots was markedly higher. This is also reflected in the Spearman rank correlation between  $\text{pH}$  and  $R_m$ , which were significantly lower ( $p < 0.05$ ) for 'wet' plots ( $R_s = 0.59$ ,  $p \leq 0.01$ ) compared to moist ( $R_s = 0.87$ ,  $p \leq 0.001$ ) and dry plots ( $R_s = 0.93$ ,  $p \leq 0.001$ ). Hence, wet plots contributed substantially to the noise in the overall relationship. This might indicate that species adapted to wet conditions are indeed indifferent or less susceptible to  $\text{pH}$  over a wide  $\text{pH}$  range, but it can also imply strong spatial variation in  $\text{pH}$  within wet plots, which is further analysed in the next section.

### Effects of spatiotemporal variation of $\text{pH}$ in the upper soil profile

To investigate the effect of vertical  $\text{pH}$  gradients on the relation we analysed the 80 paired measurements (Figure 5.4). The paired measurements were in line with the indicative  $\text{pH}$  profiles as measured in the field with Merck paper. The mean of the dataset measured at 5-25 cm was significantly larger than that of the shallow measurements ( $p < 0.001$ ). The mean difference between the two datasets was 0.35  $\text{pH}_{\text{KCl}}$ , with a 95% confidence interval of 0.21-0.49  $\text{pH}_{\text{KCl}}$  units. The significant increase of soil  $\text{pH}$  with depth is in line with our expectations, given the precipitation surplus and acid deposition in the Netherlands. Only fourteen plots had an opposite  $\text{pH}$  gradient, probably caused by inundation with alkaline river water. Investigation of soil profiles of two extreme data points, denoted with an 'A' in Figure 5.2, revealed a steep vertical  $\text{pH}$  gradient ranging from  $\text{pH}$  4.0 to 7.0 (measured with Merck paper) over less than 50 cm. The dominant species in these plots (e.g. *Carex paniculata* L. and *Calla palustris* L.) are relatively deep rooting and they presumably have benefited from the more alkaline water beneath the

more acid top layer where the soil sample was taken. Despite this difference, the Spearman rank correlation was comparable for either the shallow or the deeper  $\text{pH}_{\text{KCl}}$  dataset ( $R_s(0-5) = 0.80$ ,  $p \leq 0.001$ ,  $R_s(5-25) = 0.81$ ,  $p \leq 0.001$ ). The strength of the relationship thus does not decline or improve when measured at a different depth. Combining measurements from different depths will however, given the significant shift in pH with depth, result in an increase of noise around a regression line.

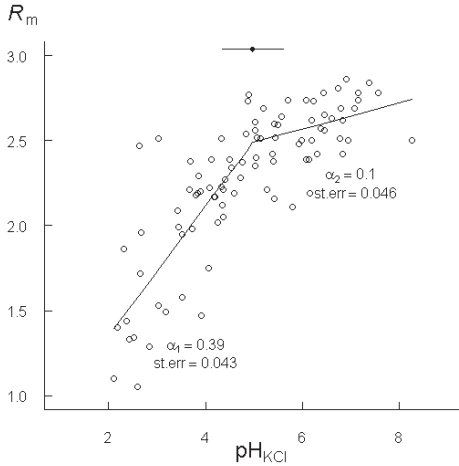


**Figure 5.2.**  $\text{pH}_{\text{KCl}}$  vs  $R_m$  and fitted segmented regression model including the confidence interval of the estimated breakpoint. The slopes of the segments are denoted, respectively, as:  $\alpha_1$  and  $\alpha_2$ . The  $R^2$  and RMSE, respectively are: 0.692 and 0.236 ( $n = 91$ ) for the total regression, 0.541 and 0.289 ( $n = 50$ ) for the left segment and 0.159 and 0.165 ( $n = 41$ ) for the right segment.

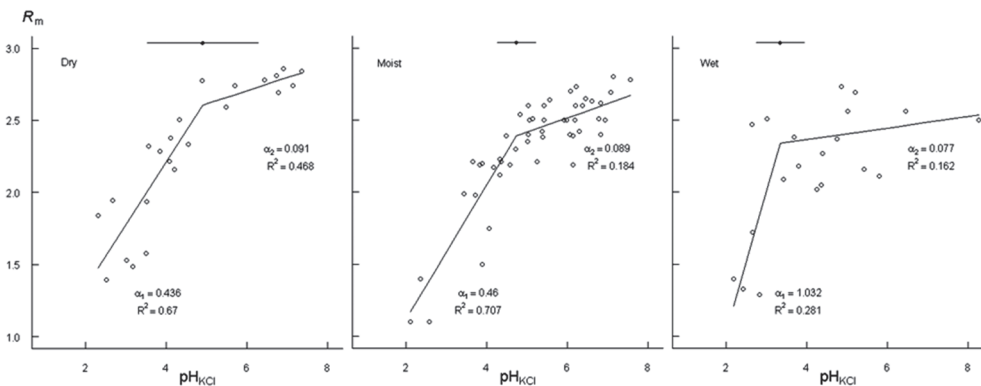


**Figure 5.3.**  $\text{pH}_{\text{KCl}}$  vs  $R_m$  and fitted segmented regression models for ‘dry’, ‘moist’ and ‘wet’ plots. Slopes and coefficients of determination,  $R^2$ , are given for the segments. Total  $R^2$  are respectively 0.84, 0.81 and 0.39 for the dry, moist and wet plots.

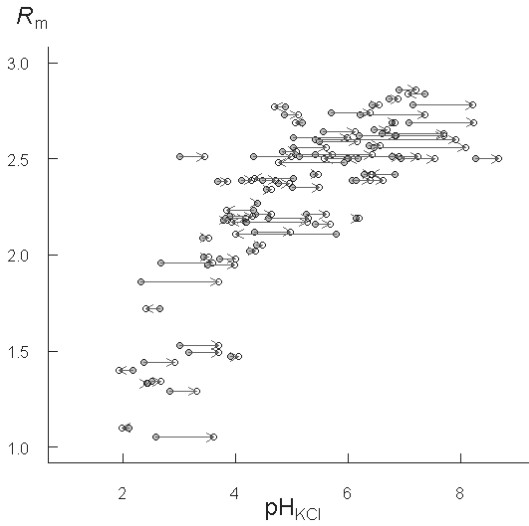


**Figure 5.4.**  $\text{pH}_{\text{KCl}}$  measurements taken at 0-5 (grey dots) and 5-25 cm (open dots) below surface level at the same location per plot. Arrows denote the direction of the vertical pH gradient.

The detailed measurements at the ‘Meeuwenkampje’ site showed substantial small-scale spatial variation of soil acidity within the 2\*2 m plots (Table 5.1, Figure 5.5). The spatial range in pH values was largest at the wettest sites (plot three and four), ranging up to as much as 1.9 pH units in May and September and smallest (0.75 pH units) at the topographically highest and relatively driest site (plot two). Plots three and four are characterized by shallow groundwater tables, high upward seepage of alkaline groundwater (Figure 5.1) and, compared to plots one and two, substantial microtopographical variation (Random roughness estimates (Kamphorst et al., 2000) of 0.2 m for plot three and four vs. 0.1 m for plots one and two, measured on a 5\*10 cm grid). The pH measurements within each plot were predominantly spatially structured (Appendix 5.B). The spatial scale ( $r$ ) of the acidity patterns is shown in Figure 5.6. The wettest plots (three and four) had a significantly smaller  $r$  (51 cm for plot three) and a throughout the year more constant  $r$  than the better drained plots one and two (Appendix 5.B). Lowest structural variance and relatively large nugget variance occurred at the wettest plots three and four. The relatively large nugget variance indicates spatial sources of variation smaller than the sampling interval.

For each calculation of  $R_{m,25}$ , seven to 22 indicator species were available. Highest  $R_{m,25}$  values were found in plot four, mainly due to the presence of *Ranunculus lingua* L. (indicative for wet alkaline conditions) in almost all grid-cells. Largest variation in  $R_{m,25}$  was observed for plot one and is related to the positioning along a ditch, resulting in a small-scale gradient over the plot. Vegetation composition of the other three plots was

much more homogeneous. The small spatial variation in  $R_{m,25}$  (e.g. 1.85 - 2.07 for plot three) found especially at the wettest plots contrasted with the large variation in soil acidity (e.g. pH 5.32-7.25 for plot three) within the same plots (Table 5.1, Figure 5.6). This is in line with the large variation in  $\text{pH}_{\text{KCl}}$  found around  $R_m = 2.0$  at wet and very moist plots in the national dataset.

Comparison of mean pH among measurement dates also showed profound and highly significant changes in acidity during the growing season for all four plots (Table 5.1). Significant changes in variances occurred at plots two, three and four between March and May. Whereas the variance for plot two decreased, it increased for plot three and four. The significant decrease in variance between the March and May measurements of plots three and four in particular was caused by ponding with alkaline groundwater in early spring, a process that levels out local pH differences. The temporary low pH values might explain the relatively low  $R_m$  value for plot 3.

**Table 5.1.** pH means, variances and ranges for March, May and September and the  $R_{m,25}$  range per plot. The range of  $R_{m,25}$  was calculated from grid-cell mean  $R$  indicator values.

Location		March	May	September	Probability of difference			$R_{m,25}$ (n= 64)
					$P_{(\text{March-May})}$	$P_{(\text{May-Sep})}$	$P_{(\text{March-Sep})}$	
Plot 1	Mean	6.54	6.00	5.25	< 0.001	< 0.001	< 0.001	2.08
	Variance	0.11	0.09	0.07	> 0.1	> 0.1	< 0.05	0.007
	Range	5.63–7.11	5.43–6.81	4.84–6.15				1.86 – 2.23
Plot 2	Mean	6.17	5.33	5.48	< 0.001	< 0.001	< 0.001	1.94
	Variance	0.08	0.03	0.03	< 0.001	> 0.1	< 0.001	0.003
	Range	5.77–6.86	4.79–5.75	5.14–5.89				1.80-2.04
Plot 3	Mean	7.49	6.55	6.69	< 0.001	< 0.05	< 0.001	1.99
	Variance	0.02	0.12	0.12	< 0.001	> 0.1	< 0.001	0.002
	Range	7.08-7.87	5.32–7.25	6.04–7.95				1.85 – 2.07
Plot 4	Mean	6.91	5.78	5.51	< 0.001	< 0.001	< 0.001	2.39
	Variance	0.004	0.117	0.136	< 0.001	> 0.1	< 0.001	0.003
	Range	6.62-7.10	5.05–6.51	4.92-6.36				2.19 – 2.51

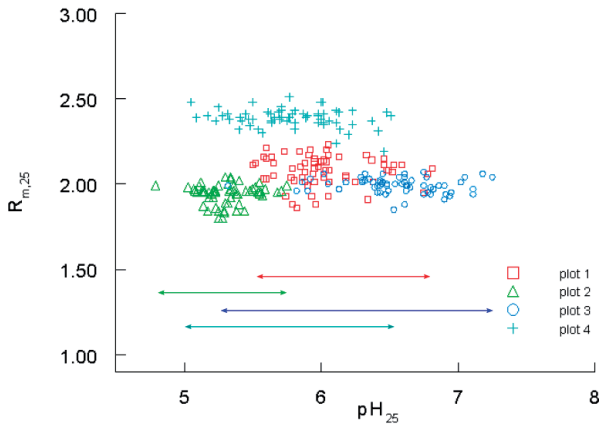


**Figure 5.5.** Relation between  $R_m$  and  $pH$  measured on a 25\*25 cm grid scale. Data points from the better drained plots 1 and especially 2 are more clustered.

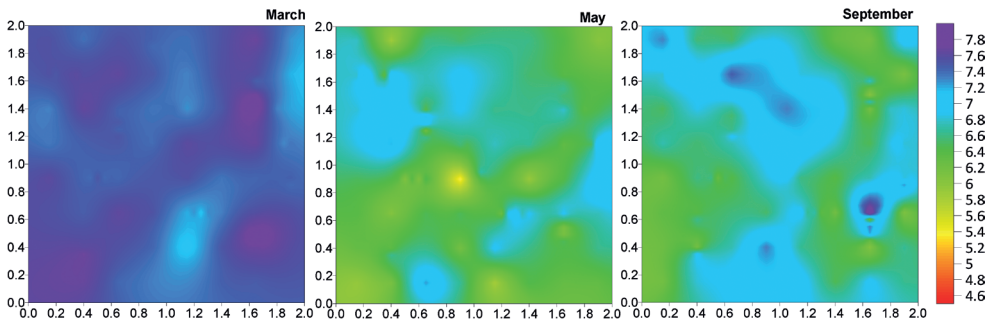


**Figure 5.6.** Spatiotemporal variation of in situ measured  $pH$ , data shown for plot 3.

## Discussion

### $R_m$ as proxy for adaptations to soil acidity

The use of species based indicator values, is often criticized because they are not fully based on detailed measurements but to a large extent on field experience. Nonetheless,  $R_m$  seems to be a good proxy integrating various adaptations of plants to soil acidity. We show that the relationship is highly non-linear, as the national dataset revealed a significant shift in slope around  $pH_{KCl}$  5.0. Previous research by e.g. Falkengren-Grerup et al. (1995), Hill and Carey (1997), Dzwonko (2001) and Wamelink et al. (2002) all using Ellenberg indicator values, did not acknowledge the non-linear nature of the relationship, although their data points show a distribution similar to the data presented in this study. Schaffers and Sýkora (2000) noticed the change of slope in the distribution of their data

points, but hypothesised that it was caused by a violation of the assumption of equal acidity tolerances for species (Ter Braak and Barendregt, 1986), when calculating mean indicator values. In our dataset however, we found no evidence supporting this hypothesis (see Appendix 5.A).

We propose that, instead of statistical inadequacies, there are several pH-dependent biogeochemical processes that influence the suitability of a site for species to persist. The impacts of these processes are consistent with the shape of the relationship: The steep slope of the relationship below  $\text{pH}_{\text{KCl}} 5.0$  might be explained by phytotoxic effects of predominantly Al, which reaches toxic levels in soil solution at pH values of less than 5.0 for sensitive species (Bolt and Bruggenwert, 1976; Poozesh et al., 2007). This indicates that sites with  $\text{pH} < 5.0$  will be dominated by species which have evolved various mechanisms to deal with toxic levels of  $[\text{Al}^{3+}]$  and  $[\text{H}^+]$ . Moreover, we hypothesize that above approximately  $\text{pH}_{\text{KCl}} 5.0$  plants respond much less to soil acidity, because toxic effects become less pronounced and pH-controlled deficiencies of elements crucial for plant growth (like P, Fe and Zn) slowly become more important. Phosphate availability for instance is optimal around pH 6, but declines at higher pH values due to the formation of (hydroxy)apatites (Bolt and Bruggenwert, 1976). In well-aerated soils,  $[\text{Fe}^{2+}]$  and  $[\text{Fe}^{3+}]$  decline with increasing pH. At  $\text{pH}_{\text{KCl}} 5.0$ , iron activity is already below that required by plants for optimal growth ( $0.01 \mu\text{mol/l}$ ) (Guerinot, 2001; Loeppert, 1986), which might explain the mild but distinct slope of the pH- $R_m$  relation for the dry sites. In calcite-rich soils particularly (buffered at  $\text{pH}_{\text{KCl}}$  values  $> 6.5-7.0$ ), Fe and P become practically unavailable and only species adapted to extreme deficiencies will survive. The need for adaptations may cause an increased slope at  $\text{pH} > 6.5 - 7.0$ , as was apparent in Schaffers and Sýkora (2000). Such increase did not arise in our dataset, presumably caused by a lack of data from calcite-rich soils.

Although the discussion above might provide an explanation for the general shape and nature of the relationship, it gives no explanation for the strong variability in the pH- $R_m$  relation encountered at especially very moist and wet sites. Our extensive national dataset and detailed measurements enabled us to evaluate sources of variation causing this variability and allowing to improve future predictions.

### Indifference of wetland species to soil acidity

One hypothesis to explain the large variability in the relationship between pH and  $R_m$  is that certain, but not all, species are indifferent to pH over a broad range of pH values. In our datasets, this seems especially the case for various species from very moist and wet sites. This was subsequently proven by the detailed local measurements in which  $R_{m,25}$  was unrelated to pH from  $5 < \text{pH} < 8$ . Wet conditions commonly imply relatively low redox potentials and, consequently, high  $\text{Fe}^{2+}$  levels due to  $\text{Fe}^{3+}$  reduction. This will have an ameliorating effect on iron deficiencies, which might explain the flattening of the relation at moist and especially wet sites. At truly low redox potentials even toxic levels of  $\text{Fe}^{2+}$  may occur. Species containing aerenchyma, however, can survive in anoxic soils due to

their ability to transport oxygen to respiring root tissues via internal porous tissues (Drew, 1983). The oxygen leaking out of the roots results in oxidation of ferrous iron and thus a decreased pH around the roots (Ahmad and Nye, 1990; Hinsinger et al., 2009; Pierce et al., 2009; Snowden and Wheeler, 1993). Moreover, increased pCO<sub>2</sub> will result in a decreased pH in all but very acid soils due to the rapid formation of H<sub>2</sub>CO<sub>2</sub>, which is a weak acid (Hinsinger et al., 2003). Furthermore, the release of protons by roots to balance excess intake of cations (such as NH<sub>4</sub><sup>+</sup>) over anions will result in an additional drop in pH.

As shown for rice by Begg et al. (1994), aerenchyma containing species can lower soil acidity by one to two pH units in the vicinity of the roots. The oxidation and acidification is beneficial for the suppression of toxic Fe<sup>2+</sup> levels and the availability of sparingly soluble nutrients such as P and Zn (Hinsinger et al., 2003). The ability to influence rhizosphere acidity makes these species relatively indifferent for differences in soil pH, providing an explanation for the breakdown of the pH-R<sub>m</sub> relation for wet sites in Figure 5.3. In our dataset aerenchyma containing species like sedges and rushes occurred over a broad pH range. In contrast, shallow rooting species and mosses seemed to occur over a much smaller range (see next section). As high concentrations of aluminium are frequently found in sites supporting iron tolerant species, it seems that some wetland plants have co-tolerance to these metals (Snowden and Wheeler, 1993), widening their pH tolerance even further.

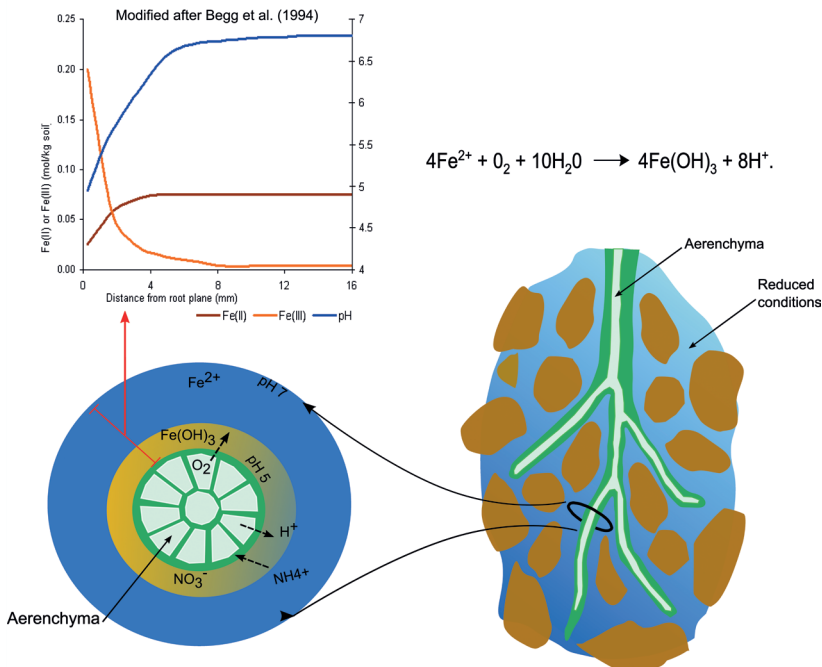


**Figure 5.7.** Rhizosphere processes affecting redox conditions and soil acidity in a wetland soil (figure not part of published manuscript).

## Spatial heterogeneity of soil acidity as a source of variation

Besides indifference to soil pH due to physiological adaptations, Van Wirdum (1991) and Wamelink et al. (2004) proposed an alternative hypothesis for the large variability in the pH- $R_m$  relationship. They suggested that variability in pH for a given  $R_m$  value may indicate strong local pH variation within a plot, which is not reflected in the plot mean  $R_m$  value. If true, this might imply that the scale of vegetation plots (typically  $> 4 \text{ m}^2$  in most studies) is inappropriate for relations between plant response and soil acidity measurements. Additional strong vertical stratification in soil pH may result in a measured pH that is different from the pH actually encountered by the roots, resulting in biased estimates of pH, even at an appropriate plot scale.

The occurrence of vertical stratification and local variation in soil pH has been extensively described for forest soils (e.g. Falkengren-Grerup et al. (1995), Skjellberg (1990)). Our national dataset shows that vertical stratification in soil pH can also be apparent in grasslands and wetlands. Strongest stratification seems, in our dataset, to be related to the influence of upward seepage of alkaline groundwater. Different sampling depths did indeed result in different  $R_m$ -pH relationships but the strength of the relationships was not significantly different. Mixing up datasets with different sampling depths will however result in increased noise.

Detailed pH measurements at the Meeuwenkampje site provide evidence that besides vertical stratification, substantial spatial (horizontal plane) pH heterogeneity can be found even within relatively small plots of  $4 \text{ m}^2$ . Within-plot variation of soil acidity ranges up to almost two pH units, whereas temporal changes over the growing season can be even larger. The distinct differences in spatial variability in soil acidity patterns among the four plots within the same meadow provide insight in the causes of spatial heterogeneity in a wetland setting. Strong spatial variation in soil acidity was found to be related with very wet conditions in combination with high upward seepage and substantial micro-topographical variation. The combination of micro-topographical variation and a shallow groundwater table results in saturation excess overland flow at micro scale depressions, while on hummocks infiltration of precipitation water can still continue. This process results in micro scale gradients from relatively alkaline hollows to more acidic hummocks. Moreover, hollows will experience longer periods of inundation, and consequently longer periods with low redox potential, which are accompanied by consumption of  $\text{H}^+$  and production of  $\text{HCO}_3^-$ .

Remarkably, despite of the large spatial variation of soil acidity at the wet plots, within plot variation of  $R_{m,25}$  is small and values are consistent with the plot mean  $R$  values. This indicates that the current plot scale is appropriate and points to indifference of the occurring wetland species to a broad pH range. This is supported by the relatively high nugget value for the wettest plots three and four, which indicates that a large part of pH variation occurs at even smaller scales than the 25 cm sampling intervals. One source of this small-scale variation can be the acidifying effect of root respiration and release of protons due to ammonium uptake, mentioned earlier. However, one has to keep in mind

that it is, under field conditions, hard to distinguish between root induced alterations of pH and pre-existing heterogeneity in soil conditions. Most of the prevailing species occupied almost the complete pH range found in the wet plots. It is noticeable that the majority of these species contain aerenchyma as adaptation to wet conditions. An example is *Carex pulicaris* L. (Figure 5.8), found at the Meeuwenkampje site at pH values ranging from 5.25 to 7.25. *Carex pulicaris* is a very tolerant species to high levels of  $\text{Fe}^{2+}$  Snowden and Wheeler (1993) due to its ability to conserve oxygen supplies (Armstrong and Beckett, 1987). Oxygen leaking out of its root tissue results in oxidation of  $\text{Fe}^{2+}$  and consequently acidification of the rhizosphere. Assuming comparable soil pH distributions in a large number of sites containing indifferent wetland species, sampling from these sites will not result in a plant response function to soil pH, but in a description of micro scale variability of soil pH within these sites instead. In contrast, plant species with a superficial root system as adaptation to reduced conditions, for instance *Lychnis flos-cuculi* L. (Blacqui re, 1986) and mosses seem to occur over a much smaller pH range. For these species, micro-scale heterogeneity of soil acidity is indeed an important ordering factor. For a statistical justification, however, many more observations are needed.

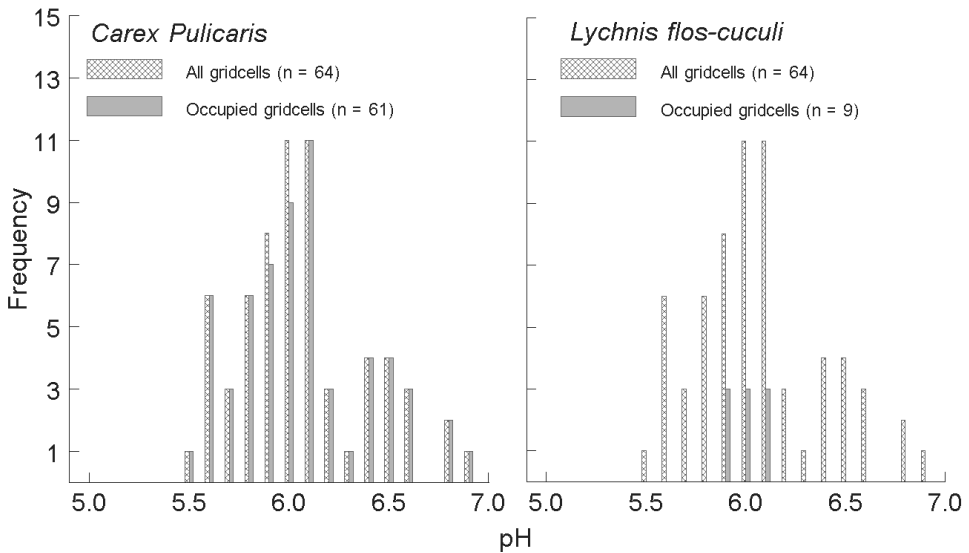


**Figure 5.8.** Frequency of occurrence per pH class of a  $[\text{Fe}^{2+}]$  tolerant wetland species (e.g. *Carex pulicaris*) and a sensitive species (e.g. *Lychnis flos-cuculi*) for plot one in comparison to the overall pH distribution. *C. pulicaris* seems to show a unimodal response to pH, but in reality this reflects the spatial distribution of the pH within the plot.

## Temporal variation of soil acidity as a source of variation

Variation of soil acidity is, in view of the mentioned processes, not expected to occur only in space but also in time. For the Meeuwenkampje site, we showed significant differences between three measurement dates during one growing season. With the start of the growing season, increased evapotranspiration causes water levels to drop, which leads to an increase in redox potential and decrease in pH, clearly visible in Figure 5.6. In addition, respiring roots result in extra acidity and further decrease of soil pH during the season. On the other hand, increased evapotranspiration also leads to a depletion of infiltrated precipitation water and increased influence of alkaline seepage water which will result in a pH increase (Figure 5.6, Table 5.1, September measurements compared to May measurements). This of course leads to the question to what plants respond to; extremes or average soil acidity conditions and in which growth stage plants are sensitive to pH. Most  $R_{m,25}$  values of the Meeuwenkampje plots are below the regression line on the national dataset, which might indicate that the occurrence of truly 'alkaline' species is limited by the temporarily occurring low pH values of around 5.0. This might imply that the extremes of seasonal pH fluctuations are of great significance for the species composition. The national dataset consists of measurements taken at different times during the growing season. It is thus likely that temporal variation will affect the found pH- $R_m$  relationships. However, because both wet, moist and dry plots were sampled at different periods during the growing season, we expect some extra noise but no significant bias.

## Conclusions

Notwithstanding the body of evidence pointing to the ecological importance of soil acidity, this factor is hardly if ever recognised as an important driver within plant strategy schemes. In this chapter, we showed strong relationships between soil acidity and plant responses (with  $R_m$  as a proxy for various adaptive strategies). Moreover, the shape of the relation was consistent with several pH-dependent biogeochemical processes known to influence plant life. The strength of the pH- $R_m$  relationship in especially the weakly acid to alkaline range was negatively related to the wetness of plots, which was probably caused by indifference for soil acidity of aerenchyma containing species. Plant species with shallow root systems, as adaptation to hypoxia, or mosses seem more responsive to soil acidity in wetland habitats and are probably better predictors of local soil pH. For predictions, it is thus important to differentiate between sites with and without severe oxygen stress. Although indifference is identified as the main cause of variation in the relationship between pH and  $R_m$ , strong spatiotemporal variation in soil pH may cause additional systematic errors and statistical noise. These errors may be avoided by systematically sampling soil acidity (at least same depth for each plot, more than one measurement per plot and for several predefined moments during the growing season). Especially the effect of (large) temporal changes in soil pH on vegetation composition and possible exclusion of sensitive species should be further investigated and is in need of

appropriate data. Ackerly and Cornwell (2007) argue that variation of plant traits within plots reflects the effects of within plot partitioning of traits among environmental gradients. In addition, our study shows that adaptation to one site factor, in our case aerenchyma as adaptation to oxygen stress, can result in indifference to gradients of other site factors such as iron and soil acidity. This might imply competitive advantage for species equipped with this kind of multi effect adaptations.

## **Acknowledgements**

We would like to thank the Dutch state forestry service for kindly providing the nationwide dataset and Yuki Fujita for proof reading the manuscript. This study was carried out within the framework of the Netherlands Organization for Scientific Research (NWO) CASIMIR programme (018.002.007) and the Dutch Water Utility Sector joint research programme (BTO).

## Appendix 5A Equal tolerances

Schaffers and Sýkora (2000) hypothesise that the change in slope around pH 5 is caused by a violation of the equal tolerances requirement (Ter Braak and Barendregt, 1986) when calculating plot mean indicator values. We tested whether this assumption holds for our dataset. In Figure 5.A.1 we related species tolerances, expressed as fractions of the total  $\text{pH}_{\text{KCl}}$  range, to the  $\text{pH}_{\text{KCl}}$  optima. Extremely narrow tolerances around pH 4 as observed by Schaffers and Sýkora (2000) are not visible in our dataset and can thus not explain the change in slope.

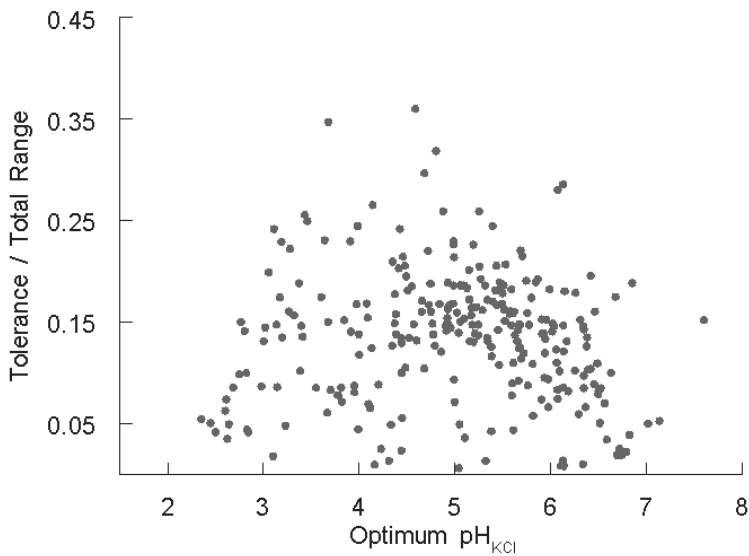


**Figure 5A.1.** Relative tolerances calculated for our national dataset. A violation of the equal tolerances assumption is, in contrast to the data of Schaffers and Sýkora (2000), not obvious.

## Appendix 5B Spatial analysis of pH patterns

Semivariogram models were fitted to determine the extent of spatial dependence using the R package GeoR (Ribeiro and Diggle, 2001). Maximum likelihood estimation and Akaike's Information Criterion (AIC) were used to select the best fitting semivariogram model. The spatial structure of the data was described by (1) the relative structural variance expressed as  $C/(C + C_0)$ , in which  $C$  = partial sill and  $C_0$  = nugget variance and (2) the correlation range,  $r$  (m), which represents the distance where spatial dependence has decayed (Webster and Oliver, 2001). For the Exponential and Gaussian model, the practical correlation range (PCR) which corresponds to the range at which 95% of the sill is being reached, was used for  $r$ .

To gain insight into the sensitivity of the PCR estimates, we also analysed inferior models deviating less than 2 AIC from the 'best' model (Burnham and Anderson, 2002). The analysis was limited to lag distances with more than 30 comparisons, since at least 30-50 data pairs per lag distance are required for a reliable estimate (Olea, 2006). The maximum lag distance for the semivariogram model was set to  $h_{\max} = 1/2 \cdot x_{\max} = 1.40\text{m}$  (Journel and Huijbregts, 1978). The lag interval was set to the smallest lag distance (5 cm).

**Table 5B.1.** Applied semivariogram models

Model	Equation
Spherical	$\gamma(h) = \begin{cases} c \left\{ \frac{3h}{2a} - \frac{1}{2} \left( \frac{h}{a} \right)^3 \right\} & \text{for } h < a \\ c & \text{for } h > a \end{cases}$
Exponential	$\gamma(h) = c \left\{ 1 - \exp\left(-\frac{h}{r}\right) \right\}$
Gaussian	$\gamma(h) = c \left\{ 1 - \exp\left(-\frac{h^2}{r^2}\right) \right\}$
Pure nugget	$\gamma(h) = c_0$
<b>C</b>	<b>Partial Sill</b>
<b>r</b>	<b>Correlation range (m)</b>
<b>C<sub>0</sub></b>	<b>Nugget variance</b>

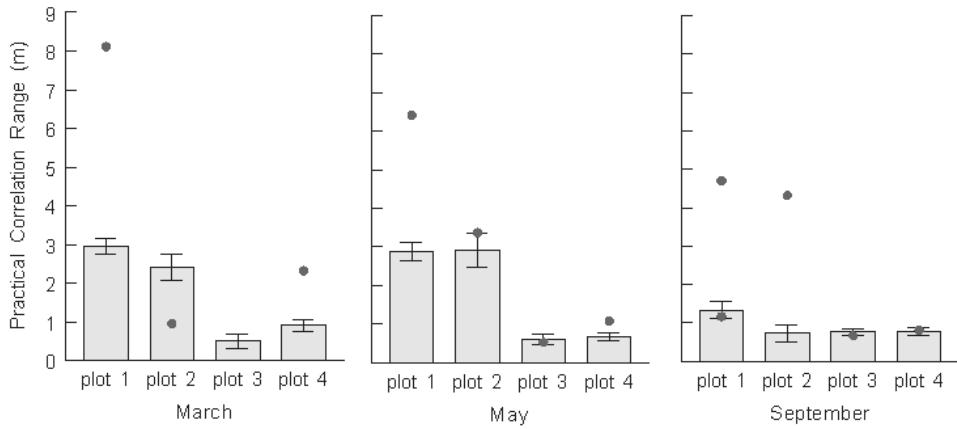


**Figure 5B.1.** Practical correlation ranges (m) of soil water acidity measurements for the different plots and measurement dates, derived from best fitting semivariogram models. Error bars represent bootstrapped 95% confidence intervals. PCR values of inferior semivariogram models deviating less than  $\pm 2$  AIC from the 'best' model are shown with dots.



## CHAPTER

# 6

### Microtopography as a driving mechanism for ecohydrological processes in shallow groundwater systems

This chapter is a modified and extended version of the published manuscript:

Van der Ploeg, M.J., Appels, W.M., Cirkel, D.G., Oosterwoud, M.R., Witte, J.-P. M. and S.E.A.T.M. van der Zee (2012) *Vadose Zone Journal*, 11(3) doi:10.2136/vzj2011.0098

## Abstract

Microtopography can have a large effect on flow processes at the soil surface and the composition of soil water. Microtopography is often represented by a roughness parameter in hydrological models. In areas without a strong topographical gradient, microtopography may be underestimated when accumulated in a single parameter, especially in shallow groundwater systems. This study reviews the intricate relationships between microtopography, surface runoff, and ecohydrology in systems featuring shallow water tables. We specifically focus on relations between microtopography and runoff, impact of microtopography on response times of shallow groundwater ecosystems and microtopography and spatial distribution of groundwater quality parameters and site factors. We advocate the use of microtopography in modelling approaches by examples that feature typical ecosystems with shallow groundwater under influence of microtopography. With a simple modelling approach, we show how microtopography could add flexibility to the acrotelm-catotelm concept in raised bog hydrology. The classic acrotelm-catotelm concept hinders progress in understanding small scale hydrological variations and other ecohydrological relations. Furthermore, we illustrate possible self-organization properties of wetlands. Finally, we show how microtopography and surface runoff affect the mixing of water with different chemical signatures, resulting in variations of the occurrence of plant species.

## Introduction

Surface runoff is the free flow of water over the soil surface, and is an important term in the hydrological cycle (Beven, 2004). Surface runoff occurs as soon as the water supplied to the soil surface cannot infiltrate, either because it exceeds the maximum infiltration rate, or because the capacity of the vadose zone to store additional water is exceeded. The soil water storage capacity is mainly influenced by the depth of the water table, whereas sealing and crust formation at the soil surface, poor wettability of the soil matrix, and subsoil compaction influence the infiltration capacity of the soil. Surface runoff caused by saturation excess and infiltration excess are known as Dunne and Horton runoff, respectively. Surface runoff may also occur when phreatic groundwater seeps up and exfiltrates at the soil surface (Dunne and Black, 1970). It is evident, from the different weather, soil, soil cover, and geohydrological conditions, that many features of surface runoff, such as magnitude, frequency of occurrence, and distance of overland displacement of water is difficult to predict (Sophocleous, 2002).

In hilly areas, the large scale topographical gradient is the dominant aspect in determining such surface runoff features, as is apparent from early distributed runoff models (Freeze and Harlan, 1969) and later ones such as SHE (Abbott et al., 1986) and TOPMODEL (Beven et al., 1995). As the topographical gradient influences both the convergence and velocity of flow, a larger slope implies a larger risk of erosion (Hairsine and Rose, 1992). Accounting for microtopography on a hillslope results in an increase of effective infiltration rate with hillslope length as the downslope increase of overland flow

depth and discharge progressively inundate the higher and more permeable parts of microtopography (Dunne et al., 1991; Thompson et al., 2010). In areas with a negligible large scale elevation gradient, microtopography, consisting of (ir)regular topographical features such as soil clods, crop rills, clumps of vegetation or washed on sediments, is the main factor in routing non-infiltrating water. Representing microtopography with a roughness parameter only would misrepresent the importance of retention of water that does not flow, but is stored in depressions to await infiltration or evaporation (Antoine et al., 2009). Surface runoff modelling in flat areas received much less attention than in sloping areas, as is apparent from the common simplification to describe surface runoff as sheet flow of uniform depth over a tilted rough surface in most process-based models (Beven, 2002).

As surface runoff is an ephemeral process and typically comprises only a small fraction of average catchment discharge, neglecting it may be understandable from a quantitative point of view. However, ignoring it is inappropriate. During storm events, surface runoff provides a considerable contribution to peak discharges at the catchment scale and to inundation and ponding at field scale. Moreover, even a limited amount of surface runoff facilitates fast transport of solutes, such as nutrients, pesticides, and other contaminants, and can significantly contribute to surface water loading (Louchart et al., 2001; Mueller et al., 2007; Turtola and Jaakkola, 1995; van der Velde et al., 2009; van der Velde et al., 2010). Particularly solutes that are strongly sorbed to the top layer of soil can by-pass the (un)saturated zone. The strong link between surface runoff and solute fate makes surface runoff in relatively flat areas an environmentally important hydrological process.

For systems with shallow groundwater levels, wetlands that are inundated or saturated at a frequency and duration sufficient to support vegetation adapted for hypoxia, the interaction between surface runoff, groundwater quantity and quality, and ecology is of particular interest (He et al., 2010). Wetlands are often located in the lowlands of deltaic areas (e.g. of Mississippi, Rhine-Meuse, and Nile) and other coastal areas. More inland, shallow groundwater may be found in areas, adjacent to streams and rivers and in areas where groundwater flow is impeded. Raised bogs and fens are types of ecosystems that require wet conditions to form, and are therefore characterized by shallow groundwater (Belyea and Baird, 2006; Belyea and Clymo, 2001; Ingram, 1978; Van Wirdum, 1991).

A wetland's ecology is not only determined by the frequency and duration of saturation, but also by the local groundwater quality. Groundwater flowing through the subsurface geochemically interacts with the solid matrix. With organic matter as the driving reductant, groundwater chemistry may change due to the dissolution of calcite, denitrification, the dissolution of manganese and iron, and the reduction of sulfate. These biogeochemical processes gradually change the chemical fingerprint of the groundwater from the moment of infiltration until the moment of discharge (Klijn and Witte, 1999; Kvarner and Kløve, 2006; Mulder et al., 1995; Van Wirdum, 1991). As the chemical signature of groundwater depends on the geochemical characteristics and the exposure time to the soil and bedrock, classifications for different groundwater types have been

developed. For instance, Van Wirdum (1991) distinguished atmocline (recently infiltrated precipitation water), lithocline (old ground water), and thallassocline (saline groundwater), based simply on the calcium chloride ratio and EC. More elaborate water quality characterization and classification methods were developed by Stiff (1951), Piper (1953) and Stuyfzand (1986).

In systems with shallow groundwater levels, infiltrating water, direct precipitation and groundwater from upward seepage meet close to the soil surface, causing different chemical signatures (atmocline, lithocline) to meet in the root zone (Cirkel et al., 2010; Schot et al., 2004; Van Wirdum, 1991). A transition zone caused by mixing is formed between these two types of water. The resulting chemical gradients may create opportunities for very different plant species and soil organisms (Moser et al., 2007; Peach and Zedler, 2006; Sterling et al., 1984; Vivian-Smith, 1997). An intuitively attractive explanation for the high biodiversity in wetlands with upward seepage is that the proximity of groundwater with different chemical signatures offers opportunities to plant species that differ in ecological demands. Plants find the environment to compete successfully at close distances, owing to different root density profiles and growing seasons (Figure 6.1, Cirkel et al. (2014), Van Wirdum (1991).

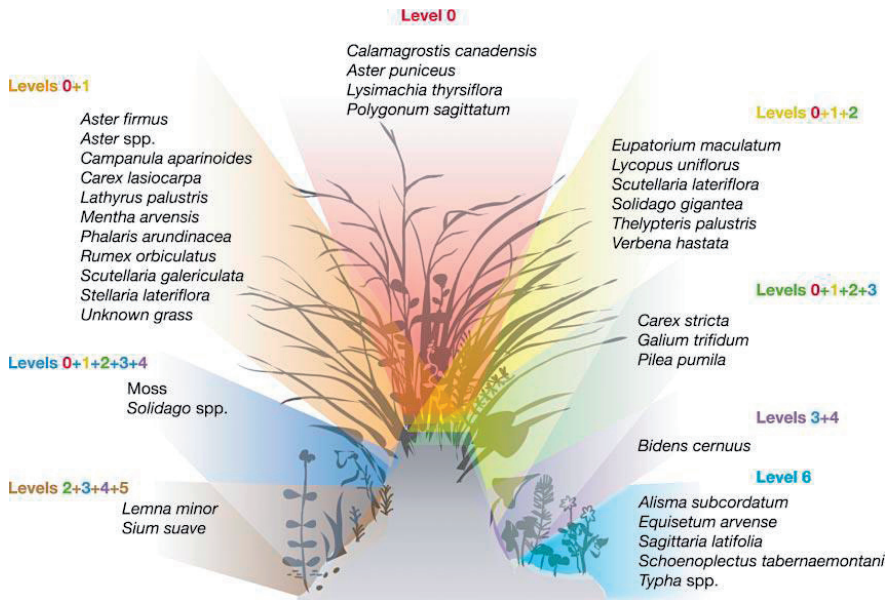


**Figure 6.1.** Example of species preference driven by microtopography: Tussock microhabitats Peach and Zedler (2006): “Patterns of species preferences for tussock microhabitats. Each “level” is either the top (level 0), the off-tussock position (level 6) or a range of side positions (levels 1–5) 6 the top or 6 the off-tussock position. Only the 34 species that showed significant spatial pattern are illustrated.” With kind permission from Springer Science and Business Media).

Vegetation affects surface runoff in several ways. Firstly, plant roots keep soil particles together and intercepting vegetation decreases the impact of rain drops, thereby preventing soil erosion caused by surface runoff (De Baets et al., 2006). Secondly, vegetation stimulates the infiltration capacity of the soil, through preventing sealing of the soil and increasing soil organic matter and macroporosity (Abrahams et al., 2003; Dunne et al., 1991; Weiler and Naef, 2003) leading to a net displacement of surface runoff from bare soil to vegetated patches (HilleRisLambers et al., 2001; Mueller et al., 2007). These vegetated patches are mainly found in semi-arid areas where plant growth is limited by water availability. The increased infiltration capacity allows the persistence of self-organized vegetation patterns, whereas the plants would die, had they been homogeneously distributed (Rietkerk et al., 2002). Thirdly, stems and other parts of plants contribute to hydraulic resistance to water flow, thereby delaying and impounding the water (Holden et al., 2008; Nepf, 1999). The hydraulic resistance caused by vegetation depends on the size of the plants, their structural properties, plant location in the channel, and the local flow conditions (Green, 2005). This dependency means that approaches for the definition of roughness and resistance formulated for macrophytes with protruding and bending stems found in streams and floodplains (e.g. Lane and Hardy (2002), Luhar et al. (2008)) cannot be applied automatically to wetlands, where vegetation has a completely different structure and size relative to flow depth than in vegetated streams and floodplains (Holden et al., 2008). Fourthly, clumps and tussocks of plants create a microtopography of their own (Peach and Zedler, 2006). Some plant species form higher tussocks, because they produce large amounts of litter that is not easily decomposed. In peat bogs, natural differences in peat moss growth create a hollow and ridges pattern within 10-30 years from initiation of peat formation (Pouliot et al., 2011).

It is clear that interactions between microtopography, surface runoff, groundwater quantity and quality, and vegetation are intricate and numerous. Here, we focus on the influence of microtopography on mass transfer processes just above and under the surface from an ecohydrological perspective in flat wetland ecosystems. We therefore consider i) microtopography and runoff, ii) microtopography and response time in shallow groundwater ecosystems, and iii) microtopography and spatial distribution of groundwater quality parameters and site factors. We discuss these topics using published literature and selected examples to illustrate the significance of such interacting processes. We show the ecohydrological importance of considering microtopography for flat areas with shallow groundwater.

## Microtopography and runoff

To call an area flat, instead of sloping, is a qualitative attribute, because a soil surface's elevation varies at different scales. In flat areas, topographic features with dimensions in the range of centimeters and decimeters control storage of water at the soil surface and surface runoff, whereas in sloping areas the global gradient in elevation of the soil surface is dominant (global referring to the system scale, such as an agricultural field or an area

with natural vegetation). The demarcation between flat and sloping areas itself, remains a relatively arbitrary choice. However, it seems logical that the size of microtopographical features relative to the global gradient is a factor in that demarcation.

In ecosystems in flat areas with shallow groundwater, surface runoff occurs ephemerally as sheet flow and channel flow in micro-channels. We distinguish it from streams, because the underlying soil may be unsaturated (Horton flow) or because the surface runoff occurs incidentally (Dunne flow). As soon as the global gradient of elevation is sufficiently smaller than the size of local microtopography variations, a fill-and-spill process of depressions becomes important (Darboux et al., 2002). The fill-and-spill process adds complexity to the flow pattern, as ponded depressions may merge through wetting, or separate through drying. In turn, local horizontal flow directions may reverse, even repeatedly, as a function of time during either a wetting or a drying sequence. Moreover, the rate of surface runoff and the quantity and timing of its discharge in the open channel or stream network may be strongly affected by the temporal storage of water in ponds at the soil surface.

Our focus on relatively flat areas has implications for the modelling approach that is taken. A readable account of simplifications and approaches to the conservation of mass and the momentum equations is provided by Lane (1998). In view of the commonly shallow water layer that is involved in surface runoff, the two-dimensional unsteady flow equations known as the Saint Venant equations, which are depth-averaged adaptations of the hydrodynamic Navier-Stokes equations, are suitable (Beven, 2002). Modelling of flow over two-dimensional soil surfaces is challenging, both with regard to parameterization and numerically (Bates et al., 1992; Bates et al., 1997; Fiedler and Ramirez, 2000). For this reason, additional simplifications are often needed to address complex surfaces with both a slope and microtopography (Tayfur and Kavvas, 1998). Mathematical models for surface runoff over an infiltrating surface often use less complex approximations of the Saint Venant equations such as the kinematic wave approximation when microtopography is neglected and the water surface slope equals the topographic slope (Meng et al., 2008; Morbidelli et al., 2006) or the diffusive wave approximation when microtopography is accounted for (Antoine et al., 2009). When simulating water flow in a watershed, these models are computationally demanding. Simpler water transfer approaches can have computational benefits while preserving the main characteristics of the surface runoff process. When the ‘dead storage’ (i.e. water retained at the soil surface in micro-depressions) is large compared to ‘live storage’ (i.e., water that is detained at the soil surface in the layer of flowing water), the development of surface runoff can be simulated well with an instantaneous water transfer algorithms instead of a 2D hydraulic model (Antoine et al., 2009). With these fast models, the effect of size and spatial organization of microtopography on the onset and development of surface runoff can be investigated systematically. Real topographies consist of a complex of features on macroscale, mesoscale, and microscale. Focusing on a peat bog as an example of flat, wet ecosystems, these scales are reflected in the small gradient of a bog from its centre towards its outer boundaries, the hollows and ridges pattern that characterize parts of

peat bog slopes (Belyea, 2007) and the patterning of different types of vegetation. Simulating fast runoff processes in these ecosystems with a fill-and-spill model (extendable with groundwater module) could therefore lead to more insight in the hydrological response of these ecosystems. In the following paragraph, we explore the use of detailed surface topography data and surface runoff concepts to model water flow on a raised bog.

It is possible to numerically simulate flow for the heterogeneous coupled groundwater-vadose zone-surface runoff system we described above to obtain an understanding of the complexities involved. Frei et al. (2010) built a model in the HydroGeoSphere code (Therrien et al., 2008) to explore the feedbacks between groundwater levels, ponding, and surface runoff in a riparian wetland with a (synthetic) heterogeneous microtopography. As was already noted, exploring such a system with a fully coupled physically based computer model, comes at a price. In this case a simulation of one hydrological year could take up to seven weeks of computation time. We illustrate an alternative approach with a simulation of depression filling and surface runoff on a slope of the Männikjärve raised bog in Estonia. We measured an elevation profile from the centre to the margin of the raised bog (the bog is surrounded by open water), with a length of 400 m, width 1 m and a vertical elevation drop of 1.5 m ( $\approx 0.4\%$ ). We simulated microtopography with a spatial structure that visually matches field observations of microtopography (as it was not measured). The random topography was generated in R Statistical Software with the RandomFields package. We used an exponential covariance function for the definition of the semivariogram shape with a standard deviation of 5 cm and correlation length of 30 cm. This microtopography was superposed on the measured elevation profile. We then analysed how often surface runoff reached the margin of the raised bog subject to a designated rainfall forcing measured at Männikjärve bog during spring, summer, and autumn of 2009. The analysis was performed with an algorithm for ponding and redistribution of water (Appels et al., 2011). For illustrative purposes, the analysis was kept simple and therefore featured no groundwater or Richard's subsurface flow. Infiltration and evaporation losses were assumed to occur at a constant rate throughout the entire slope during rainfall events and under ponded areas during the periods between rainfall events. At the start of the simulation all ponds at the slope were filled with water, originating from melting of snow cover on the bog in winter.

In Figure 6.2 the rainfall and surface runoff rates are plotted together with the volume of water that is stored in the microtopography. Surface runoff occurs only when more than 80% of the available depression storage capacity of 50 mm is filled with water. This amount is plausible in the waterlogged ecosystem we investigated. We find several values of surface runoff rate occurring with the same amount of water stored at the surface because of two reasons. The first cause is the variation in rainfall rate; once a flowpath towards the bog margin has been established through ponds filled with water, the surface runoff rate depends on the rainfall rate in the timestep under consideration. Secondly, even though the infiltration rate was fixed at a constant value, the cumulative water losses from pools in periods between rainfall events depend on the pools' dimensions. Deep

pools, featuring a large depth-width ratio, will dry up slower than shallow pools with a small depth-width ratio. This, combined with a variation of area contributing excess water to each pool, leads to a change in activation of the flow paths on the bog over time. The occurrence of surface runoff becomes a function of characteristics of the rainfall sequence as well. The spatial differences are amplified when we consider the whole raised bog, instead of just a thin (semi 2D) profile. The various morphological features of the raised bog have specific relations between amount of water stored at the soil surface and surface runoff rate at boundaries between morphologies. Therefore, the total surface runoff rate of a bog will reflect the presence of these different morphological features.

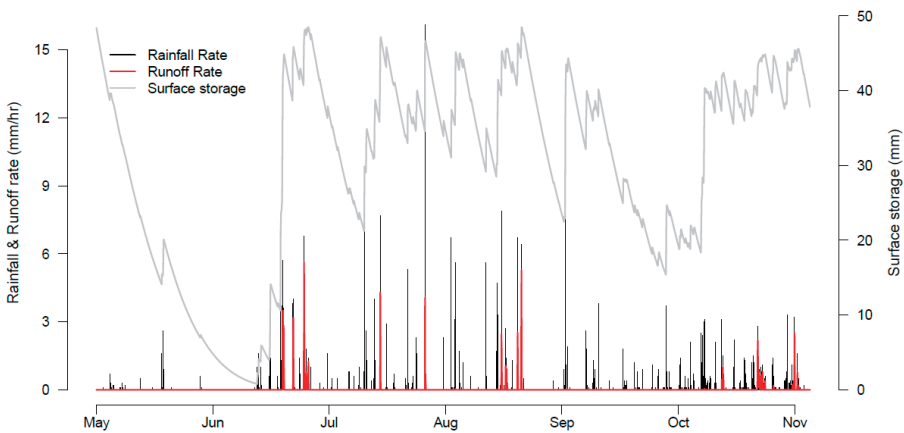


**Figure 6.2.** Rainfall and surface runoff rate and amount of water stored at the soil surface of a raised bog. The surface topography of the raised bog was based on elevation measurements in Männikjärve bog (Estonia) and a synthetic microtopography. The hourly precipitation data were measured in Männikjärve bog in 2009.

## Microtopography and response time in shallow groundwater ecosystems

As mentioned in the previous section, raised bogs are a typical example of systems with shallow groundwater levels. Raised bogs are dome-shaped and have the groundwater level typically located within a few decimetres below the ground surface (Baird et al., 2008). Raised bogs develop from lakes or flat marshy areas, over mineral substrates. With time, the peat progresses to a level where it is only fed by precipitation and the groundwater develops an atmocline signature. At this point the bog starts to form its dome shape. In NW-Germany, Eggelsmann (1967) found an average dome-height of 5 m for 64 raised bogs with an average diameter of 6 km. These peat bodies drain horizontally by gravity to adjacent areas with lower groundwater levels. The integrity of these bogs is only ascertained when water is stored in the peat body in periods of a precipitation deficit

and efficiently removed in wet periods (Baird et al., 2008; Tsuboya et al., 2001). The vegetation that constitutes the raised bogs requires shallow groundwater levels to avoid consolidation and mineralization, but cannot survive prolonged periods of flooding. To maintain a relatively stable water table, the bog's top layer swells in response to precipitation excess, and shrinks under evaporative demand, thereby influencing its hydraulic conductivity, while deeper layers have a much lower hydraulic conductivity as a result of compaction despite water contents up to 90% (Rezanezhad et al., 2010; Rycroft et al., 1975).

The surface topography of peatlands (Figure 6.3 features examples) consists of several morphological features: pools, wet depressions with *Sphagnum* species and sedges (hollows), stretches of *Sphagnum* species (lawns), drier mounds with *Sphagnum* species and vascular plants (hummocks), and higher, drier areas with terrestrial vegetation (ridges) (Belyea and Clymo, 2001; van Breemen, 1995; Wallén et al., 1988). Hummocks and hollows have a characteristic spatial scale of 10-100 m<sup>2</sup>, and reported heights from a few centimetres to over 50 cm. On bogs, the higher ridges can feature smaller scale compositions of lawns and hummocks, whereas on fens the ridges tend to have a more uniform small-scale surface topography. In boreal to sub-arctic zones, and sometimes in maritime and alpine parts of the mid-temperate zone, raised bogs are characterized by a surface pattern of pools and ridges (Belyea, 2007). Pools form secondarily on such bogs and the cause of their formation remains an open question. The width of the pools ranges from less than 1 m on sloping sites to over 100 m in flat areas. Once formed, the topographic features are sustained by a positive feedback mechanism, in which hummocks and ridges have a higher growth rate in comparison to hollows and pools and therefore keep their elevated position in the peat bog (Belyea and Clymo, 2001; Sjörs, 1990). Ridge-pool patterning mainly orients perpendicular to a bog's slope and has a profound influence on surface runoff by determining the length and orientation of flowpaths. In wet periods, the depression storage capacity of pools may be exceeded, leading to coalescence of pools and rapid drainage by surface flow (Quinton and Roulet, 1998). In addition, microtopography increases species richness in peatlands and other wet ecosystems (Peach and Zedler, 2006; Vivian-Smith, 1997). An increase in species richness can directly influence the routing of surface runoff. It was shown by Holden et al. (2008) that *Sphagnum* provided a greater effective hydraulic roughness than peatland grasses. Variation in hydraulic roughness may have an influence on the convergence or divergence of surface runoff, in turn affecting the amount of water a neighboring patch of vegetation receives. Similar feedbacks are found in semi-arid areas where vegetation patches influence hydraulic conductivity and direction of flowpaths (Bergkamp, 1998; Mueller et al., 2007; Rietkerk et al., 2002).

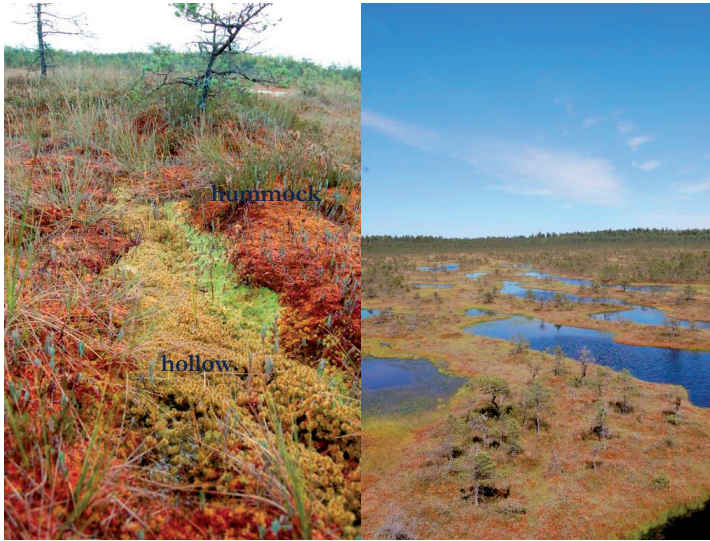


**Figure 6.3.** Surface topography at two spatial scales on Männikjärve raised bog in Estonia. Left: a hollow surrounded by hummocks, right: secondary formed pools between ridges.

The structure and the hydraulic properties of raised bogs make a sharp distinction between the surface and the subsurface difficult. In the mid-twentieth century, Russian scientists therefore separated surface and subsurface processes with the acrotelm-catotelm concept to explain peatland functioning. The concept comprises an upper active ‘acrotelm’ layer with a high hydraulic conductivity, storage capacity, and a fluctuating water table and a more inert lower ‘catotelm’ layer that corresponds to the permanently saturated main body of peat (Ivanov, 1981; Romanov, 1968). Outside Russia, the acrotelm-catotelm concept was adopted by Ingram (1978) who considered it a fundamental concept for all understanding of the hydrology, ecology, and pedology of peatlands. The distinction between acrotelm and catotelm is a conceptual one, the layers cannot be separated in the sense of physical or morphometrical properties like soil horizons. The concept is mainly based on the position of the lowest groundwater level during a year with drought. Clymo (1978);(1984) defined the acrotelm and catotelm differently, by partitioning the oxic and anoxic decomposition of peat. This concept is often used in peatland decomposition and accumulation studies (e.g. Frolking et al. (2001)). Both definitions were then mixed and perceived as linked (Morris et al., 2011), and nowadays they are used regularly in ecohydrology and peat-development modelling.

In the acrotelm-catotelm concept the raised bog is modelled with a groundwater equation based on Darcy’s law and the equation of the conservation of mass. The acrotelm is treated as an aquifer layer, and the catotelm as an aquitard. The concept definition implies that most runoff will occur within the upper peat layer, close to or at the peat surface as groundwater flow, and that this layer (the acrotelm) has a hydraulic

conductivity that is much larger than that of the lower catotelm layer. Reported hydraulic conductivities for the catotelm range from  $10^{-4}$  to  $10^2$  m d<sup>-1</sup> (Chason and Siegel, 1986; Rycroft et al., 1975), which sometimes raises the question if the catotelm acts as the aquitard or rather the underlying sediment (Reeve et al., 2000). In the acrotelm hydraulic conductivities are highly variable. Rosa and Larocque (2008) reported hydraulic conductivity variations over a factor of 44 within the upper 40 cm of the acrotelm, and may exceed values of  $10^5$  m d<sup>-1</sup> (Holden and Burt, 2003a; van der Schaaf, 2004). Hydraulic conductivities in peat also depend on the formation of methane gas bubbles that may block pores and decrease the hydraulic conductivity (Baird and Gaffney, 1995; Beckwith and Baird, 2001).

Although the acrotelm-catotelm concept has broad utility, it ignores the important role of macropores and soil pipes in connecting deep and shallow parts of a peat profile (Holden and Burt, 2003b). All ecological, hydrological and biochemical processes and structures have to be explained by a single boundary, rendering the concept inflexible, and incapable of representing a range of ecohydrological phenomena (Morris et al., 2011). These phenomena include heterogeneity in the structure and function of bogs and fens, fast processes occurring near the surface and interactions between peat growth and hydrological processes (Belyea and Baird, 2006). The horizontal spatial heterogeneity found in peat properties is linked to the topographic features found in peatlands (Waddington et al., 2010). This spatial variability impacts flow patterns over the bog (Baird et al., 2008; Eppinga et al., 2009; Lapen et al., 2005). Ronkanen and Kløve (2007) used both oxygen and hydrogen isotopes as well as conventional tracers (KBr, KI) in tracer tests to find water flow paths in a treatment system established on natural peatland in Finland. They found that beside preferential flow paths, water flows mainly in the top of the peat layer. This implies that for the water flow dynamics in peatlands, surface flow processes need to be considered and that an integrated approach of surface and subsurface flow is desired. Considering fast and slow water movement in raised bogs and fens by combining surface runoff and groundwater flow would allow to account for vegetation, related (micro)topography and preferential flowpaths; important three-dimensional components of peatland hydrology (Waddington et al., 2010) that cannot be fitted into the acrotelm-catotelm concept. Adding a concept capturing the effect of surface topography on water flow, as a different approach to model peatland hydrology will, even with a simple approach as described in the previous section (Figure 6.2), increase the understanding of the hydrological functioning of raised bogs.

In ecosystems such as raised bogs and lowland peats, the hydrology and vegetation are adjusted to each other. Besides routing surface runoff, microtopography influences characteristic response times of the groundwater-surface runoff system, the relevance of which we show here by considering the groundwater system as a linear reservoir, drained by a set of parallel streams (Figure 6.4). In the reservoir, the recession of the groundwater level after cessation of groundwater recharge ( $R = 0$ ) is a function of time (Kraijenhoff van de Leur, 1958):

$$h(t) = h(0)e^{-\frac{t}{j}} \quad (6.1)$$

where  $h(t)$  is the groundwater level [L] relative to surface water level at designated time  $t$  [T],  $h(0)$  is the initial groundwater level, and  $j$  is the reservoir coefficient [T], which is the time in which the groundwater level drops by a factor  $e^{-1}$  or by 37%.

For a phreatic aquifer domain in between two parallel streams, schematized in Figure 6.4, the equation of Kraijenhoff van de Leur (1958) is a good approximation of the reservoir parameter:

$$j = \frac{\mu L^2}{\pi^2 k D} \quad (6.2)$$

where  $L$  (L) is the distance between the streams (or ephemeral channels),  $\mu$  (-) is the phreatic storage coefficient,  $k$  (L/T) is the hydraulic conductivity, and  $D$  the average thickness of the phreatic aquifer (L). The reservoir coefficient can be used to simulate the dynamics of the groundwater level as a function of groundwater recharge (Bierkens and van den Hurk, 2007; Kraijenhoff van de Leur, 1958). It gives insight in the dynamics of the groundwater level: if  $j$  is small, the level reacts quickly to inputs and if  $j$  is large it reacts slowly. The  $j$ -values range from 1 d for small wet systems to 1000 d for large dry systems, depending on the hydrologic properties of the system. Examples of values of the reservoir parameter and its constituents are given in Table 6.1.

**Table 6.1.** Values for the reservoir parameter  $j$  (Kraijenhoff van de Leur, 1958) and its constituents of two hydrological systems (Hendriks, 2010; Werkgroep Herziening Cultuurtechnisch Vademecum, 1988).

	$\mu$ (-)	L (m)	k (m/d)	D (m)	j (d)
Managed fen	0.1	10	0.1	4	2.5
Ice pushed ridge	0.3	1000	5	30	203

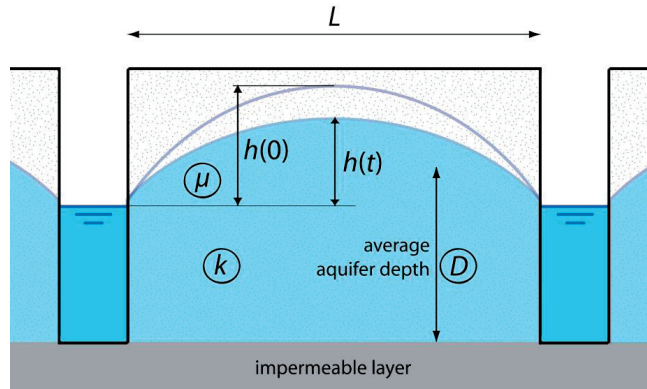


**Figure 6.4.** Schematization of field between two major streams.  $L$  is the distance between the streams,  $\mu$  the phreatic storage coefficient,  $k$  the hydraulic conductivity,  $D$  the average thickness of the phreatic aquifer,  $h(0)$  is the initial groundwater level between the streams, and  $h(t)$  the level at designated time  $t$  during the recession period.

At a smaller scale ( $j$ -range less extensive), the reservoir concept is relevant for wetlands too. Small values of  $j$  imply that the groundwater level fluctuations are small and the horizontal discharge  $q$  ( $L/T$ ), proportional to  $h$  ( $L$ ), will quickly flatten out the water table. Hence, large systems (large  $L$ ) that respond slowly lead to a large value of  $j$ , while highly conductive materials (coarse sand, gravel) allow groundwater to flow quickly, and lead to a decrease of  $j$ . This equation suggests that geometry ( $L$ ) has a larger effect on groundwater level response than hydraulic properties and neglects slight topographical height variations: the equation mainly emphasizes the importance of the distance between draining streams. Both the loss of storage in time and the resistance to water flow are proportionally related to  $L$ , therefore  $j$  depends on  $L^2$ .

It is interesting, though, that when  $k$  and  $D$  are large, a large distance  $L$  between draining streams will be sufficient to discharge all precipitation in wet periods. Likewise, when water flow in the soil is slow due to small  $kD$ , a fast discharge of precipitation can only be obtained when systems develop a small distance  $L$  between draining streams. Such streams develop by soil erosion in wet periods, when saturation excess surface runoff occurs in microchannels. Hence,  $kD$  and  $L$  are related.

In wet ecosystems,  $j$  varies considerably with the groundwater level. The  $j$ -function is an ecosystem feedback function as in wet periods both  $L$  and  $j$  are small and rainwater is quickly discharged, whereas in dry conditions  $L$  and  $j$  are large and water is retained. This feedback can be considered an example of hydrologic self-organization.

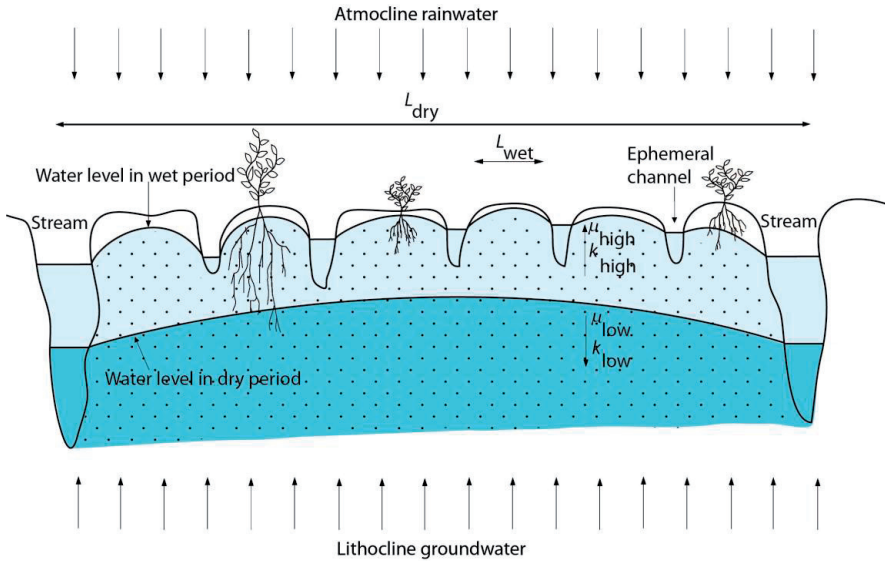


**Figure 6.5.** Self-organized ecosystem, where feedback processes between hydrology and topography create favourable conditions for various plant species.

The surface of natural wetlands is characterised by a complex pattern of ephemeral channels and streams and intermediate higher terrain. A broad variety of patterns has been observed (Larsen and Harvey, 2011), most of which can be conceptualized as a complex of nested systems (Figure 6.5). In prolonged wet periods, a wetland ecosystem features a small reservoir coefficient because the hydraulic conductivity is large and  $L_{wet}$  is small, even though the storage coefficient maybe higher than in dry periods, especially in peat soils. Under prolonged dry conditions (when  $L=L_{dry}$  and hydraulic conductivity is small) the reservoir coefficient is large. This corresponds conceptually with the acrotelm-catotelm concept: the fast acrotelm flow is characterised by a small reservoir coefficient and the slow catotelm flow by a large value. The self-organization of the system with regard to the hazards of drought and wetness are in essence captured adequately with the dependence of  $j$  on  $k$ ,  $L$ , and  $\mu$ .

The above illustration reveals that horizontal drainage distance is the key determinant of the response time of the system. In essence, the presence of nested systems of streams and channels ensure optimal growth conditions for the wetland vegetation, because these systems enable both the discharge and the storage of water under conditions where either of the two is most needed.

## Microtopography and spatial distribution of groundwater quality parameters and site factors

*The content of this section is expanded with respect to the VZJ publication*

As was mentioned in the previous section, it is plausible that complex patterns of ephemeral channels and streams in wetlands affect the hydrological response of the groundwater systems. However, this is not the only impact of draining channels and streams. In areas with upwelling groundwater, infiltrating precipitation water meets groundwater with a different chemical signature and is diverted towards the streams. The volume that is characterized by the infiltrated precipitation water is lens-shaped and for this reason, such water bodies are called precipitation lenses. The interface between locally infiltrated precipitation water and the lithocline upward seeping groundwater is located deepest at the hydrological divide and monotonously becomes shallower in the direction of the draining streams.

This general pattern, depicted by e.g. Cirkel (2003), Schot et al. (2004), Dekker et al. (2005) for fresh water systems and Eeman et al. (2011) for a rainwater lens on saline groundwater, becomes much more complicated when (small) channels convey surface runoff during a limited wet period only. In those periods, part of the infiltrating precipitation does not flow towards the main streams, but towards these more shallow ephemeral channels (Figure 6.6). Close to these channels, the hydraulic gradient is directed towards the shallow draining channels (Figure 6.7) and the interface between infiltrated precipitation water and upward seeping groundwater water becomes situated closer to the soil surface. As Figure 6.6 shows, the interface cones up at places where shallow channels drain by surface flow, thereby mirroring the topography of the soil surface at these places. The interactions described above will of course depend on the ratio of upward and downward fluxes and the duration of high groundwater levels and consequent activation of ephemeral channels.

Ecologically, the interaction between the topography of the soil surface and groundwater quality is important. Obviously, the proximity of the phreatic groundwater level is important for the availability of oxygen to plant roots, which directly, via oxygen stress (Bartholomeus et al., 2008) and indirectly, via redox processes (Hinsinger et al., 2009; Koch et al., 1990; van der Welle et al., 2008), and the release of nutrients by mineralization (Koerselman et al., 1993), affects plant species composition. In view of the different chemical signatures of infiltrated precipitation water and upward seeping groundwater, zonation will also occur with regard to acidity and base cations, availability of macro and micro nutrients and phytotoxic substances such as  $\text{H}_2\text{S}$  and  $\text{Fe}^{2+}$ .

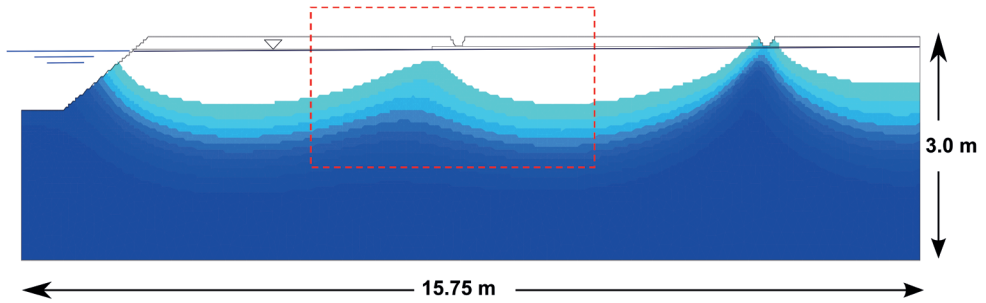


**Figure 6.6.** Calculated transition zone between young infiltrated precipitation water (white) and older upward seeping groundwater (blue), as affected by small ephemeral channels. Calculations were performed with Hydrus-2D for a loamy sand soil with an upward seepage flux of 0.6 mm/d. The red dashed box indicates the position of Figure 6.7.

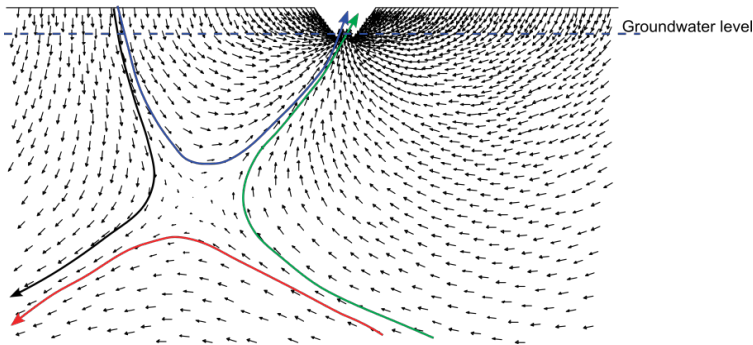


**Figure 6.7.** Flow pattern as affected by an ephemeral channel during a wet period.

Studies linking vegetation patterns to microtopographic features are however very scarce and mainly limited to the raised bog literature. In these studies, microtopography is mainly described in a qualitative manner using the earlier mentioned terms ‘hummock’, ‘hollow’, ‘lawn’ etc. (Eldridge et al., 1991). The advantage of such a description is that it gives a quick impression of the characteristics of a certain sites, but it limits the comparability of different studies and make it impossible to derive quantitative relationships. Recently, more quantitative descriptions of microtopography in groundwater fed wetlands were given by Smith et al. (2012), showing height variation between 15 and 25 cm and hummock diameters between 50 and 110 cm. Information on small scale water quality and vegetation patterns related to microtopography (described by geostatistical parameters) is to our knowledge largely unavailable in this context.

To this end, we combined our detailed pH measurements and vegetation samples (see Chapter 5) with detailed measurements of microtopography using a pin frame measuring device (Figure 1.5). Using the pin frame, we took 800 height measurements per 4 m<sup>2</sup> sampling plot (Figure 4.2) for each of the four plots in the Meeuwenkampje nature reserve. We expressed the microtopographical variation quantitatively using generic height characteristics Relief (difference between minimum and maximum measurements) and Random Roughness (RR) (standard deviation of measurements corrected for trends) as proposed by Kamphorst et al. (2000). The spatial structure of the microtopographic patterns was described using semivariogram analysis as discussed in Chapter 5. An overview of the microtopographic characteristics of the four plots is given in Table 6.2.

In the Meeuwenkampje reserve, hummock growth by brown mosses and tussock growth by sedges and *Molinia* is suppressed by yearly mowing of the vegetation. Nonetheless, significant microtopographical variation was observed. The spatial scale of the hummocks, as expressed by PCR, was about one meter for the lower lying wet plots 1,3 and 4, which is in line with the results of Smith et al. (2012). Relief varies between 0.09 and 0.16 and is highest in plot 4. The relatively high value for Relief in plot 4 is caused by *Carex elata* tussocks (see Figure 4.2). RR is clearly higher in the poorly drained plots 2 and 4, which points to significant (random) microtopographical variation.

As was hypothesized by Van Wirdum (1991) and shown by Vivian-Smith (1997) and Peach and Zedler (2006), vegetation can respond to very subtle topography variations and resulting abiotic gradients. Nonetheless, abiotic heterogeneity as driver for floral biodiversity remains subject of significant debate, including studies showing no effect (Reynolds et al., 2007). Our detailed measurements in the Meeuwenkampje reserve (Figure 6.8) however support the above notion for very wet sites with microtopography. *Molinia caerulea*, a drought and acid tolerant plant species, is clearly more abundant on the higher and thus dryer and more acid ridges. Another example, *Calliergon cuspidatum*, a moss species resistant to inundation but sensitive to acidification, is clearly more abundant in the hollows of the plot and absent in the most acid parts of the plot. However, other species such as *Carex pulicaris* and *Carex hostiana*, although abundant, do not show any spatial correlation with microtopography in our plots. An explanation for this might be that clonal species are able to integrate their resource use across patch types, thus using homogeneous and heterogeneous habitats (Reynolds et al., 2007), or that these aerenchyma containing species are indifferent for spatial variation in redox conditions and soil acidity as discussed in Chapter 5.

**Table 6.2.** Generic height characteristics, Relief and RR and fitted semivariogram parameters (see Appendix 5B, Chapter 5 for explanation) per plot. For the location of the plots in the Meeuwenkampje reserve see Figure 4.2.

Plot	av. height (m+ MSL)	Stdev	Min (m+ MSL)	Max (m+ MSL)	Relief (m)	RR (m)	c0	c+ c0	PCR (m)	c/c+ c0
1	5.55	0.016	5.50	5.59	0.09	0.012	$3.19 \cdot 10^{-5}$	$3.13 \cdot 10^{-4}$	1.03	0.90
2	5.77	0.020	5.72	5.82	0.10	0.012	$2.50 \cdot 10^{-5}$	$5.79 \cdot 10^{-4}$	3.94	0.96
3	5.66	0.019	5.61	5.72	0.11	0.019	$2.96 \cdot 10^{-5}$	$4.36 \cdot 10^{-4}$	1.00	0.93
4	5.59	0.026	5.53	5.64	0.16	0.022	$9.38 \cdot 10^{-6}$	$7.18 \cdot 10^{-4}$	1.17	0.99

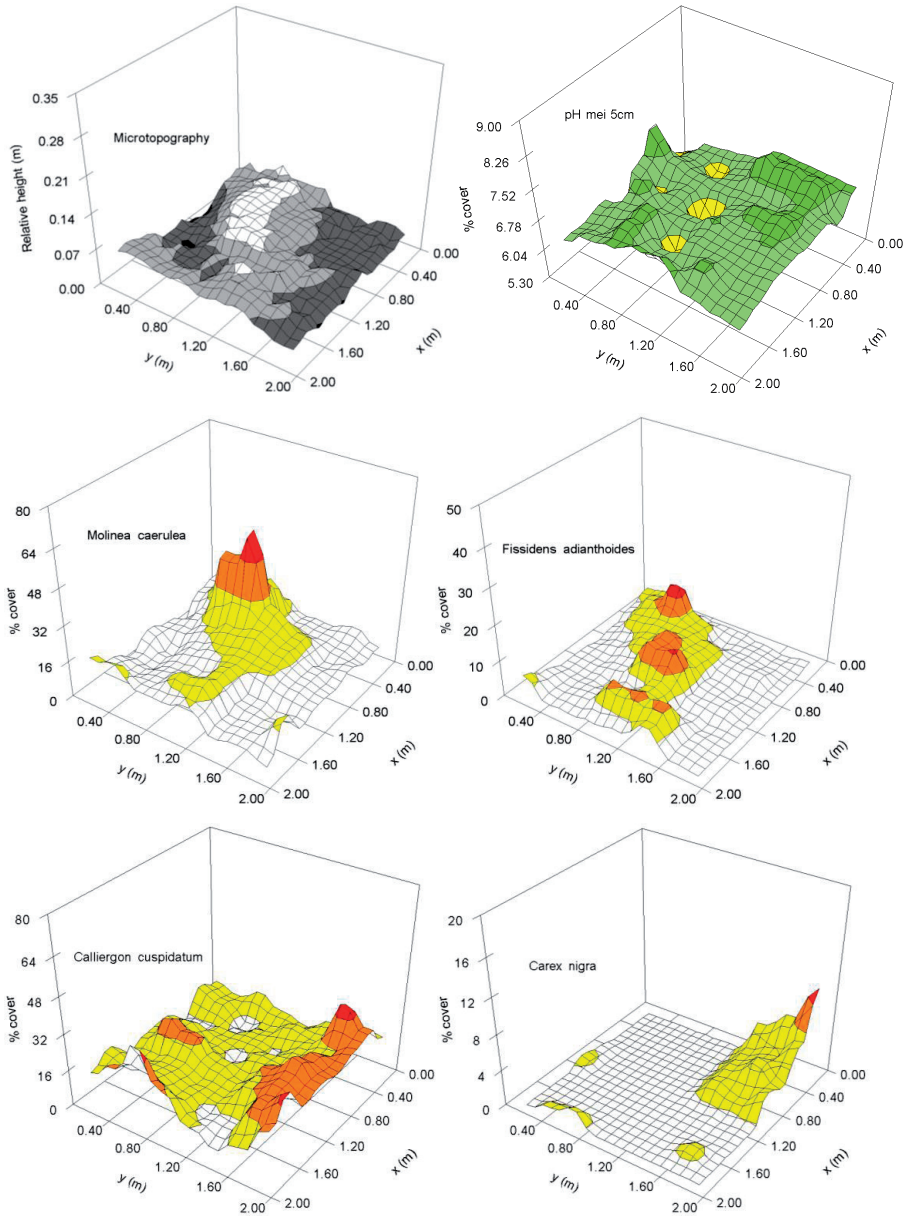


**Figure 6.8.** Microtopography, soil-pH and relative cover of four plant and moss species in a seepage dependent wetland area. Data from fen meadow reserve “Het Meeuwenkampje” (plot 3, see Chapter 4 and 5) in the Netherlands. Microtopography was measured with a pin-meter on a 5-10 cm grid. Vegetation was mapped on a 25 – 25 cm grid.

Although it is clear that microtopography can significantly influence patterns of groundwater flow (Frei et al., 2010) and groundwater quality (Frei et al., 2012), it proves difficult to pinpoint the actual driver for the distribution of plant species over a height gradient. This is due to the correlation between microtopography and important site factors such as soil moisture status, soil aeration (redox status) and pH. Another factor is that abiotic preferences of individual species are still largely unknown and habitat dependent. Moreover, the feedback between vegetation and microtopography can be self-enhancing. *Molinia* for instance forms tussocks due to the production of large amounts of litter that is hard to decompose and thus increases local elevation. In a groundwater fed wetland, this increase in elevation will in turn result in more aerated conditions and less influence of groundwater and as a result more acid conditions. This may result in competitive advantage for *Molinia* compared to co-occurring species adapted to wet, alkaline conditions. To better understand the intricate relationships between microtopography and vegetation composition, more detailed measurements are needed in different wetland habitats.

## Closing remarks

In this chapter, we have discussed some of the interactions between surface runoff and groundwater flow under the influence of microtopography in flat ecosystems with shallow groundwater levels. Microtopography creates a complex spatiotemporal pattern of ponding and redistribution, which in turn results in variability of infiltration into the soil. Microtopography also influences the exfiltration of groundwater and the residence time of water in the system. The in- and exfiltration fluxes of groundwater directly influence the dynamics of chemical transport in the rainwater lens, deeper groundwater, and in particular the transition zone between the two. Dynamics in fluxes and chemistry impact the occurrence of vegetation, and vegetation enhances the spatial variation of soil saturation and microtopography. Therefore, aggregating the nested structure of microtopography into a roughness parameter hampers interpretation of the ecohydrology of flat ecosystems with shallow groundwater levels. Despite much ecological research, the impact of flow and (solute) transport processes on vegetation and possible feedbacks have received little attention from the physics point of view, although the impact of e.g. anaerobicity, and acidity on vegetation development have been demonstrated.

To deal with such complexity, both high resolution data and software tools are needed for improved prediction of surface runoff and soil surface water redistribution. This study shows that high resolution sampling in wetland ecosystems is very laborious, but can provide valuable insight in the influence of microtopography on vegetation composition of wetland ecosystems. Modelling the interaction between surface runoff and groundwater flow under the influence of surface complexity in a fully physical way remains a computational challenge, permitting the use of simple conceptual alternative modelling strategies. This type of models allows a thorough sensitivity analysis of combining several scales of spatial complexity and examine the effect on spatial variability

of hydrological and other site factors in ecosystems with a shallow groundwater level. The increasing availability of detailed topographical data (e.g. LiDAR) of these ecosystems in various regions of the world allows a better investigation of the relation between topography and vegetation patterns. Comparing measured complex topographies with synthetic ones with an increasing level of complexity, will facilitate the understanding of the complex interactions governing the hydrologic responses in these ecosystems.

## **Acknowledgements**

This study was carried out within the framework of the Netherlands Organization for Scientific Research (NWO) CASIMIR programme (018.002.007), the Dutch Water Utility Sector joint research programme (BTO) and the Knowledge for Climate programme. Parts of this work have been sponsored by the Dutch Ministry of Agriculture OBN-Hoogveen research programme, and Alterra (Wageningen UR), the Netherlands.





CHAPTER

**7**

| **Synthesis and outlook**

## Summary of results

Seepage dependent mesotrophic meadows are regarded as the Dutch crown jewels of floral biodiversity, but have nevertheless declined dramatically in area and quality. In order to restore these ecosystems to their full floristic glory and to protect them against future threats, insight is needed of the intricate hydrological and biogeochemical processes driving small scale (cm-dm) gradients in abiotic conditions. It is these small scale gradients that provide the greatest species diversity as long as a functionally diverse species pool is available (Questad and Foster, 2008). Insight in the spatiotemporal variation of water flow and water quality patters contributes to sound management of these ecosystems and better understanding of the effects of changes in water management, changes in climatic conditions and pollution of inflowing groundwater. Therefore, the general aim of the research presented in this thesis was *to provide quantitative insights into the small scale, hydrological and biogeochemical relationships between upward seeping groundwater, infiltrating precipitation water and vegetation patterns*. In response to the specific aims as stated in Chapter 1, the major results presented in this thesis are summarised:

*Aim: Develop a method to infer seepage intensities on an appropriate ecological scale, from measured time series of ground and surface levels and quantify the accuracy and uncertainty associated with the estimation.*

Chapter 2 presents a method to make reliable estimates of seepage intensities from data provided by easy to place and operate piezometers and water level gauges. The method presented here provides insight into the maximum level of accuracy and the minimum level of uncertainty associated with seepage intensity estimates, depending on the measurement time interval of input data and on the accuracy of inferred local geo-hydrological properties and boundary conditions. It appears that combined measurements of groundwater levels, hydraulic heads and especially surface water levels are needed for reliable estimates. Data supplied every fortnight (as is common in the Netherlands) was found to be just as valuable for seepage estimation as modern high frequency measurements.

*Aim: Model the dispersive and chromatographic mixing behaviour at the interface between infiltrated rainwater and upwelling  $\text{Ca}^{2+}$  rich groundwater in order to gain insight in the influence of oscillating flow conditions on (vertical) transport of solutes in precipitation lenses.*

Numerical transport modelling in ORCHESTRA allowed us to explore the combination of physical processes such as convection and dispersion with non-linear sorption chemistry (Chapter 3). Oscillating flow conditions are shown to be an important factor controlling transport of base cations. For an inert solute, we showed that the width of the mixing zone of an oscillating (precipitation lens) interface can be described as a function of the travelled distance of the interface divided by the total time. This illustrates that it does not matter how the interface fluctuates and thus also holds for highly erratic oscillations, for instance as a result of weather forcing. The applied (Gapon type) non-

linear cation exchange lead to Traveling Wave or Rarefied Wave behaviour, depending on the flow direction, matching well with analytical approximations. It was shown that for oscillating flow, the front shape does not shift between the extremes that agree with the analytical approximations, but shows gradual spreading converging to a pure diffusion, non-linear exchange transport case. For practical applications it is therefore possible to ignore convective transport and account for the spreading behaviour by introducing an effective diffusion coefficient. Besides the relevance for soil chemical processes in wetlands, we advocate that our finding may also be relevant for other applications where concentration front positions fluctuate as a function of time, e.g. aquifer storage and recovery, aquifer thermal energy storage, with their own non-linear chemistry.

*Aim: Measure and explain field scale spatial and temporal variation in ground- and soil water quality of mesotrophic meadows with upward seepage, surrounded by intensive agricultural land use*

This aim was explored in Chapter 4, presenting the results of a case study, with hydrological and biogeochemical field measurements in a small seepage dependent nature reserve. This relatively well preserved meadow reserve, called “het Meeuwenkampje”, is located in one of the most intensive agricultural areas of Western Europe. Our field measurements showed that elevation differences of 0.2-0.3 m had a significant influence on field scale water quality patterns, resulting in the development of a precipitation lens. The lens was thin or absent in part of the field with groundwater levels in the vicinity of, or temporarily above, the soil surface. The observed patterns were in agreement with the theory discussed in Chapter 6. Furthermore, upward seeping groundwater was shown to be influenced by agricultural activities in the infiltration area, resulting in very high sulphate concentrations, alkalinity and hardness. Reduction and precipitation processes were observed to strongly determine the water quality profile and ultimately the abiotic conditions of the root zone where the precipitation lens was absent. Chapter 4 shows that seepage dependent fen ecosystems can be remarkably resilient to biogeochemical changes as a result of inflow of sulphate polluted groundwater. Counter intuitively, a fen might even benefit, due to the fact that sulphate pollution often coincides with increased hardness and alkalinity. The reduction of sulphate produces extra alkalinity which might result in active calcite precipitation, ameliorating internal eutrophication, as was shown for the Meeuwenkampje reserve.

*Aim: Determine the influence of small-scale spatiotemporal variation on empirical relationships between soil acidity and vegetation. Main objective is to gain insight in possible mechanistic relations between soil acidity and plant response, with special focus on seepage dependent ecosystems.*

Soil acidity is involved in many complex processes that control plant growth as is reviewed in Chapter 5, but is also influenced by a wide variety of biogeochemical processes. This makes quantifications of mechanistic plant responses (i.e. using a physiologically based variable for plant traits) to soil acidity difficult. A commonly applied alternative is the use of semi quantitative acidity indicator values, as proxy for the various

adaptations of plants to soil acidity. Although relationships between acidity indicator values and soil acidity (expressed as pH) are generally strong, they often show systematic bias and still contain high residual variances. We investigated possible sources of variation and bias on the basis of data from 91 well-documented plots throughout the Netherlands and extremely detailed, within plot, vegetation recordings and pH measurements collected in our case area, the Meeuwenkampje nature reserve. The strength of the relationship was negatively affected by data from wet plots in the neutral to alkaline range. Probably this is caused by indifference for soil acidity of aerenchyma containing species. Plant species with shallow root systems, as adaptation to hypoxia, or mosses seem more responsive to soil acidity in wetland habitats and are probably better predictors of local soil pH. For predictions, it is thus important to differentiate between sites with and without severe oxygen stress. Furthermore, spatiotemporal variation of soil acidity appeared to be a critical source of systematic errors and high residual variances. Consequently, data harmonisation is crucial when combining different datasets. Moreover, our detailed pH measurements showed significant spatial and temporal variation of soil pH in the topsoil. The spatial scale (PCR) of the pH patches corresponds well with the spatial scale of micro-topographic features (Chapter 6), but is not very well reflected by the spatial distribution of indicator values, within a plot. This might be caused by the occurrence of clonal and/or by aerenchyma containing species (Chapter 6).

*Aim: Illustrate the influence of micro-topographical variation on ecohydrological and biogeochemical processes and vegetation patterns in wetlands.*

Micro-topography and surface runoff are shown to be important, yet are often ignored ‘ordering factors’ in wetland ecohydrology (Chapter 6). Microtopography in wetlands creates a complex spatiotemporal pattern of ponding and redistribution of water over the soil surface, which in turn results in variability of infiltration into the soil. This directly influences spatial patterns of shallow groundwater flow and results in small scale abiotic gradients in for instance soil pH (Chapter 5) which impact vegetation composition. Pinpointing the actual driver for small scale distribution of plant species remains a challenge, due to the multiple and interrelated effects of microtopography on abiotic conditions and plant growth. However, the increasing availability of detailed topographical and biochemical data and development of conceptual alternative modelling strategies, such as proposed in Chapter 6, allow a better investigation of the complex interactions between micro-topography, hydrology and vegetation in these ecosystems.

## General discussion and outlook

Combination of a physically based Soil-Water-Plant-Atmosphere model with a modern optimization algorithm as proposed in Chapter 2, enables reliable estimation of seepage intensities from easy to place piezometers and water level gauge data. In practise, however, combined measurements of phreatic groundwater levels, hydraulic heads and especially surface water levels are scarce. This severely hampers application of the method

on field data, such as the 200 relevé dataset mentioned in the end of Chapter 2. For future research, I therefore advocate to equip nature monitoring networks with at least a well-placed phreatic as well as a deep piezometer and monitor water level fluctuations of all relevant drainage levels per relevé. Measuring discharge of the drainage system may further improve predictions. Although the presented method provides local information on seepage intensities, it does not provide information on whether the upward seeping groundwater will actually reach the root zone. To elucidate these patterns, investigation of natural tracers (Chapter 4), representative for the different water types, is crucial.

As is shown in Chapter 4 and 6, shallow flow patterns of seepage and infiltrating precipitation water are strongly dependent on complex interactions between topography and local (ephemeral) drainage systems. Moreover, the infiltration and exfiltration fluxes of groundwater and precipitation water directly influence the dynamics of chemical transport in the precipitation lens, deeper groundwater, and, in particular the transition zone between the two (Chapter 4, Chapter 6). In Chapter 3, we theoretically investigated this mixing behaviour using a simple 1D modelling approach, but part of our findings have been confirmed by more complex 2D modelling (Eeman et al., 2012). Validation of our findings on field data is, however, still urgently needed. Unfortunately, the observations presented in Chapter 4 were not sufficient for this purpose. For instance, very fine scaled water sampling is needed to capture sharpening behaviour as a result of cation exchange. Moreover, a much longer monitoring period is necessary to sufficiently capture climatic forcing. The sandy subsoil of plot 3 in the Meeuwenkampje reserve, would be a good sampling location to perform such a study.

Our finding in Chapter 3, that oscillative mixing can be described with a (non-linear) diffusion equation can be applied for downscaling upward seepage fluxes derived from regional groundwater models. For this, the diffusion model needs to be combined with relatively simple bucket models as for example proposed by Van Immerzeel et al. (1996), Poot and Schot (2000). These models can provide the absolute average movement of the precipitation lens interface needed for the effective diffusion coefficient, yet are not computationally demanding. Using this downscaled data might strongly enhance the predictive power of habitat distribution models.

In Chapter 4 we showed that sulphate polluted groundwater is already reaching the Meeuwenkampje nature reserve. As Mendizabal et al. (2012) shows that sulphate pollution is widespread and increasing in many Dutch aquifers, it is therefore likely that inflow of sulphate will become apparent in many more seepage dependent nature reserves in the coming years. Although the Meeuwenkampje reserve proved remarkably resilient to this threat, it is unclear whether this is the case for other nature reserves. To assess whether that is the case, many more reserves should be investigated obtaining detailed soil profile data on sulphur, iron and carbonate chemistry. The need for detailed profile data on soil chemical properties is also stressed in Chapter 5. In many ecological studies, abiotic conditions are determined by taking a single soil sample from the root zone, or bulking several root zone samples per relevé. In this way, important information on small

scale spatial variation of abiotic conditions is either not taken into account or lost due to the bulking of samples. Moreover, as is shown in Chapter 4 a good interpretation of the processes determining the abiotic conditions of a site is only possible by combining spatial and temporal biogeochemical and hydrological data.

Microtopography structures vegetation in wetland ecosystems (Chapter 6) and influences several important site factors such as soil moisture status, soil aeration (redox status) and pH. Small-scale non-invasive measurements are often very laborious as we encountered measuring soil pH (Chapter 5). Nonetheless these measurements are crucial for understanding how microtopography affects plant growth. For this reason, I recommend to combine microtopography measurements with detailed (micro-invasive) measurements of pH, oxygen, base cations, bicarbonate and redox sensitive elements such as  $\text{Fe}^{2+}$  and  $\text{H}_2\text{S}$ .

If computation times of models integrating 3D groundwater flow, surface runoff and reactive transport can be reduced, it would be interesting to assess the sensitivity of micro-topography related abiotic gradients to different scenarios of drainage conditions, soil physical parameters, seepage intensities meteorological conditions.

## Final conclusions

Although seepage dependent mesotrophic meadows have been the subject of several Dutch ecological dissertations, there has been little quantitative hydrological and hydrochemical research into the controls and relations between upward seepage of groundwater and vegetation composition in these areas. The results presented in this thesis provide new insights into the complex, often small scaled, hydrological and biogeochemical processes driven by the subtle balance between upward seeping groundwater and infiltrating precipitation in these areas. The results can be used to improve empirical relationships between site factors and vegetation, form a step to more mechanistic approaches and identify important processes, which may help the management and restoration of these ecosystems to maximise floral biodiversity.





## | Bibliography

- Abbott, M.B., Bathurst, J.C., Cunge, J.A., O'Connell, P.E., Rasmussen, J., 1986. An introduction to the European Hydrological System – Systeme Hydrologique Europeen, "SHE", 1: History and philosophy of a physically-based, distributed modelling system. *Journal of Hydrology*, 87(1-2): 45-59.
- Abrahams, A.D., Parsons, A.J., Wainwright, J., 2003. Disposition of rainwater under creosotebush. *Hydrological Processes*, 17(13): 2555-2566.
- Ackerly, D.D., Cornwell, W.K., 2007. A trait-based approach to community assembly: partitioning of species trait values into within- and among-community components. *Ecology Letters*, 10(2): 135-145.
- Ahmad, A.R., Nye, P.H., 1990. Coupled diffusion and oxidation of ferrous iron in soils. I. Kinetics of oxygenation of ferrous iron in soil suspension. *Journal of Soil Science*, 41(3): 395-409.
- Ali, M.A., Dzombak, D.A., 1996. Interactions of copper, organic acids, and sulfate in goethite suspensions. *Geochimica et Cosmochimica Acta*, 60(24): 5045-5053.
- Almendinger, J.E., Leete, J.H., 1998. Peat characteristics and groundwater geochemistry of calcareous fens in the Minnesota River Basin, U.S.A. *Biogeochemistry*, 43(1): 17-41.
- Alvarez, R., Evans, L.A., Milham, P.J., Wilson, M.A., 2004. Effects of humic material on the precipitation of calcium phosphate. *Geoderma*, 118(3-4): 245-260.
- Anonymous, 1988. *Cultuurtechnisch vademecum*. Cultuurtechnische vereniging, Utrecht.
- Antoine, M., Javaux, M., Bielders, C., 2009. What indicators can capture runoff-relevant connectivity properties of the micro-topography at the plot scale? *Advances in Water Resources*, 32(8): 1297-1310.
- Antoniou, E.A., van Breukelen, B.M., Putters, B., Stuyfzand, P.J., 2012. Hydrogeochemical patterns, processes and mass transfers during aquifer storage and recovery (ASR) in an anoxic sandy aquifer. *Applied Geochemistry*(0).
- Appelo, C.A.J., 2000. Comment on "Sulfate transport in a Coastal Plain confining unit, New Jersey, USA" (Pucci 1999). *Hydrogeology Journal*, 8(4): 455-456.
- Appelo, C.A.J., Drijver, B., Hekkenberg, R., de Jonge, M., 1999. Modeling In Situ Iron Removal from Ground Water. *Ground Water*, 37(6): 811-817.
- Appelo, C.A.J., Postma, D., 2005. *Geochemistry, Groundwater And Pollution*. Balkema Publishers, Leiden, The Netherlands.
- Appels, W.M., Bogaart, P.W., van der Zee, S.E.A.T.M., 2011. Influence of spatial variations of microtopography and infiltration on surface runoff and field scale hydrological connectivity. *Advances in Water Resources*, 34(2): 303-313.
- Armstrong, W., Beckett, P.M., 1987. Internal Aeration and the Development of Stelar Anoxia in Submerged Roots. A Multishelled Mathematical Model Combining Axial Diffusion of Oxygen in the Cortex with Radial Losses to the Stele, the Wall Layers and the Rhizosphere. *New Phytologist*, 105(2): 221-245.
- Aronovici, V.S., Donnan, W.W., 1946. Soil permeability as a criterion for drainage design. *Transactions of the American Geophysical Union*, 27: 95-101.
- Atkins, W.R.G., 1921. Relation of the Hydrogen-ion Concentration of the Soil to Plant Distribution. *Nature*, 108: 80-81.
- Badon Ghyben, W., 1888. Nota in verband met de voorgenomen putboring nabij Amsterdam. *Tijdschr. Van Koninklijk Instituut Van Ingenieurs*, 5: 8-22.
- Baird, A.J., Eades, P.A., Surridge, B.W.J., 2008. The hydraulic structure of a raised bog and its implications for ecohydrological modelling of bog development. *Ecohydrology*, 1(4): 289-298.
- Baird, A.J., Gaffney, S.W., 1995. A partial explanation of the dependency of hydraulic conductivity on positive pore water pressure in peat soils. *Earth Surface Processes and Landforms*, 20(6): 561-566.
- Bakker, M., 2000. The size of the freshwater zone below an elongated island with infiltration. *Water Resources Research*, 36(1): 109-117.

- Bakker, M., 2010. Radial Dupuit interface flow to assess the aquifer storage and recovery potential of saltwater aquifers. *Hydrogeology Journal*, 18(1): 107-115.
- Bakker, M., Nieber, J.L., 2004. Analytic Element Modeling of Cylindrical Drains and Cylindrical Inhomogeneities in Steady Two-Dimensional Unsaturated Flow. *Vadose Zone Journal*, 3(3): 1038-1049.
- Bartholomeus, R.P. et al., 2012. Process-based proxy of oxygen stress surpasses indirect ones in predicting vegetation characteristics. *Ecohydrology*, 5(6): 746-758.
- Bartholomeus, R.P., Witte, J.P.M., Van Bodegom, P.M., Van Dam, J.C., Aerts, R., 2008. Critical soil conditions for oxygen stress to plant roots: substituting the Feddes-function by a process-based model. *Journal of Hydrology*, 360: 147-165.
- Bates, P.D., Anderson, M.G., Baird, L., Walling, D.E., Simm, D., 1992. Modelling floodplain flows using a two-dimensional finite element model. *Earth Surface Processes and Landforms*, 17(6): 575-588.
- Bates, P.D., Horritt, M.S., Smith, C.N., Mason, D., 1997. Integrating remote sensing observations of flood hydrology and hydraulic modelling. *Hydrological Processes*, 11(14): 1777-1795.
- Bear, J., 1972. *Hydraulics of Groundwater*. McGraw-Hill, New York, USA.
- Beckwith, C.W., Baird, A.J., 2001. Effect of biogenic gas bubbles on water flow through poorly decomposed blanket peat. *Water Resources Research*, 37(3): 551-558.
- Beemster, J., Wendt, T.A., Schipper, P., 2002. Ontwerp grondwaterkwaliteitsmeetnet winning Veenendaal. Koatsuryoku no Kagaku to Gijutsu. Grontmij Advies & Techniek, Houten.
- Beersma, J.J., Buishand, T.A., 2007. Drought in the Netherlands - Regional frequency analysis versus time series simulation. *Journal of Hydrology*, 347(3-4): 332-346.
- Beets, C.P., Hommel, P.W.F.M., de Waal, R.W., 2003. Selectie van referentiepunten t.b.v. het SBB-project terreincondities. Staatsbosbeheer, afdeling Terreinbeheer, Driebergen, 268 pp.
- Begg, C.B.M., Kirk, G.J.D., Mackenzie, A.F., Neue, H.U., 1994. Root-Induced Iron Oxidation and pH Changes in the Lowland Rice Rhizosphere. *New Phytologist*, 128(3): 469-477.
- Bellin, A., Rinaldo, A., Bosma, W.J.P., van der Zee, S.E.A.T.M., Rubin, Y., 1993. Linear equilibrium adsorbing solute transport in physically and chemically heterogeneous porous formations: 1. Analytical solutions. *Water Resources Research*, 29(12): 4019-4030.
- Belyea, L.R., 2007. Climatic and topographic limits to the abundance of bog pools. *Hydrological Processes*, 21(5): 675-687.
- Belyea, L.R., Baird, A.J., 2006. Beyond "the limits to peat bog growth": cross-scale feedback in peatland development. *Ecological Monographs*, 76(3): 299-322.
- Belyea, L.R., Clymo, R.S., 2001. Feedback control of the rate of peat formation. *Proceedings of the Royal Society of London. Series B: Biological Sciences*, 268(1473): 1315-1321.
- Bergkamp, G., 1998. A hierarchical view of the interactions of runoff and infiltration with vegetation and microtopography in semiarid shrublands. *CATENA*, 33(3-4): 201-220.
- Beven, K., Binley, A., 1992. The future of distributed models: Model calibration and uncertainty prediction. *Hydrological Processes*, 6(3): 279-298.
- Beven, K., Freer, J., 2001. Equifinality, data assimilation, and uncertainty estimation in mechanistic modelling of complex environmental systems using the GLUE methodology. *Journal of Hydrology*, 249(1-4): 11-29.
- Beven, K., Lamb, R., Quinn, P., Romanowicz, R., Freer, J., 1995. Topmodel. In: Singh, V.P. (Ed.), *Computer models of watershed hydrology*. Water Resources Publications Colorado, USA, pp. 627-668.
- Beven, K.J., 2002. *Rainfall-runoff modelling, the primer*. Wiley, Chichester, U.K.
- Beven, K.J., 2004. Robert E. Horton's perceptual model of infiltration processes. *Hydrological Processes*, 18(17): 3447-3460.

- Bierkens, M.F.P., van den Hurk, B.J.J.M., 2007. Groundwater convergence as a possible mechanism for multi-year persistence in rainfall. *Geophysical Research Letters*, 34(2): L02402.
- Blacqui re, T., 1986. Nitrate reduction in the leaves and numbers of nitrifiers in the rhizosphere of *Plantago lanceolata* growing in two contrasting sites. *Plant and Soil*, 91(3): 377-380.
- Bloemen, G.W., 1968. Determination of constant rate deep recharge or discharge from groundwater level data. *Journal of Hydrology*, 6(1): 58-68.
- Boeye, D., van Straaten, D., Verheyen, R.F., 1995. A recent transformation from poor to rich fen caused by artificial groundwater recharge. *Journal of Hydrology*, 169(1-4): 111-129.
- Bolt, G.H., 1982. Soil chemistry. B. Physico-Chemical Models. Elsevier, Amsterdam.
- Bolt, G.H., Bruggenwert, M.G.M., 1976. Soil chemistry. A. Basic Elements. Elsevier, Amsterdam.
- Boman, A., Fr jld , S., Backlund, K.,  str m, M.E., 2010. Impact of isostatic land uplift and artificial drainage on oxidation of brackish-water sediments rich in metastable iron sulfide. *Geochimica et Cosmochimica Acta*, 74(4): 1268-1281.
- Bonte, M., Stuyfzand, P.J., van den Berg, G.A., Hijnen, W.A., 2011. Effects of aquifer thermal energy storage on groundwater quality and the consequences for drinking water production: a case study from The Netherlands. *Water science and technology : a journal of the International Association on Water Pollution Research*, 63(9): 1922-1931.
- Bootsma, M.C., Van de Broek, T., Barendregt, A., Beltman, B., 2002. Rehabilitation of acidified floating fens by addition of buffered surface water. *Restoration Ecology*, 10(1): 112-121.
- Bosma, W.J.P., van der Zee, S.E.A.T.M., 1993. Transport of reacting solute in a one-dimensional, chemically heterogeneous porous medium. *Water Resources Research*, 29(1): 117-131.
- Boyer, M.L.H., Wheeler, B.D., 1989. Vegetation Patterns in Spring-Fed Calcareous Fens: Calcite Precipitation and Constraints on Fertility *Journal of Ecology*, 77(2): 597-609.
- Bruggeman, G.A., 1972. Tweedimensionale stroming in semi-spanningswater, Bijlage 5, rapport 'De Groeve'. RID, Leidschendam.
- Bruggeman, G.A., 1999. Analytical Solutions of Geohydrological Problems. *Developments in water science*, 46. Elsevier, Amsterdam.
- Brunner, P., Simmons, C.T., 2012. HydroGeoSphere: A Fully Integrated, Physically Based Hydrological Model. *Ground Water*, 50(2): 170-176.
- Burnham, K.P., Anderson, D.R., 2002. Model Selection and Multi-model Inference: A Practical Information-Theoretic Approach. Springer, New York.
- Casagrande, D.J., Gronli, K., Sutton, N., 1980. The distribution of sulfur and organic matter in various fractions of peat: origins of sulfur in coal. *Geochimica et Cosmochimica Acta*, 44(1): 25-32.
- Chason, D.B., Siegel, D.I., 1986. Hydraulic Conductivity and Related Physical Properties of Peat, Lost River Peatland, Northern Minnesota. *Soil Science*, 142(2): 91-99.
- Cirkel, D.G., 2003. Neerslaglenzen in natte natuurgebieden, een modelstudie naar vorm en functioneren van neerslaglenzen in blauwgraslanden en trilvenen, Afstudeerscriptie, Wageningen Universiteit, Wageningen.
- Cirkel, D.G., 2010. Verdrogingsbestrijding TOP-gebied Meeuwenkampje. Systeemanalyse, knelpuntenanalyse en maatregelen. Provincie Utrecht, Utrecht.
- Cirkel, D.G., Beek, C.G.E.M., Witte, J.P.M., Zee, S.E.A.T.M., 2013. Sulphate reduction and calcite precipitation in relation to internal eutrophication of groundwater fed alkaline fens. *Biogeochemistry*: 1-19.
- Cirkel, D.G., Witte, J.-P.M., van Bodegom, P.M., Nijp, J.J., van der Zee, S.E.A.T.M., 2014. The influence of spatiotemporal variability and adaptations to hypoxia on empirical relationships between soil acidity and vegetation. *Ecohydrology*, 7(1): 21-32.
- Cirkel, D.G., Witte, J.-P.M., van der Zee, S.E.A.T.M., 2010. Estimating seepage intensities from groundwater level time series by inverse modelling: A sensitivity analysis on wet meadow scenarios. *Journal of Hydrology*, 385(1-4): 132-142.

- Cirpka, O.A., Frind, E.O., Helmig, R., 1999. Numerical methods for reactive transport on rectangular and streamline-oriented grids. *Advances in Water Resources*, 22(7): 711-728.
- Cirpka, O.A., Kitanidis, P.K., 2000. Characterization of mixing and dilution in heterogeneous aquifers by means of local temporal moments. *Water Resources Research*, 36(5): 1221-1236.
- Clark, M.P., Slater, A.G., 2006. Probabilistic Quantitative Precipitation Estimation in Complex Terrain. *Journal of Hydrometeorology*, 7(1): 3-22.
- Clark, M.P. et al., 2008. Framework for Understanding Structural Errors (FUSE): A modular framework to diagnose differences between hydrological models. *Water Resources Research*, 44: W00B02.
- Clymo, R.S., 1962. An Experimental Approach to Part of the Calcicole Problem. *Journal of Ecology*, 50(3): 707-731.
- Clymo, R.S., 1978. A Model of Peat Bog Growth. In: Heal, O.W., Perkins, D.F. (Eds.), *Production Ecology of British Moors and Montane Grasslands*. Ecological Studies. Springer Berlin Heidelberg, pp. 187-223.
- Clymo, R.S., 1984. The Limits to Peat Bog Growth. *Philosophical Transactions of the Royal Society of London. B, Biological Sciences*, 303(1117): 605-654.
- Dagan, G., 1989. *Flow and Transport in Porous Media*. Springer, New York.
- Danen-Louwerse, H.J., Lijklema, L., Coenraats, M., 1995. Coprecipitation of phosphate with calcium carbonate in Lake Veluwe. *Water Research*, 29(7): 1781-1785.
- Darboux, F., Davy, P., Gascuel-Oudou, C., Huang, C., 2002. Evolution of soil surface roughness and flowpath connectivity in overland flow experiments. *CATENA*, 46(2-3): 125-139.
- Davies, R.B., 1987. Hypothesis testing when a nuisance parameter is present only under the alternative. *Biometrika*, 74(1): 33-43.
- De Baets, S., Poesen, J., Gyssels, G., Knapen, A., 2006. Effects of grass roots on the erodibility of topsoils during concentrated flow. *Geomorphology*, 76(1-2): 54-67.
- De Josselin de Jong, G., 1958. Longitudinal and transverse diffusion in granular deposits. *Transactions American Geophysical Union*, 39: 67-74.
- De Josselin de Jong, G., Van Duijn, C.J., 1986. Transverse dispersion from an originally sharp fresh-salt interface caused by shear flow. *Journal of Hydrology*, 84(1-2): 55-79.
- De Lange, W.J., 1996. *Groundwater modeling of large domains with analytic elements*, Delft University of Technology, Delft.
- de Louw, P.G.B. et al., 2011. Shallow rainwater lenses in deltaic areas with saline seepage. *Hydrol. Earth Syst. Sci. Discuss.*, 8(4): 7657-7707.
- DeGaetano, A.T., Wilks, D.S., 2009. Radar-guided interpolation of climatological precipitation data. *International Journal of Climatology*, 29(2): 185-196.
- Dekker, S.C., Barendregt, A., Bootsma, M.C., Schot, P.P., 2005. Modelling hydrological management for the restoration of acidified floating fens. *Hydrological Processes*, 19(20): 3973-3984.
- Devau, N., Cadre, E.L., Hinsinger, P., Jaillard, B., Gérard, F., 2009. Soil pH controls the environmental availability of phosphorus: Experimental and mechanistic modelling approaches. *Applied Geochemistry*, 24(11): 2163-2174.
- Diaz, S. et al., 2004. The plant traits that drive ecosystems: Evidence from three continents. *Journal of Vegetation Science*, 15(3): 295-304.
- Diekmann, M., 1995. Use and improvement of Ellenberg's indicator values in deciduous forests of the Boreo-nemoral zone in Sweden. *Ecography*, 18: 178-189.
- Diekmann, M., 2003. Species indicator values as an important tool in applied plant ecology - a review. *Basic and Applied Ecology*, 4(6): 493-506.
- Dierschke, H., 1994. *Pflanzensoziologie Grundlagen und Methoden*. Eugen Ulmer: Stuttgart.
- Dillon, P. et al., 2006. Role of aquifer storage in water reuse. *Desalination*, 188(1-3): 123-134.

- Drew, M.C., 1983. Plant injury and adaptation to oxygen deficiency in the root environment: A review. *Plant and Soil*, 75: 179-199.
- Duff, S.M.G., Sarath, G., Plaxton, W.C., 1994. The role of acid phosphatases in plant phosphorus metabolism. *Physiologia Plantarum*, 90(4): 791-800.
- Dunne, T., Black, R.D., 1970. An Experimental Investigation of Runoff Production in Permeable Soils. *Water Resources Research*, 6(2): 478-490.
- Dunne, T., Zhang, W., Aubry, B.F., 1991. Effects of rainfall, vegetation, and microtopography on infiltration and runoff. *Water Resources Research*, 27(9): 2271-2285.
- Dzwonko, Z., 2001. Assessment of light and soil conditions in ancient and recent woodlands by Ellenberg indicator values. *Journal of Applied Ecology*, 38: 942-951.
- Eeman, S., Leijnse, A., Raats, P.A.C., van der Zee, S.E.A.T.M., 2011. Analysis of the thickness of a fresh water lens and of the transition zone between this lens and upwelling saline water. *Advances in Water Resources*, 34(2): 291-302.
- Eeman, S., van der Zee, S.E.A.T.M., Leijnse, A., de Louw, P.G.B., Maas, C., 2012. Response to recharge variation of thin rainwater lenses and their mixing zone with underlying saline groundwater. *Hydrology and Earth System Sciences*, 16(10): 3535-3549.
- Efron, B., 1979. Bootstrap Methods: Another Look at the Jackknife. *The Annals of Statistics*, 7(1): 1-26.
- Eggelsman, R., 1981. Oekologische Aspekte von antropogen beeinflussten und unbeeinflussten Mooren Norddeutschlands. Universität Oldenburg, Bremen.
- Eggelsmann, R., 1967. Oberflächengefälle und Abflussregime der Hochmoore. *Wasser und Boden*, 19: 247-252.
- Eldridge, D.J., Westoby, M., Holbrook, K.G., 1991. Soil-surface characteristics, microtopography and proximity to mature shrubs: effects on survival of several cohorts of *Atriplex vesicaria* seedlings. *The Journal of Ecology*: 357-364.
- Ellenberg, H. et al., 1991. Zeigerwerte von Pflanzen in Mitteleuropa. *Scripta Geobotanica*, 18. Verlag Erich Goltze KG, Göttingen, 77 pp.
- Eppinga, M.B., de Ruiter, P.C., Wassen, M.J., Rietkerk, M., 2009. Nutrients and hydrology indicate the driving mechanisms of peatland surface patterning. *The American Naturalist*, 173(6): 803-818.
- Ernst, R.F., 1956. Calculation of the steady flow of groundwater in vertical cross sections. *Netherlands Journal of Agricultural Science*, 4: 126-131.
- Ernst, R.F., 1983. Wegzijing en kwel; de grondwaterstroming van hogere naar lagere gebieden, Instituut voor Cultuurtechniek en Waterhuishouding, Wageningen.
- Ertsen, A.C.D., 1999. Ecohydrological impact-assessment modeling: an example for terrestrial ecosystems in Noord-Holland, the Netherlands. *Environmental Modeling and Assessment*, 4(1): 13-22.
- Ertsen, A.C.D., Alkemade, J.R.M., Wassen, M.J., 1998. Calibrating Ellenberg indicator values for moisture, acidity, nutrient availability and salinity in the Netherlands. *Plant Ecology*, 135: 113-124.
- Falkengren-Grerup, U., Quist, M.E., Tyler, G., 1995. Relative importance of exchangeable and soil solution cation concentrations to the distribution of vascular plants. *Environmental and Experimental Botany*, 35(1): 9-15.
- Feddes, R.A., Kowalik, P.J., Zaradny, H., 1978. Simulation of field water use and crop yield. *Simulation Monographs*. Pudoc, Wageningen, 189 pp.
- Fiedler, F.R., Ramirez, J.A., 2000. A numerical method for simulating discontinuous shallow flow over an infiltrating surface. *International Journal for Numerical Methods in Fluids*, 32(2): 219-239.
- Fitter, A.H., Hay, R.K.M., 2001. *Environmental physiology of plants*. London: Academic Press, 367 pp.
- Fowler, D. et al., 2007. Long Term Trends in Sulphur and Nitrogen Deposition in Europe and the Cause of Non-linearities. *Water, Air, & Soil Pollution: Focus*, 7(1-3): 41-47.

- Freeze, R.A., Harlan, R.L., 1969. Blueprint for a physically-based digitally simulated hydrologic response model. *Journal of Hydrology*, 9: 237-258.
- Frei, S., Knorr, K.H., Peiffer, S., Fleckenstein, J.H., 2012. Surface micro-topography causes hot spots of biogeochemical activity in wetland systems: A virtual modeling experiment. *Journal of Geophysical Research: Biogeosciences*, 117.
- Frei, S., Lischeid, G., Fleckenstein, J.H., 2010. Effects of micro-topography on surface-subsurface exchange and runoff generation in a virtual riparian wetland – A modeling study. *Advances in Water Resources*, 33(11): 1388-1401.
- Frolking, S. et al., 2001. Modeling Northern Peatland Decomposition and Peat Accumulation. *Ecosystems*, 4(5): 479-498.
- Gao, Q., Li, M., Yu, M., Spitler, J.D., Yan, Y.Y., 2009. Review of development from GSHP to UTES in China and other countries. *Renewable and Sustainable Energy Reviews*, 13(6-7): 1383-1394.
- Geelhoed, J.S., Hiemstra, T., Van Riemsdijk, W.H., 1997. Phosphate and sulfate adsorption on goethite: Single anion and competitive adsorption. *Geochimica et Cosmochimica Acta*, 61(12): 2389-2396.
- Gelman, A., Rubin, D., 1992. Inference from iterative simulation using multiple sequences. *Statistical Science* 7: 457-511.
- Glaser, P.H., Janssens, J.A., Siegel, D.I., 1990. The Response of Vegetation to Chemical and Hydrological Gradients in the Lost River Peatland, Northern Minnesota. *Journal of Ecology*, 78(4): 1021-1048.
- Goreau, T.J. et al., 1980. Production of NO<sub>2</sub>- and N<sub>2</sub>O by Nitrifying Bacteria at Reduced Concentrations of Oxygen. *Applied and Environmental Microbiology*, 40(3): 526-532.
- Green, J.C., 2005. Modelling flow resistance in vegetated streams: review and development of new theory. *Hydrological Processes*, 19(6): 1245-1259.
- Grime, J.P., 1963. Factors Determining the Occurrence of Calcifuge Species on Shallow Soils Over Calcareous Substrata. *Journal of Ecology*, 51(2): 375-390.
- Grime, J.P., 1977. Evidence for the Existence of Three Primary Strategies in Plants and Its Relevance to Ecological and Evolutionary Theory. *The American Naturalist*, 111(982): 1169-1194.
- Grootjans, A.P., 1985. Changes of groundwater regime in wet meadows., PhD thesis, Rijksuniversiteit Groningen, Groningen.
- Grootjans, A.P. et al., 2006. Hydrological landscape settings of base-rich fen mires and fen meadows: an overview. *Applied Vegetation Science*, 9(2): 175-184.
- Grootjans, A.P. et al., 2005. Calcareous spring mires in Slovakia; Jewels in the Crown of the Mire Kingdom. *Stapfia 85, zugleich Kataloge der OÖ. Landesmuseen*(35): 97-115.
- Grootjans, A.P., Van Diggelen, R., Wassen, M.J., Wiersinga, W.A., 1988. The effects of drainage on groundwater quality and plant species distribution in stream valley meadows. *Vegetatio*, 75(1-2): 37-48.
- Guerinot, M.L., 2001. Improving rice yields; ironing out the details. *Nat Biotech*, 19(5): 417-418.
- Hairsine, P.B., Rose, C.W., 1992. Modeling water erosion due to overland flow using physical principles: 1: sheet flow. . *Water Resources Research*, 28(1): 237-243.
- Hájková, P. et al., 2011. How a Sphagnum fuscum-dominated bog changed into a calcareous fen: the unique Holocene history of a Slovak spring-fed mire. *Journal of Quaternary Science*, 27: 233-243.
- He, G. et al., 2010. Factors Controlling Surface Water Flow in a Low-gradient Subtropical Wetland. *Wetlands*, 30(2): 275-286.
- Hell, R., Stephan, U., 2003. Iron uptake, trafficking and homeostasis in plants. *Planta*, 216(4): 541-551.
- Hendriks, M.R., 2010. *Introduction to Physical Hydrology*. Oxford University Press.
- Herzberg, A., 1901. Die Wasserversorgung einiger Nordseebäder. *J Gasbeleucht Wasserversorgung*, 44: 815-819.

- Hill, M.O., Carey, P.D., 1997. Prediction of yield in the Rothamsted Park Grass Experiment by Ellenberg indicator values. *Journal of Vegetation Science*, 8: 579-586.
- Hill, M.O., Roy, D.B., Mountford, J.O., Bunce, R.G.H., 2000. Extending Ellenberg's indicator values to a new area: an algorithmic approach. *Journal of Applied Ecology*, 37(1): 3-15.
- HilleRisLambers, R., Rietkerk, M., van den Bosch, F., Prins, H.H., de Kroon, H., 2001. Vegetation pattern formation in semi-arid grazing systems. *Ecology*, 82(1): 50-61.
- Hinsinger, P., 2001. Bioavailability of soil inorganic P in the rhizosphere as affected by root-induced chemical changes: a review. *Plant and Soil*, 237(2): 173-195.
- Hinsinger, P., Bengough, A.G., Vetterlein, D., Young, I., 2009. Rhizosphere: biophysics, biogeochemistry and ecological relevance. *Plant and Soil*, 321(1-2): 117-152.
- Hinsinger, P., Plassard, C., Tang, C., Jaillard, B., 2003. Origins of root-mediated pH changes in the rhizosphere and their responses to environmental constraints: A review. *Plant and Soil*, 248(1): 43-59.
- Holden, J., Burt, T.P., 2003a. Hydraulic conductivity in upland blanket peat: measurement and variability. *Hydrological Processes*, 17(6): 1227-1237.
- Holden, J., Burt, T.P., 2003b. Hydrological studies on blanket peat: the significance of the acrotelm-catotelm model. *Journal of Ecology*, 91(1): 86-102.
- Holden, J. et al., 2008. Overland flow velocity and roughness properties in peatlands. *Water Resources Research*, 44(6).
- Hoogendoorn, J.H., 1990. Enige gedachtenvorming met betrekking tot eco-geohydrologie. Rapport PN 90-01-A, Dienst Grondwaterverkenning TNO, Delft.
- Hooghoudt, S.B., 1940. Bijdragen tot de kennis van enige natuurkundige grootheden van de grond. *Verslagen van Landbouwkundig Onderzoek*, 46: 515-707.
- Houba, V.J.G., van der Lee, J.J., Novozamsky, I., 1989. Soil and Plant Analysis, a Series of Syllabi. Part 5. Soil Analysis Procedures. Wageningen Agricultural University, Wageningen.
- Huisman, J.A., Snepvangers, J.J.C., Bouten, W., Heuvelink, G.B.M., 2002. Mapping spatial variation in surface soil water content: comparison of ground-penetrating radar and time domain reflectometry. *Journal of Hydrology*, 269(3-4): 194-207.
- Ingram, H.A.P., 1978. Soil layers in mires: Function and Terminology. *Journal of Soil Science*, 29(2): 224-227.
- Ivanov, K.E., 1981. Water movement in mirelands. Academic press, London.
- Jansen, A.J.M., 2000. Hydrology and restoration of wet heathland and fen meadow communities, PhD thesis Rijksuniversiteit Groningen, Groningen.
- Jansen, A.J.M., Grootjans, A.P., Jalink, M.H., 2000. Hydrology of Dutch Cirsio-Molinietum meadows: Prospects for restoration. *Applied Vegetation Science*, 3(1): 51-64.
- Jansen, P.C., 1995. Verdamping van korte vegetaties in natte natuurgebieden. *H2O*, 28(15).
- Jansen, P.C., Kemmers, R.H., 1995. Ecohydrologisch onderzoek in het natuureservaat 'Het Meeuwenkampje'. Rapport 398, DLO-Staring Centrum, Wageningen.
- Janssen, G.M.C.M., Cirpka, O.A., van der Zee, S.E.A.T.M., 2006. Stochastic analysis of nonlinear biodegradation in regimes controlled by both chromatographic and dispersive mixing. *Water Resources Research*, 42(1): W01417.
- Jelgersma, S., Breeuwer, J.B., 1975. Toelichting bij de geologische overzichtsprofielen door Nederland. In: Staalduin, W.H.Z.C.J. (Ed.), Toelichting bij de geologische overzichtskaarten van Nederland, 91-93. Rijksgeologische dienst, Haarlem.
- Jørgensen, B.B., 1977. Bacterial sulfate reduction within reduced microniches of oxidized marine sediments. *Marine Biology*, 41(1): 7-17.
- Jørgensen, B.B., 1982. Mineralization of organic matter in the sea bed, the role of sulphate reduction. *Nature*, 296(5858): 643-645.
- Journel, A., Huijbregts, C., 1978. Mining Geostatistics. Academic Press, London.

- Juncher Jørgensen, C., Jacobsen, O.S., Elberling, B., Aamand, J., 2009. Microbial Oxidation of Pyrite Coupled to Nitrate Reduction in Anoxic Groundwater Sediment. *Environmental Science & Technology*, 43(13): 4851-4857.
- Käfer, J., Witte, J.P.M., 2004. Cover-weighted averaging of indicator values in vegetation analyses. *Journal of Vegetation Science*, 15(5): 647-652.
- Kamphorst, E.C. et al., 2000. Predicting Depressional Storage from Soil Surface Roughness. *Soil Science Society of America Journal*, 64(5): 1749-1758.
- Karageorgiou, K., Paschalis, M., Anastassakis, G.N., 2007. Removal of phosphate species from solution by adsorption onto calcite used as natural adsorbent. *Journal of Hazardous materials*, 139(3): 447-452.
- Kavetski, D., Kuczera, G., Franks, S.W., 2006a. Bayesian analysis of input uncertainty in hydrological modeling: 1. Theory. *Water Resources Research*, 42(3): W03407.
- Kavetski, D., Kuczera, G., Franks, S.W., 2006b. Bayesian analysis of input uncertainty in hydrological modeling: 2. Application. *Water Resources Research*, 42(3): W03408.
- Kemmers, R.H., Van Delft, S.P.J., 2008. Stikstof-, fosfor- en kaliumbeschikbaarheid en kritische depositiewaarden voor stikstof in korte vegetaties., Alterra, Wageningen.
- Kidd, P.S., Proctor, J., 2001. Why plants grow poorly on very acid soils: are ecologists missing the obvious? *Journal of Experimental Botany*, 52(357): 791-799.
- Kirkby, C.A. et al., 2011. Stable soil organic matter: A comparison of C:N:P:S ratios in Australian and other world soils. *Geoderma*, 163(3-4): 197-208.
- Klijn, F., Witte, J.-P.M., 1999. Eco-hydrology: Groundwater flow and site factors in plant ecology. *Hydrogeology Journal*, 7(1): 65-77.
- Koch, M.S., Mendelssohn, I.A., McKee, K.L., 1990. Mechanism for the Hydrogen Sulfide-Induced Growth Limitation in Wetland Macrophytes. *Limnology and Oceanography*, 35(2): 399-408.
- Koerselman, W., Beltman, B., 1988. Evapotranspiration from fens in relation to Penman's potential free water evaporation (EO) and pan evaporation. *Aquatic Botany*, 31(3-4): 307-320.
- Koerselman, W., Kerkhoven, M., Verhoeven, J., 1993. Release of inorganic N, P and K in peat soils; effect of temperature, water chemistry and water level. *Biogeochemistry*, 20(2): 63-81.
- Konert, M., Vandenberghe, J.E.F., 1997. Comparison of laser grain size analysis with pipette and sieve analysis: a solution for the underestimation of the clay fraction. *Sedimentology*, 44(3): 523-535.
- Koster, E.A., 2005. Recent advances in luminescence dating of Late Pleistocene (cold-climate) aeolian sand and loess deposits in western Europe. *Permafrost and Periglacial Processes*, 16(1): 131-143.
- Kraijenhoff van de Leur, D., 1958. A study of non-steady groundwater flow with special reference to a reservoir coefficient. *De Ingenieur*, 70(87-94).
- Kroes, J.G., Van Dam, J.C., Groenendijk, P., Hendriks, R.F.A., Jacobs, C.M.J., 2008. SWAP version 3.4, Theory description and user manual. Alterra report 1649, Wageningen University and Research Centre, Wageningen.
- Kværner, J., Kløve, B., 2006. Tracing sources of summer streamflow in boreal headwaters using isotopic signatures and water geochemical components. *Journal of Hydrology*, 331(1): 186-204.
- Lamers, L., Dolle, G., Van Den Berg, S., Van Delft, S., Roelofs, J., 2001. Differential responses of freshwater wetland soils to sulphate pollution. *Biogeochemistry*, 55(1): 87-101.
- Landolt, E., 1977. *Okologische Zeigerwerte zur Schweizer Flora*. Veroff. Geobot. Inst. Rubel, 64.
- Lane, S., Hardy, R., 2002. Porous rivers: A new way of conceptualising and modelling river and floodplain flows? *Transport Phenomena in Porous Media*, 2: 425-449.
- Lane, S.N., 1998. Hydraulic modelling in hydrology and geomorphology: a review of high resolution approaches. *Hydrological Processes*, 12(8): 1131-1150.

- Lapen, D.R., Price, J.S., Gilbert, R., 2005. Modelling two-dimensional steady-state groundwater flow and flow sensitivity to boundary conditions in blanket peat complexes. *Hydrological Processes*, 19(2): 371-386.
- Larsen, L.G., Harvey, J.W., 2011. Modeling of hydroecological feedbacks predicts distinct classes of landscape pattern, process, and restoration potential in shallow aquatic ecosystems. *Geomorphology*, 126(3-4): 279-296.
- Lee, D.R., 1977. A device for measuring seepage flux in lakes and estuaries. *LIMNOL. & OCEANOGR.*, 22(1, Jan.1977): 140-147.
- Lefohna, A.S., Husarb, J.D., Husarb, H.B., 1999. Estimating Historical Anthropogenic Global Sulfur Emission Patterns for the Period 1850-1990. *Atmospheric Environment*, 33: 3435-3444.
- Leijnse, H., Uijlenhoet, R., Stricker, J.N.M., 2008. Microwave link rainfall estimation: Effects of link length and frequency, temporal sampling, power resolution, and wet antenna attenuation. *Advances in Water Resources*, 31(11): 1481-1493.
- Levenspiel, O., 1972. *Chemical reaction engineering*. John Wiley & Sons, New York.
- Loeppert, R.H., 1986. Reactions of iron and carbonates in calcareous soils. *Journal of Plant Nutrition*, 9,195-214.(3): 195-214.
- Louchart, X., Voltz, M., Andrieux, P., Moussa, R., 2001. Herbicide Transport to Surface Waters at Field and Watershed Scales in a Mediterranean Vineyard Area. *Journal of Environment Quality*, 30(3): 982-991.
- Luhar, M., Rominger, J., Nepf, H., 2008. Interaction between flow, transport and vegetation spatial structure. *Environmental Fluid Mechanics*, 8(5-6): 423-439.
- Maas, K., 2007. Influence of climate change on a Ghijben-Herzberg lens. *Journal of Hydrology*, 347(1-2): 223-228.
- Makkink, G.F., 1957. Testing the Penman formula by means of lysimeters. *Journal of the Institution of Water Engineers*, 11: 277-288.
- Marschner, H., 1991. Mechanisms of adaptation of plants to acid soils. *Plant and Soil*, 134(1): 1-20.
- McIntyre, N.R., Wheeler, H.S., 2004. A tool for risk-based management of surface water quality. *Environmental Modelling & Software*, 19(12): 1131-1140.
- Meeussen, J.C.L., 2003. ORCHESTRA: An Object-Oriented Framework for Implementing Chemical Equilibrium Models. *Environmental Science & Technology*, 37(6): 1175-1182.
- Meijboom, F.W., Van Noordwijk, M., 1996. Rhizon soil solution samplers as artificial roots. In: Kutcher, L., Huebl, E., Lichtenegger, E., Persson, H., Sobotnik, M. (Eds.), *Root ecology and its practical application*. ISSR, Vienna, pp. 793-795.
- Mendizabal, I., 2011. Public supply well fields as a valuable groundwater quality monitoring network, PhD thesis, VU University Amsterdam.
- Mendizabal, I., Baggelaar, P.K., Stuyfzand, P.J., 2012. Hydrochemical trends for public supply well fields in The Netherlands (1898-2008), natural backgrounds and upscaling to groundwater bodies. *Journal of Hydrology*, 450-451: 279-292.
- Meng, H., Green, T.R., Salas, J.D., Ahuja, L.R., 2008. Development and testing of a terrain-based hydrologic model for spatial Hortonian Infiltration and Runoff/On. *Environmental Modelling & Software*, 23(6): 794-812.
- Miller, E.E., Miller, R.D., 1956. Physical theory for capillary flow phenomena. *Journal of Applied Physics*, 27: 324.
- Morbidelli, R., Corradini, C., Govindaraju, R.S., 2006. A field-scale infiltration model accounting for spatial heterogeneity of rainfall and soil saturated hydraulic conductivity. *Hydrological Processes*, 20(7): 1465-1481.
- Morris, P.J., Waddington, J.M., Bencotter, B.W., Turetsky, M.R., 2011. Conceptual frameworks in peatland ecohydrology: looking beyond the two-layered (acrotelm-catotelm) model. *Ecohydrology*, 4(1): 1-11.

- Moser, K., Ahn, C., Noe, G., 2007. Characterization of microtopography and its influence on vegetation patterns in created wetlands. *Wetlands*, 27(4): 1081-1097.
- Mualem, Y., 1976. A new model for predicting the hydraulic conductivity of unsaturated porous media. *Water Resources Research*, 12(3): 513-522.
- Mueller, E.N., Wainwright, J., Parsons, A.J., 2007. Impact of connectivity on the modeling of overland flow within semiarid shrubland environments. *Water Resources Research*, 43(9): W09412.
- Muggeo, V.M.R., 2003. Estimating regression models with unknown break-points. *Statistics in Medicine*, 22(19): 3055-3071.
- Muggeo, V.M.R., 2004. Segmented package for R Version 0.1-4.
- Mulder, J., Christophersen, N., Kopperud, K., Fjeldal, P., 1995. Water flow paths and the spatial distribution of soils as a key to understanding differences in streamwater chemistry between three catchments (Norway). *Water, Air, and Soil Pollution*, 81(1-2): 67-91.
- Myers, L., Sirois, M.J., 2004. Spearman Correlation Coefficients, Differences between, *Encyclopedia of Statistical Sciences*. John Wiley & Sons, Inc.
- Nash, J.E., Sutcliffe, J.V., 1970. River flow forecasting through conceptual models part I -- A discussion of principles. *Journal of Hydrology*, 10(3): 282-290.
- Neeper, D.A., 2001. A model of oscillatory transport in granular soils, with application to barometric pumping and earth tides. *Journal of Contaminant Hydrology*, 48(3-4): 237-252.
- Neeper, D.A., Stauffer, P.H., 2012. Transport by Oscillatory Flow in Soils with Rate-Limited Mass Transfer: 1. Theory. *Vadose Zone Journal*, 11(2).
- Nepf, H., 1999. Drag, turbulence, and diffusion in flow through emergent vegetation. *Water Resources Research*, 35(2): 479-489.
- Nicholson, B.J., Vitt, D.H., 1990. The paleoecology of a peatland complex in continental western Canada. *Canadian Journal of Botany*, 68(1): 121-138.
- Oenema, O., 1999. Vermindering nutriëntenverlies uit landbouw; van nutriëntenoverschotten naar evenwicht tussen aanvoer en afvoer. *Landschap*, 16(3): 141-152.
- Økland, R., 1990. Vegetation ecology: theory, methods and applications with reference to Scandinavia. *Sommerfeltia Supplement*, 1: 1-233.
- Olde Venterink, H., Wassen, M.J., Verkroost, A.W.M., De Ruiter, P.C., 2003. Species-richness-productivity patterns differ between N-, P-, and K-limited wetlands. *Ecology*, 84(8): 2191-2199.
- Olea, R., 2006. A six-step practical approach to semivariogram modeling. *Stochastic Environmental Research and Risk Assessment*, 20(5): 307-318.
- Oosterbaan, R.J., Sharma, D.P., Singh, K.N., Rao, K.V.G.K., 1990. Crop production and soil salinity: evaluation of field data from India by segmented linear regression with breakpoints. , *Proceedings of the Symposium on Land Drainage for Salinity Control in Arid and Semi-Arid Regions*, pp. 373-383.
- Parkhurst, D.L., Appelo, C.A.J., 1999. A computer program for speciation, batch-reaction, one-dimensional transport, and inverse geochemical calculations, Denver Colorado.
- Parton, W.J., Stewart, J.W.B., Cole, C.V., 1988. Dynamics of C, N, P and S in Grassland Soils: A Model. *Biogeochemistry*, 5(1): 109-131.
- Peach, M., Zedler, J., 2006. How tussocks structure sedge meadow vegetation. *Wetlands*, 26(2): 322-335.
- Pierce, S.C., Pezeshki, S.R., Larsen, D., Moore, M.T., 2009. Hydrology and species-specific effects of *Bacopa monnieri* and *Leersia oryzoides* on soil and water chemistry. *Ecohydrology*, 2: 279-286.
- Piper, A.M., 1953. A graphic procedure for the geo-chemical interpretation of water analysis, USGS Groundwater Note no. 12.

- Plant, L.J., House, W.A., 2002. Precipitation of calcite in the presence of inorganic phosphate. *Colloids and Surfaces A: Physicochemical and Engineering Aspects*, 203(1-3): 143-153.
- Poelman, J.N.B., 1972. Soil material rich in pyrite in non-coastal areas. In: Dost, H. (Ed.), *International symposium on acid sulphate soils*. International Institute for Land Reclamation and Improvement, Wageningen, The Netherlands.
- Poot, A., Schot, P., 2000. Regenwater lenzen: vorm en dynamiek. *Stromingen*, 6(4): 13-26.
- Poozesh, V., Cruz, P., Cholera, P., Bertoni, G., 2007. Relationship between the AI Resistance of Grasses and their Adaptation to an Infertile Habitat. *Annals of Botany*, 99(5): 947-954.
- Postma, D., Jakobsen, R., 1996. Redox zonation: Equilibrium constraints on the Fe(III)/SO<sub>4</sub>-reduction interface. *Geochimica et Cosmochimica Acta*, 60(17): 3169-3175.
- Pouliot, R., Rochefort, L., Karofeld, E., 2011. Initiation of microtopography in revegetated cutover peatlands. *Applied Vegetation Science*, 14(2): 158-171.
- Prommer, H., Barry, D.A., Zheng, C., 2003. MODFLOW/MT3DMS-Based Reactive Multicomponent Transport Modeling. *Ground Water*, 41(2): 247-257.
- Pyne, R.D.G., 2005. *Aquifer storage recovery: a guide to groundwater recharge through wells*. ASR press.
- Questad, E.J., Foster, B.L., 2008. Coexistence through spatio-temporal heterogeneity and species sorting in grassland plant communities. *Ecology Letters*, 11(7): 717-726.
- Quinton, W.L., Roulet, N.T., 1998. Spring and summer runoff hydrology of a subarctic patterned wetland. *Arctic and Alpine Research*: 285-294.
- R Development Core Team, 2008. *R: A language and environment for statistical computing*. R Foundation for Statistical Computing, Vienna.
- Raat, K.J., Vrugt, J.A., Bouten, W., Tietema, A., 2004. Towards reduced uncertainty in catchment nitrogen modelling: Quantifying the effect of field observation uncertainty on model calibration. *Hydrology and Earth System Sciences Discussions*, 8(4): 751-763.
- Raats, P.A.C., 1969. The effect of a finite response time upon the propagation of sinusoidal oscillations of fluids in porous media. *Zeitschrift für Angewandte Mathematik und Physik (ZAMP)*, 20(6): 936-946.
- Raats, P.A.C., 1973. Propagation of Sinusoidal Solute Density Oscillations in the Mobile and Stagnant Phases of a Soil. *Soil Science Society of America Journal*, 37(5): 676-680.
- Raats, P.A.C., Scotter, D.R., 1968. Dynamically Similar Motion of Two Miscible Constituents in Porous Mediums. *Water Resources Research*, 4(3): 561-568.
- Reeve, A.S., Siegel, D.I., Glaser, P.H., 2000. Simulating vertical flow in large peatlands. *Journal of Hydrology*, 227(1-4): 207-217.
- Regina, K., Nykänen, H., Silvola, J., Martikainen, P., 1996. Fluxes of nitrous oxide from boreal peatlands as affected by peatland type, water table level and nitrification capacity. *Biogeochemistry*, 35(3): 401-418.
- Reiniger, P., Bolt, G.H., 1972. Theory of chromatography and its application to cation exchange in soils. *Netherlands Journal of Agricultural Science*, 20: 301-313.
- Reynolds, H.L., Mittelbach, G.G., Darcy-Hall, T.L., Houseman, G.R., Gross, K.L., 2007. No effect of varying soil resource heterogeneity on plant species richness in a low fertility grassland. *Journal of Ecology*, 95(4): 723-733.
- Rezanezhad, F. et al., 2010. Influence of pore size and geometry on peat unsaturated hydraulic conductivity computed from 3D computed tomography image analysis. *Hydrological Processes*, 24(21): 2983-2994.
- Ribbius, C.P.E., 1904. De duinwatertheorie in verband met de verdeling van het zoete en zoute water in den ondergrond onzer zeeduinen. *De Ingenieur*, 19: 71-77.
- Ribeiro, P.J., Diggle, P.J., 2001. *geoR: A package for geostatistical analysis*. R-NEWS, 1: 15-18.

- Rietkerk, M. et al., 2002. Self-organization of vegetation in arid ecosystems. *The American Naturalist*, 160(4): 524-530.
- Roem, W.J., Berendse, F., 2000. Soil acidity and nutrient supply ratio as possible factors determining changes in plant species diversity in grassland and heathland communities. *Biological Conservation*, 92(2): 151-161.
- Romanov, V.V., 1968. *Hydrophysics of bogs* (translated). Israel Programme for Scientific Translations, Jerusalem.
- Römheld, V., 1991. The role of phytosiderophores in acquisition of iron and other micronutrients in graminaceous species: An ecological approach. *Plant and Soil*, 130(1): 127-134.
- Ronkanen, A.-K., Kløve, B., 2007. Use of stable isotopes and tracers to detect preferential flow patterns in a peatland treating municipal wastewater. *Journal of Hydrology*, 347(3-4): 418-429.
- Rosa, E., Larocque, M., 2008. Investigating peat hydrological properties using field and laboratory methods: application to the Lanoraie peatland complex (southern Quebec, Canada). *Hydrological Processes*, 22(12): 1866-1875.
- Rosenberry, D.O., LaBaugh, J.W., Hunt, R.J., 2008. Application of existing wells, portable piezometers, and seepage meters to the determination of water flux between surface water and ground water. In: Rosenberry, D.O., LaBaugh, J.W. (Eds.), *Field Techniques for Estimating Water Fluxes between Surface Water and Ground Water*. US Geological Survey Techniques and Methods, Denver, pp. 43-70.
- Runhaar, H., Witte, F., Verburg, P., 1997. Ground-water level, moisture supply, and vegetation in the Netherlands. *Wetlands*, 17(4): 528-538.
- Runhaar, J., 1989. *Toetsing van het ecotopensysteem* [Testing of the ecotope system]. Centrum voor Milieukunde. Rijksuniversiteit Leiden, Leiden, 138 pp.
- Rycroft, D.W., Williams, D.J.A., Ingram, H.A.P., 1975. The Transmission of Water Through Peat: II. Field Experiments. *Journal of Ecology*, 63(2): 557-568.
- Schaap, M.G., Leij, F.J., 2000. Improved Prediction of Unsaturated Hydraulic Conductivity with the Mualem-van Genuchten Model. *Soil Science Society of America Journal*, 64(3): 843-851.
- Schaap, M.G., Leij, F.J., van Genuchten, M.T., 2001. Rosetta: a computer program for estimating soil hydraulic parameters with hierarchical pedotransfer functions. *Journal of Hydrology*, 251(3-4): 163-176.
- Schaap, M.G., van Genuchten, M.T., 2006. A Modified Mualem-van Genuchten Formulation for Improved Description of the Hydraulic Conductivity Near Saturation. *Vadose Zone J.*, 5(1): 27-34.
- Schaffers, A.P., Sýkora, K.V., 2000. Reliability of Ellenberg indicator values for moisture, nitrogen and soil reaction: a comparison with field measurements. *Journal of Vegetation Science*, 11: 225-244.
- Schaminée, J.H.J., Stortelder, A.H.F., Westhoff, V., 1995a. *De vegetatie van Nederland, deel 1*. Opulus Press, Uppsala, Leiden.
- Schaminée, J.H.J., Weeda, E.J., Westhoff, V., 1995b. *De vegetatie van Nederland 2. Wateren, moerassen, natte heiden*. Opulus Press, Uppsala, SE, Leiden, NL.
- Scherrer, D., Körner, C., 2011. Topographically controlled thermal-habitat differentiation buffers alpine plant diversity against climate warming. *Journal of Biogeography*, 38(2): 406-416.
- Schiff, S.L., Spoelstra, J., Semkin, R.G., Jeffries, D.S., 2005. Drought induced pulses of sulfur from a Canadian shield wetland: use of  $\delta^{34}\text{S}$  and  $\delta^{18}\text{O}$  in to determine sources of sulfur. *Applied Geochemistry*, 20(4): 691-700.
- Schot, P.P., Dekker, S.C., Poot, A., 2004. The dynamic form of rainwater lenses in drained fens. *Journal of Hydrology*, 293(1-4): 74-84.
- Schouwenaars, J.M., 1993. Hydrological differences between bogs and bog-relicts and consequences for bog restoration. *Hydrobiologia*, 265: 217-224.

- Schuurmans, J.M., Bierkens, M.F.P., Pebesma, E.J., Uijlenhoet, R., 2007. Automatic Prediction of High-Resolution Daily Rainfall Fields for Multiple Extents: The Potential of Operational Radar. *Journal of Hydrometeorology*, 8(6): 1204-1224.
- Scotter, D.R., Raats, P.A.C., 1968. Dispersion in Porous Mediums Due to Oscillating Flow. *Water Resources Research*, 4(6): 1201-1206.
- ŠeffEROVÁ StanOVÁ, V., ŠeffER, J., Janák, M., 2008. Management of Natura 2000 habitats. 7230 Alkaline fens. The European Commission (DG ENV B2).
- Šimůnek, J., Šejna, M., Van Genuchten, M.T., 1999. The HYDRUS-2D software package for simulating two-dimensional movement of water, heat, and multiple solutes in variably saturated media Version 2.0, IGWMC - TPS - 53, International Ground Water Modeling Center, Colorado School of Mines, Golden, Colorado.
- Sjörs, H., 1990. Divergent successions in mires, a comparative study. *Aquilo, Series Botanica*, 28: 67-77.
- Skyllberg, U., 1990. Correlation between pH and depth in the mor layer of a *Picea abies* (L.) Karst stand on till soils in northern Sweden. *Scandinavian Journal of Forest Research*, 5: 143-153.
- Smith, M., Meiman, P., Brummer, J., 2012. Characteristics of hummocked and non-hummocked Colorado riparian areas and wetlands. *Wetlands Ecology and Management*, 20(5): 409-418.
- Smolders, A., Lucassen, E., Bobbink, R., Roelofs, J., Lamers, L., 2010. How nitrate leaching from agricultural lands provokes phosphate eutrophication in groundwater fed wetlands: the sulphur bridge. *Biogeochemistry*, 98(1): 1-7.
- Smolders, A.J.P. et al., 2006. Changes in pore water chemistry of desiccating freshwater sediments with different sulphur contents. *Geoderma*, 132(3-4): 372-383.
- Snowden, R.E.D., Wheeler, B.D., 1993. Iron Toxicity to Fen Plant Species. *Journal of Ecology*, 81(1): 35-46.
- Sophocleous, M., 2002. Interactions between groundwater and surface water: the state of the science. *Hydrogeology Journal*, 10(1): 52-67.
- Sterling, A., Peco, B., Casado, M., Galiano, E., Pineda, F., 1984. Influence of microtopography on floristic variation in the ecological succession in grassland. *Oikos*: 334-342.
- Stern, D.I., 2005. Global sulfur emissions from 1850 to 2000. *Chemosphere*, 58(2): 163-175.
- Stiff, H., 1951. The interpretation of chemical water analysis by means of patterns. *Journal of Petroleum Technology*, 3(10).
- Stoppelenburg, F.J., 1999. Een overzicht van de toepassing van intreeweerstanden in modelstudies. Nationaal onderzoeksprogramma verdroging: nov-rapport, 13(3) Ministerie van Verkeer en Waterstaat, Directoraat-generaal Rijkswaterstaat (RWS), Rijksinstituut voor Integraal Zoetwaterbeheer en Afvalwaterbehandeling (RIZA), Den Haag, pp. 40.
- Stumm, W., Morgan, J.J., 1996. *Chemical Equilibria and Rates in Natural Waters*. John Wiley & Sons, New York, 1022 pp.
- Stuyfzand, P.J., 1986. Een nieuwe hydrochemische classificatie van watertypen, met Nederlandse voorbeelden van toepassing. *H2O*, 19: 562-568.
- Tang, D.H., Frind, E.O., Sudicky, E.A., 1981. Contaminant transport in fractured porous media: Analytical solution for a single fracture. *Water Resources Research*, 17(3): 555-564.
- Tayfur, G., Kavvas, M.L., 1998. Areal-averaged overland flow equations at hillslope scale. *Hydrological Sciences Journal*, 43(3): 361-378.
- Ter Braak, C.J.F., Barendregt, L.G., 1986. Weighted averaging of species indicator values: Its efficiency in environmental calibration. *Mathematical Biosciences*, 78(1): 57-72.
- Therrien, R., McLaren, R.G., Sudicky, E.A., Panday, S.M., 2008. *HydroGeoSphere a three-dimensional numerical model describing fully-integrated subsurface and surface flow and solute transport (manual)*. University of Waterloo: Groundwater Simulations Group.
- Thompson, S.E., Katul, G.G., Porporato, A., 2010. Role of microtopography in rainfall runoff partitioning: An analysis using idealized geometry. *Water Resources Research*, 46(7): W07520.

- Triska, F., Jackman, A., Duff, J., Avanzino, R., 1994. Ammonium sorption to channel and riparian sediments: A transient storage pool for dissolved inorganic nitrogen. *Biogeochemistry*, 26(2): 67-83.
- Tsuboya, T., Takagi, K., Takahashi, H., Kurashige, Y., Tase, N., 2001. Effect of pore structure on redistribution of subsurface water in Sarobetsu Mire, northern Japan. *Journal of Hydrology*, 252(1-4): 100-115.
- Turtola, E., Jaakkola, A., 1995. Loss of phosphorus by surface runoff and leaching from a heavy clay soil under barley and grass ley in Finland. *Acta Agriculturae Scandinavica, Section B - Soil & Plant Science*, 45(3): 159-65.
- Van Beek, C.G.E.M., 1980. A model for the induced removal of iron and manganese from groundwater in the aquifer, Proc. 3rd Water-Rock Interaction Symp., Edmonton, Canada, pp. 29-31.
- Van Beek, C.G.E.M., Jalink, M., Meuleman, A.F.M., 2001. De verzwaveling van grondwater in zandgronden. *Landschap*, 18(4): 267-272.
- van Bodegom, P.M., van Reeve, J., Denier van der Gon, H.A.C., 2003. Prediction of reducible soil iron content from iron extraction data. *Biogeochemistry*, 64(2): 231-245.
- van Breemen, N., 1995. How Sphagnum bogs down other plants. *Trends in Ecology & Evolution*, 10(7): 270-275.
- Van Dam, J.C., 2000. Field-scale water flow and solute transport, PhD thesis, Wageningen University.
- Van Dam, J.C., Groenendijk, P., Hendriks, R.F.A., Kroes, J.G., 2008. Advances of modeling water flow in variably saturated soils with SWAP. *Vadose Zone Journal*, 7(2): 640-653.
- Van Delft, B., Brouwer, F., Van der Werff, M., Kemmers, R., 2010. Natuurpotentie Willinks Weust, resultaten van een Ecopedologisch onderzoek, Alterra Wageningen UR, Wageningen.
- Van Delft, S.P.J., 1995. Humus - en bodemprofielen in natte schraalgraslanden: resultaten van een bodemkundig onderzoek in 13 referentiegebieden voor het onderzoek naar effectgerichte maatregelen tegen verzuring (EGM), DLO-Staring Centrum, Wageningen.
- Van der Hoek, D.J., 2005. The effectiveness of restoration measures in species-rich fen meadows, PhD thesis, Wageningen University.
- Van der Ploeg, M.J. et al., 2012. Microtopography as a Driving Mechanism for Ecohydrological Processes in Shallow Groundwater Systems. *Vadose Zone Journal*, 11(3).
- Van der Schaaf, S., 1998. Balanceren tussen kwel en wegzijging: hydrologisch beheer bij het herstel van soortenrijke natte graslanden. *Landschap*, 15: 87-97.
- van der Schaaf, S., 2004. A single well pumping and recovery test to measure in situ acrotelm transmissivity in raised bogs. *Journal of Hydrology*, 290(1-2): 152-160.
- van der Swaluw, E., Asman, W.A.H., van Jaarsveld, H., Hoogerbrugge, R., 2011. Wet deposition of ammonium, nitrate and sulfate in the Netherlands over the period 1992-2008. *Atmospheric Environment*, 45(23): 3819-3826.
- van der Velde, Y., de Rooij, G.H., Torfs, P.J.J.F., 2009. Catchment-scale non-linear groundwater-surface water interactions in densely drained lowland catchments. *Hydrology and Earth System Sciences Discussions*, 13(10): 1867-1885
- van der Velde, Y., Rozemeijer, J.C., de Rooij, G.H., van Geer, F.C., Broers, H.P., 2010. Field-Scale Measurements for Separation of Catchment Discharge into Flow Route Contributions. *Vadose Zone Journal*, 9(1): 25-35.
- van der Welle, M.E.W., Roelofs, J.G.M., Lamers, L.P.M., 2008. Multi-level effects of sulphur-iron interactions in freshwater wetlands in The Netherlands. *Science of the Total Environment*, 406(3): 426-429.
- Van der Zee, S.E.A.T.M., 1990. Analytical traveling wave solutions for transport with nonlinear and nonequilibrium adsorption. *Water Resources Research*, 26(10): 2563-2578.
- Van Diggelen, R., 1998. Moving gradients. Assessing restoration prospects of degraded brook valleys, PhD thesis, University of Groningen.

- Van Duijn, C.J., Knabner, P., 1992. Travelling waves in the transport of reactive solutes through porous media: Adsorption and binary ion exchange – Part 1. *Transport in Porous Media*, 8(2): 167-194.
- Van Duijn, C.J., Peletier, L.A., 1977. A class of similarity solutions of the nonlinear diffusion equation. *Nonlinear Analysis, Theory, Methods & Applications*, 1(3): 223-233.
- Van Genuchten, M.T., 1980. A closed-form equation for predicting the hydraulic conductivity of unsaturated soils. *Soil Science Society of America Journal*, 44: 892-898.
- Van Genuchten, M.T., Alves, W.J., 1982. Analytical Solutions of the One-Dimensional Convective-Dispersive Solute Transport Equation, U.S. Department of Agriculture, Technical bulletin no. 1661.
- van Helvoort, P.-J., Griffioen, J., Hartog, N., 2007. Characterization of the reactivity of riverine heterogeneous sediments using a facies-based approach; the Rhine-Meuse delta (The Netherlands). *Applied Geochemistry*, 22(12): 2735-2757.
- Van Immerzeel, C.H., Vegter, U., Schot, P.P., 1996. Toepassing van een neerslaglenzenmodel bij hydro-ecologische herstelprojecten. *H2O*, 29(10): 293-296.
- Van Moorsel, R.C.M.J., Barendregt, H.E., 1993. Dotterbloem en Waterviolier in Nederland. *Gorteria*, 19: 33-44.
- Van Wirdum, G., 1991. Vegetation and hydrology of floating rich fens. Phd Thesis, PhD thesis, University of Amsterdam.
- Vandenbohede, A., Van Houtte, E., Lebbe, L., 2008. Groundwater flow in the vicinity of two artificial recharge ponds in the Belgian coastal dunes. *Hydrogeology Journal*, 16(8): 1669-1681.
- Vermulst, J.A.P.H., Kroon, T., De Lange, W.J., 1998. Modelling the hydrology of the Netherlands on a nationwide scale. *Hydrology in a Changing Environment*, 1: 91-100.
- Violle, C. et al., 2007. Let the concept of trait be functional! *Oikos*, 116(5): 882-892.
- Vivian-Smith, G., 1997. Microtopographic heterogeneity and floristic diversity in experimental wetland communities. *Journal of Ecology*: 71-82.
- Vogel, T., Cislerova, M., Hopmans, J.W., 1991. Porous Media With Linearly Variable Hydraulic Properties. *Water Resources Research*, 27(10): 2735-2741.
- Vogel, T., Van Genuchten, M.T., Cislerova, M., 2001. Effect of the shape of the soil hydraulic functions near saturation on variably-saturated flow predictions. *Advances in Water Resources*, 24(2): 133-144.
- Vrugt, J.A., Bouten, W., Gupta, H.V., Sorooshian, S., 2002. Toward improved identifiability of hydrologic model parameters: The information content of experimental data. *Water Resources Research*, 38(12): 1312.
- Vrugt, J.A., Gupta, H.V., Bouten, W., Sorooshian, S., 2003. A Shuffled Complex Evolution Metropolis algorithm for optimization and uncertainty assessment of hydrologic model parameters. *Water Resources Research*, 39(8): 1201.
- Vrugt, J.A. et al., 2004. Inverse modeling of large-scale spatially distributed vadose zone properties using global optimization. *Water Resources Research*, 40(6): W06503.
- Vrugt, J.A., ter Braak, C.J.F., Clark, M.P., Hyman, J.M., Robinson, B.A., 2008. Treatment of input uncertainty in hydrologic modeling: Doing hydrology backward with Markov chain Monte Carlo simulation. *Water Resources Research*, 44: W00B09.
- Vrugt, J.A., Van Wijk, M.N., Hopmans, J.W., Šimunek, J., 2001. One-, two-, and three-dimensional root water uptake functions for transient modeling. *Water Resources Research*, 37: 2457-2470.
- Waddington, J.M., Kellner, E., Strack, M., Price, J.S., 2010. Differential peat deformation, compressibility, and water storage between peatland microforms: Implications for ecosystem function and development. *Water Resources Research*, 46(7): W07538.
- Wallén, B., Falkengren-Grerup, U., Malmer, N., 1988. Biomass, productivity and relative rate of photosynthesis of *Sphagnum* at different water levels on a South Swedish peat bog. *Ecography*, 11(1): 70-76.

- Wallis, I. et al., 2011. Process-Based Reactive Transport Model To Quantify Arsenic Mobility during Aquifer Storage and Recovery of Potable Water. *Environmental Science & Technology*, 45(16): 6924-6931.
- Wamelink, G.W.W., Goedhart, P.W., van Dobben, H.F., 2004. Measurement errors and regression to the mean cannot explain bias in average Ellenberg indicator values. *Journal of Vegetation Science*, 15(6): 847-851.
- Wamelink, G.W.W., Joosten, V., van Dobben, H.F., Berendse, F., 2002. Validity of Ellenberg indicator values judged from physico-chemical field measurements. *Journal of Vegetation Science*, 13: 269-278.
- Wang, M.K., Tzou, Y.M., 1995. Phosphate sorption by calcite, and iron-rich calcareous soils. *Geoderma*, 65(3-4): 249-261.
- Wassen, M.J., Barendregt, A., Bootsma, M.C., Schot, P.P., 1988. Groundwater chemistry and vegetation of gradients from rich fen to poor fen in the Naardermeer (the Netherlands). *Vegetatio*, 79(3): 117-132.
- Webster, R., Oliver, M.A., 1992. Sample adequately to estimate variograms of soil properties. *Journal of Soil Science*, 43(1): 177-192.
- Webster, R., Oliver, M.A., 2001. *Geostatistics for Environmental Scientists*. John Wiley & Sons, Ltd., Chichester.
- Weiler, M., Naef, F., 2003. An experimental tracer study of the role of macropores in infiltration in grassland soils. *Hydrological Processes*, 17(2): 477-493.
- Weng, L., Vega, F.A., Van Riemsdijk, W.H., 2011. Competitive and Synergistic Effects in pH Dependent Phosphate Adsorption in Soils: LCD Modeling. *Environmental Science & Technology*, 45(19): 8420-8428.
- Werkgroep Herziening Cultuurtechnisch Vademecum, 1988. *Cultuurtechnisch Vademecum*. Cultuurtechnische Vereniging Utrecht, The Netherlands.
- Wesseling, J.G., Wesseling, J., 1984. The influence of seepage on the depth of water tables in drainage. *Journal of Hydrology*, 73(3-4): 289-297.
- Westoby, M., 1998. A leaf-height-seed (LHS) plant ecology strategy scheme. *Plant and Soil*, 199(2): 213-227.
- Wheeler, B.D., 1980. Plant Communities of Rich-Fen Systems in England and Wales: III. Fen Meadow, Fen Grassland and Fen Woodland Communities, and Contact Communities *Journal of Ecology*, 68(3): 761-788.
- Wherry, E.T., 1922. Recent Work on Soil Acidity and Plant Distribution. *Science*, 55: 568-570.
- Wiebe, W.J., 1981. Anaerobic respiration and fermentation. In: Pomeroy, L.R., Wiegert, R.G. (Eds.), *The ecology of a salt marsh*. Springer, pp. 137-159.
- Witte, J.P.M., 1998. *National Water Management and the Value of Nature*, PhD Thesis Wageningen Agricultural University, Wageningen.
- Witte, J.P.M. et al., 2012. An ecohydrological sketch of climate change impacts on water and natural ecosystems for the Netherlands: bridging the gap between science and society. *Hydrology and Earth System Sciences*, 16: 3945-3957.
- Witte, J.P.M., Wójcik, R.B., Torfs, P.J.J.F., de Haan, M.W.H., Hennekens, S., 2007. Bayesian classification of vegetation types with Gaussian mixture density fitting to indicator values. *Journal of Vegetation Science*, 18: 605-612.
- Wösten, J.H.M., Pachepsky, Y.A., Rawls, W.J., 2001. Pedotransfer functions: bridging the gap between available basic soil data and missing soil hydraulic characteristics. *Journal of Hydrology*, 251(3-4): 123-150.
- Yapo, P.O., Gupta, H.V., Sorooshian, S., 1996. Automatic calibration of conceptual rainfall-runoff models: sensitivity to calibration data. *Journal of Hydrology*, 181(1-4): 23-48.

- Zeeman, W.P.C., 1986. Application in Land, Nature and Water Management: The Reitema a case study. In: Hooghart, J.C. (Ed.), *Water Management in relation to nature, forestry and landscape management*. CHO-TNO, The Hague, pp. 117-126.
- Zhang, Y.-C., Slomp, C.P., Broers, H.P., Passier, H.F., Cappellen, P.V., 2009. Denitrification coupled to pyrite oxidation and changes in groundwater quality in a shallow sandy aquifer. *Geochimica et Cosmochimica Acta*, 73(22): 6716-6726.
- Zuurbier, K., Bakker, M., Zaadnoordijk, W., Stuyfzand, P., 2013a. Identification of potential sites for aquifer storage and recovery (ASR) in coastal areas using ASR performance estimation methods. *Hydrogeology Journal*, 21(6): 1373-1383.
- Zuurbier, K.G., Hartog, N., Valstar, J., Post, V.E.A., van Breukelen, B.M., 2013b. The impact of low-temperature seasonal aquifer thermal energy storage (SATES) systems on chlorinated solvent contaminated groundwater: Modeling of spreading and degradation. *Journal of Contaminant Hydrology*, 147(0): 1-13.



## DANKWOORD

Het was alweer in 2002 dat Flip Witte mij attendeerde op de mogelijkheid voor een afstudeeronderzoek naar de dynamiek van neerslaglenzen in kwelafhankelijke natuurgebieden. Een leuk onderwerp op het raakvlak van hydrologie, hydrochemie en ecologie. Nieuwe programmatuur en krachtiger computers maakten het mogelijk om gedetailleerd aan de stromingspatronen en stoftransport in deze systemen te rekenen. Het rekenwerk bleek echter geen sinecure, met numerieke problemen en rekentijden van weken, maar resulteerde wel in een mooie scriptie. Na mijn afstuderen in 2003 introduceerde Flip mij bij het voor mij toen nog onbekende instituut Kiwa Water Research, waar ik al snel aan de slag kon. Na mijn introductie in waterleidingland verschoof mijn aandacht gedurende een aantal jaren naar aan waterwinning gerelateerde aspecten zoals putverstopping en bescherming van grondwater als grondstof voor drinkwater. De tijdens mijn afstuderen gewekte interesse voor fysische processen in kwelafhankelijke natuurgebieden bleef echter onverminderd aanwezig.

Arthur Meuleman, mijn toenmalige afdelingshoofd zag in 2006 mogelijkheden voor het aanvragen van een Casimir beurs bij NWO. Samen met Sjoerd van der Zee, Flip en Arthur werd een onderzoeksvorstel geschreven voor een studie naar de ‘Spatiotemporele fysische en chemische eigenschappen van regenwaterlenzen in natuurgebieden’. Dit voorstel werd in 2007 door NWO gehonoreerd, waarna ik aan de slag kon met mijn onderzoek. Het afronden van lopende projecten en tijd vrijmaken voor het onderzoek viel niet helemaal mee, maar in 2008 kwam het onderzoek op stoom, waarbij ik de donderdagen op de vakgroep in Wageningen doorbracht. Arthur, Flip en Sjoerd, ik wil jullie bedanken voor jullie vertrouwen en het bieden van de mogelijkheid voor mijn promotieonderzoek.

Flip en Sjoerd, ik wil jullie als promotoren in het bijzonder bedanken. Voor jullie kennis en creativiteit waar ik veel van heb mogen leren, de goede discussies, jullie snelle en uitgebreide commentaar op aangeleverde teksten en in het bijzonder de relativerende en bemoedigende woorden als de moed me weer eens in de schoenen zakte. Ik zie er naar uit om met jullie samen te blijven werken.

Collega's van de WUR, het was leuk om, al was het maar voor een dag in de week, terug te zijn op de vakgroep in Wageningen. Ik wil jullie bedanken voor jullie interesse, meedenken en gezelligheid. Willemijn en Marieke, het bij jullie aanschuiven op de kamer was een waar genoegen. Dank voor de lol en goede gesprekken en mooi dat we op onze kamer kennis hebben kunnen integreren in een publicatie die is opgenomen in hoofdstuk 6! Toon, bedankt voor je fysische inzicht en bemoedigende woorden. Jelmer, jouw metingen in het kader van je afstudeeronderzoek hebben flink bijgedragen aan hoofdstuk 5 en 6 van dit proefschrift, hiervoor bedankt en succes met je promotieonderzoek.

Hans, ik wil je bedanken voor je hulp bij het gebruiken van Orchestra en de discussies over bodemchemie en modellen die we gevoerd hebben. Peter, bedankt voor je bodemchemische kennis en je waardevolle suggesties voor hoofdstuk 5.

Collega's van KWR, bedankt voor jullie interesse in mijn onderzoek en de ontspannende momenten tijdens koffiepauzes, lunch(wandelingen) en uitjes naar de Ardennen. Kees, ik heb de afgelopen 10 jaar bij KWR veel van je kunnen leren en het is mooi dat we samen de chemische processen in het Meeuwenkampje hebben kunnen uitknobbelen, resulterend in de H<sub>2</sub>O prijs 2012 en een mooi hoofdstuk van mijn proefschrift. Han, dank voor de discussies die we hebben gevoerd en het aanscherpen van m'n gedachten. Ruud, van het digitaliseren van de bodemeigenschappen heb jij uiteindelijk het meeste baat gehad, maar ik deed het graag! Dank voor je aanstekelijke optimisme en het lenen van je proefschrift layout.

Zonder de mogelijkheden die Staatsbosbeheer me heeft geboden om in kwetsbare natuurgebieden metingen uit te voeren, was een groot deel van dit onderzoek niet mogelijk geweest. Bjørn, dank voor het verlenen van toestemming en het aanleveren van bestaande data. Rein, Bert, dank voor jullie veldkennis en het in goede banen leiden van maaiactiviteiten langs de meetopstellingen.

Ruben, 't is al weer 16 jaar geleden dat we elkaar op Larenstein tegenkwamen. Sindsdien veel goede momenten gedeeld. Dank voor je prikkelende vragen en goede discussies. Fijn dat je m'n paranimf wilt zijn.

Coert, hoewel ik je promotiewerk inhoudelijk niet geheel kon volgen, konden we ons promotie wel en wee wel delen. Het was dan ook een eer om je paranimf te wezen. Nu zijn de rollen omgekeerd! Onze jaarlijkse vakantie in Limburg en de Ardennen met Marieke, Annelene en de kids is altijd weer een week om naar uit te kijken.

Brie, bedankt voor je hulp bij het goed in het Engels verwoorden van de stellingen.

Paps, mams, zonder jullie had dit boekje er niet gelegen. Dank voor jullie vertrouwen en steun ook toen het niet 'vanzelf' ging op de middelbare school.

Tobias en Matthijs, jullie weten niet beter dan dat ik met m'n promotieonderzoek bezig ben, dank voor jullie relativerende levensvreugde en de ontspannende uurtjes bouwen met Lego en Kapla. Tobias, je opmerking: "papa, wanneer is je boekje klaar, dan kunnen we weer leuke dingen doen" was een extra stimulans om m'n proefschrift af te ronden.

Lieve Marieke, de afgelopen jaren hebben best wat van jou gevraagd. Dank voor je steun, liefde en vertrouwen, ik zie uit naar onze verdere leven samen.

## LIST OF PUBLICATIONS

### *Peer reviewed publications:*

- Ramaker, T.A.B., A.F.M. Meuleman, L. Bernardi & D.G. Cirkel (2005) Climate change and drinking water production in the Netherlands: a flexible approach, *Water Science & Technology*, 51(5), 37-44.
- Meuleman, A.F.M., D.G. Cirkel & J.J.G. Zwolsman (2007) When climate change is a fact! Adaptive strategies for drinking water production in a changing natural environment. *Water Science & Technology*, 56(4), 137-144.
- Cirkel, D.G., J.P.M. Witte & S.E.A.T.M. van der Zee (2010) Estimating seepage intensities from groundwater level time series by inverse modelling: A sensitivity analysis on wet meadow scenarios, *Journal of Hydrology*, 385, 132–142.
- Van der Ploeg, M.J., W.M. Appels, D.G. Cirkel, M.R. Oosterwoud, J.-P. M. Witte & S.E.A.T.M. van der Zee (2012) Microtopography as a driving mechanism for ecohydrological processes in shallow groundwater systems. *Vadose zone Journal* 11(3) doi: 10.2136/vzj2011.0098
- Von Asmuth, J.R., C. Maas, M.F.P. Bierkens, M. Bakker, T.N. Olsthoorn, D.G. Cirkel, I. Leunk, F. Schaars & D.C. von Asmuth (2012) *Menyanthes*: software for hydrogeologic time series analysis, interfacing data with physical insight. *Environmental Modelling & Software* 38: 178-190.
- Cirkel, D.G., C.G.E.M. van Beek, J.P.M. Witte & S.E.A.T.M. van der Zee (2013) Sulphate reduction and calcite precipitation in relation to internal eutrophication of groundwater fed alkaline fens. *Biogeochemistry* doi 10.1007/s10533-013-9879-4
- Cirkel, D.G., J.P.M. Witte, P.M. van Bodegom, J.J. Nijp & S.E.A.T.M. van der Zee (2014) How moisture regime and spatiotemporal variability shape empirical relationships between soil acidity and vegetation. *Ecohydrology* 7(1): 21-32 doi: 10.1002/eco.1312
- Cirkel, D.G., S.E.A.T.M. van der Zee & J.C.L. Meeussen. (*Submitted*) Mixing Behaviour at Oscillating Fronts.

*Publications in professional journals:*

- Cirkel, D.G. & C.G.E.M. van Beek (2012) Pyrietoxidatie en Sulfaatreductie, bedreiging of kans voor vorming kalkmoeras? *H<sub>2</sub>O* 1: 31-33
- Rothuizen, R.D & Cirkel, D.G. (2011) Regulering vloeistofdrukken cruciaal bij aanleg HDDW. *Geotechniek* 2: 25-27
- Cirkel, D.G., P. van der Wens, R.D. Rothuizen, & J.W. Kooiman (2011) Waterwinning met HDD-boringen; Eén horizontaal putfilter voor meerdere verticale. *Land+Water* 1(2): 22-23
- Rothuizen, R.D. & D.G. Cirkel (2010) Horizontal Directional Drilled Wells – HDDW; Nieuwe techniek voor horizontale filters. *Civiele Techniek* 65, 7: 30-32
- Cirkel, D. G., F. Rambags, I. van de Hoeve, B. Pittens & P. van der Wens (2010), Doorbraak met geslaagde horizontaal gestuurd geboorde put. *H<sub>2</sub>O* 17: 9-11
- Berg, Gerard van den, Gijsbert Cirkel & Benno Drijver (2007), Aanpak putverstopping door chemische neerslagen kan en moet effectiever. *H<sub>2</sub>O* 8:16-17
- Cirkel, D.G., E. van Griensven & E. Broers (2006), Klimaatverandering en grondwaterwinning. *H<sub>2</sub>O* 22: 39-42
- Putters, B., C. Maas, D.G. Cirkel, F. Vaessen, M. Juhász & J.R. von Asmuth (2006), Voorkómen en voorspellen van nitraatconcentraties in kalksteenwinningen in Zuid-Limburg, *Stromingen* 12(3): 31-40
- Cirkel, D.G., J.R. von Asmuth (2005), Schatgraven in grondwaterstands tijdreeksen, *Trends in water*, 16
- Von Asmuth, J.R., C. Maas & D.G. Cirkel (2004), Tijdreeksanalyse nu binnen ieders handbereik. *H<sub>2</sub>O* 24: 31-33

## CURRICULUM VITAE

Gijsbert Cirkel was born in Zoetermeer, the Netherlands, on 27 June 1979 and grew up in Ede. After graduating from secondary school (HAVO, Streeklyceum Ede) in 1997, he studied Land and Water Management at Hogeschool Larenstein in Velp. After his BSc graduation in 2001 he continued with the MSc study Hydrology and Quantitative Water Management, with a specialisation in Soil Physics, Agrohydrology and Groundwater Management, at Wageningen University and graduated in 2003 (Cum Laude). In 2004 his Master thesis: “Effects of re-wetting measures and climate change on extreme high flow conditions” was rewarded the Wageningen University Fund thesis price. After graduation, he started his professional career as a hydrologist at Kiwa Water Research (from 2008 KWR Watercycle Research Institute). After receiving a NWO CASIMIR grant, he started his PhD research at the Soil Physics Ecohydrology and Groundwater group (currently Soil physics and Land Management group) at Wageningen University on a part time basis. The results of this research are reported in this thesis.



The research described in this thesis was carried out at KWR Watercycle Research Institute and Wageningen University. The research was financially supported by both the Netherlands Organisation for Scientific Research (NWO) CASIMIR programme (018.002.007) and the joint research program of the Dutch Water Utility sector (BTO).



Cover design: Erwin Timmerman

Printing: Optima Grafische Communicatie



